FINAL REPORT
GTI PROJECT NUMBER 22428 / 22429
OTD PROJECT NUMBER 4.14.c.2
DOT Project #729
DOT/PHMSA CONTRACT NUMBER: 693JK31810003

Validating Non-Destructive Tools for Surface to Bulk Correlations of Yield Strength, Toughness, and Chemistry

Date Submitted
September 28, 2021

Submitted To
U.S. DOT/PHMSA
Operations Technology Development, OTD

Project Manager / Administrative Contact
Matt Manning
Gas Technology Institute
847.971.1214
mmanning@gti.energy

Principal Investigator / Technical Contact
Daniel Ersoy
Element Resources, LLC
847.343.9755
dersoy@elementresourcesllc.com

Authors
Daniel Ersoy (Element Resources)
Brian Miller (GTI)
Marta Guerrero Merino (GTI)
Dr. Yongming Liu, Qiongfang Zhang, Jie Chen, Nan Xu (ASU, Ch. 6)

GTI
1700 S. Mount Prospect Rd.
Des Plaines, Illinois 60018
www.gti.energy

LEGAL NOTICE

This information was prepared by Gas Technology Institute ("GTI") for U.S. DOT/PHMSA and Operations Technology Development, OTD.

Neither GTI, the members of GTI, the Sponsor(s), nor any person acting on behalf of any of them:

Makes any warranty or representation, express or implied with respect to the accuracy, completeness, or usefulness of the information contained in this report, or that the use of any information, apparatus, method, or process disclosed in this report may not infringe privately-owned rights. Inasmuch as this project is experimental in nature, the technical information, results, or conclusions cannot be predicted. Conclusions and analysis of results by GTI represent GTI's opinion based on inferences from measurements and empirical relationships, which inferences, and assumptions are not infallible, and with respect to which competent specialists may differ.

Assumes any liability with respect to the use of, or for any and all damages resulting from the use of, any information, apparatus, method, or process disclosed in this report; any other use of, or reliance on, this report by any third party is at the third party's sole risk.

The results within this report relate only to the items tested/reviewed.

TABLE OF CONTENTS

LIST OF FIGURES

Page

LIST OF TABLES

Page

PART I: SUMMARY, TECHNICAL APPROACH, AND DATA ORGANIZATION

Part I contains:

- Chapter 1: Executive Summary
- Chapter 2: Technical Approach and Data Organization

Chapter 1: Executive Summary

1.1 Project Objective

The deliverables of this project will facilitate the use of non-destructive surface testing: micro-indentation, micro-machining, in situ chemistry, and replicate microscopy analysis as accurate, efficient, and cost-effective tools for material property confirmation.

This work will provide benefits to pipeline safety, energy continuity, and integrity assessment programs since the developed techniques and models and validated testing technology will not require a line to be taken out of service or destructively cut out samples from the in-service pipeline.

The results of this project will also be applicable to DOT/PHMSA regulations that require operators to backfill their material property records for grandfathered pipeline segments and/or those that do not have adequate material records.

1.2 Acknowledgements

Sponsors

The project team greatly thanks the two sponsors of this effort:

U.S. Department of Transportation Pipeline and Hazardous Materials Safety Administration, under project #729, agreement 693JK31810003.

Public project web page at: https://primis.phmsa.dot.gov/matrix/PrjHome.rdm?prj=729

Operations Technology Development, under project OTD 4.14.c.2

Further information available at: https://www.otd-co.org.

Technical Advisory Panel (TAP)

- DOT/PHMSA, OTD
- GTI, Element Resources, and ASU
- Gas Pipeline Participants
  - Ameren
  - Peoples Gas
  - North Shore Gas
  - National Fuel
  - Southwest Gas
  - Intermountain Gas
  - Dominion
  - National Grid

Project Team

- **U.S. DOT / PHMSA**: Joseph Pishnery (AOR) and Robert Smith (Prgm Mgr.)
- **OTD**: Mike Adamo
- **Element Resources**: Daniel Ersoy
- **Gas Technology Institute:** Brian Miller and Marta Guerrero-Merino
- **Arizona State University**: Dr. Yongming Liu, Jie Chen, Qionfang Zhang, Sonam Dahire, and Nan Xu

1.3 Report Structure

The report represents a significant body of work over 3 years+. Therefore, the report is broken up into five "Parts" which each house Chapters related to the Part.

The five Parts are:

- Part I: Summary, Technical Approach, and Data Organization
- Part II: Surface / Bulk Testing Comparisons
- Part III: Modeling
- Part IV: Project Conclusions and Recommendations
- Part V: Appendices, References, and Attachments

1.4 Concise Report Chapter Summaries

This section provides a high level and concise summary of each of the five Parts and related eight Chapters. The remainder of the report provides further details for each section and the attachments which number 1,000 pages provide much more detail and supporting information.

Part I: Summary, Technical Approach, and Data Organization

Chapter 1: Executive Summary

Provides concise summary of the project: objective, team, and chapter content.

Chapter 2: Technical Approach and Data Organization

The test results from thousands of lab and field material tests done on actual pipeline samples have been used to develop models that account for pipe material thermo-mechanical process variations and through-wall variability of material, mechanical, and chemical properties.

A Technical Advisory Panel (TAP) was formed with the sponsors, the technical team, and eight pipeline operators. The TAP was used to solicit input on scope of work details, operational considerations, and deliverable design.

A separate "training set" of twenty pipelines was made available to GTI, Element Resources, and ASU to allow initial model testing and prove-out prior to the seventy primary samples that were used to fully characterize pipeline properties and the correlation of surface to bulk properties, as well as develop predictive models of bulk properties based solely on surface obtained pipeline data.

A set of seventy pipeline samples (termed Pipe Library) that were in service from the natural gas industry were selected for the project testing and modeling. A great deal of care and effort was put forth to select a reasonable number that provided the adequate breadth of variety as typically encountered by the industry in the field.

The Pipe Library detailed breakdown in the report is termed the design of experiments (DOE). The ranges for the key pipeline attributes are:

- Installation years from 1930 to 2004 with over 60% pre-code pipelines
- Diameters from 4 to 30 inches
- Grades from A to X52
- All steel types: rimmed/capped, semi-killed, and fully killed
- All key long seam types: ERW, SAW, Seamless, and Spiral
- Wall thickness over wide range: 0.156 to 0.460 inches
- Chemistry grade variety, e.g.: 1008, 1010, 1015, 1016, 1021, 1022, 1023, 1025, 1026, 1030, 1522, 1525, and vanadium and niobium High Strength Low Allow (HSLA) grades
- ASTM Grain Size (log scale) range spanning: 7.0 to 13.0

A structured, column database was developed with 203 variables (fields) to collect and organize all project test data from the lab and field-based testing. A separate, similar but smaller database, was designed to collect and organize a supplemental toughness testing program. These databases house nearly 15,000 data entries from lab and field-based testing and are provided as Appendix A and Appendix B external Excel files in column database orientations.

Part II: Surface / Bulk Testing Comparisons

Chapter 3: Material Yield and Tensile Strength, Grain Size, and Chemistry

This chapter describes the trends and comparisons between surface and bulk pipe properties. Methodologies are listed in Chapter 2 and the associated and very detailed Attachments to this report. Readers are directed to these sections for more information related to methods and procedures.

The chapter is broken down into four main sections, one each focused on: yield strength, ultimate tensile strength, chemistry, and grain size. Chemistry is also very important to determine steel type.

The testing uncovered a range of variation across the pipe wall thickness. The data used in this Chapter is provided in Appendix A.

For the normalized/annealed *seamless* pipelines, the properties were mostly uniform or isotropic across the pipe wall, meaning that the nondestructive evaluation technologies done on the pipe outer wall surface are representative of the rest of the wall and therefore the bulk properties needed for characterization.

For *non-seamless* pipes (that have long seam welds) there can be significant anisotropic properties of *yield strength* and *chemistry* (specifically carbon segregation) between the surface obtained values and an average across the wall and/or bulk chemistry and full-wall mechanical testing results.

The reasons for this difference between the surface and bulk properties is discussed in detail in this chapter, but in summary the major categorical factors are: (a) cold work and forming stress from pipe manufacturing (without post production normalizing/annealing as in seamless pipe), (b) chemical segregation from primary steel production (e.g., rimmed/capped centerline carbon segregation), (c) HSLA steel grain refinement especially near the outer surfaces of the pipe wall, and (d) other thermomechanical factors.

The surface NDE test results from two technologies (Frontics AIS and MMT HSD) for yield strength and ultimate tensile strength were compared to the full-wall lab test results.

The observed trends likely indicate that the MMT HSD "surface scratch-type" technique (see Attachments) interrogates mostly the outer layers of the pipe wall while the Frontics AIS "indentation-type" technique (see Attachments) may in effect test deeper into the pipe wall.

Seamless pipe is normalized/annealed and is therefore very homogenous across its thickness. Welded pipe on the other hand is produced from hot rolled plate or strip that usually exhibits through-thickness variations in microstructure. These differences in grain size or in pearlite interlamellar distance are produced by localized through-thickness differences in temperature as the plate is rolled and then cooled on the run-out table. In addition, forming the pipe through the U-bend, O-bend, and Expansion (UOE) process followed by welding often produces significant residual stresses and cold work that tends to make the outer layers of the pipe "stronger" from a yield testing standpoint. Finally, the cold expansion step (and potential mill hydrotest) may or may not have been performed which introduces another element of uncertainty in properties prediction.

The same can be said for HSLA steels that due to the chemistry and grain refiners added, and thermomechanical processing, may lead to a finer (smaller diameter) grain size structure on the outer walls of the pipe thickness. This could also increase the yield strength near the surface due to the well-known Hall-Petch phenomenon that finer grain sizes contribute to higher yield strengths. While the properties of all steels are affected by thermomechanical processing factors, HSLA or micro-alloyed steels are produced in way so as to maximize the strengthening mechanisms available through controlled rolling and accelerated cooling.

Taken as a whole, and on average, welded and/or HSLA pipes and steels lead to a pipe stronger on the outside layers than the inside layers. From the data, this appears to be a likely reason why the MMT surface yield strengths (prior to any modeling) are higher for these situations than the full-wall lab tensile tests.

Both NDE techniques exhibited little difference between the lab and their NDE surface-derived tensile strengths. This is consistent with the reality that the factors that produce a gradient of yield strength across a pipe wall do not affect the ultimate tensile strength the same way. The yield strength is very sensitive to any changes that reduce or increase the ability for atomic slip planes and dislocations to move through the material matrix, whereas tensile strength is actual breaking of these bonds outright.

Chapter 4: Material Toughness (Supplemental Section)

A subset of 30 of the 70 pipeline samples from the DOE had extensive Charpy V-notch (CVN) toughness testing completed on them. The data for these is provided in Appendix B.

This chapter analyzes the results of the testing which included CVN absorbed energy, lateral expansion, and percent shear over various temperatures. Enough temperatures were performed to establish the CVN upper shelf energy level.

Frontics also tested these 30 pipeline samples in the form of coupons for K_{IC} fracture toughness. Those results are presented in Attachment #4 but are not compared directly to the CVN values since the testing direction and mode are different.

In general, the CVN energy went down when temperature was reduced and phosphorous and sulfur levels increased for non-HSLA steels.

The research team feels that this Chapter will provide an excellent foundation for future research and development as new field-ready and non-destructive toughness test methods are developed.

Part III: Modeling

Chapter 5: Causally Based Regression

This chapter contains the regression and model fits (when provided) from the nondestructive technology and the causal models from the analysis developed during this project, as well as historical models from the literature.

The causality of each model is a function of the choices of independent variables and how they are interacted or not. The choices for the structure of the causal models were based on the range of API steels tested and expected in the field, i.e., the DOE. These include lower to moderate carbon steels with ferritic and/or pearlitic phase structures. The inclusion of the key alloy elements used to strengthen the steels through solid solution and precipitation strengthening were accounted for as well.

Many historic models recorded in the literature were tested but it became evident that although these models did have some merit, that the lack of ubiquitous computing power from the decades that they were developed potentially resulted in a limited number of terms for the least square regressions and exclusion of some key, higher order terms. With the availability of very powerful personal computers and equally important the associated statistical analysis packages, there were no restrictions on the causal model terms and forms selected for modeling in this project.

The best causal models for the Frontics and MMT NDE technologies were developed for yield strength and outperformed all the other models from historical research or those that were developed at the time by the technology provider in some cases.

The modeling of the ultimate tensile strength was a much simpler formula from a causal basis. It is highly dependent on manganese and carbon content. There are only minimal differences between all of the models for ultimate tensile strength for both the custom and the historic models in the literature.

In summary, the project was highly successful with the model development. The causal model developed and combined with the Frontics AIS output for yield strength was able to achieve a predicted vs. actual regression fit with a 95% confidence for predicting yield strength across the entire pipe sample DOE. The MMT technology showed non-conservative bias in all models for yield strength, especially near or above 50 ksi actual (full-wall) yield strength for the aforementioned reasons. The ultimate tensile strength causal models achieved the same 95% confidence level for both NDE technologies across the full pipe DOE range.

Chapter 6: Data Analytics Modeling: OLS, BMA, BNM, GPM, and MBGPM

Several classical and novel data analytics methods are demonstrated, compared, and validated using the collected experimental datasets. They are: ordinary least-square regression (OLS), Bayesian Model Averaging (BMA), Bayesian Network Model (BNM), Gaussian Process Model (GPM), and Manifold-Based Gaussian Process Model (MBGPM). The results showed that the Bayesian averaging and updating principle is able to show the best prediction performance with large uncertainties from measurements. It also shows that the Frontics measurements have less prediction error in the investigated data analytics methods which is consistent with the causal-based OLS modeling of Chapter 5. The models developed in this chapter are included as R-language source code in Appendix D.

Part IV: Project Conclusions and Recommendations

Chapter 7: Conclusions

1. The project successfully measured and categorized the mechanical, chemical, and physical differences across a broad range of pipe sample walls through methodical full-wall and bulk testing as compared to surface-collected physical, mechanical, and chemical NDE testing.

2. Differences in yield strength between the surface derived values and bulk, full-wall were analyzed via a sensitivity study and explained through the changes in surface yield strength due to primary steel production processes, seam type and pipe forming process, and steel chemistry. All these factors/variables can be determined from surface testing.

3. Based on the extensive testing and analysis an ambitious set of modeling tasks were completed include causal-based OLS and data analytics-based modeling. Successful models for yield strength and ultimate tensile strength were developed to predict bulk properties from purely surface obtained information for yield strength and tensile strength.

4. The optimum causal models combined with the Frontics AIS technology surface data achieved a 95% confidence in yield strength predictions by overlapping the full-wall yield strength from lab tests across the entire pipe sample DOE. The optimal models for the MMT HSD exhibited bias in the yield strength for certain pipe configurations related to non-isotropic properties across the pipe wall. The models reduced the bias of the MMT results, but could not completely adjust for it particularly at higher yield strengths.

5. Both NDE technologies optimal models, coupled with the surface data, achieved 95% confidence in ultimate tensile strength predictions by overlapping the full-wall ultimate tensile strength from lab testing across the entire pipe sample DOE.

6. Chemistry values were correlated successfully for 15 key elements, and the only significant variation of chemical properties across the pipe wall was noted from surface to bulk values for carbon and sulfur. A set of chemical element kernel distributions were developed to estimate the magnitude of these differences across the pipe wall based on steel type and other factors.

7. A supplemental body of detailed toughness testing was completed on over 40% of the pipe samples in the DOE and collected and analyzed as a supplemental task of the project. This work will provide invaluable to future NDE technology development aimed at estimating pipe toughness through surface nondestructive testing.

Chapter 8: Recommendations

1. The relations, models, and distributions developed under this project can be used to predict full-wall yield and ultimate strengths from surface-based NDE technology such as Frontics AIS and MMT HSD for *seamless* pipes.

2. The Frontics AIS technology also was successful at a 95% confidence for predicting *yield* strength across the entire pipe sample DOE on *non-seamless* pipes, i.e., pipes with long seam welds like ERW, SAW, etc.

3. Further research is warranted/advised into the promising MMT HSD technology to help reduce bias in the full-wall yield strength predictions based on surface readings for non-seamless pipe that have variation of yield strength across the pipe thickness cross section. The current models provided by the manufacturer and developed under this project could not remove the bias in these measurements, particularly for higher yield strengths.

4. The relations, models, and distributions developed under this project can be used to predict full-wall *ultimate tensile* strengths from surface-based NDE technology such as Frontics AIS and MMT HSD. Using the causal-based models developed, both technologies achieved a 95% confidence for predicting tensile strength across the entire pipe sample DOE, seamless or non-seamless.

Part V: Appendices, References, and Attachments

Appendices

- **Appendix A**: External File - Project Master Data Table for 70 Pipeline Samples in Excel (778KB). APPENDIX_A_MASTER_DATA_TABLE_V01.xlsx

- **Appendix B**: External File - Charpy Toughness and Related Data 30 Pipeline Samples in Excel (195 KB). APPENDIX_B_CHARPY_DATA_TABLE_V01.xlsx

- **Appendix C**: Contained in this report - Causal-Based Regression Output Tables.

- **Appendix D**: External File - R-Code for Regressions in Chapter 6 in a ZIP file (53 KB). APPENDIX_D_CH6_R-CODE.zip

References

- Final report citations are expanded in this section. Contained in this report.

Attachments

- **Attachment #1** - Frontics: Measurement of Yield strength, Tensile strength and Fracture toughness of API 5L pipe using Instrumented Indentation Testing (328 pages pdf). FARE-190603-1 Part I.pdf

- **Attachment #2** - Frontics: Measurement of Yield strength, Tensile strength and Fracture toughness of API 5L pipe using Instrumented Indentation Testing - Part II (298 pages). FARE-190603-1 Part II.pdf

- **Attachment #3** - Frontics: Measurement of Yield strength, Tensile strength and Fracture toughness of API 5L pipe using Instrumented Indentation Testing - Additional Sample (8 pages). FARE-190723-1 Part I Appendix 2.pdf

- **Attachment #4** - Frontics: Measurement of Yield strength, Tensile strength and Fracture toughness of API 5L pipe samples using Instrumented Indentation Testing - Coupon testing (108 pages). FARE-201122A.pdf

- **Attachment #5** - MMT: Procedure Bundle (47 pages). 2020MMTProcedureBundle_2021.03.01.pdf

- **Attachment #6** - MMT: Final report for nondestructive HSD Testing for 70 cutout samples (267 pages). 2021.02.10-MMTFinalNDEReportForGTI19006.pdf

Chapter 2: Technical Approach and Data Organization

2.1 Overview

Focus

This project's focus is to test and model state-of-the-art technology from Massachusetts Materials Technologies (MMT), Frontics America (Frontics), SciApps, Arizona State University (ASU), Element Resources, and the Gas Technology Institute (GTI).

The test results from thousands of lab and field material tests done on actual pipeline samples have been used to develop models that account for pipe material thermo-mechanical process variations and through-wall variability of material, mechanical, and chemical properties.

A simplified interrelation diagram between properties is shown in Figure 1 below.

Figure 1. A Simplified Interrelation Diagram.

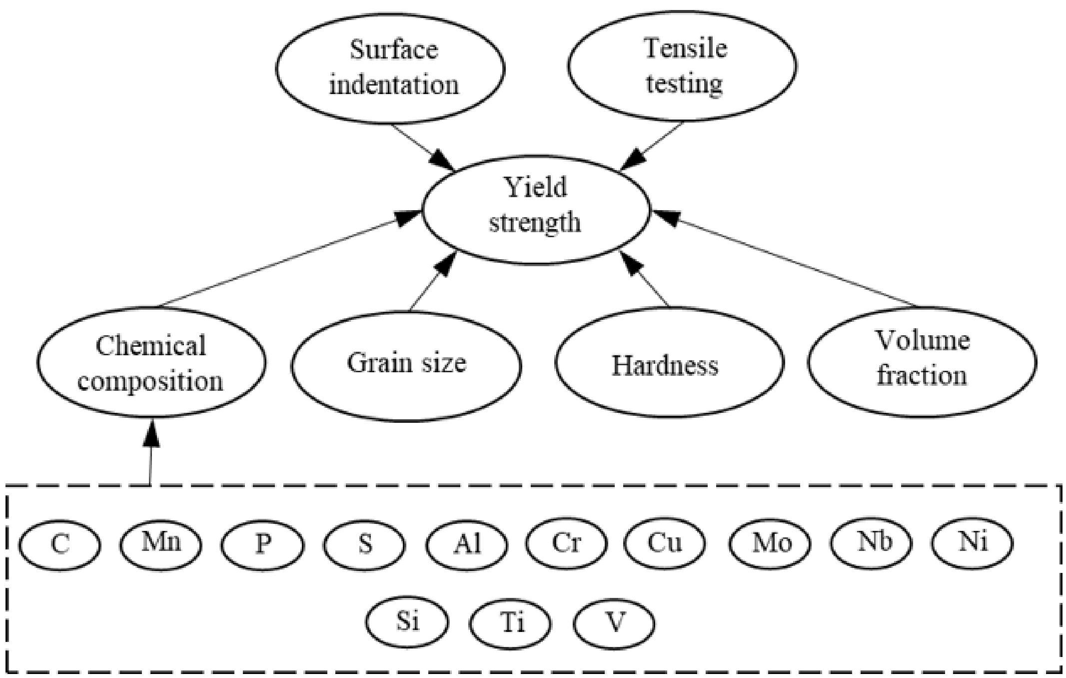

These correlations will allow surface-obtainable information from indentation and other surface testing techniques, surface chemistry analysis, and surface optical microscopy to be used for material property validation for pipelines.

Project Structure and Implementation Plan

The project team structure is shown in Figure 2.

Figure 2. Project Team Structure.

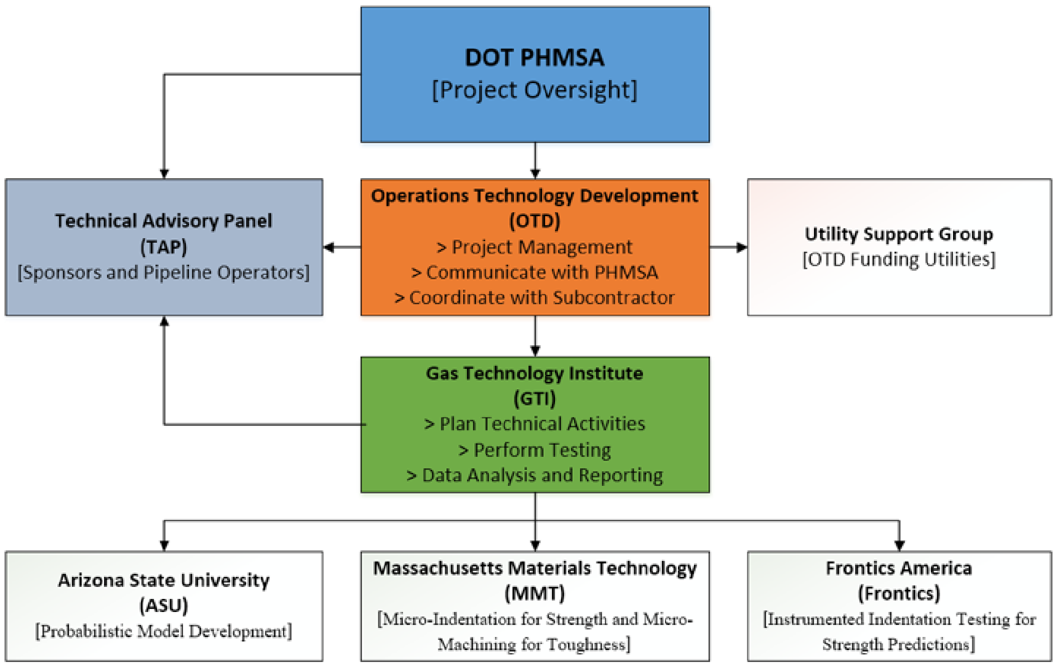

2.2 Approach by Task

Task 1: Form Technical Advisory Panel and Scope Confirmation

- The project was kicked off via a teleconference with DOT PHMSA and OTD to confirm scope, schedule, and communication plans
- A Technical Advisory Panel (TAP) was formed with the sponsors, the technical team, and eight pipeline operators. The TAP was used to solicit input on scope of work details, operational considerations, and deliverable design.

Task 2: Develop Project Database and Pipeline Sample Library

- Previously tested and available material properties of pipeline steels were organized and compiled, including: surface and bulk chemistry; surface and bulk mechanical properties (yield and tensile strength, toughness, hardness); and surface and bulk metallurgical grain size.
- Pipeline samples were selected from the extensive GTI pipeline library and supplemented with testing samples received from the TAP and other utility and pipeline operators.
- A training set of twenty pipelines was made available to GTI, Element Resources, and ASU to allow initial model testing and prove out prior to the seventy additional samples that needed comprehensive testing done.

Task 3: Develop Testing Matrix and Execute Testing

A testing matrix was developed using the MMT, Frontics, ICP, and field microscopy testing technology and methods, coupled with the database design and physical samples from Task 2. These tests were executed and correlated with full-wall and bulk tests of the same pipeline specimens.

A high level summary of the extensive tests completed is listed directly below. The test data/matrix is contained in **Appendix A** and **Appendix B** which are external Excel spreadsheet files with flat-table column oriented databases. The test data represents approximately 15,000 cells or data points from the tests noted below. Several photos of testing equipment are presented in Figure 3 as well.

Surface, field-based testing includes technology from MMT, Frontics, and Sci-Apps:

- **Surface Yield and Tensile Strength** remote and across welds
  - **MMT** Hardness, Strength, and Ductility (**HSD**)
  - **Frontics** Advanced Indentation System (**AIS**)
- **Surface Toughness**
  - **Frontics AIS K_{IC} fracture toughness** estimates (supplemental task)
- **Surface Chemistry**
  - SciApps field-ready, surface-based Handheld Laser Induced Breakdown Spectroscopy (**HH LIBS**) Optical Emission Spectroscopy (**OES**)
  - Surface removed **filings**
- **Surface Microstructure and Grain Size**
  - Field-based **replicates**
  - In situ **microscopy**

Baseline (referee) lab-based testing includes

- **Lab-based Strength** via full wall tensile tests per **ASTM A370** Fig A2.3 specimen 5 with 1"-gauge length longitudinal specimens and an average of 3 specimens
- **Lab-based Chemistry**
  - Lab Glow Discharge Spectroscopy (**GDS)** chemistry at 4 different depths. (0.005", 0.020", 3/4 thickness and mid thickness). Includes C, S, and P by GDS. 15 elements are included for baseline chemistry
  - Bulk Inductively Coupled Plasma (**ICP**) **OES**
  - Bulk **LECO ASTM E1019** for C, S, and N
- **Lab-based Grain Size** near surface, ¼ pt, and center for both longitudinal and transverse sections, average of 6 readings; then average of near surface grain sizes (~0.005" deep) longitudinal and transverse specimens
- **Lab-based Hardness** via OD **Rockwell B Hardness** after ~ 0.005" surface grind; ID Rockwell B hardness after ~ 0.005" surface grind
- **Lab-based Toughness** via full **Charpy** S-curve toughness curve testing and development

Figure 3. Examples of Several Testing Methods.

(a) Frontics AIS, (b) MMT HSD, (c) SciApps HH LIBS-OES, (d) Tensile Bars, (e) Grains Size Computer, (f) Lab ICP-OES Chemistry, (g) Hardness Tester, (h) Charpy Small Hammer, (i) OES Units.

Task 4: Data Analysis and Model Development and Optimization

Element Resources, GTI, and ASU provided advanced statistical analysis and surface-to-bulk causal-based regression and associated model development. This included developing chemical-physical-mechanical models for predicting the bulk mechanical properties (yield and tensile strength) of the steels from surface located measurements.

The causal-based models incorporated factor interactions and variation in testing results and provided solutions. Also included was the creation of probability distribution functions of the surface-to-bulk differences (mechanical and chemical data) and performing a sensitivity analysis by pipeline steel type, pipeline manufacture method, and other attributes.

The modeling task was subdivided into eight broad categories as shown in Table 1 below. The first three, led by Element Resources are presented in detail in Chapter 5, and the remaining five led by ASU, are presented in detail in Chapter 6.

Table 1. Modeling Categories.

Modeling Categories			
Team Lead	**Category**	**Description**	**Model Abbreviation**
Element Resources *Chapter 5*	**1**	Descriptive Statistics of All Data	**DS**
	2	Sensitivity Study of Independent on Dependent Variables	**SS**
	3	Causal-Based - Ordinary Least Squares Models	**CB-OLS**
Arizona State University *Chapter 6*	**4**	Ordinary Least Squares Models	**OLS**
	5	Bayesian Update Model Averaging	**BMA**
	6	Bayesian Network Model s	**BNM**
	7	Gaussian Process Models	**GPM**
	8	Manifold-Based Gaussian Process Models	**MB-GPM**

Task 5: Final Report and Implementation Guide

- Development of this report and all supporting materials.
- This report includes the final databases, completed causal models with coefficients by technology type for yield and tensile strength, and advanced numerical prediction models and the associated "R" programming language modeling source code (R is an open source, free application to the public).

Task 6: Project Management and Communications

- This task included regular communication and monthly updates to PHMSA and OTD, quarterly reporting activities, coordination with the TAP, subcontractors, and outside organizations and users, annual PHMSA Peer Reviews, and a final virtual presentation of the project results via a web-based meeting that PHMSA will organize and announce to the public.
- A project presentation to at least one public pipeline conference/workshop/forum or published periodical/magazine.
- A peer review paper from this research was accepted and published, "Probabilistic bulk property estimation using multimodality surface non-destructive measurements for vintage pipes", on June 22, 2020, in the Journal of Structural Safety (Elsevier)[1]. Additional papers are submitted and planned.

2.3 Pipe Sample Library Summary and Raw Testing Data

A set of seventy pipeline samples that were in service from the natural gas industry were selected for the project testing and modeling. A great deal of care and effort was put forth to select a reasonable number that provided the adequate breadth of variety as typically encountered by the industry in the field.

Table 2 to Table 6 and Figure 4 to Figure 8 show the excellent range of pipeline samples by installation year, diameter, reported grade, steel type, long seam type, wall thickness, API grade, and chemistry (UNS) grade. The points in the plots are jittered since they would otherwise overlap.

The pipeline sample set proved to be very robust and provided an excellent range of seam types, HSLA and non-HSLA steels, ingot and slabs with and without significant carbon segregation, grain size variations, etc.

The modeling section will show that the relationship between surface yield strength and bulk yield strength are sensitive to many of these factors and their variation from the outer surface of the pipe toward the centerline.

Table 2. Pipeline Samples by Installation Year.

Install Year	Freq.	Percent	Cum.
1930	1	1.43	1.43
1947	5	7.14	8.57
1950	2	2.86	11.43
1952	1	1.43	12.86
1953	1	1.43	14.29
1954	3	4.29	18.57
1956	1	1.43	20.00
1958	2	2.86	22.86
1959	1	1.43	24.29
1960	6	8.57	32.86
1961	1	1.43	34.29
1963	3	4.29	38.57
1965	4	5.71	44.29
1966	3	4.29	48.57
1967	2	2.86	51.43
1968	6	8.57	60.00
1970	1	1.43	61.43
1972	3	4.29	65.71
1973	1	1.43	67.14
1981	1	1.43	68.57
1983	2	2.86	71.43
1992	1	1.43	72.86
1995	1	1.43	74.29
2004	1	1.43	75.71
Unknown	17	24.29	100.00
Total	**70**	**100.00**	

Table 3. Pipeline Samples by Diameter.

Pipe Diam (in)	Freq.	Percent	Cum.
4	5	7.14	7.14
6	9	12.86	20.00
8	16	22.86	42.86
10	12	17.14	60.00
12	10	14.29	74.29
16	5	7.14	81.43
18	3	4.29	85.71
20	4	5.71	91.43
24	3	4.29	95.71
26	2	2.86	98.57
30	1	1.43	100.00
Total	**70**	**100.00**	

Table 4. Two Way Table of Pipeline Samples by Installation Year and Diameter.

	Pipe Diameter											
	4	**6**	**8**	**10**	**12**	**16**	**18**	**20**	**24**	**26**	**30**	**Total**
Installation Year												
1930				1								1
1947			5									5
1950						2						2
1952											1	1
1953						1						1
1954			2		1							3
1956					1							1
1958			1							1		2
1959	1											1
1960	3	2	1									6
1961					1							1
1963				2	1							3
1965		2	1		1							4
1966	1		2									3
1967			1	1								2
1968			3				3					6
1970						1						1
1972						1		2				3
1973								1				1
1981		1										1
1983				1	1							2
1992		1										1
1995				1								1
2004					1							1
Unknown		3		6	3			1	3	1		17
Total	**5**	**9**	**16**	**12**	**10**	**5**	**3**	**4**	**3**	**2**	**1**	**70**

Table 5. Two Way Table of Pipeline Samples by Installation Year and Reported Grade.

	Pipe Grade Reported								
Installation Year	**GradeA**	**GradeB**	**NotReported**	**X30**	**X42**	**X42-X52**	**X46**	**X52**	**Total**
1930	1								1
1947		5							5
1950			2						2
1952								1	1
1953		1							1
1954			3						3
1956			1						1
1958			2						2
1959			1						1
1960			6						6
1961			1						1
1963			2				1		3
1965			3		1				4
1966			3						3
1967		1	1						2
1968			3		1			2	6
1970			1						1
1972			1		2				3
1973					1				1
1981			1						1
1983			2						2
1992			1						1
1995			1						1
2004					1				1
Unknown			14	1		2			17
Total	**1**	**7**	**49**	**1**	**6**	**2**	**1**	**3**	**70**

It is important to note that after lab testing, the full-wall yield strengths ranged from 30 ksi to over 73 ksi in round numbers. This includes the 49 unknown grades in the table above for the 70 samples. This is an excellent range and distribution of yield strengths that represents pipe strengths in service of most interest to this project and the associated surface to bulk property relationships. This distribution can be seen and ordered as desired in the Appendix A, Master Data Table.

Table 6. Two Way Table of Pipeline Samples by Installation Year and Steel Type.

	Steel Type				
	KilledAl	KilledSi	RimmedCapped	SemiKilled	Total
Installation Year					
1930			1		1
1947		5			5
1950		2			2
1952				1	1
1953				1	1
1954	1		2		3
1956	1				1
1958			1	1	2
1959			1		1
1960	1		1	4	6
1961			1		1
1963	2	1			3
1965		2		2	4
1966	1		1	1	3
1967		1	1		2
1968		2	3	1	6
1970			1		1
1972	1			2	3
1973			1		1
1981	1				1
1983	1		1		2
1992		1			1
1995		1			1
2004		1			1
Unknown	1	8	5	3	17
Total	**10**	**24**	**20**	**16**	**70**

Figure 4. Pipeline Sample by Steel and Long Seam Type.

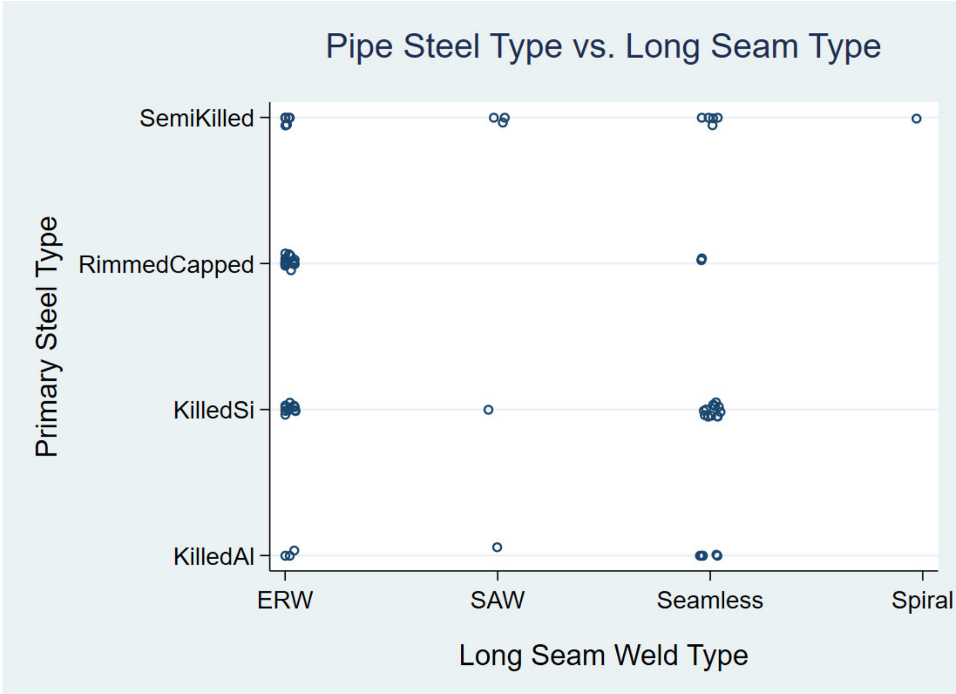

Figure 5. Pipeline Sample by Installation Year and Pipe Grade.

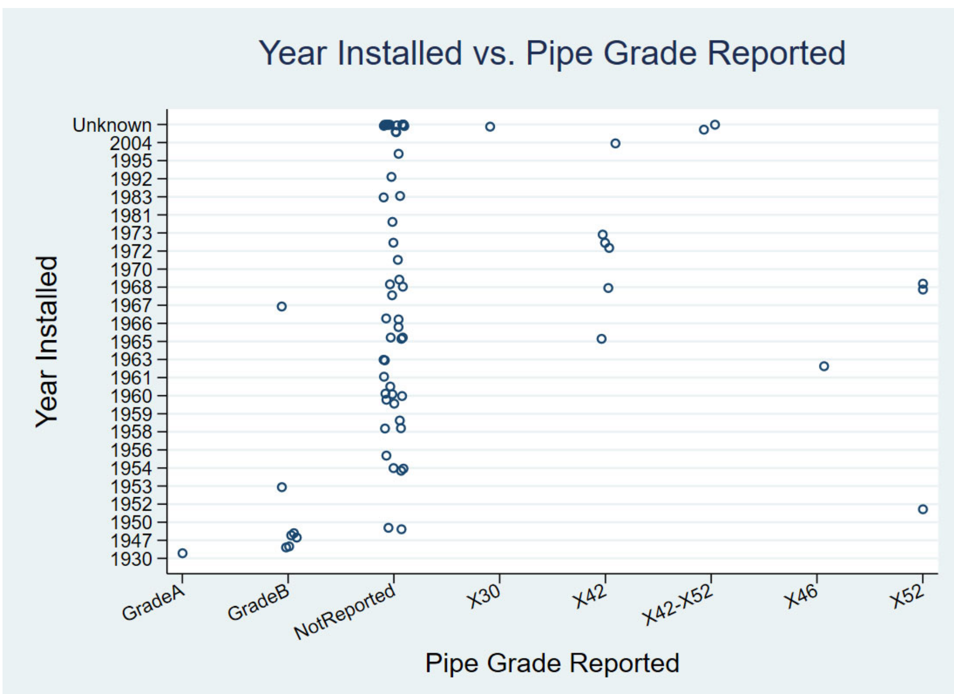

Figure 6. Pipeline Sample by Diameter and Wall Thickness.

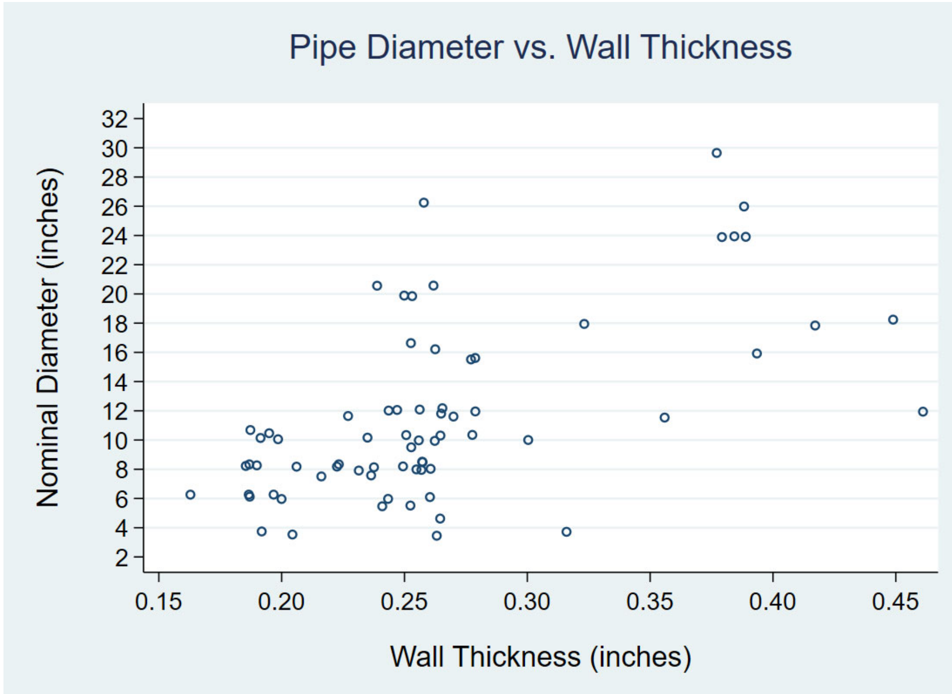

Figure 7. Pipeline Sample by Chemistry Grade and API Grade Reported.

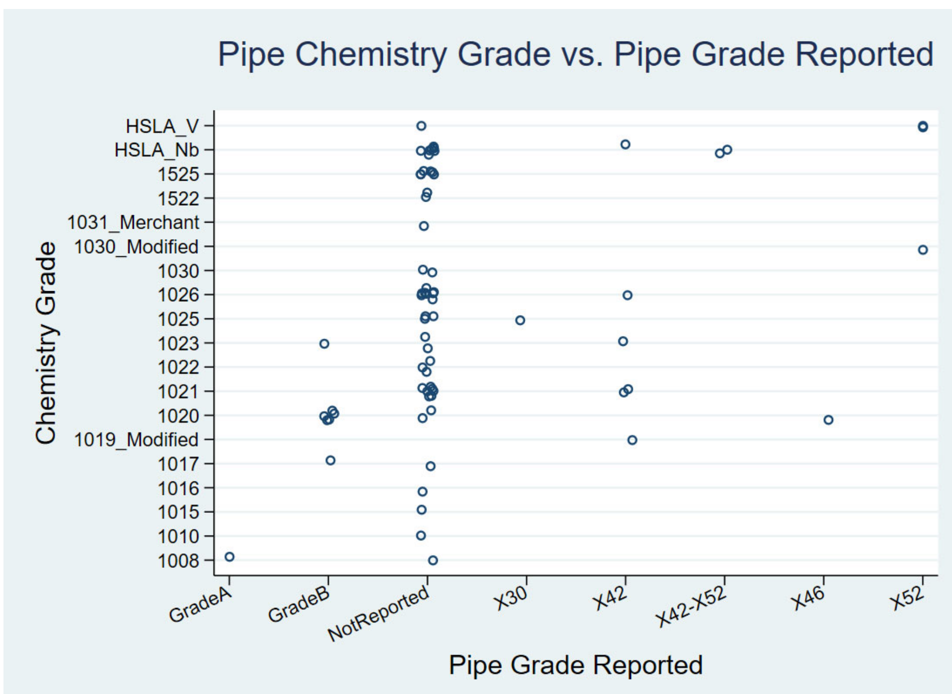

Figure 8. Pipeline Sample by Steel Type and ASTM Grain Size.

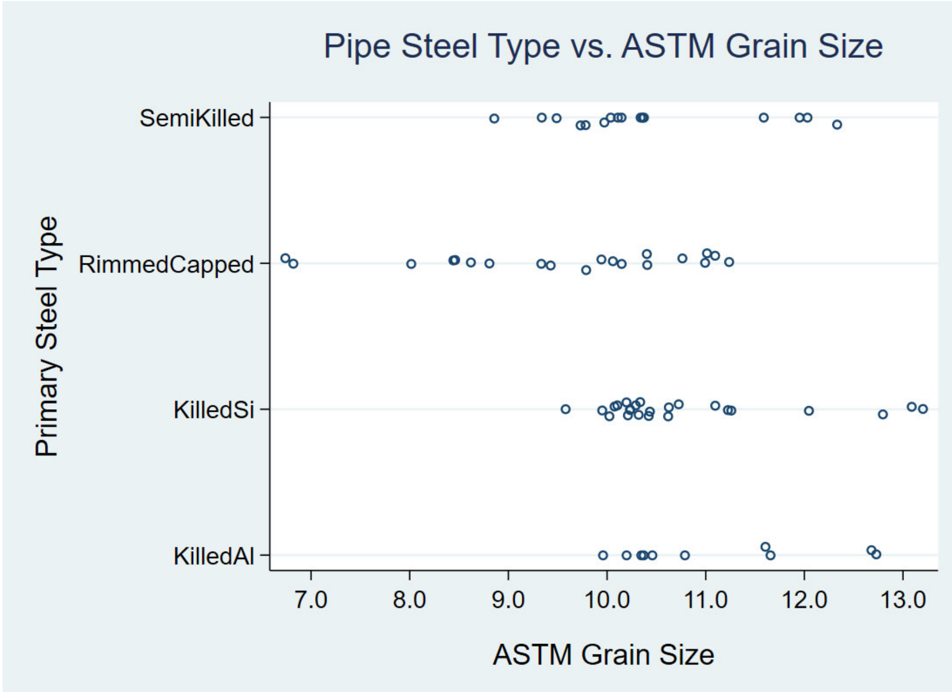

2.4 Data Organization and Test Methods Used

The master column database for the project is provided as a separate Excel Spreadsheet due to its size, see **Appendix A** for the main database and the supplemental **Appendix B** for the Charpy Toughness data and metadata used to create the plots in this report. Table 7 below describe the database columns of data. Table 8 provides a glossary of abbreviations and initialisms used in the database.

Database Columns, Titles, and Descriptions with Test Method

Table 7. Project Master Database Structure, Fields, and Testing Methods.

Column No.	Short Title	Description
1A	PIPE_NUMBER	Pipe number given by GTI for sample identification
2A	DIAMETER_NOMINAL	Nominal diameter of the pipe in inches
3A	WALL_THICKNESS_AS_RECEIVED	States the wall thickness of the pipe in inches without any treatment to the sample, i.e.: including corrosion products, adhesions
3B	WALL_THICKNESS_LAB_SAMPLE	States the wall thickness of the pipe in inches after preparation of the sample for testing
4A	INSTALLATION_YEAR	Specifies the installation date as provided by the utilities
5A	GRADE_REPORTED	Shows the steel grade as known by the utilities
6A	STEEL_TYPE_ESTIMATE	Specifies the GTI estimate of steel (rimmed, capped, killed Si, killed, Al, semi-killed)
7A	GRADE_CHEMISTRY_GROUP	States the steel grade as per SAE-ASTM
8A	WELD_TYPE_GTI	Determines whether the pipe has a weld or not and what type of weld it is according to GTI inspections
8B	WELD_TYPE_MMT	Determines the type of ERW weld, either High Frequency (HF), High Frequency Normalized (HFN), or Low Frequency (LF), identified by MMT on 25 pipes of the 70 set
9A	YS_LAB_FULL_WALL	Yield Strength mini: Shows the yield strength in ksi as evaluated from a mini 1” gauge length longitudinal sample
9B	YS_FULL_WALL_HALF_PERCENT_EUL	Yield Strength mini: Shows the yield strength at 0.5% Elongation Under Load in ksi as evaluated from a mini 1” gauge length longitudinal sample
9C	UTS_LAB_FULL_WALL	Tensile Strength mini: Shows the tensile strength in ksi as evaluated from a mini 1” gauge length longitudinal sample
10A	YS_FRONTICS_BASE	Bulk Yield Strength as calculated by Frontics from their non-destructive Instrumented Indentation Testing (IIT) using AIS2100
10B	UTS_FRONTICS_BASE	Bulk Ultimate Tensile Strength as calculated by Frontics from their non-destructive IIT using AIS2100
11A	YS_MMT_SURFACE	Surface measurement of yield strength as 0.5% Elongation Under Load (EUL) obtained from MMT HSD Tester
11B	YS_MMT_SURFACE_SDV	Standard deviation for the surface measurement of yield strength as 0.5% EUL obtained from MMT HSD Tester

Column No.	Short Title	Description
11C	UTS_MMT_SURFACE	Surface measurement of Ultimate Tensile Strength (UTS) obtained from MMT HDS Tester
11D	UTS_MMT_SURFACE_SDV	Standard deviation for the surface measurement of UTS obtained from MMT HSD Tester
12A	YS_MMT_BRM	Predicted yield strength as 0.5% EUL using a Bayesian Linear Regression model
12B	YS_MMT_BRM_SDV	Standard deviation for the predicted yield strength as 0.5% EUL using a Bayesian Linear Regression model
12C	UTS_MMT_BRM	Predicted UTS using a Bayesian Linear Regression model
12D	UTS_MMT_BRM_SDV	Standard deviation for the predicted UTS using a Bayesian Linear Regression model
13A	YS_MMT_LRM	Predicted yield strength as 0.5% EUL using a Multiple Linear Regression model
13B	YS_MMT_LRM_SDV	Standard deviation for the predicted yield strength as 0.5% EUL using a Multiple Linear Regression model
13C	UTS_MMT_LRM	Predicted UTS using a Multiple Linear Regression model
13D	UTS_MMT_LRM_SDV	Standard deviation for the predicted UTS using a Multiple Linear Regression model
14A	YS_MMT_ANN	Predicted yield strength as 0.5% EUL using an Artificial Neural Network model
14B	YS_MMT_ANN_SDV	Standard deviation for the predicted yield strength as 0.5% EUL using an Artificial Neural Network model
14C	UTS_MMT_ANN	Predicted UTS using an Artificial Neural Network model
14D	UTS_MMT_ANN_SDV	Standard deviation for the predicted UTS using an Artificial Neural Network model
15A	C_BULK	Bulk chemical composition by weight percentage of carbon as per ASTM E1019 by Combustion
15B, 15C	MN_BULK, P_BULK	Bulk chemical composition using ICP (Inductively Coupled Plasma). Lab weight percentage of elements, Manganese and Phosphorus
15D	S_BULK	Bulk chemical composition by weight percentage of sulfur as per ASTM E1019 by Combustion
15E - 15N	[Element]_BULK	Bulk chemical composition using ICP (Inductively Coupled Plasma). Lab weight percentage of elements, Al, Cr, Cu, Mo, Nb, Ni, Si, Ti, V, and B
15O	N_BULK	Bulk chemical composition by weight percentage of nitrogen as per ASTM E1019 and E1409 using Fusion analysis (LECO) technique
15P	PEARLITE_PERC_BULK	Percentage pearlite estimated by the lever rule using the bulk carbon content as per column 15A
16A - 16O	[Element]_5MIL	Chemical composition by OES (optical emission spectroscopy) using a laboratory spectrometer, SPECTROMAXX, after grinding 0.005” from surface for C, Mn, P, S, Al, Cr, Cu, Mo, Nb, Ni, Si, Ti, V, B, and N in wt.%
16P	PEARLITE_PERC_5M	Percentage pearlite estimated by the lever rule using the carbon content at 0.005” from surface as per column 16A
17A - 17O	[Element]_20MIL	Chemical composition by OES (optical emission spectroscopy) using a laboratory spectrometer, SPECTROMAXX, at a depth of 0.020” from surface for C, Mn, P, S, Al, Cr, Cu, Mo, Nb, Ni, Si, Ti, V, B, and N in wt.%

Column No.	Short Title	Description
18A - 18O	[Element]_QTRTHK	Chemical composition by OES (optical emission spectroscopy) using a laboratory spectrometer, SPECTROMAXX, at a depth of one quarter of the thickness from O.D. surface for C, Mn, P, S, Al, Cr, Cu, Mo, Nb, Ni, Si, Ti, V, B, and N in wt.%
19A - 19O	[Element]_MIDWALL	Chemical composition by OES (optical emission spectroscopy) using a laboratory spectrometer, SPECTROMAXX, at midwall for C, Mn, P, S, Al, Cr, Cu, Mo, Nb, Ni, Si, Ti, V, B, and N in wt.%
20A - 20O	[Element]_AVEGDS	Average of each element at the: 0.005", 0.020", and ¼ thickness, and midwall from the surface in wt.%
20P	PEARLITE_PERC_AVE_GDS	Percentage pearlite estimated by the lever rule using the average carbon content as per column 20A
21A - 21O	[Element]_MMT_GRNDGS	Chemical composition provided by MMT and obtained from pipe grindings for C, Mn, P, S, Al, Cr, Cu, Mo, Nb, Ni, Si, Ti, V, and B in wt.%. C and S measured by combustion analysis and rest of elements measured by ICP-OES
22A - 22O	[Element]_LIBS	Surface chemical compositions obtained from SciAps Z-200 series hand-held device through Laser Induced Breakdown Spectroscopy (LIBS) for C, Mn, Al, Cr, Cu, Mo, Nb, Ni, Si, Ti, V, B, and N in wt.%
23A - 23O	[Element]_LIBS_ERR	Instrument error for the surface chemical compositions obtained from SciAps Z-200 series hand-held device LIBS for C, Mn, Al, Cr, Cu, Mo, Nb, Ni, Si, Ti, V, B, and N in wt.%
24A - 24O	[Element]_XRF	Surface chemical composition obtained from SciAps X-series hand-del device through X-Ray Fluorescence (XRF) spectroscopy for C, Mn, P, S, Al, Cr, Cu, Mo, Nb, Ni, Si, Ti, V, B, and N in wt.%
25A - 25O	[Element]_XRF_ERR	Instrument error for the surface chemical composition obtained from SciAps X-series hand-del device through X-Ray Fluorescence (XRF) spectroscopy for C, Mn, P, S, Al, Cr, Cu, Mo, Nb, Ni, Si, Ti, V, B, and N in wt.%
26A	HRBW_OD	Rockwell hardness at the outer diameter (OD) of the pipe as per ASTM E18
26B	HRBW_ID	Rockwell hardness at the inner diameter (ID) of the pipe as per ASTM E18
33A	GS_COMPOSITE	Grain size represented as an ASTM number measured as an average as per ASTM E112
33D	GS_SURFACE	Grain size represented as an ASTM number measured at the surface as per ASTM E112; typically, at about 0.005" from the surface.

Database Glossary of Acronyms and Abbreviations

Table 8. Glossary of Database Terms.

Acronym/Abbreviation	Description
AIS	Advanced Indentation System
ANN	Artificial Neural Network
ASTM	American Society for Testing and Materials
AVE	Average
BRM	Bayesian Regression Model
ERR	Error
ERW	Electric Resistance Weld
EUL	Elongation Under Load
GDS	Glow Discharge Spectroscopy
GS	Grain Size (ASTM Number)
GTI	Gas Technology Institute
HF	High Frequency
HFN	High Frequency Normalized
HSD	Hardness, Strength, and Ductility
HSLA	High Strength Low Alloy Steel
ICP	Inductively Coupled Plasma
ID	Pipe Inner Diameter
IIT	Instrumented Indentation Testing
LECO	Laboratory Equipment Corporation
LF	Low Frequency
LRM	Linear Regression Model
MIDWALL	Midwall of Pipe
MIL	One thousandth of an inch (0.001 inches)
MMT	Massachusetts Materials Technology
NAN	Not a Number (intentionally blank)
NDE	Non-Destructive Evaluation
OD	Pipe Outer Diameter
OES	Optical Emission Spectroscopy
PERC	Percent
QTRTHK	Quarter Thickness of Pipewall
SAE	Society of Automotive Engineers
SAW	Submerged Arc Welding
SDV	Standard Deviation
UTS	Ultimate Tensile Strength
YS	Yield Strength
LIBS	Laser Induced Breakdown Spectroscopy
XRF	X-Ray Fluorescence

PART II: SURFACE / BULK TESTING COMPARISONS

Part II contains:

- Chapter 3: Material Yield and Tensile Strength, Chemistry, and Grainsize
- Chapter 4: Material Toughness (Supplemental Section)

Chapter 3: Material Yield and Tensile Strength, Chemistry, and Grain Size

3.1 Overview

The data used for this chapter is listed in the **Appendix A** and **Appendix B** sections of this report in detail and *table* form.

This chapter uses plots to describe the trends and comparisons. Methodologies are listed in Chapter 2 and the associated and very detailed Attachments to this report. Readers are directed to these sections for more information related to methods and procedure.

The chapter is broken down into four main sections, one each focused on: yield strength, ultimate tensile strength, chemistry, and grain size. The latter two are very important variables to determine steel type and associated with surface-based NDE to improve the bulk predictions of strength through modeling.

Chapter 5 is focused on modeling of the surface obtainable data to provide unknown bulk predictions. This chapter focuses on the bulk compared to the NDE data. Therefore, this chapter is the basis of Chapter 5 and provides the input data and variables for the models. The same is true for the data analytics modeling used in Chapter 6.

For this chapter and the remainder of the report, when box plots are used the inner quartile region (IQR) represents 50% of the data points and the inner-box horizontal line is the median value. The whiskers of the boxes extend up to 1.5x the length of the IQR and outlier values beyond that are plotted as points and jittered (laterally offset) only if necessary.

3.2 Yield and Tensile Strength

Matrix plots are used to plot variables against each other in a systematic way. They are good at displaying trends between variables, both independent and/or dependent variables.

Figure 9 and Figure 10 contain a matrix plot of the seventy pipeline samples for yield strength and ultimate tensile strength respectively. They include the lab tests and the two NDE techniques: Frontics AIS and MMT HSD, but the as measured surface values vs. models of the same which will be shown in Chapter 5.

Matrix Plots of Bulk vs. Surface NDE Strength Comparisons

Figure 9. Matrix Plot of Yield Strength: Lab vs. Surface.

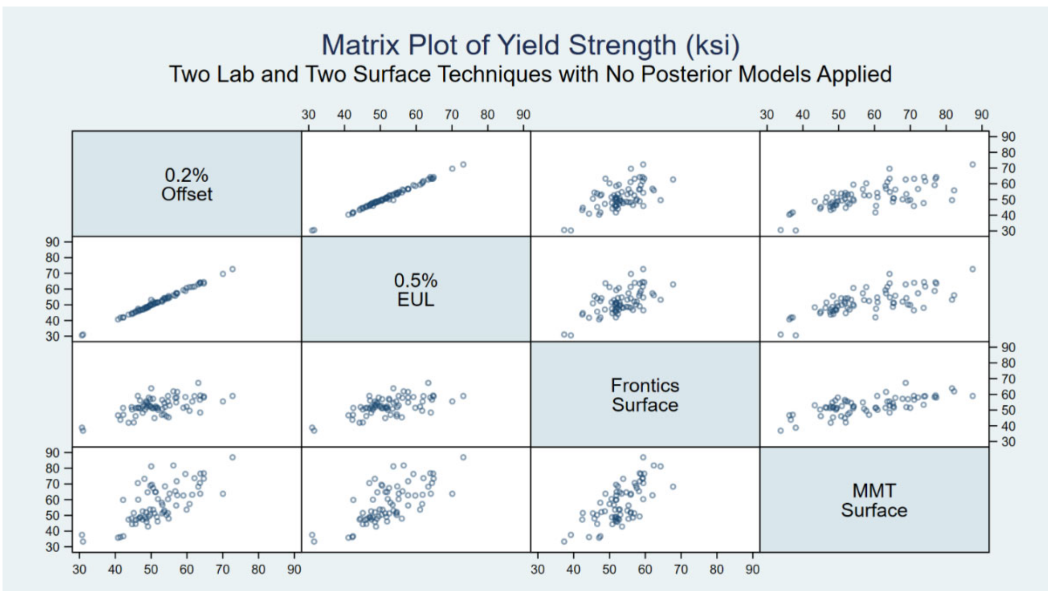

Figure 10. Matrix Plot of Tensile Strength: Lab vs. Surface.

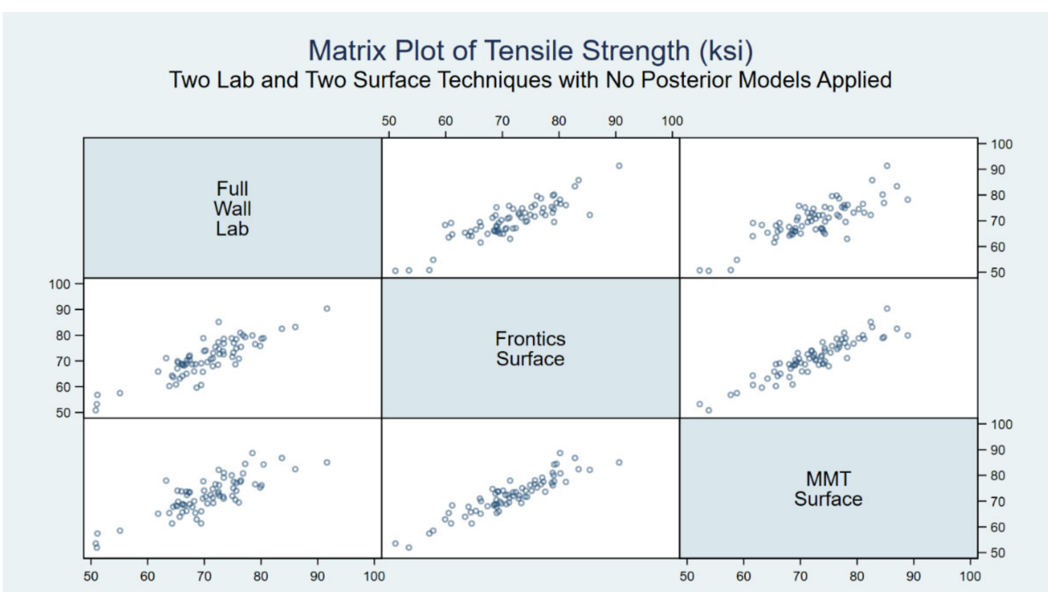

The matrix plots reveal that there is excellent agreement between the two lab yield strength techniques and measure, i.e., 0.2% offset and 0.5% elongation under load. These tests are done in an accredited lab and are intra-lab, i.e., from the same lab. The MMT results appear to have a larger spread vs. the lab testing than the Frontics results do for yield testing, regardless of the lab method selected.

The tensile results exhibit a generally tighter grouping of NDE results when compared to the lab results and there is no substantive difference noticeable on the matrix plots between the two NDE techniques themselves.

Box Plots of Bulk vs. Surface NDE Strength Comparisons

The matrix plots are more qualitative; therefore, it is useful to look at the same testing results for the seventy pipeline steels through box plots of strength.

Figure 11 is the box plot of yield strengths for the seventy pipeline samples by lab or NDE technique. The IQRs for the lab techniques, and the medians, are very close to being the same as is expected from the matrix plots. The Frontics IQR is bound within the lab techniques and the median is very close. The MMT IQR is shifted to the high side with the median value near the top of the lab IQR and the top of the MMT IQR is substantially higher than the lab or Frontics IQR. There is also a much higher top whisker for the MMT data on the same seventy pipeline samples.

These trends will be explored in later Chapters in this report, as well as later in this Chapter, where an explanation is developed based on other variable relationships.

Figure 11. Box Plot of Yield Strength by Technique.

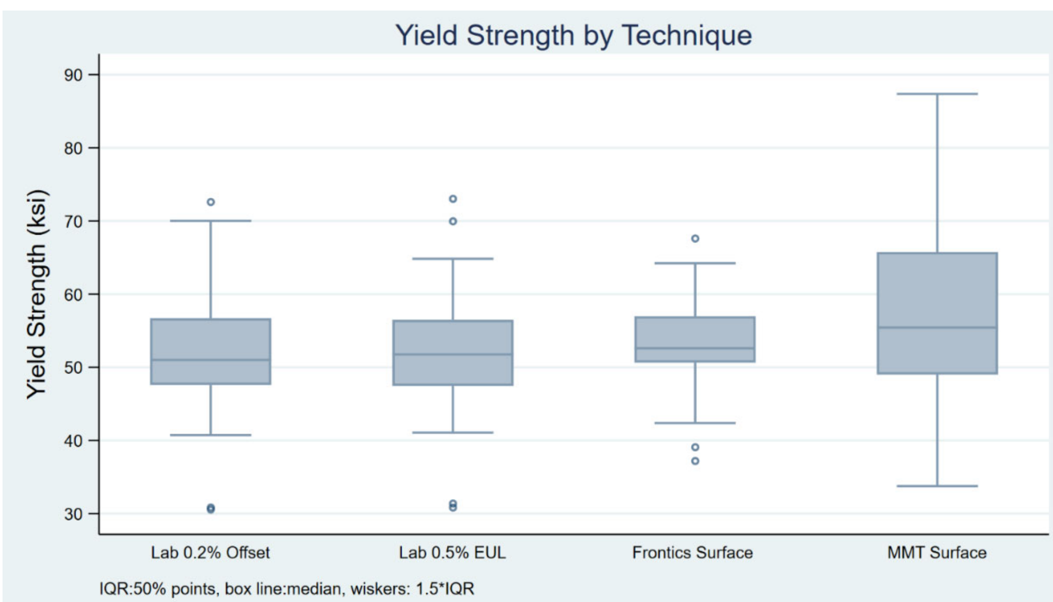

Figure 12 is a box plot of the ultimate tensile strength (referred to as tensile strength for the remainder of much of the report) for the seventy pipeline samples by lab or NDE technique. The IQRs for the lab technique, and the medians, are very close to the same for the NDE techniques. The same can be said for the overall spread of the data.

Figure 12. Box Plot of Tensile Strength by Technique.

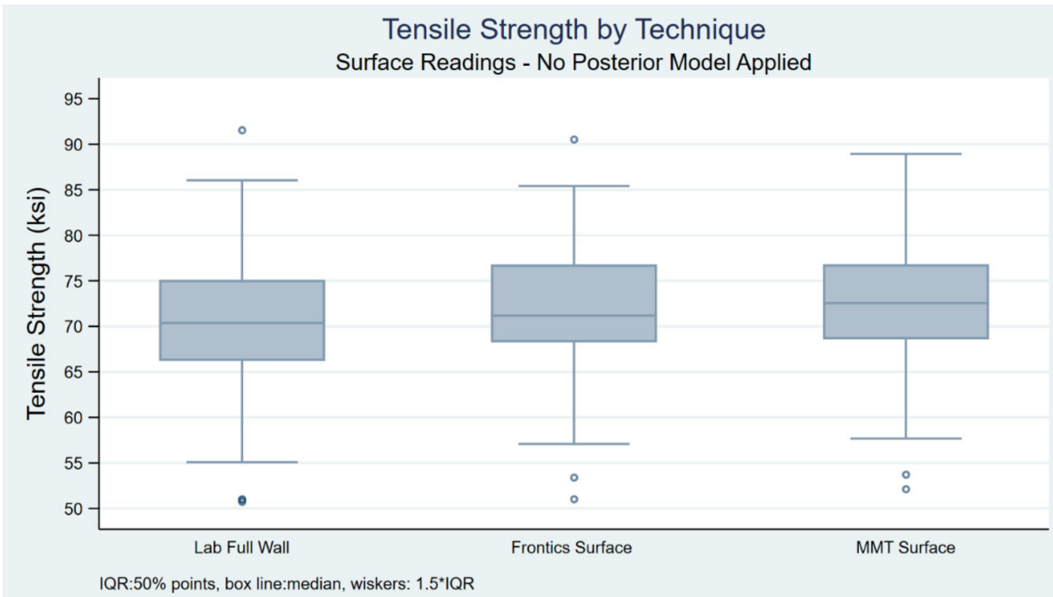

Bulk vs. Surface NDE Strength Comparisons by HSLA or Non-HSLA Grades

To further examine the trends shown in this section above, and explain why such variation might be present, the yield and tensile strength values are plotted in a series of unity plots in this section.

These plots have the lab (benchmark) yield or tensile strength on the y-axis and the surface NDE measure of the same parameter on the x-axis. The 0.2% yield strength is used for comparison since this the more common and specified yield strength for pipeline steels, and as it turns out there is little to no difference between plotting it or the 0.5% EUL since they are effectively the same for all the pipeline samples.

A 45 degree line is plotted on all the unit lines from the lower left to the upper right of the plot. If the points fall on the line, it indicates that the sample has the same value for the lab and the NDE technique. If the points are above the line, then the NDE technique has a lower strength (conservative) value and if below, the NDE technique has a higher strength (non-conservative) strength value.

Figure 13 to Figure 16 plot the lab full wall yield and tensile strengths vs. the NDE techniques separating the seventy pipeline steels into HSLA (red circles) and non-HSLA (black circles) steels.

Figure 13. Lab vs. Frontics Surface Yield Strength by HSLA.

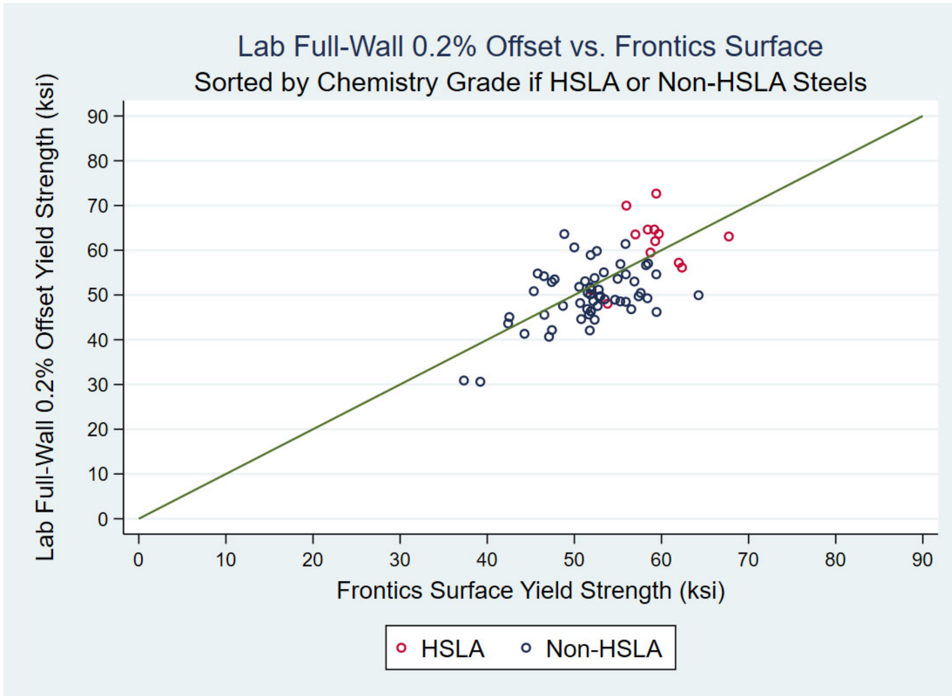

Figure 14. Lab vs. Frontics Surface Tensile Strength by HSLA.

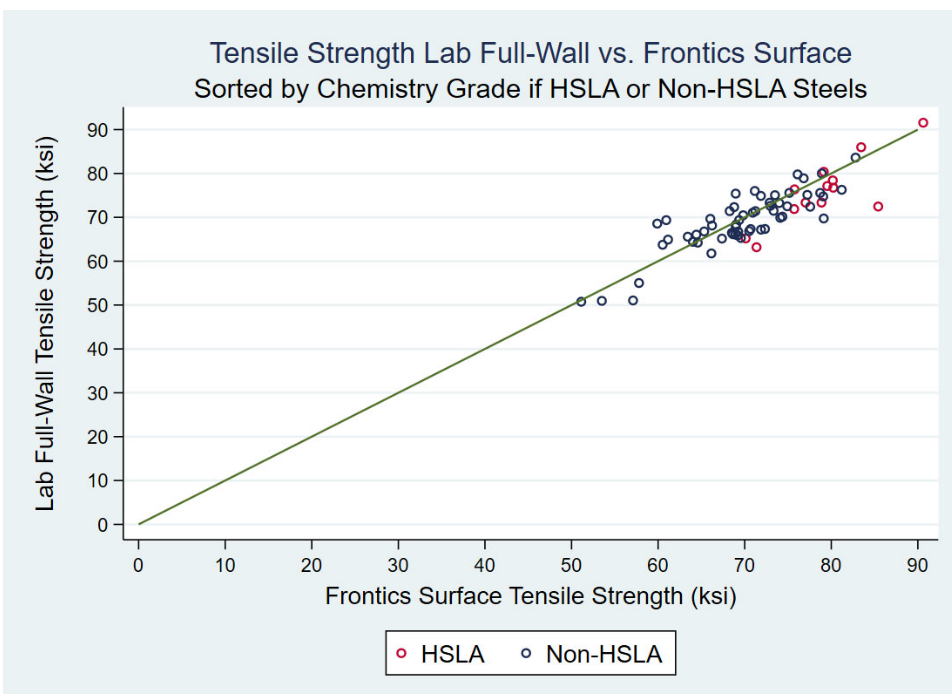

Figure 15. Lab vs. MMT Surface Yield Strength by HSLA.

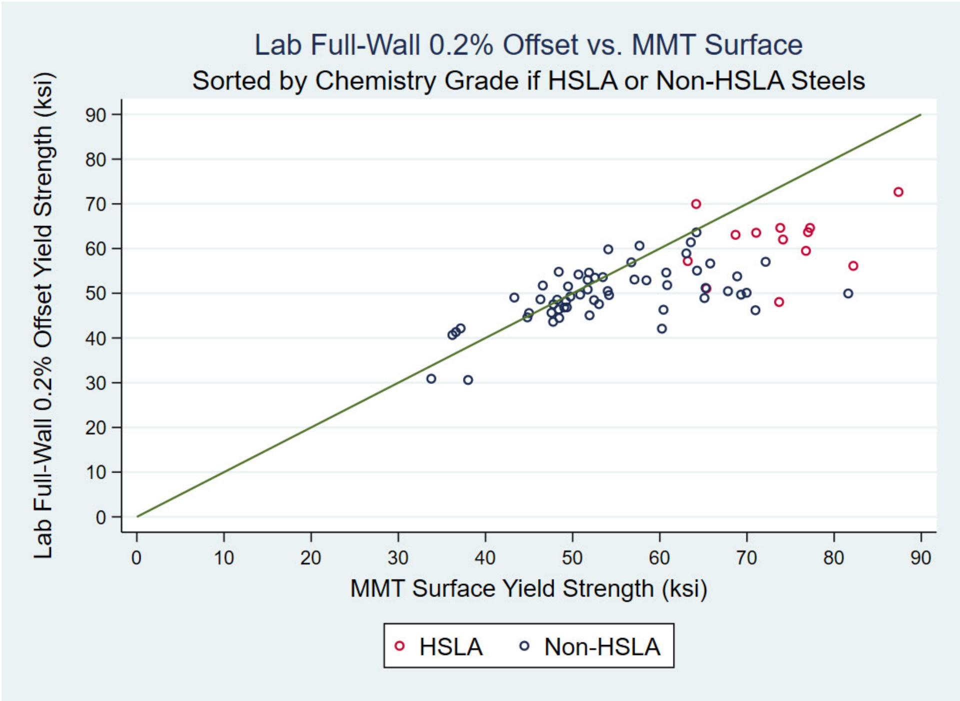

Figure 16. Lab vs. MMT Surface Tensile Strength by HSLA.

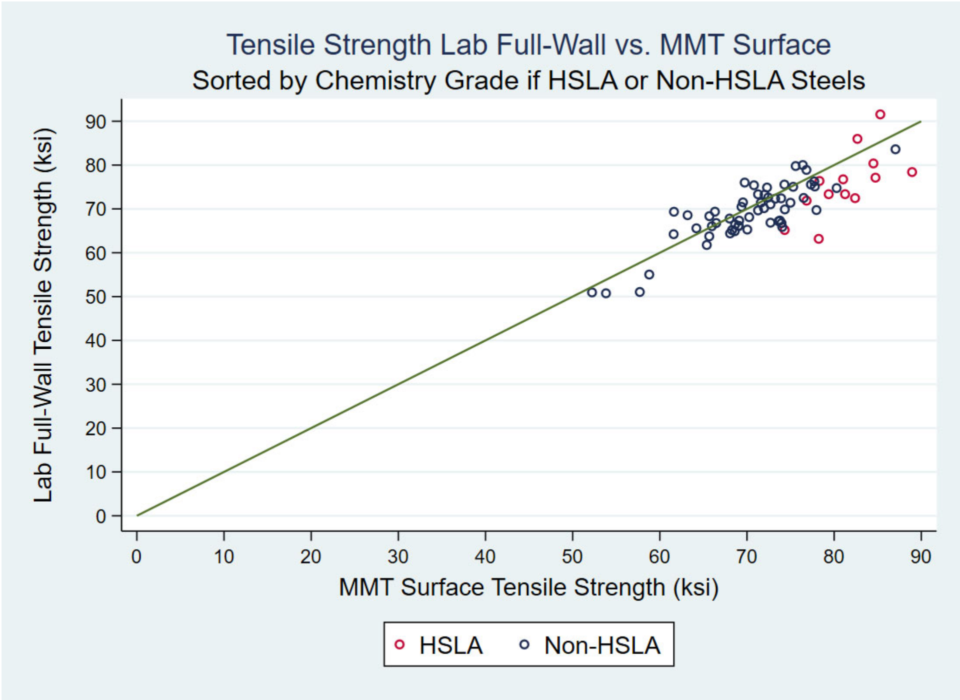

From the plots one can see that for Frontics yield and tensile strength and MMT tensile strength that there is little difference in the difference magnitude or direction between the lab and the NDE surface strength. However, for the MMT yield strength there is a clear bias for the HSLA steels to indicate a higher yield strength from the MMT surface results vs. the lab tests.

As will be shown later in this section via plot analysis and then quantitatively in the sensitivity study of the modeling Chapter, the HSLA is likely additive to the even more impactful seamless vs. non-seamless categorical variable. This variable will be shown to have a very strong effect on the MMT results and bias in predictions due to the surface cold work and residual stresses typically present in these non-annealed, long seam welded and formed pipes.

Bulk vs. Surface NDE Strength Comparisons by Steel Type and HSLA or Non-HSLA Grades

Figure 17 to Figure 20 are the same as the last section except the plots are further each divided into four subpanels by steel type. As before, the tensile strengths do not appear to have correlation to steel type and for the Frontics AIS NDE technology, it appears that the yield strength is also not affected strongly by steel type.

The MMT HSD NDE has some occurrence of non-conservative bias with all steel types for yield strength. It is also evident that the silicon killed HSLA steels show the most likely preponderance of having a surface yield strength higher than the lab baseline is from the HSLA grades within this steel type.

Figure 17. Lab vs. Frontics Surface Yield Strength by HSLA and Steel Type.

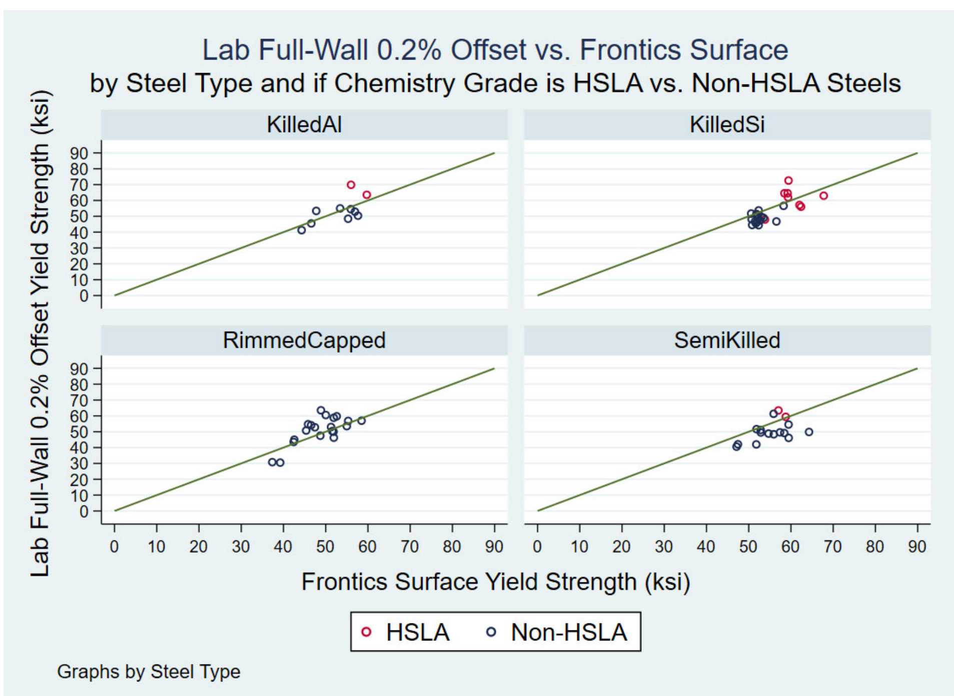

Figure 18. Lab vs. Frontics Surface Tensile Strength and Steel Type.

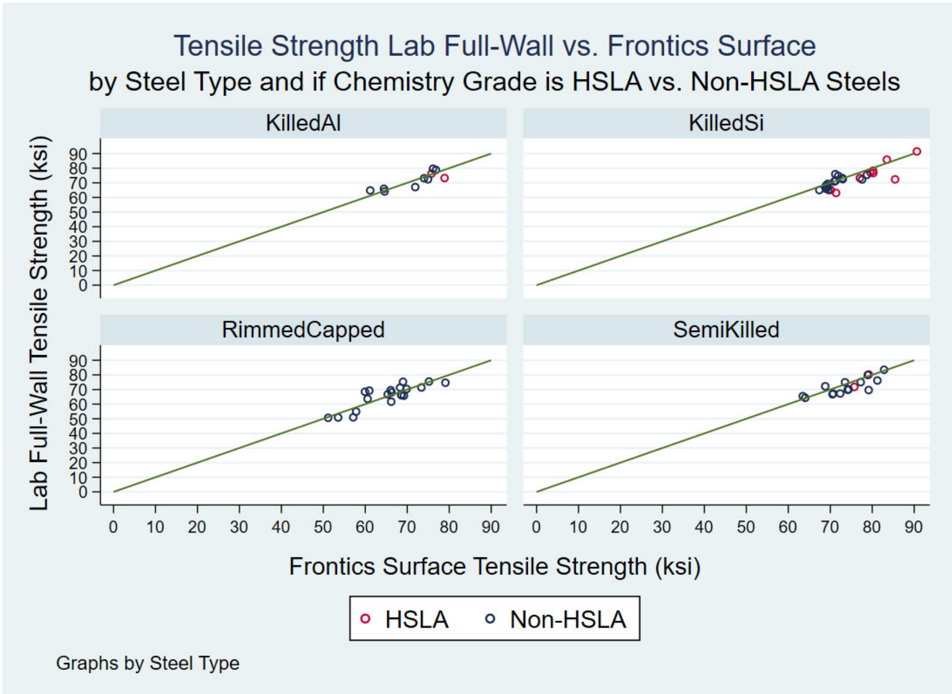

Figure 19. Lab vs. MMT Surface Yield Strength by HSLA and Steel Type.

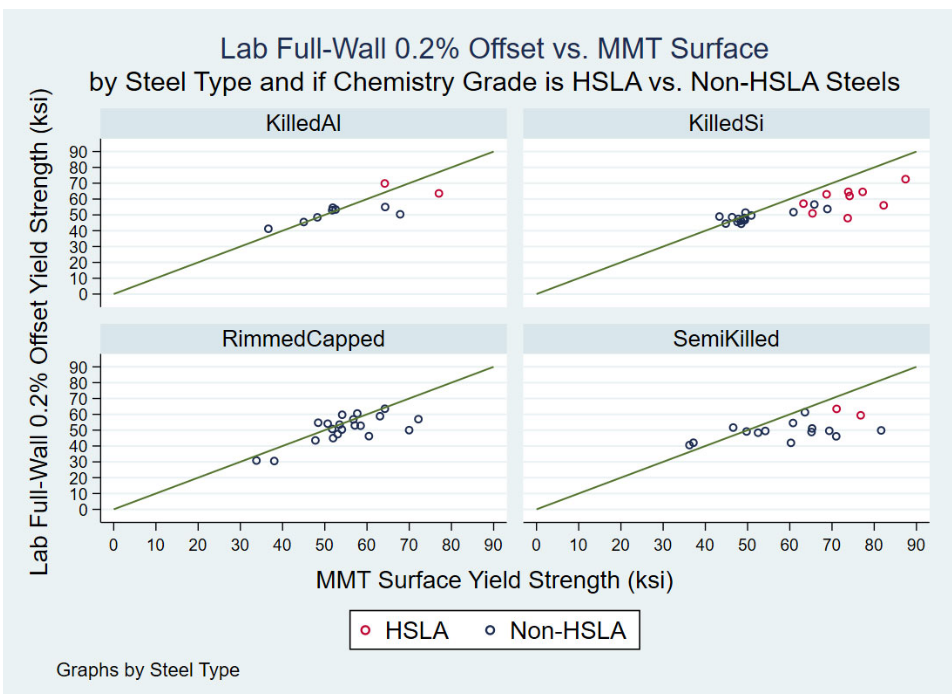

Figure 20. Lab vs. MMT Surface Tensile Strength by HSLA and Steel Type.

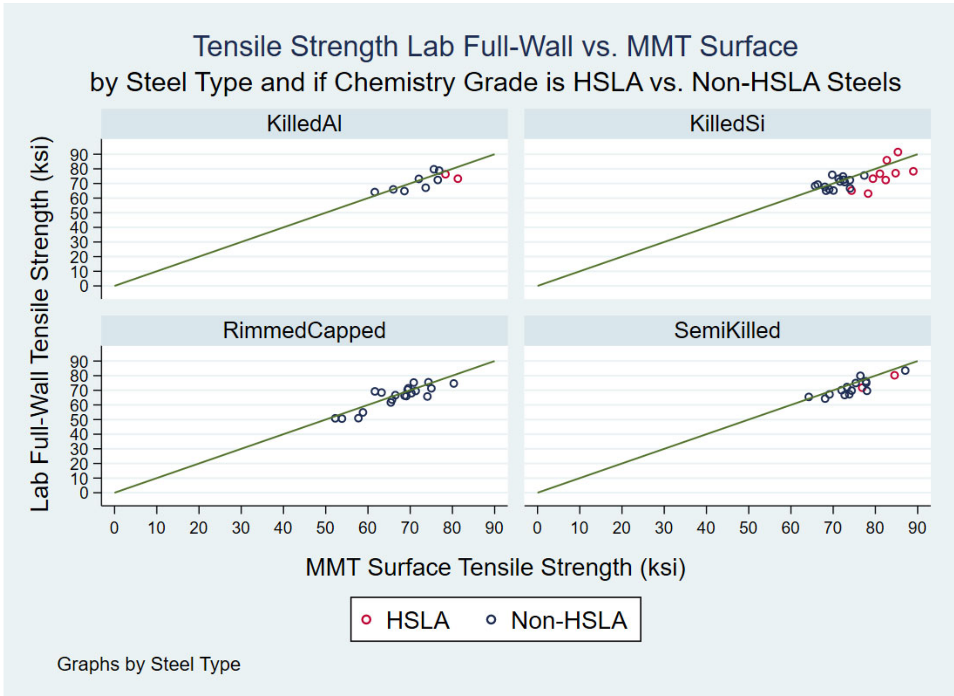

Bulk vs. Surface NDE Strength Comparisons by Weld Seam Type

The observed trends likely indicate that the MMT HSD "surface scratch-type" technique (see Attachments) interrogates mostly the outer layers of the pipe wall while the Frontics AIS "indentation-type" technique (see Attachments) may in effect test deeper into the pipe wall.

Seamless pipe is normalized/annealed and is therefore very homogenous across its thickness. Welded pipe on the other hand is produced from hot rolled plate or strip that usually exhibits through thickness variations in microstructure. These differences in grain size or in pearlite interlamellar distance are produced by localized through thickness differences in temperature as the plate is rolled and then cooled on the run-out table.

In addition, forming the pipe through the U-bend, O-bend, and Expansion (UOE) process followed by welding often produces significant residual stresses and cold work that tends to make the outer layers of the pipe "stronger" from a yield testing standpoint. Finally, the cold expansion step (and potential mill hydrotest) may or may not have been performed which introduces another element of uncertainty in properties prediction.

The same can be said for HSLA steels that due to the chemistry and grain refiners added and the processing, tend to have a finer (smaller diameter) grain size structure on the outer walls of the pipe thickness. This would also increase the yield strength due to the well-known Hall-Petch phenomenon that finer grain sizes contribute to higher yield strengths. While the properties of all steels are affected by thermomechanical processing factors, HSLA or micro-alloyed steels are produced in way so as to maximize the strengthening mechanisms available through controlled rolling and accelerated cooling.

Taken as a whole, and on average, welded and HSLA pipes and steels lead to a pipe stronger on the outside layers than the inside layers. From the data this appears to be a very possible reason why the MMT surface yield strengths (prior to any modeling) are higher for these situations than the full-wall lab tensile test. The next section contains plots that clearly show this. The modeling in Chapter 5 and 6 can help mitigate this bias from the MMT surface data, but could not remove it totally.

Figure 21 to Figure 24 show the same trends as the last two sections but each plot is subdivided by long seam weld type. Focusing on the ERW and Seamless weld types, the Frontics AIS NDE yield strength does not show bias by weld types when compared to the baseline full-wall lab results. The SAW and Spiral categories have too few samples to make a definitive statement. The MMT HSD NDE results demonstrate that the Seamless pipes show no substantive bias, but the ERW pipes do.

This could indicate that the MMT HSD "surface scratch-type" technique interrogates mostly the outer layers of the pipe wall while the Frontics AIS "indentation-type" technique may in effect test deeper into the pipe wall. Seamless pipe is normalized/annealed and is therefore very homogenous across its thickness. Welded pipe on the other hand is produced from hot rolled plate or strip that usually exhibits through thickness variations in microstructure. These differences in grain size or in pearlite interlamellar distance are produced by localized through thickness differences in temperature as the plate is rolled and then cooled on the run-out table.

In addition, forming the pipe through the U-bend, O-bend, and Expansion (UOE) process followed by welding can produce residual stresses and cold work that would tend to make the outer layers of the pipe "stronger" from a yield testing standpoint (the final cold expansion step may or may not have been performed which introduces another element of uncertainty in properties prediction).

The same can be said for HSLA steels that due to the chemistry and grain refiners added and the processing, tend to have a finer (smaller diameter) grain size structure on the outer walls of the pipe thickness. This would also increase the yield strength due to the well-known Hall-Petch phenomenon that finer grain sizes contribute to higher yield strengths. While the properties of all steels are affected by thermomechanical processing factors, HSLA or micro-alloyed steels are produced in way so as to maximize the strengthening mechanisms available through controlled rolling and accelerated cooling.

Taken as a whole, and on average, welded and HSLA pipes and steels lead to a pipe stronger on the outside layers than the inside layers. From the data this appears to be a very possible reason why the MMT surface yield strengths (prior to any modeling) are higher for these situations than the full-wall lab tensile test. The next section contains plots that clearly show this.

Figure 21. Lab vs. Frontics Surface Yield Strength by Weld Seam Type.

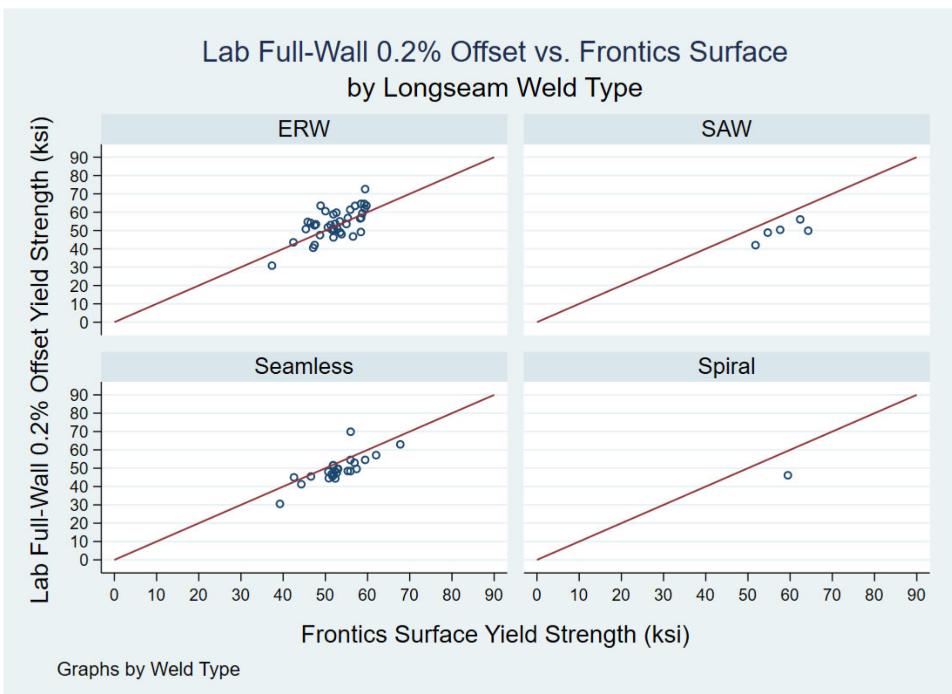

Figure 22. Lab vs. Frontics Surface Tensile Strength by Weld Seam Type.

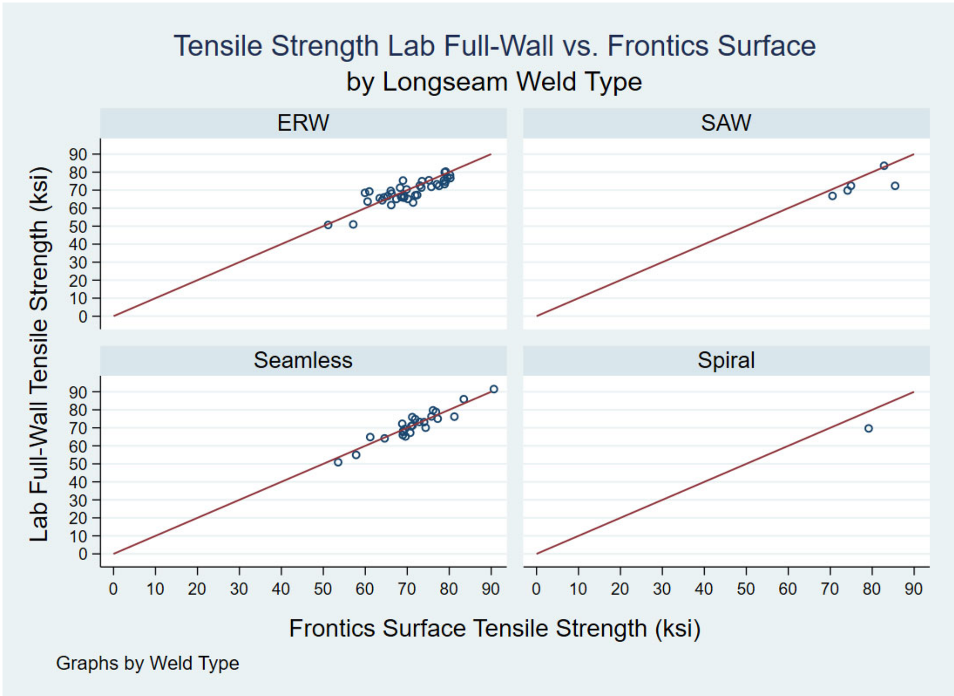

Figure 23. Lab vs. MMT Surface Yield Strength by Weld Seam Type.

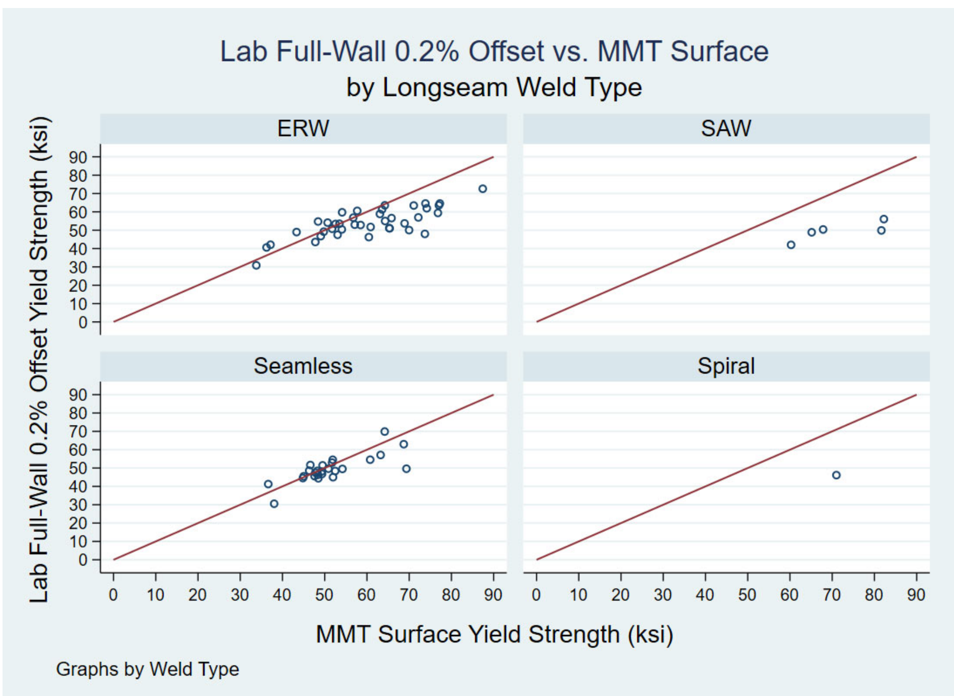

Figure 24. Lab vs. MMT Surface Tensile Strength by Weld Seam Type.

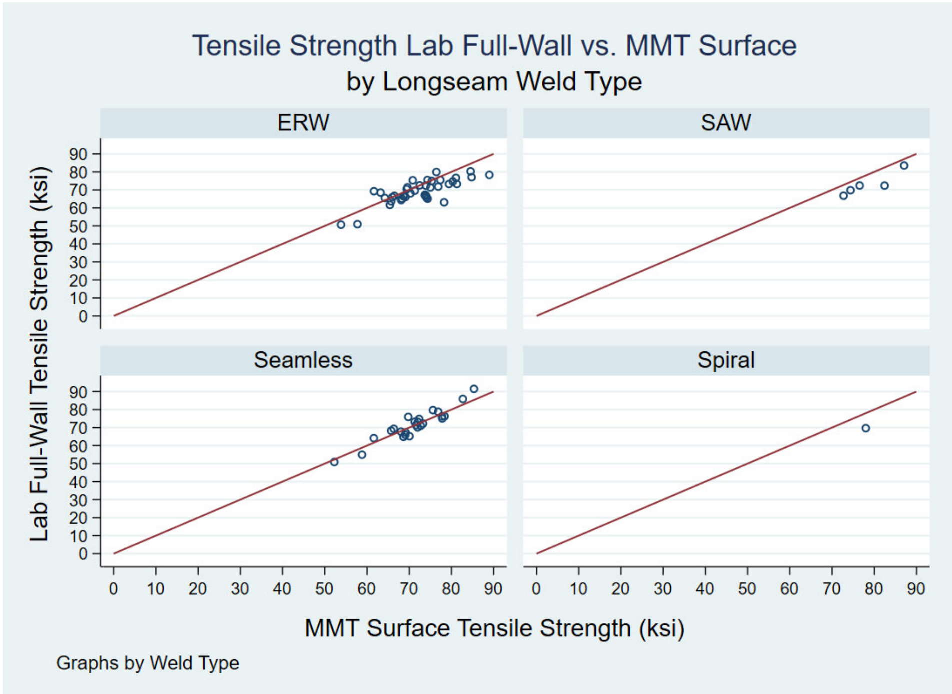

Bulk vs. Surface NDE Strength Comparisons by Steel Type and Seamless or Welded

Figure 25 to Figure 28 show the same trends as the last few sections but each plot is subdivided by steel type. The pipeline samples that are seamless are plotted as red circles and welded long seam samples are plotted as black circles.

First, it is interesting to note that the Rimmed/Capped steels in Figure 25 show a slight bias with the Frontics AIS NDE where the surface NDE yield strength is either the same or marginally lower than the baseline full-wall lab yield strength. This is expected since steels that go through the full or partial rimming process tend to have carbon center-line segregation in the ingot, leading to a lower yield strength on the surface and a higher yield strength in the center of the ingot and therefore pipe wall. The carbon segregation of these steels will be dramatically shown later in this chapter.

Figure 27 shows that the MMT HSD NDE surface yield strength with no post-processing models applied reveals seamless pipeline samples that have excellent correlation between the lab and NDE tests, regardless of the steel type. However, for the non-seamless, i.e., welded long seam pipe that is not normalized, the HSD technology mostly has a higher yield strength than the full-wall lab yield strength. This is true, except for the rimmed, welded pipes which has a good correlation to the lab tests. It is possible that the lower strength of the rimmed ingot on the outside is offset by the added strength of the non-annealed welding process of forming the pipe. This would explain all the trends in the plots discussed so far.

Figure 25. Lab vs. Frontics Surface Yield Strength by Weld Seam Type and if Seamless.

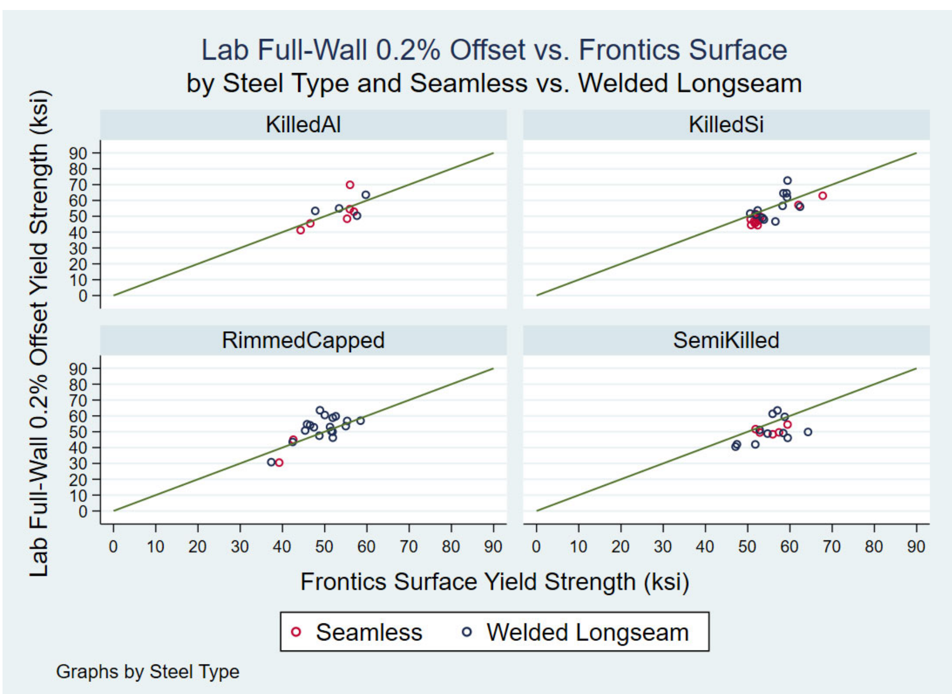

Figure 26. Lab vs. Frontics Surface Tensile Strength by Weld Seam Type and if Seamless.

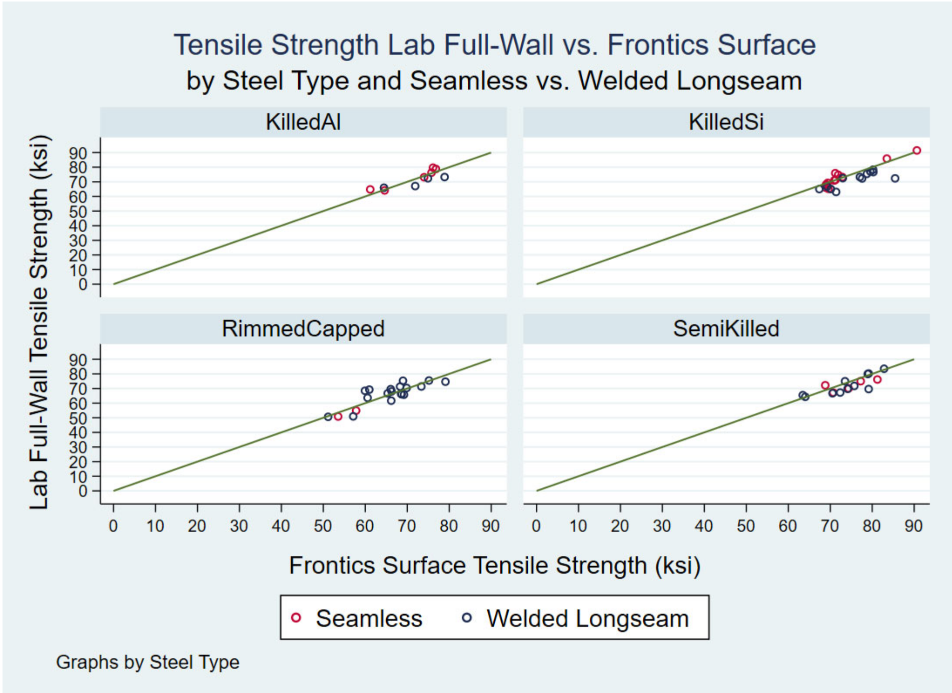

Figure 27. Lab vs. MMT Surface Yield Strength by Weld Seam Type and if Seamless.

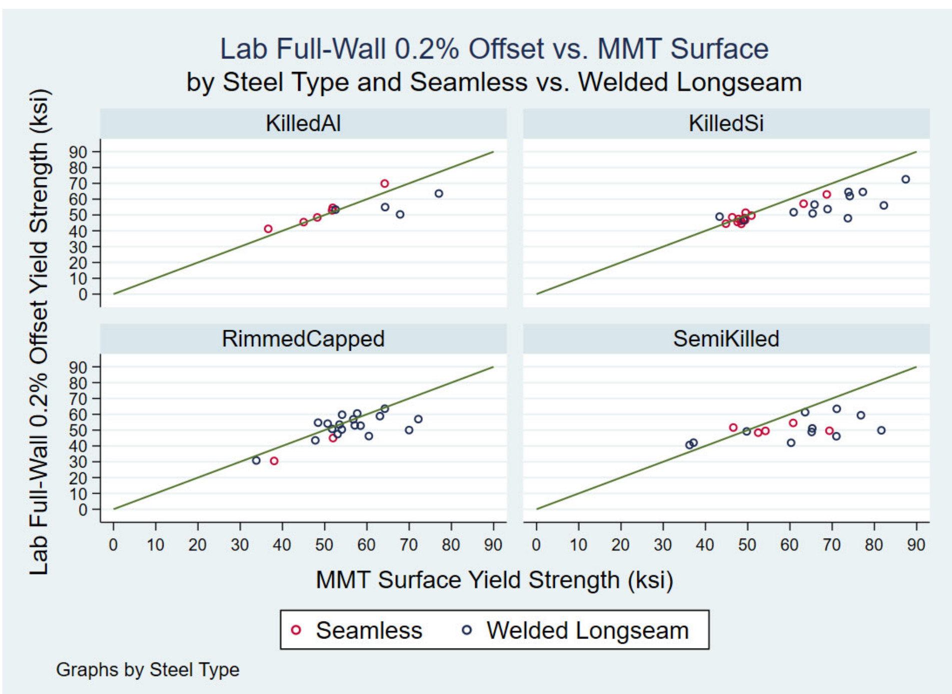

Figure 28. Lab vs. MMT Surface Tensile Strength by Weld Seam Type and if Seamless.

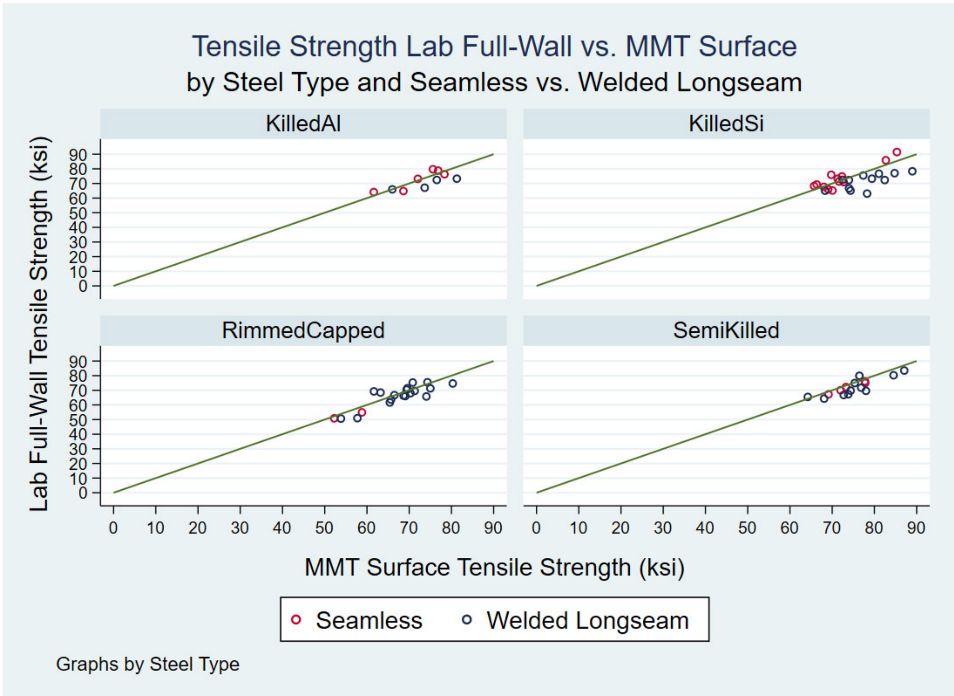

Bulk vs. Surface NDE Strength Comparisons by NDE Technology, Weld, and Grade Categories

Figure 29 and Figure 30 combine multiple pipeline factors, i.e., variables, into two side-by-side comparison plots for yield strength and ultimate tensile strength respectively. As already discussed, the MMT HSD NDE technology generally provides a higher than lab reading for yield strength, sometimes significant, for HSLA and non-seamless pipeline samples. The ultimate tensile strength readings for both NDE technologies are more uniform around the lab readings.

Figure 29. Lab vs. NDE Surface Yield Strength by Multiple Factors.

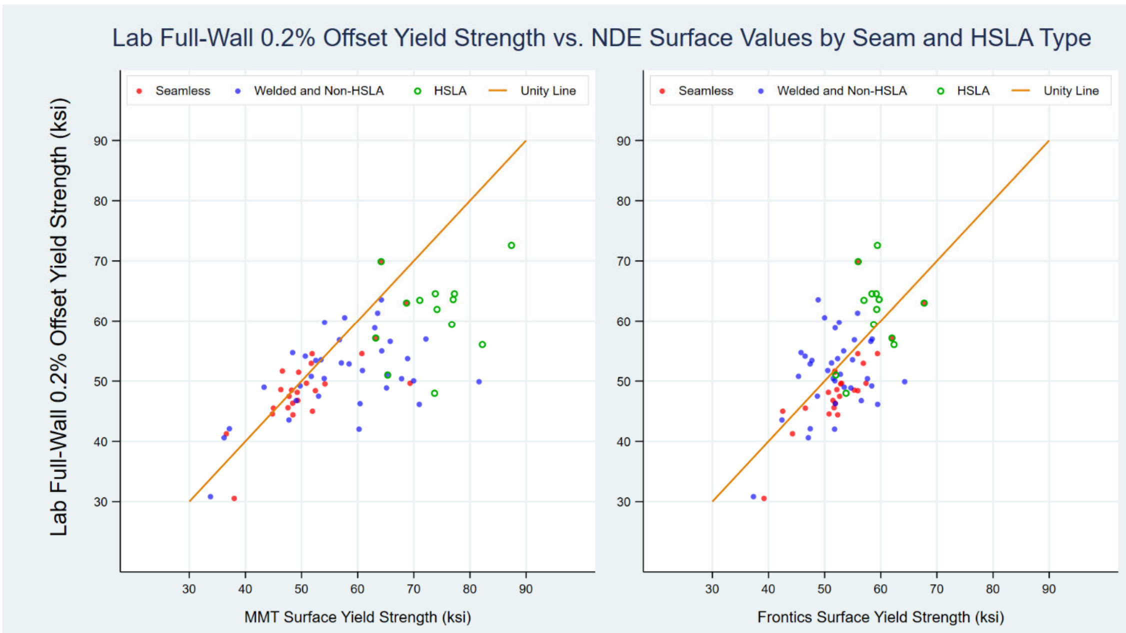

Figure 30. Lab vs. NDE Surface Tensile Strength by Multiple Factors.

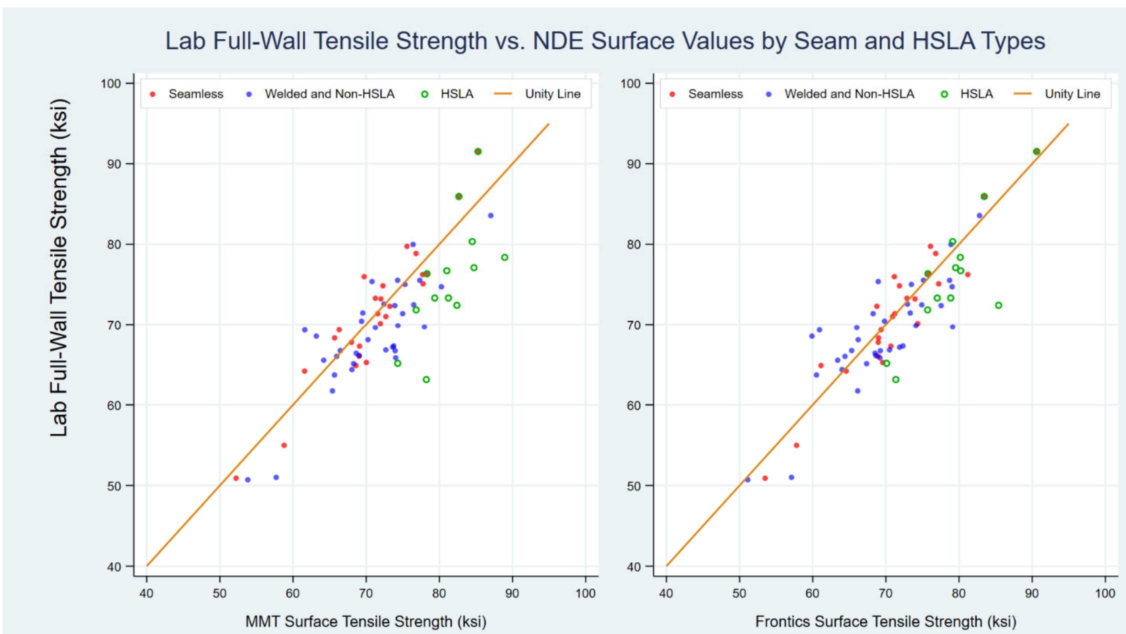

Bulk vs. Surface NDE Strength Comparisons by Pipe Diameter

Figure 31 and Figure 32 show the similar strength comparisons but for pipe diameter and Figure 33 and Figure 34 show the same as a function of pipe wall thickness. The relative diameter of the plotted values are proportional to the pipe diameter. Upon careful comparison with the steel types, the observed trends are due to the steel types vs. the diameter or thickness for the MMT NDE technology.

Figure 31. Lab vs. NDE Surface Yield Strength by Pipe Diameter.

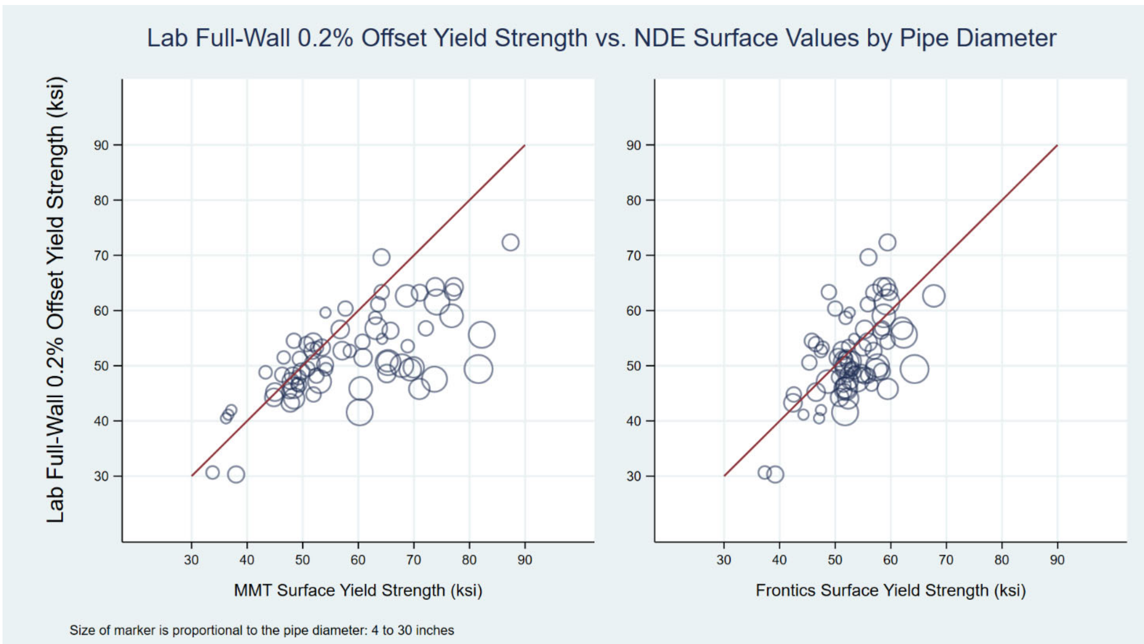

Figure 32. Lab vs. NDE Surface Tensile Strength by Pipe Diameter.

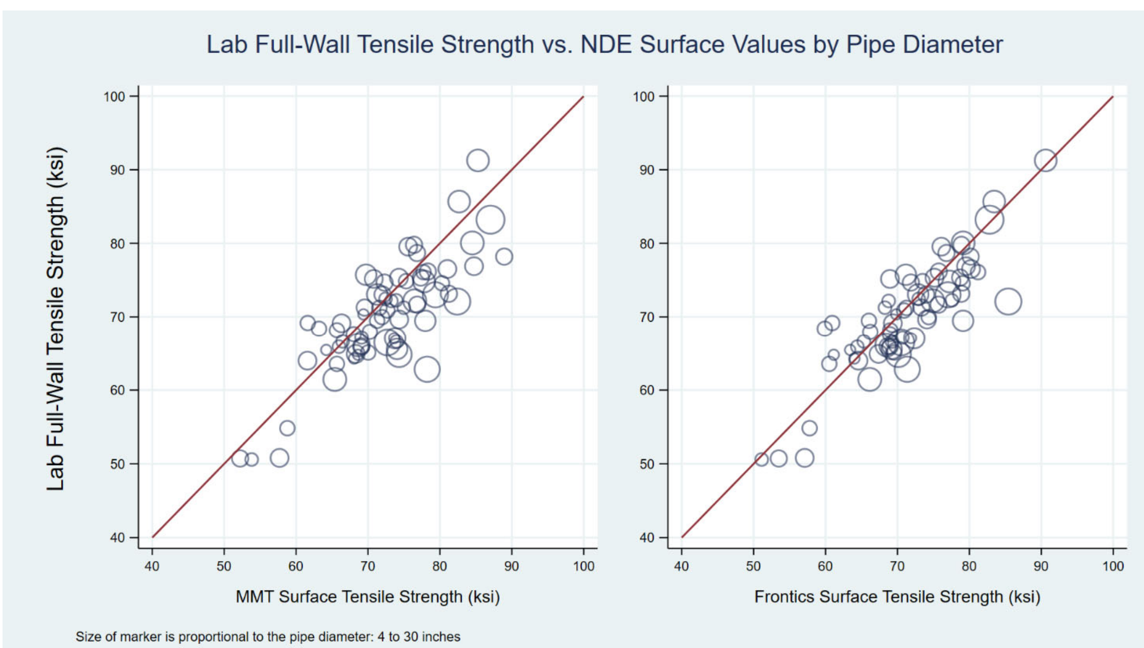

Bulk vs. Surface NDE Strength Comparisons by Pipe Thickness

Figure 33. Lab vs. NDE Surface Yield Strength by Wall Thickness.

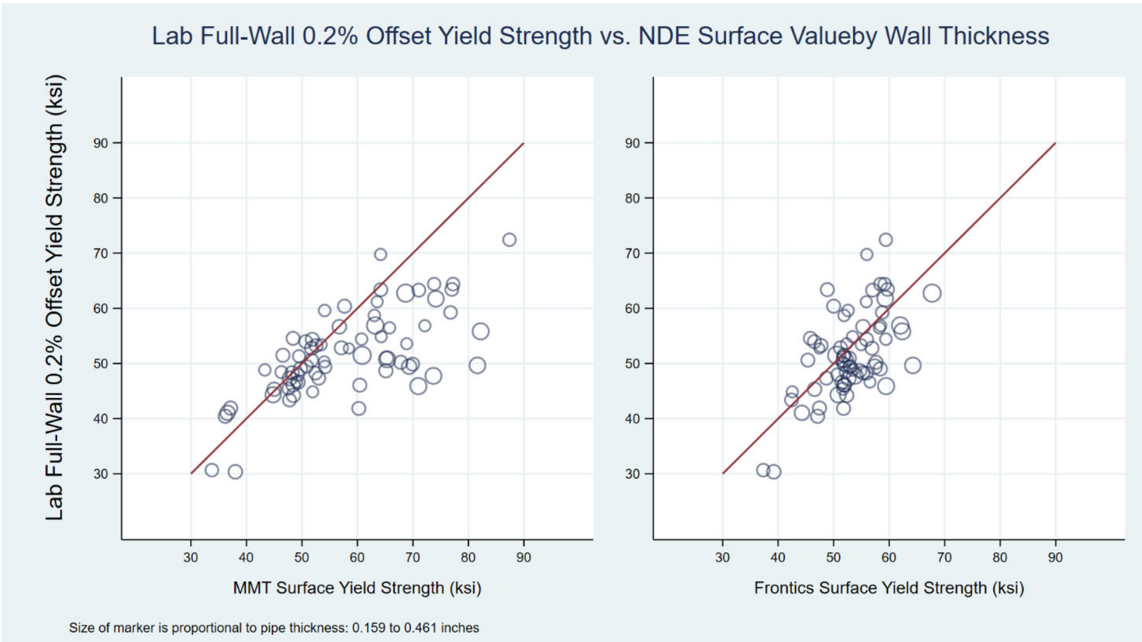

Figure 34. Lab vs. NDE Surface Tensile Strength by Wall Thickness.

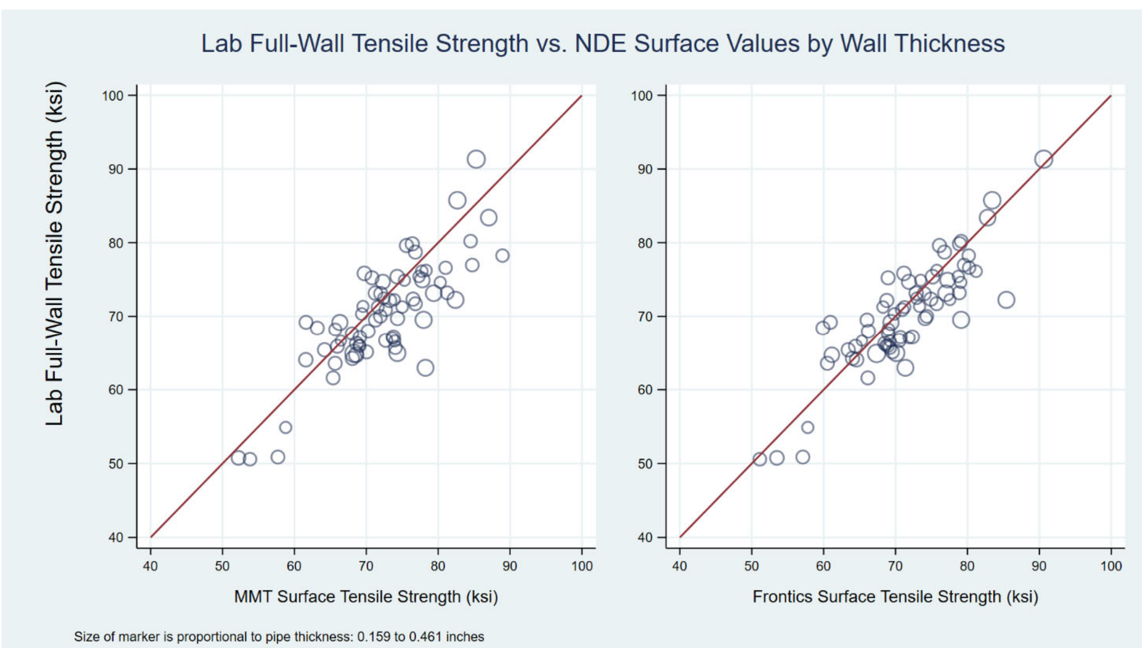

3.3 Grain Size

Figure 35 shows the grain size comparison for the seventy pipeline samples between the surface at 5 mils deep vs. the 4-depth average. The correlation is excellent, with the values tightly grouped around the unity line. The range of grain size values is also excellent as discussed in the pipe sample section earlier and represents the variety and range expected in the field. Figure 36 is the same data but further broken down by steel type as four separate panels.

Surface vs. Ave Bulk Grain Size Unity Plots

Figure 35. Grain Size Comparison - 5 mils vs. 4-Depth Composite.

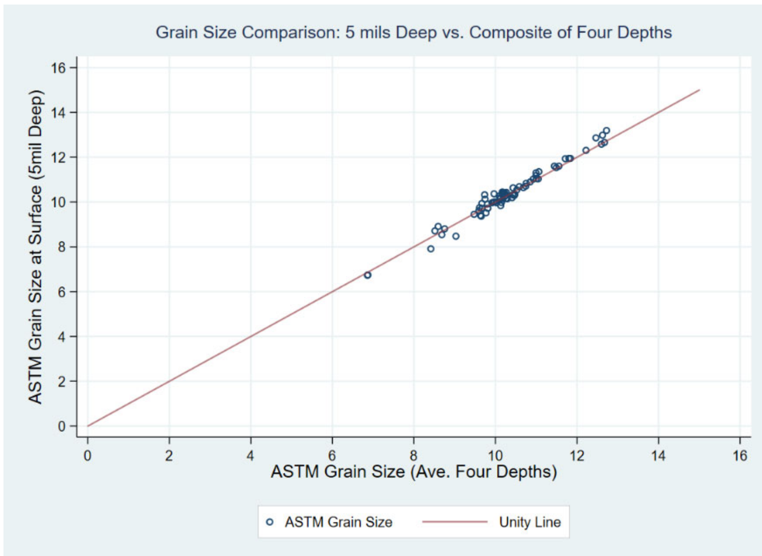

Figure 36. Grain Size Comparison - 5 mils vs. 4-Depth Composite by Steel Type.

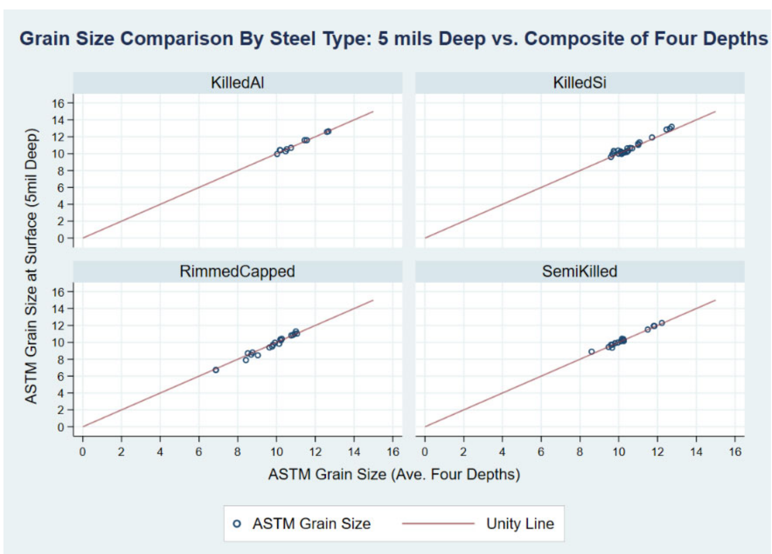

Histogram and Density Plot of Delta Between Surface - Ave Bulk Grain Size

Figure 37 shows a histogram and density plot of the difference of the surface grain size minus the 4-depth composite grain size. The plot is nearly centered on zero and the variation is across the range is normally distributed as shown by the red normal density plot overlaying the green density plot of the data. Figure 38 plots the same data, but by steel type as separate panels, again with excellent correlation between the surface and composite across all steel types.

Figure 37. Difference (Delta) Between Surface and 4-Depth Composite Grain Size.

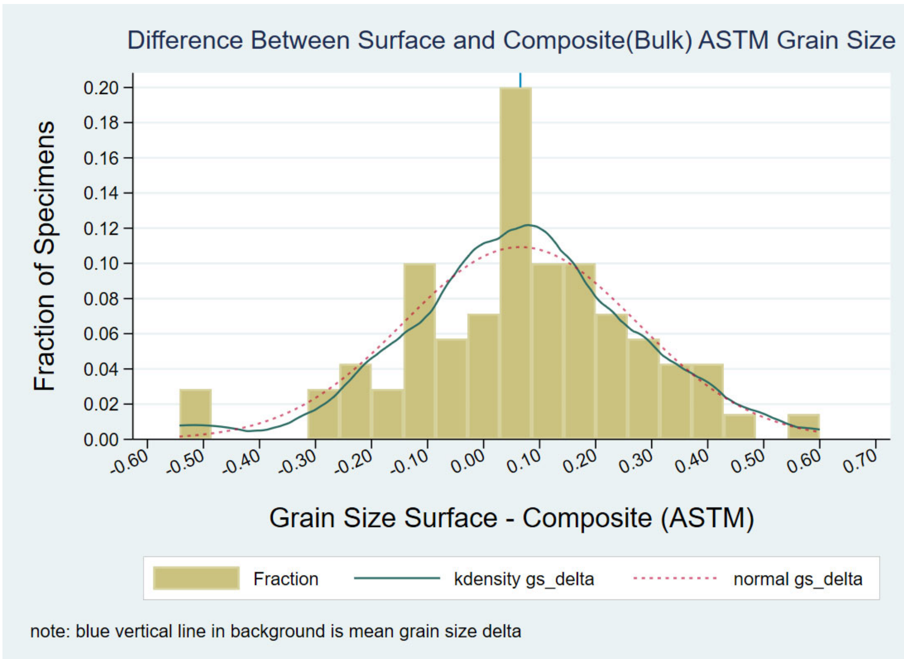

Figure 38. Difference Between Surface and 4-Depth Composite Grain Size by Steel Type.

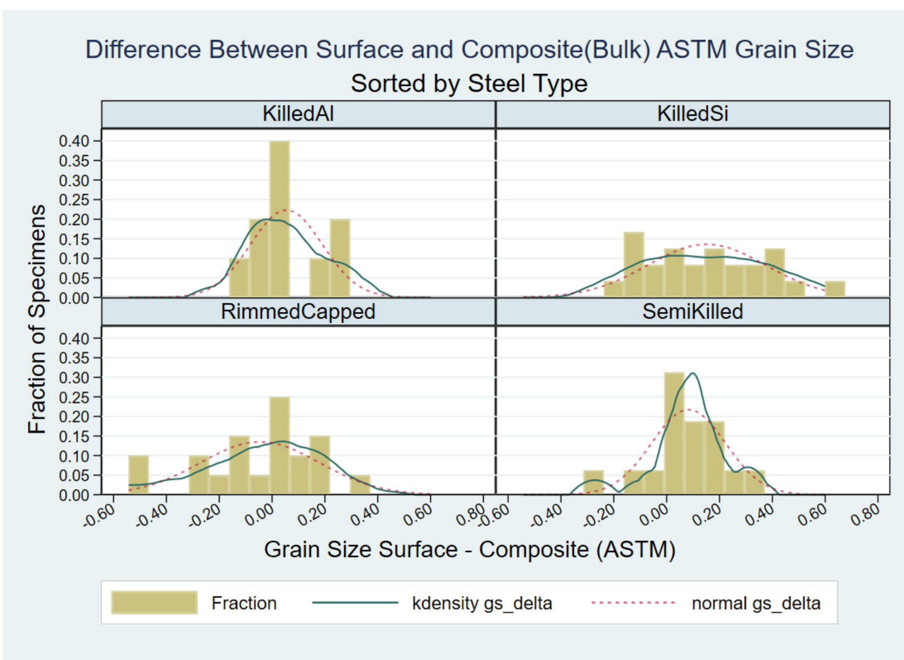

3.4 Chemistry

Compendium of Unity Comparison Scatter Plots at Various Depths by Element

Aluminum (Al)

The various depths, 4-depth average, and bulk Al chemistry weight percent values are consistent with each other. There is no substantive overall segregation from surface to bulk or midwall.

Figure 39. Aluminum Weight Percent Comparisons by Depths and Bulk.

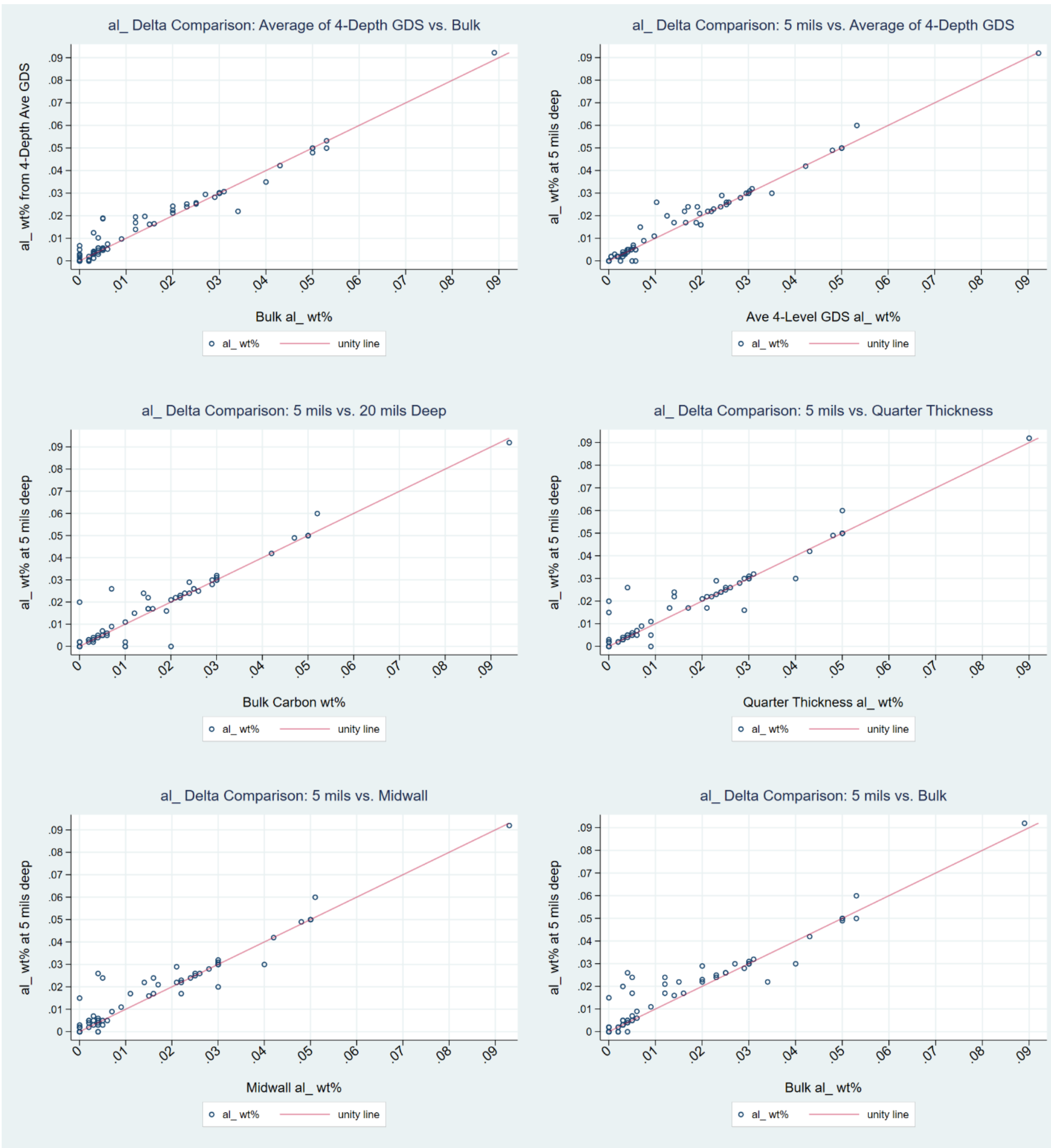

Boron (Br)

The various depths, 4-depth average, and bulk Br chemistry weight percent values are consistent with each other. There is no substantive overall segregation from surface to bulk or midwall.

Figure 40. Boron Weight Percent Comparisons by Depths and Bulk.

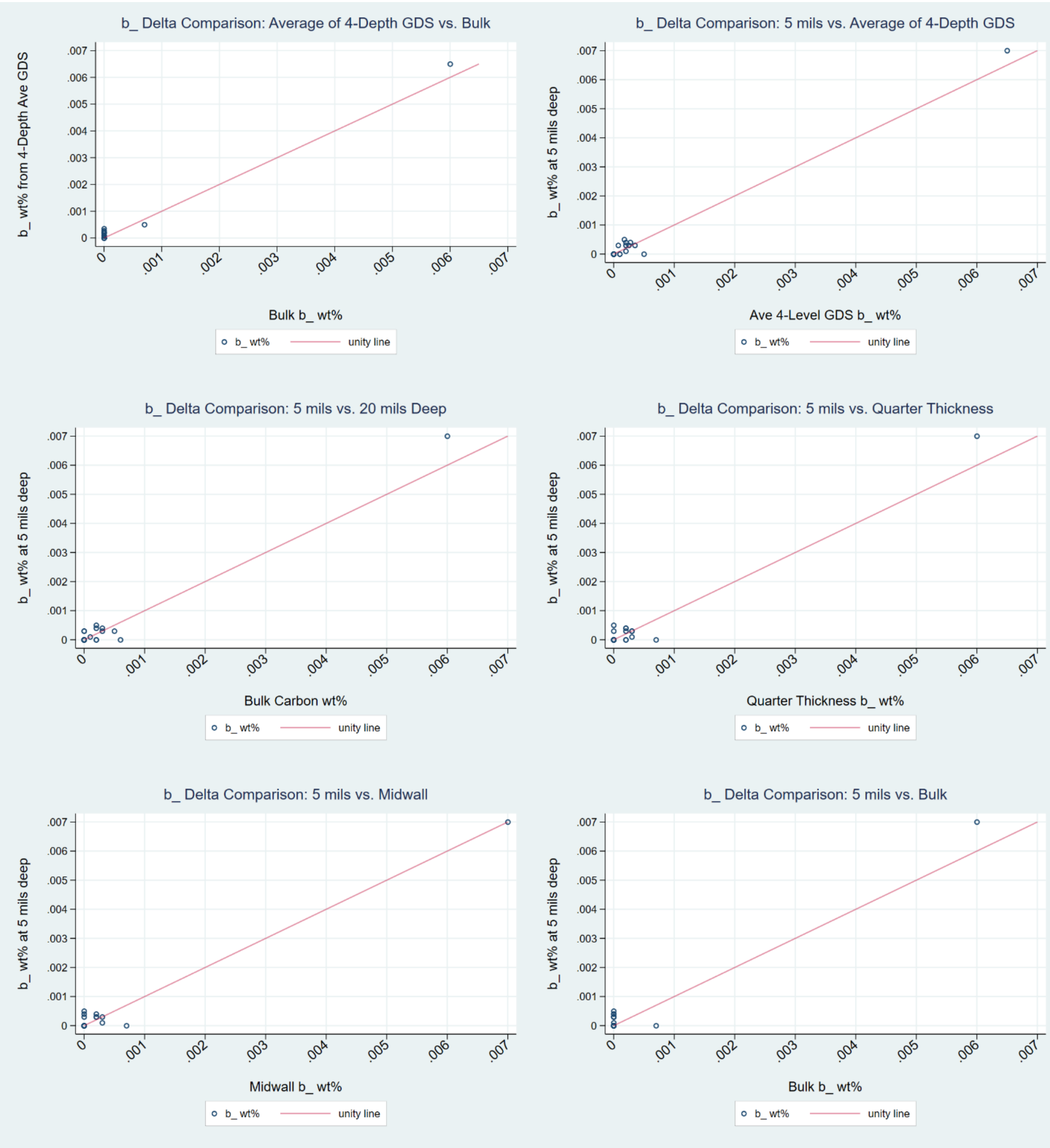

Carbon (C)

The various depths, 4-depth average, and bulk C chemistry weight percent values show significant segregation as one would expect in these pipeline steels. There is significantly lower carbon levels at and near the surface versus the 20 mil, quarter thickness, midwall, and bulk values.

Figure 41. Carbon Weight Percent Comparisons by Depths and Bulk.

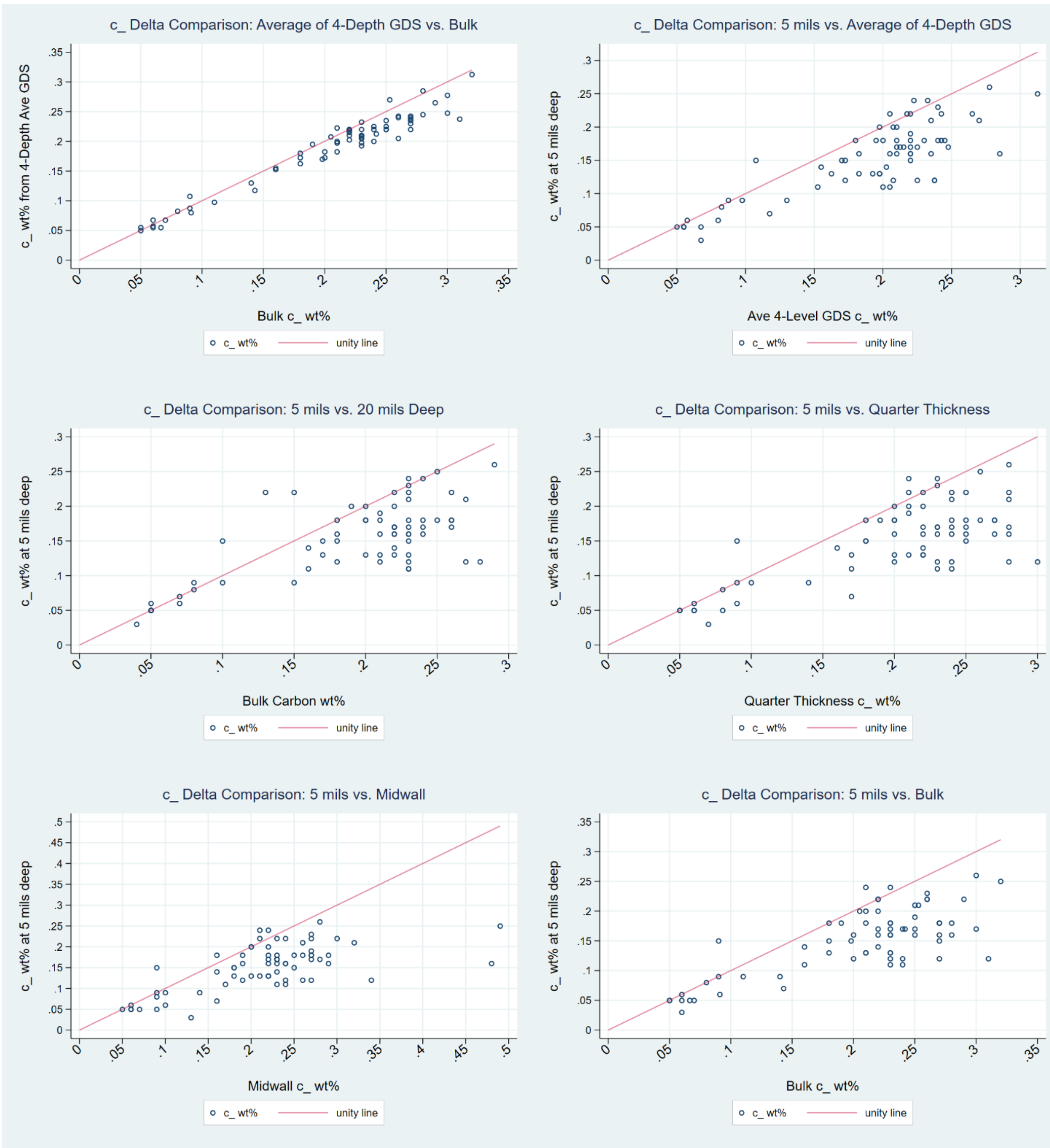

Chromium (Cr)

The various depths, 4-depth average, and bulk Cr chemistry weight percent values are consistent with each other. There is no substantive overall segregation from surface to bulk or midwall.

.

Figure 42. Chromium Weight Percent Comparisons by Depths and Bulk.

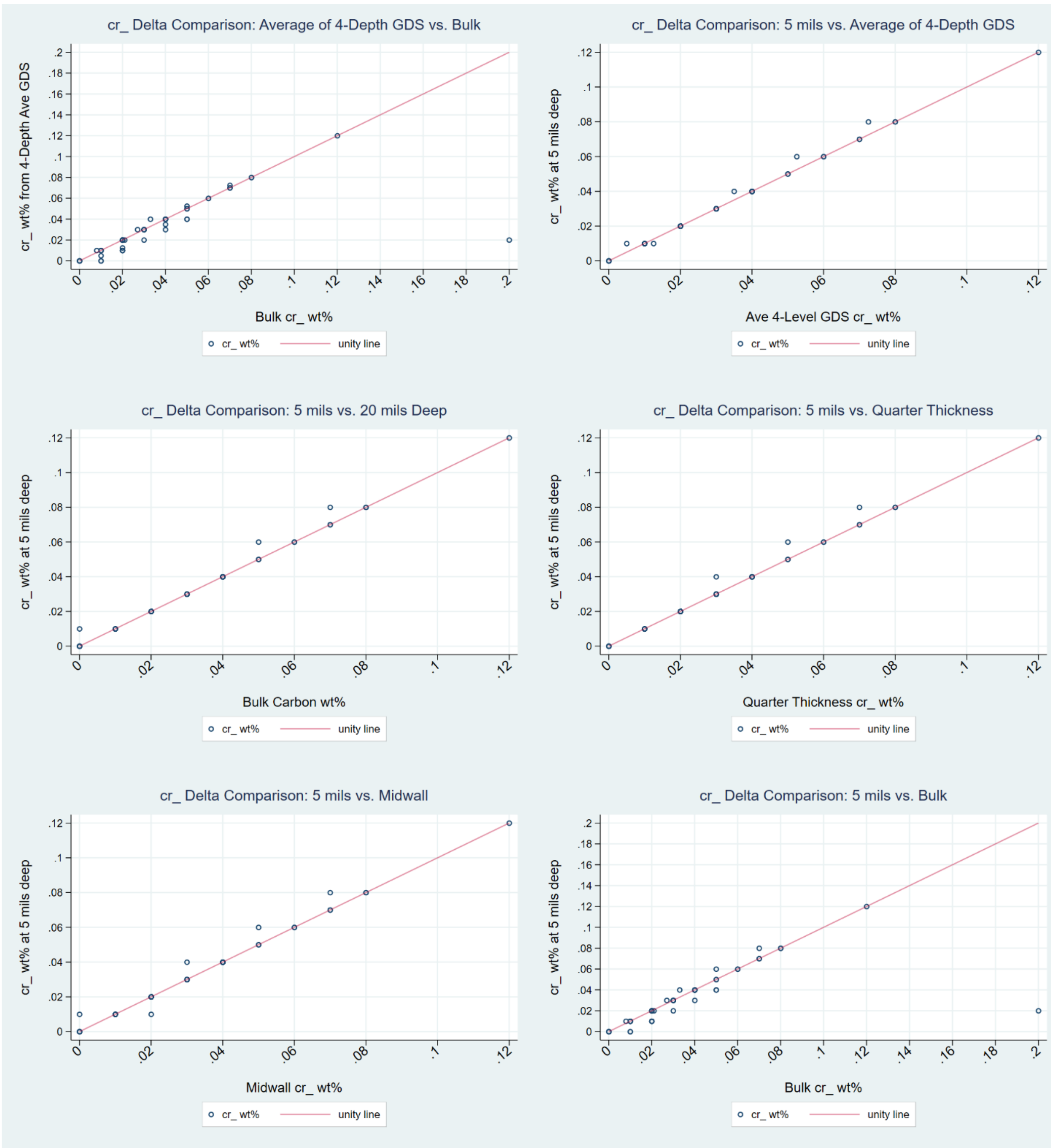

Copper (Cu)

The various depths, 4-depth average, and bulk Cu chemistry weight percent values are consistent with each other. There is no substantive overall segregation from surface to bulk or midwall.

Figure 43. Copper Weight Percent Comparisons by Depths and Bulk.

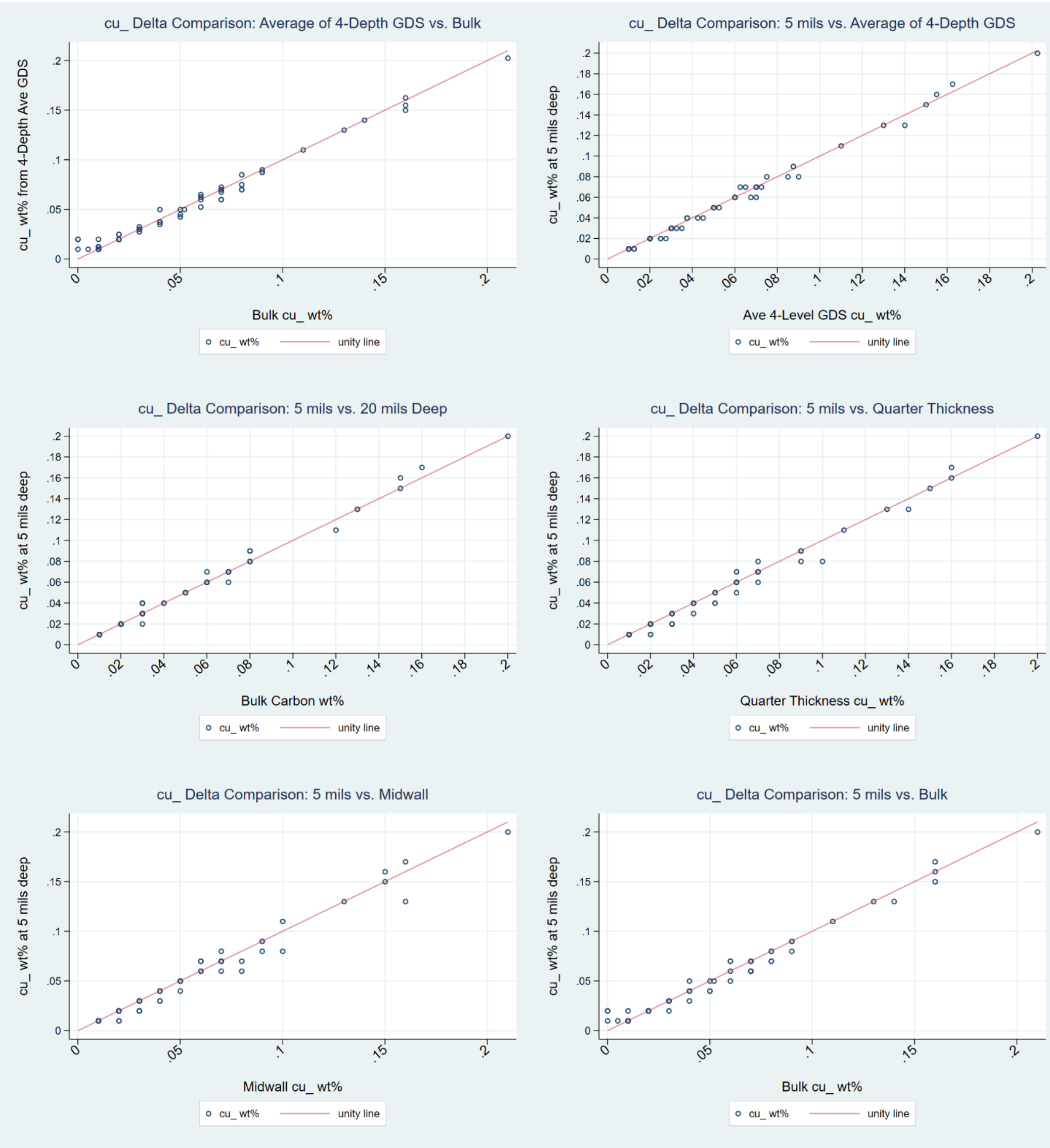

Manganese (Mn)

The various depths, 4-depth average, and bulk Mn chemistry weight percent values are consistent with each other. There is no substantive overall segregation from surface to bulk or midwall.

Figure 44. Manganese Weight Percent Comparisons by Depths and Bulk.

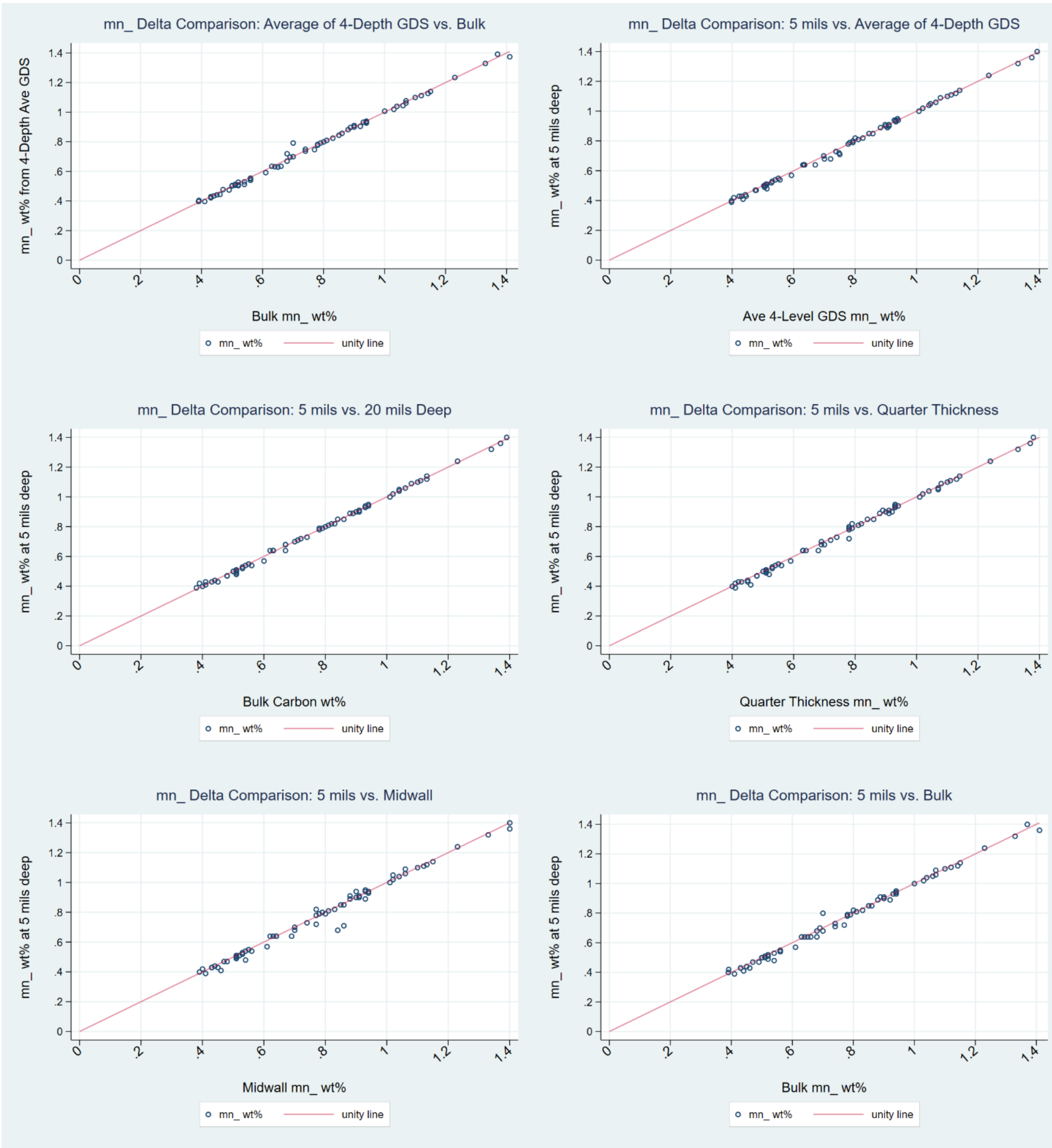

Molybdenum (Mo)

The various depths, 4-depth average, and bulk Mo chemistry weight percent values are consistent with each other. There is no substantive overall segregation from surface to bulk or midwall.

Figure 45. Molybdenum Weight Percent Comparisons by Depths and Bulk.

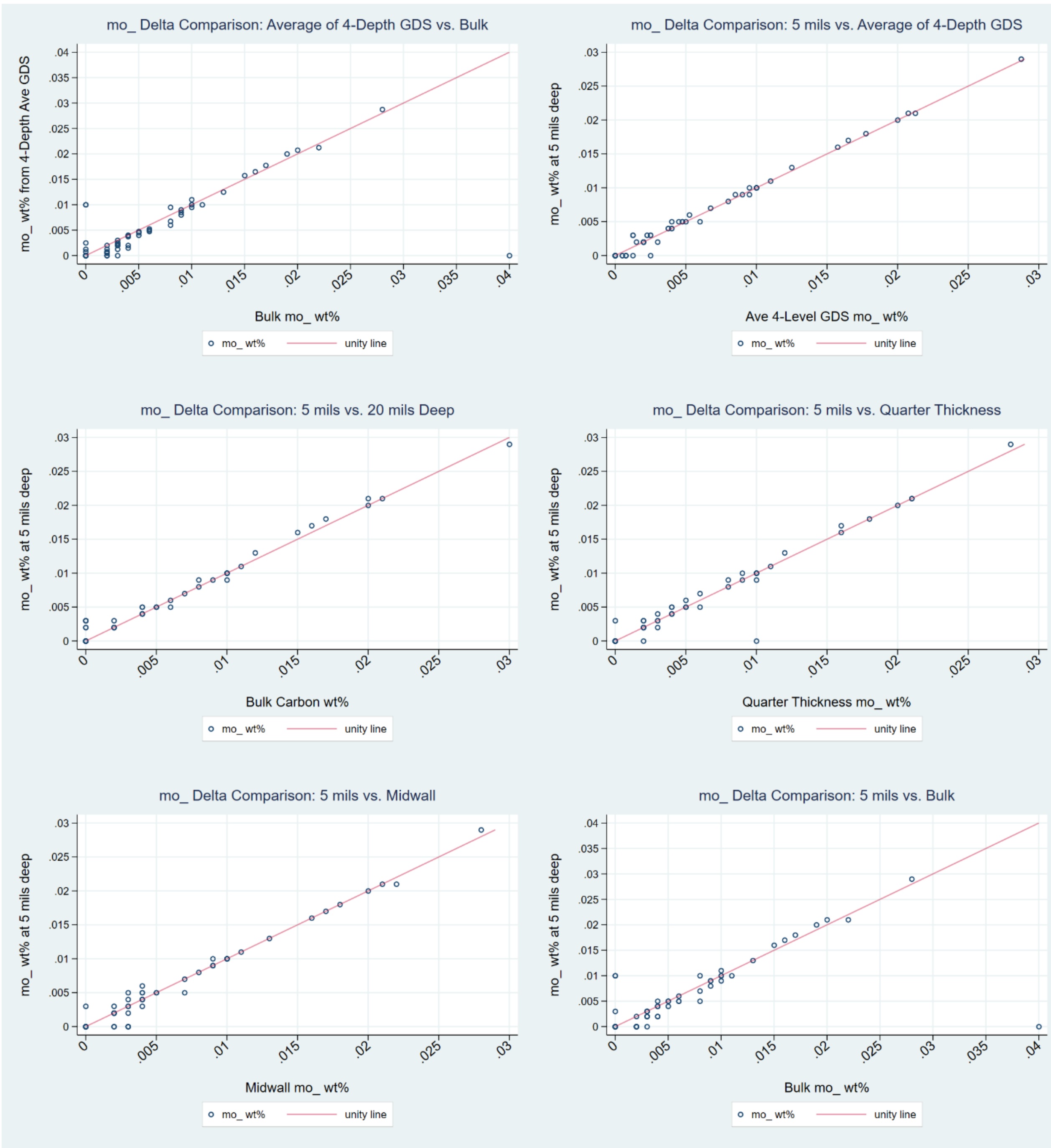

Nitrogen (N)

The various depths, 4-depth average, and bulk N chemistry weight percent values exhibit variation in both higher and lower values between the surface and the bulk or composite values. Nitrogen is at a low level in steel and is also difficult to test for. The 5 mil nitrogen level compares overall well with the 4-depth composite with some elevated levels from the surface locations.

Figure 46. Nitrogen Weight Percent Comparisons by Depths and Bulk.

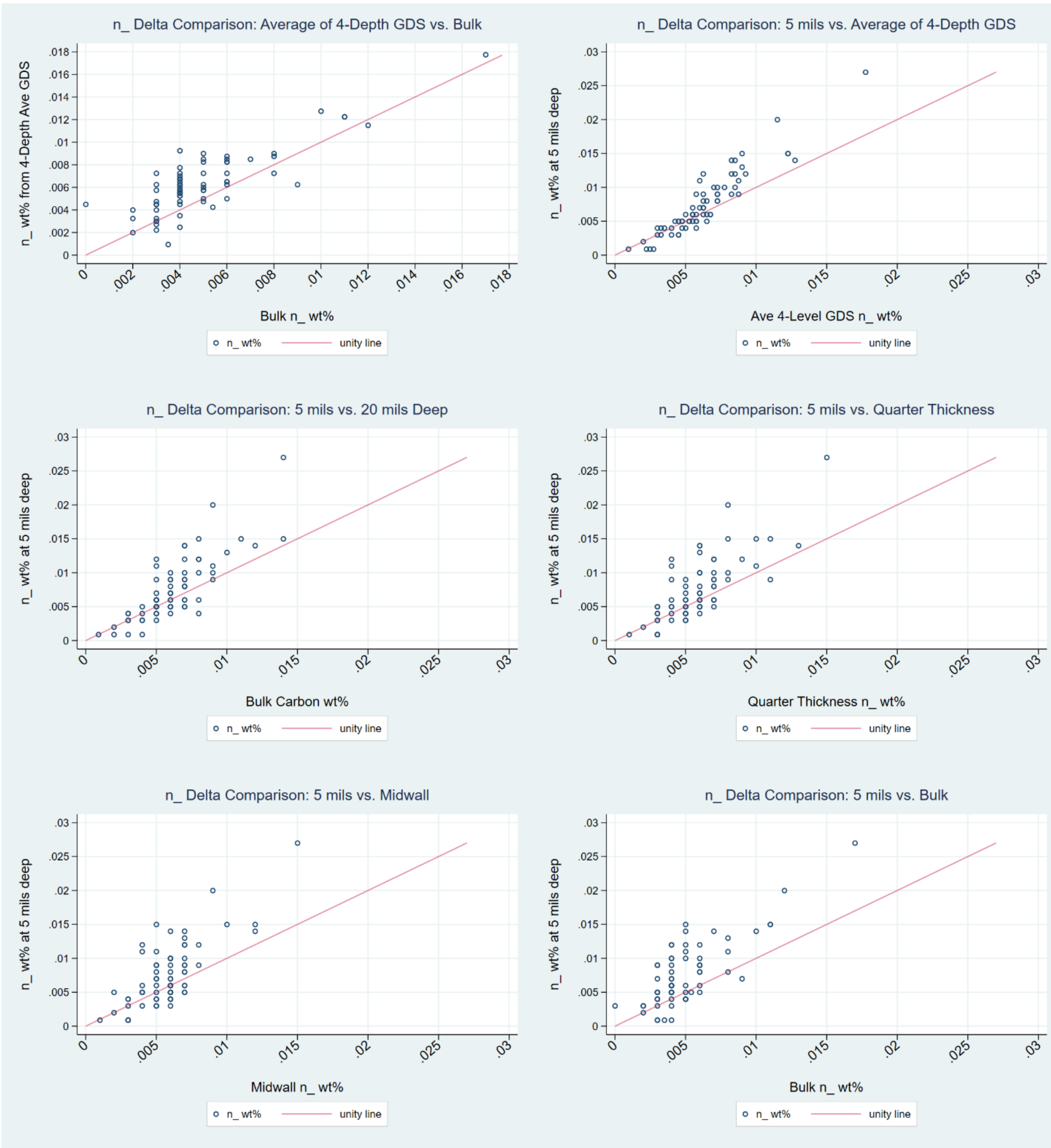

Niobium (Nb)

The various depths, 4-depth average, and bulk Nb chemistry weight percent values are consistent with each other. There is no substantive overall segregation from surface to bulk or midwall.

Figure 47. Niobium Weight Percent Comparisons by Depths and Bulk.

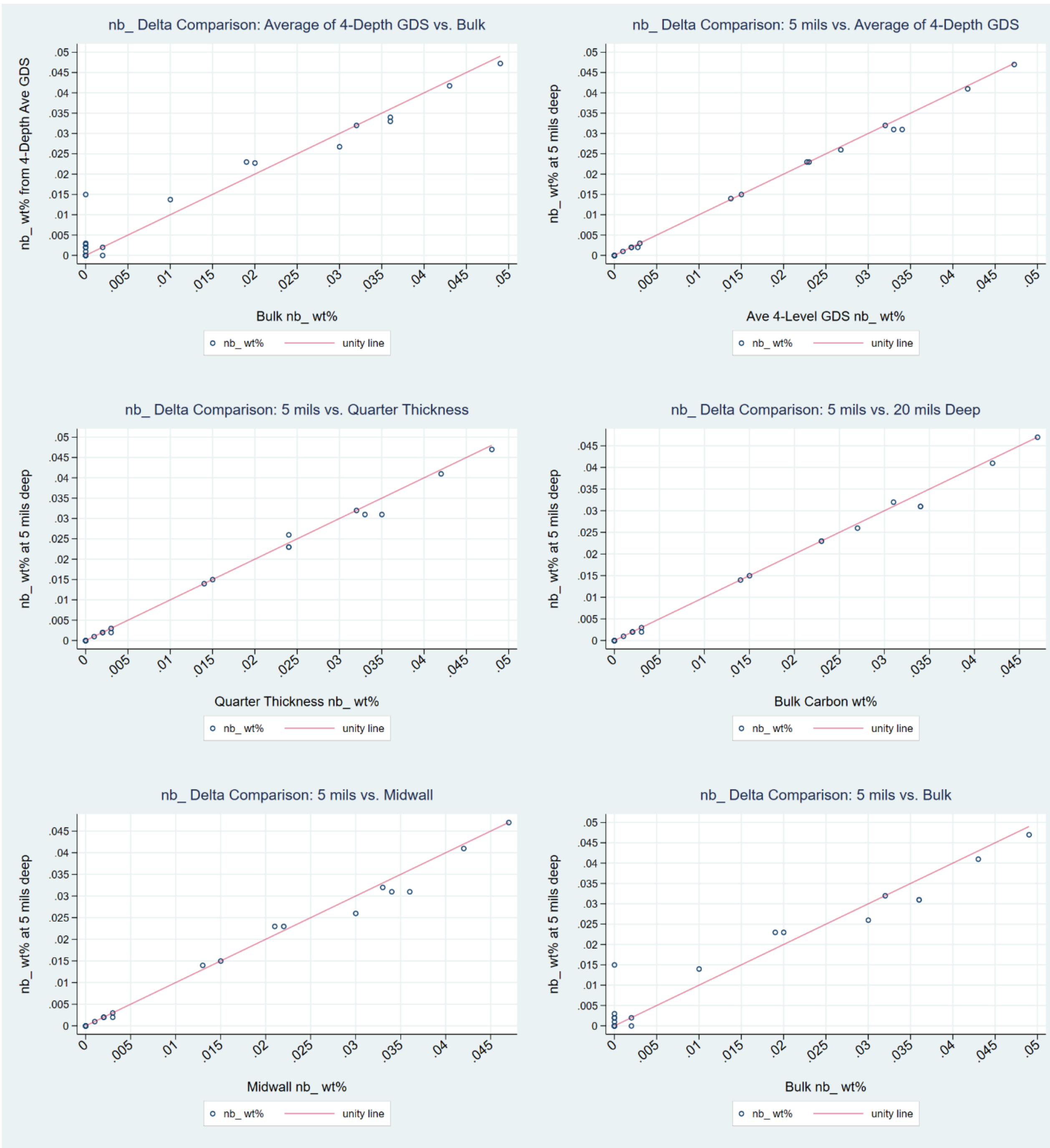

Nickel (Ni)

The various depths, 4-depth average, and bulk Ni chemistry weight percent values are consistent with each other. There is no substantive overall segregation from surface to bulk or midwall.

Figure 48. Nickel Weight Percent Comparisons by Depths and Bulk.

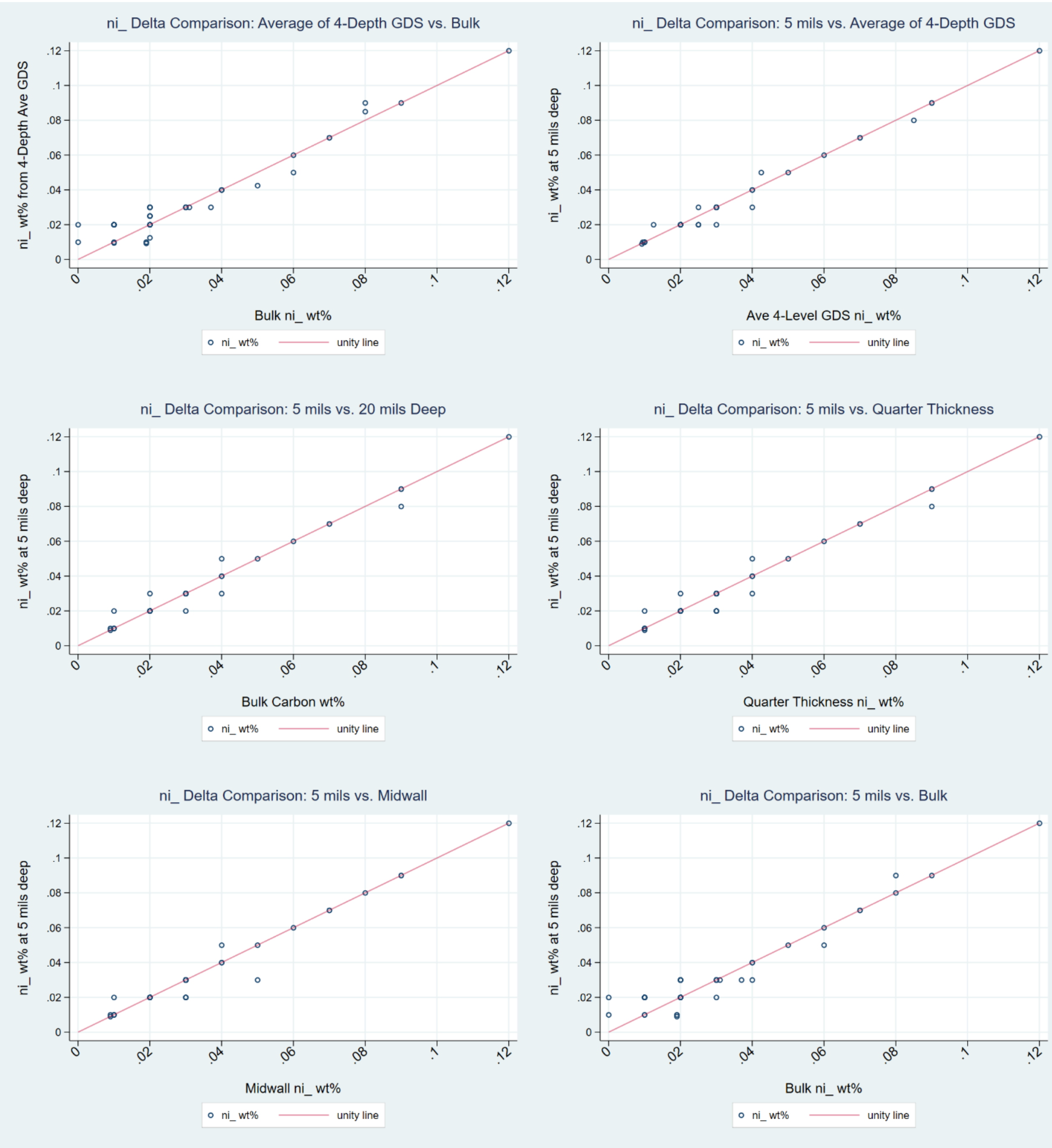

Phosphorus (P)

The various depths, 4-depth average, and bulk P chemistry weight percent values are consistent with each other. There is no substantive overall segregation from surface to bulk or midwall.

Figure 49. Phosphorus Weight Percent Comparisons by Depths and Bulk.

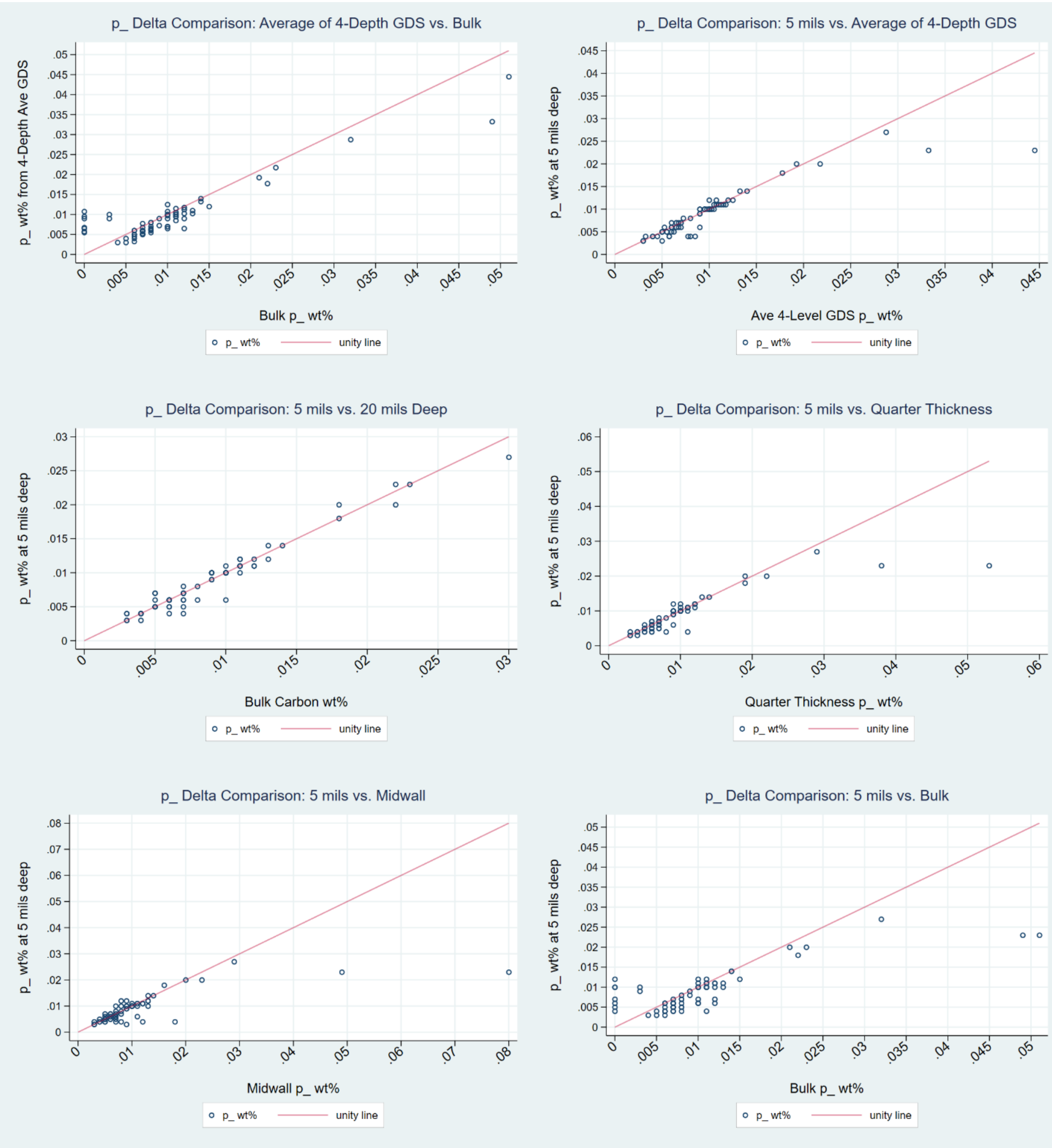

Sulfur (S)

The various depths, 4-depth average, and bulk S chemistry weight percent values show significant segregation as one would expect in these pipeline steels. There are lower sulfur levels at and near the surface versus the 4-depth composite and bulk values. Sulfur is not known to have significant effect on yield or tensile strength but it is known to have a strong effect on Charpy toughness which could be a concern if surface chemistry were used in a surface to bulk toughness model.

Figure 50. Sulfur Weight Percent Comparisons by Depths and Bulk.

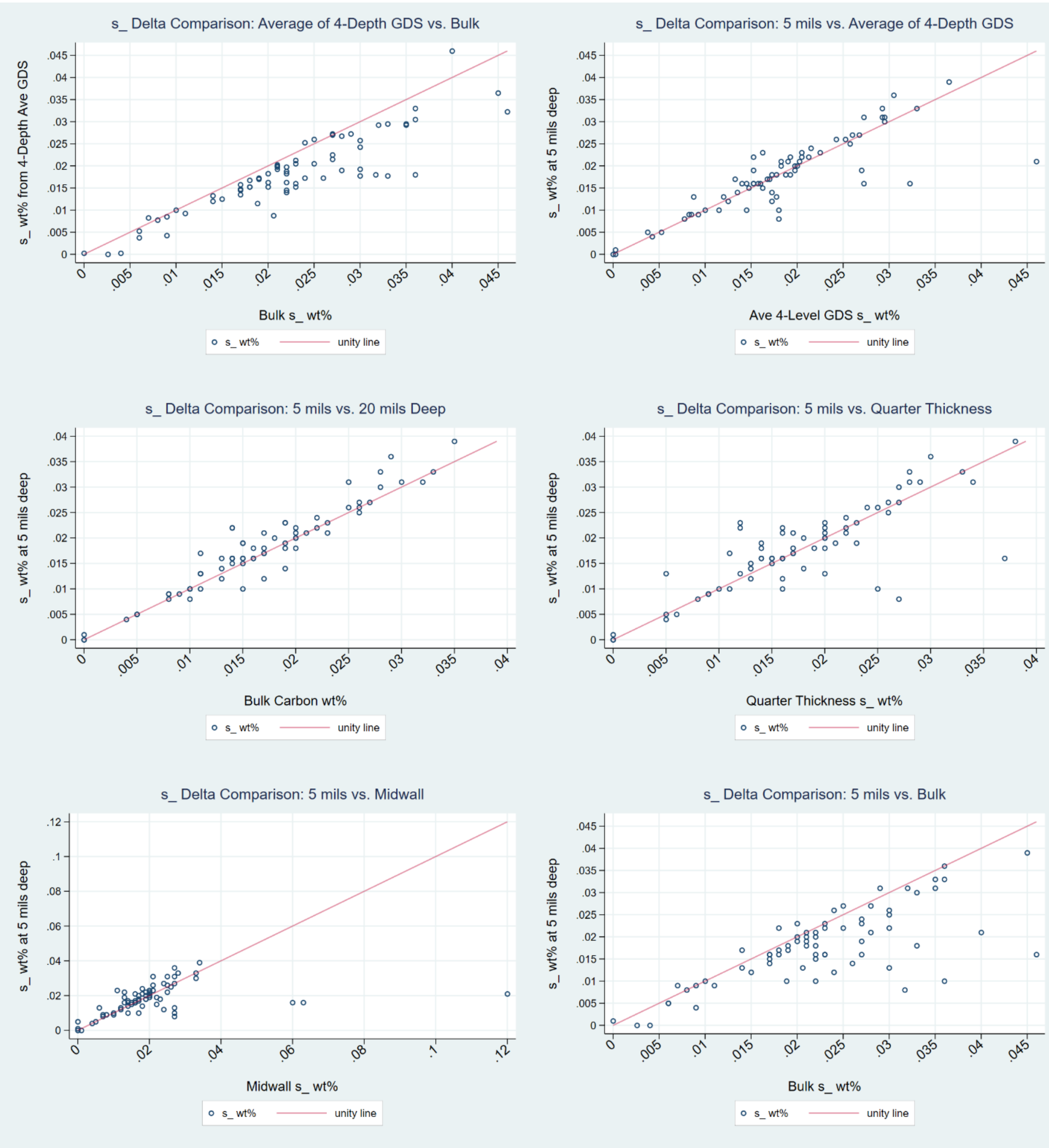

Silicon (Si)

The various depths, 4-depth average, and bulk Si chemistry weight percent values are consistent with each other. There is no substantive overall segregation from surface to bulk or midwall.

Figure 51. Silicon Weight Percent Comparisons by Depths and Bulk.

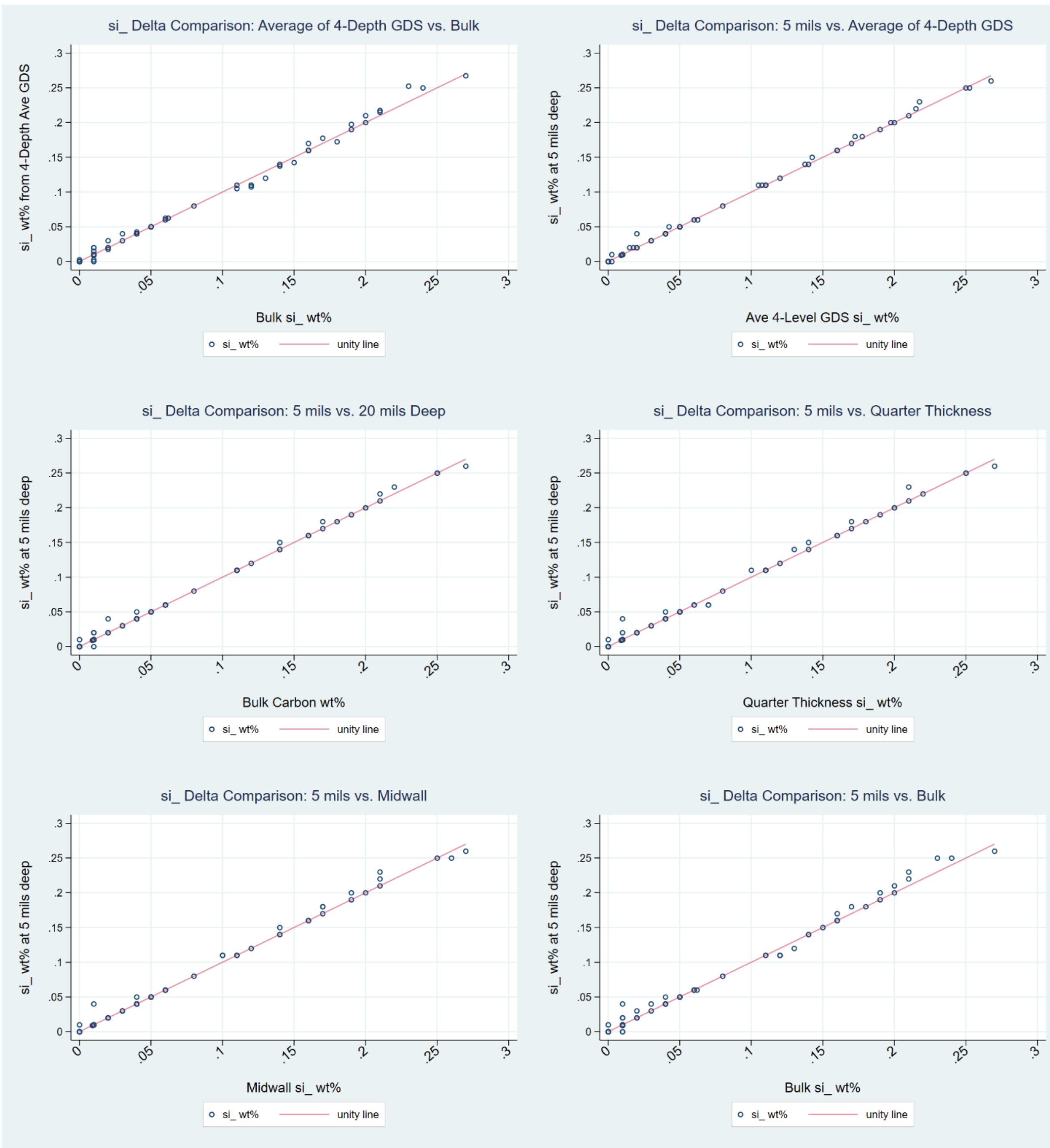

Titanium (Ti)

The various depths, 4-depth average, and bulk Ti chemistry weight percent values are consistent with each other. There is no substantive overall segregation from surface to bulk or midwall.

Figure 52. Titanium Weight Percent Comparisons by Depths and Bulk.

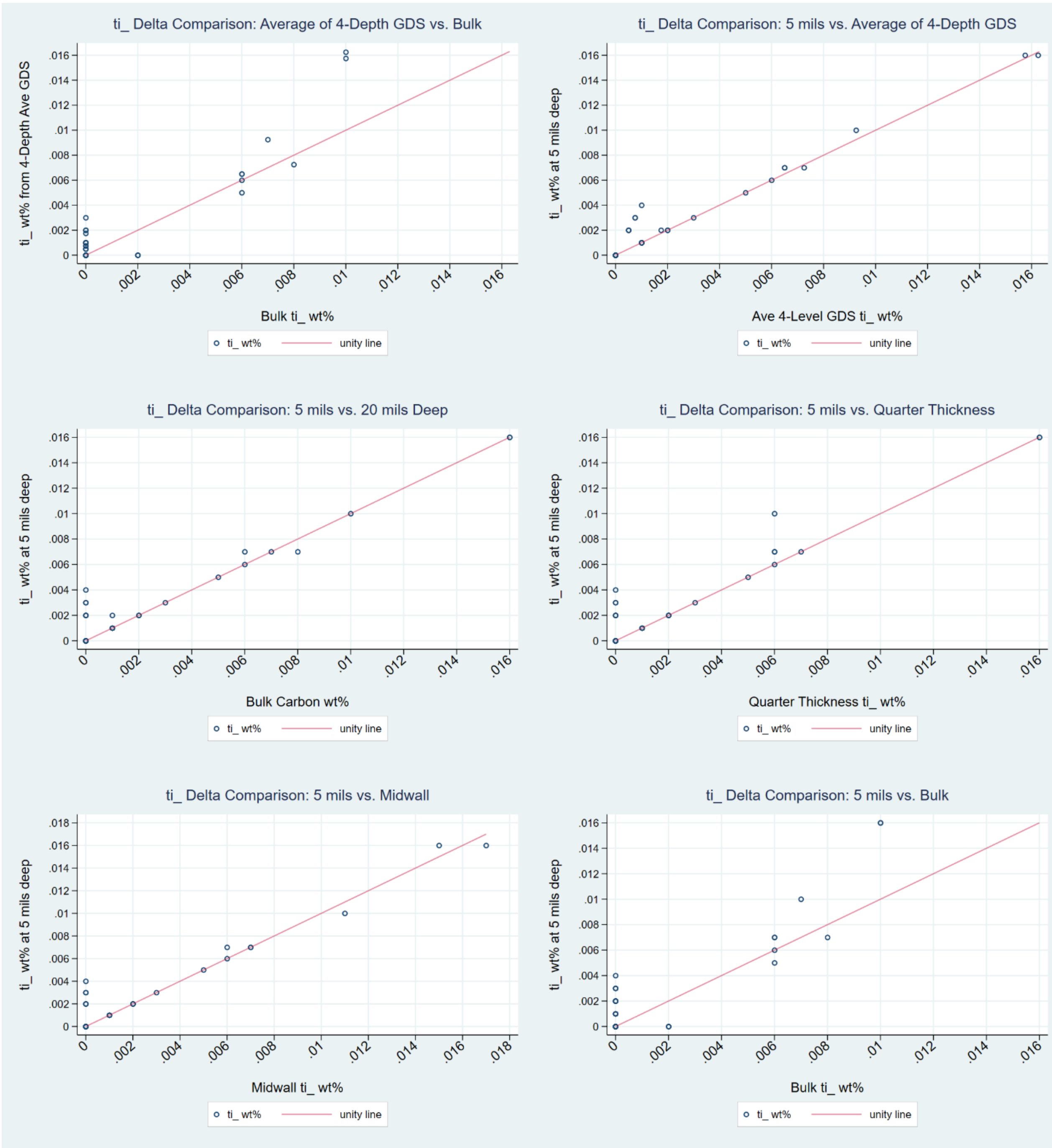

Vanadium (V)

The various depths, 4-depth average, and bulk V chemistry weight percent values are consistent with each other. There is no substantive overall segregation from surface to bulk or midwall.

Figure 53. Vanadium Weight Percent Comparisons by Depths and Bulk.

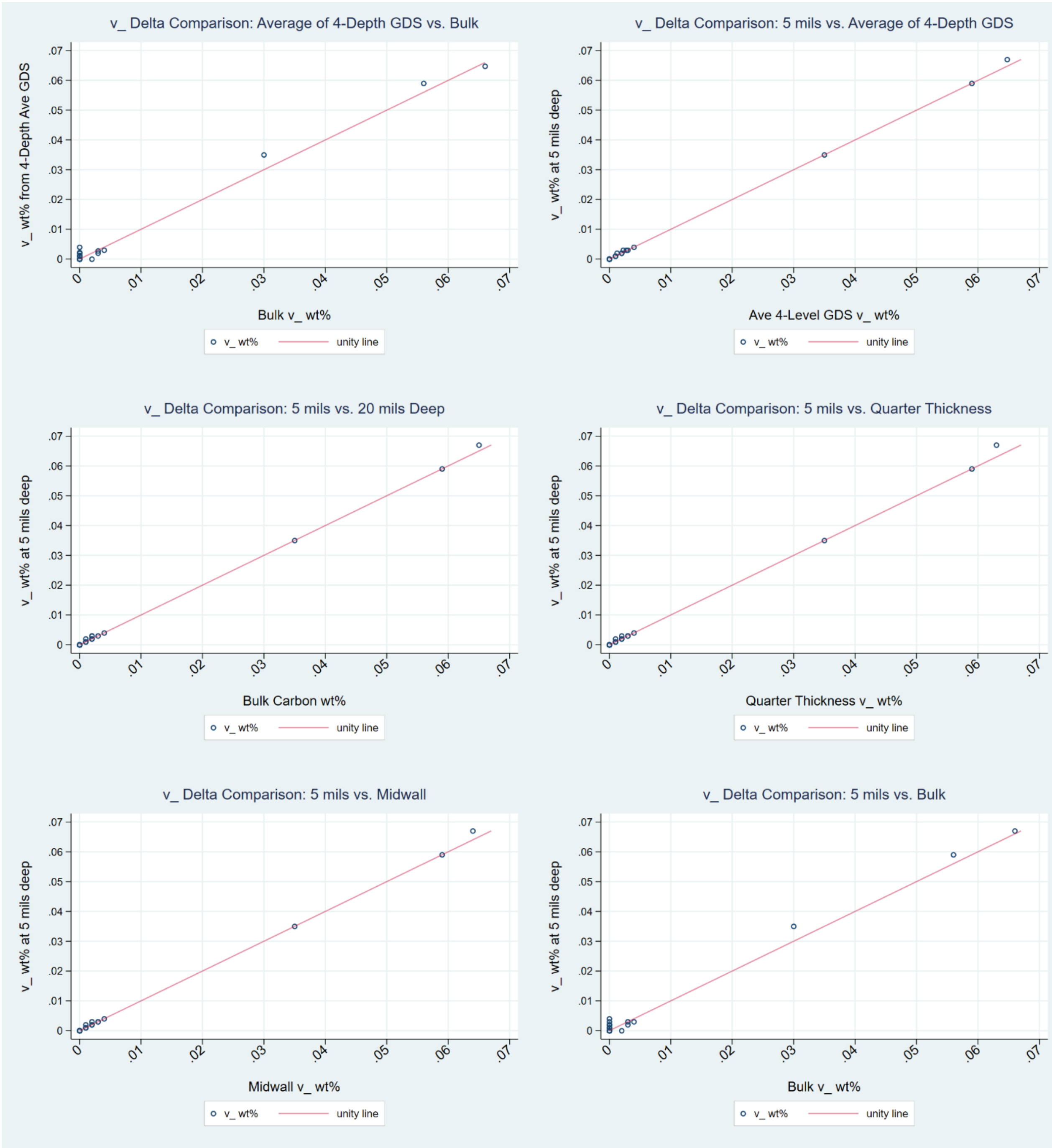

Chemistry Unity Plots by Element by Depth by Steel Type

The chemistry distribution by depth by steel types are shown for the elements in Figure 54 to Figure 74.

Most the elements do not exhibit segregation across the thickness in general as shown in the last section and the same holds true by steel type.

The main exception to this is carbon segregation by depth. Figure 56 is a histogram and density plot of carbon by steel type. The difference between the LIBS surface carbon and the bulk carbon levels is greatest negative for rimmed and capped steels. This is expected due to the centerline segregation of carbon in this steel type along the ingots which carries over to the produced pipe wall cross section. The killed and semi-killed steels do not show this trend and exhibit a difference between surface and bulk that is equally split between low and high sides and centered around a difference of zero.

Figure 57 is a box plot of all the seventy pipeline samples and shows that carbon values increase from 5 mils to 20 mills, to quarter thickness, and peak at the midwall. The average of the 4-depth composite is similar to the bulk levels and the LIBS carbon levels, which are taken on the outer surface of the sample with minimal material removal, are closest to the 5 mil values. The MMT grindings, which go deeper into the pipe wall, are closer to the 20 mil depth distribution for carbon levels.

Figure 58 shows that the carbon levels by steel type have different distributions by key depth points. The rimmed and capped steels have the highest centerline (midwall) levels due to the carbon segregation that accumulates in the midwall area during the steel boiling and rimming action. These steels even show segregation between the 20 mil depths and midwall.

The fully and semi-killed, more modern steels have a much more uniform carbon distribution, especially from 20 mil through to the midwall, unlike the rimmed and capped steels.

As discussed earlier, this carbon distribution can explain how the rimmed and capped steels help to mitigate an NDE technology that was reading higher yield strengths due to other factors on the pipe outer wall, such as the cold work effect and refined grain sizes of non-seamless pipe and HSLA steels, respectively. Both of these factors increase the outer or surface yield strengths vs. the bulk or midwall.

Figure 59 shows the general trend of lower carbon percent in all steel types between the 5 mil and 20 mil depths. Figure 61 shows similarly for between 5 mils and the bulk. However, Figure 60 shows that when one compares the 20 mil depth to the bulk, those differences are negligible for the fully and semi killed steels, while still present for the rimmed and capped steels due to the much more significant centerline carbon segregation.

Aluminum (Al)

Figure 54. Aluminum Weight Percent Comparisons at 5 mils vs. 20 mils by Steel Type.

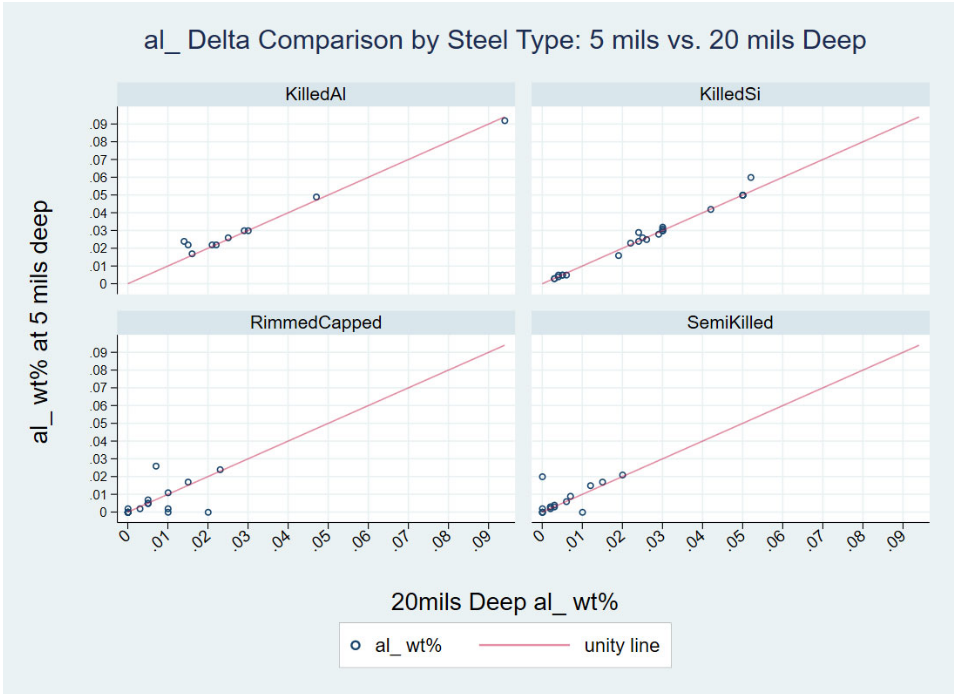

Boron (Br)

Figure 55. Boron Weight Percent Comparisons at 5 mils vs. 20 mils by Steel Type.

Carbon (C)

Figure 56. Carbon Weight Percent LIBS Surface vs. Bulk by Steel Type.

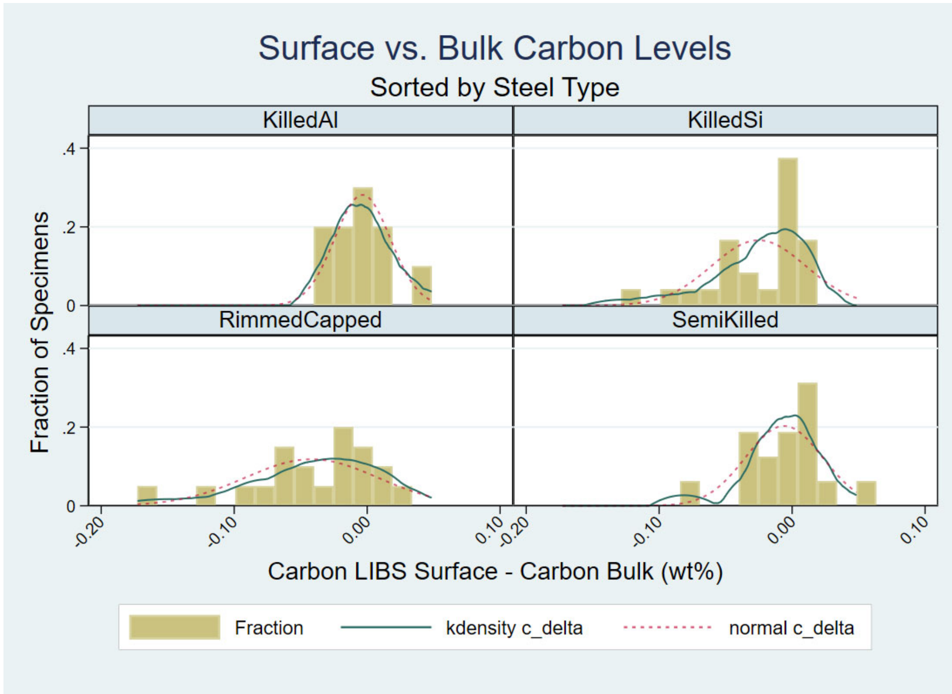

Figure 57. Carbon Weight Percent by Depth of Wall and Technique.

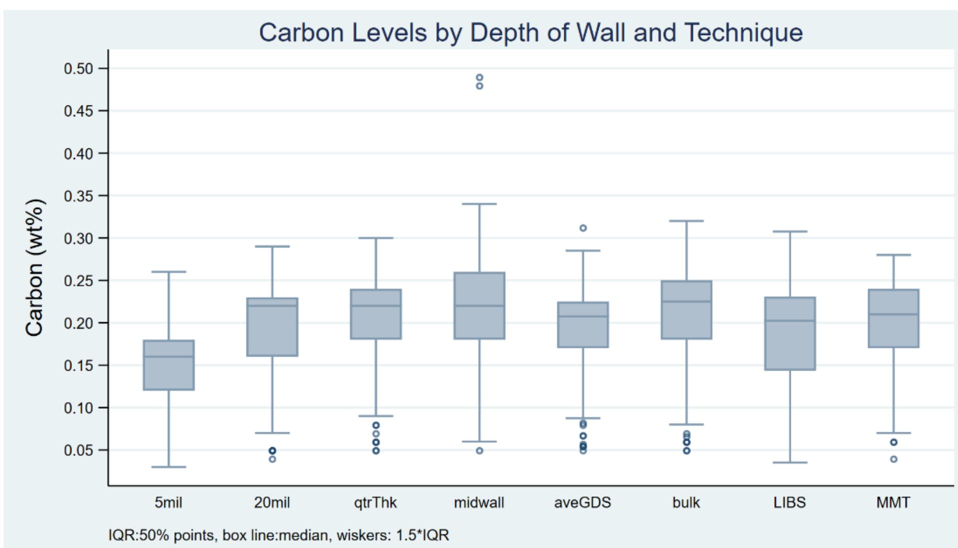

Figure 58. Carbon Weight Percent by Depth of Wall, Technique, and Steel Type.

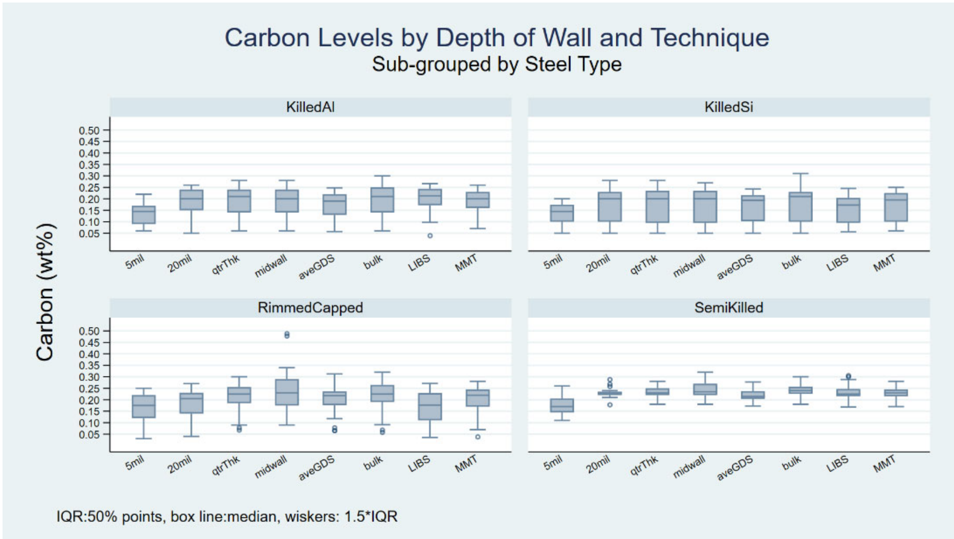

Figure 59. Carbon Weight Percent Comparisons at 5 mils vs. 20 mils by Steel Type.

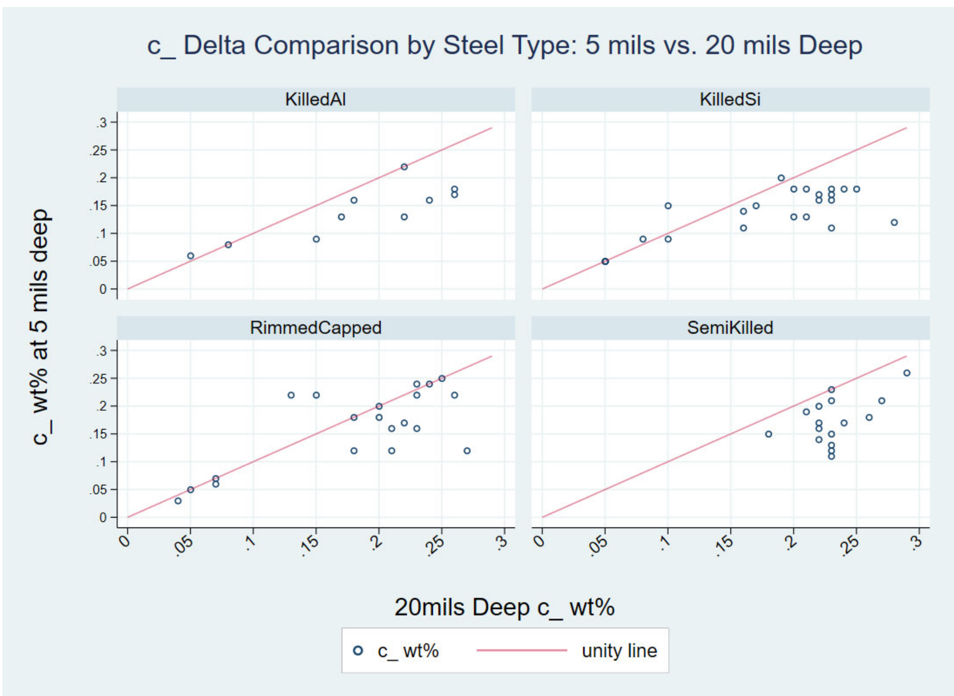

Figure 60. Carbon Weight Percent Comparisons at 20 mils vs. Bulk by Steel Type.

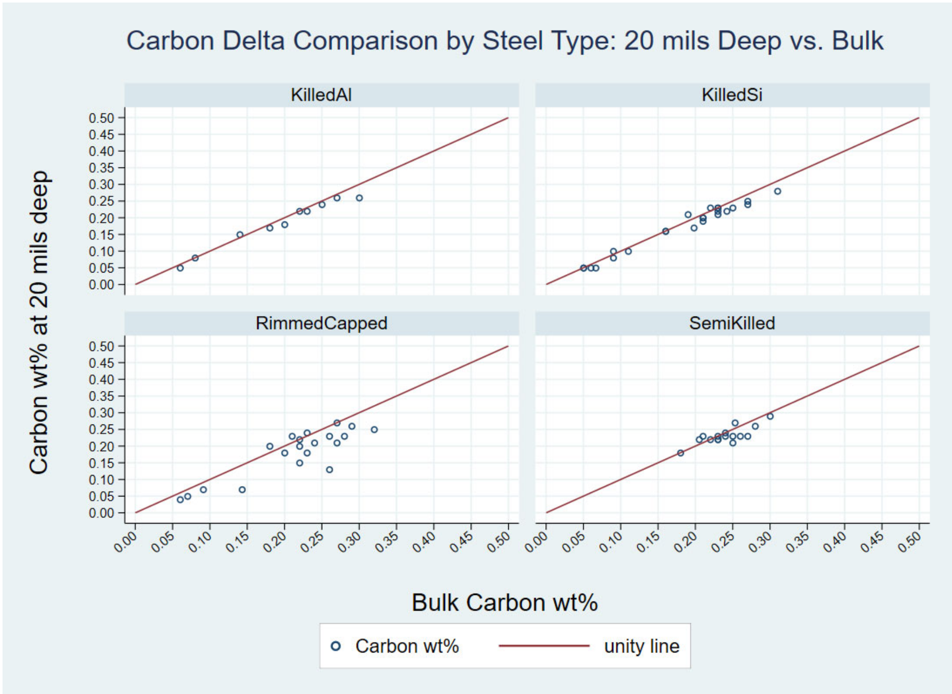

Figure 61. Carbon Weight Percent Comparisons at 5 mils vs. Bulk by Steel Type.

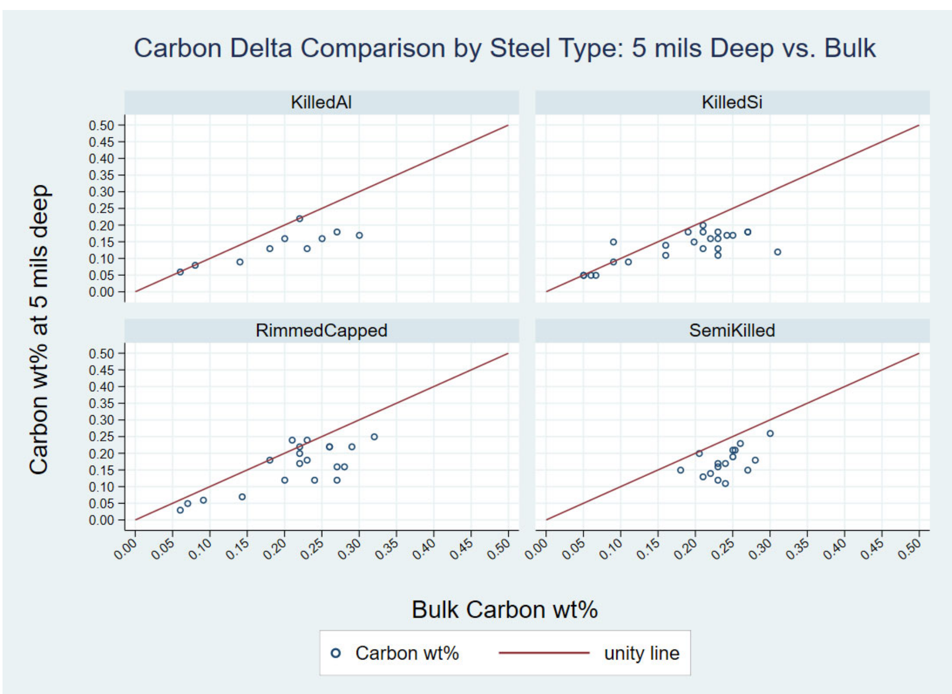

Chromium (Cr)

Figure 62. Chromium Weight Percent Comparisons at 5 mils vs. 20 mils by Steel Type.

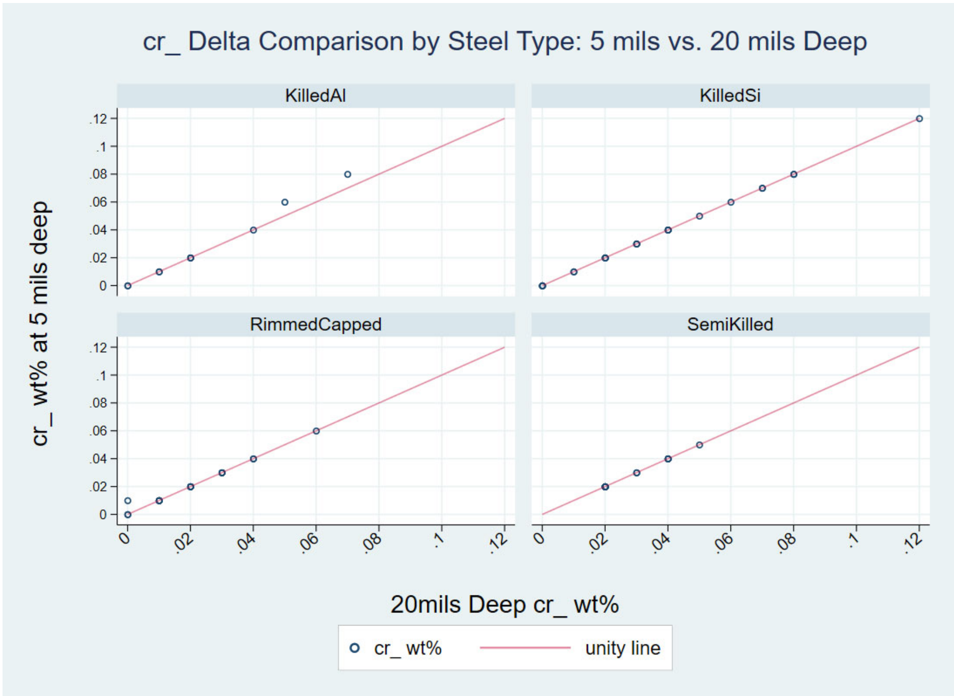

Copper (Cu)

Figure 63. Copper Weight Percent Comparisons at 5 mils vs. 20 mils by Steel Type.

Manganese (Mn)

Figure 64. Manganese Weight Percent LIBS Surface vs. Bulk by Steel Type.

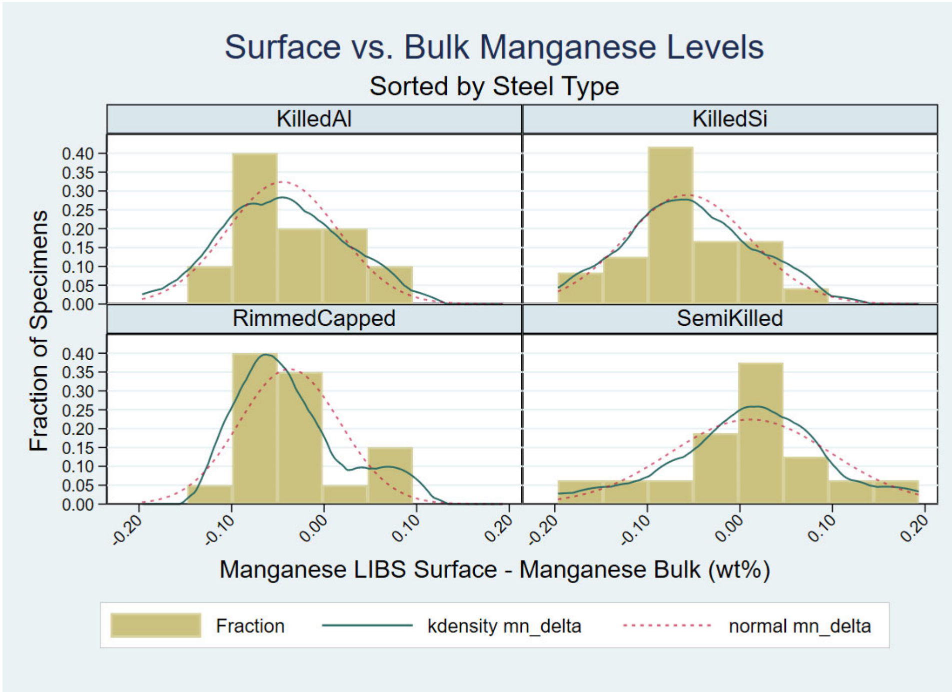

Figure 65. Manganese Weight Percent Comparisons at 5 mils vs. 20 mils by Steel Type.

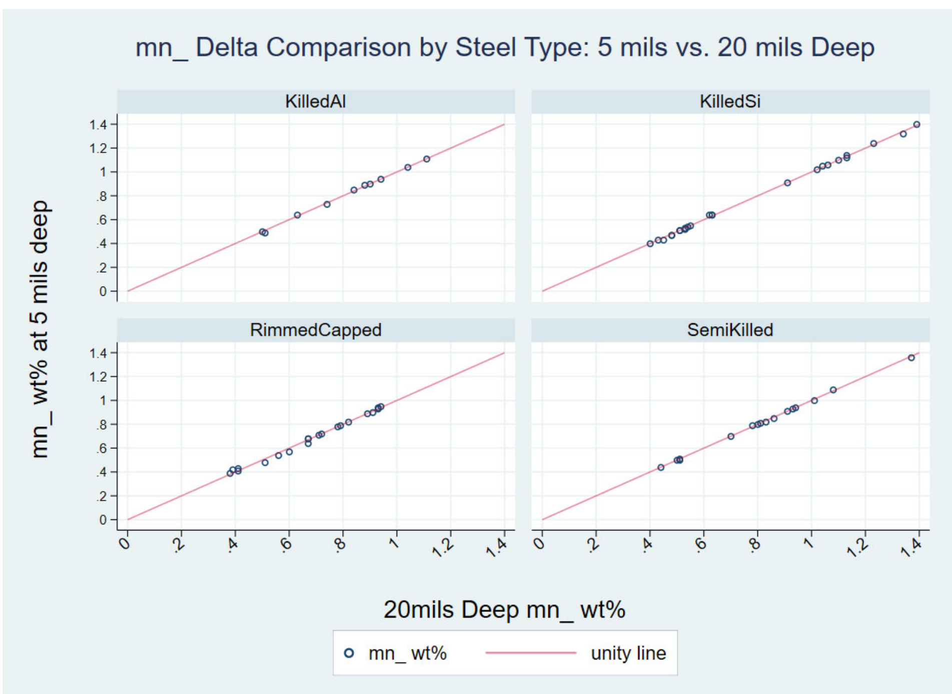

Molybdenum (Mo)

Figure 66. Molybdenum Weight Percent Comparisons at 5 mils vs. 20 mils by Steel Type.

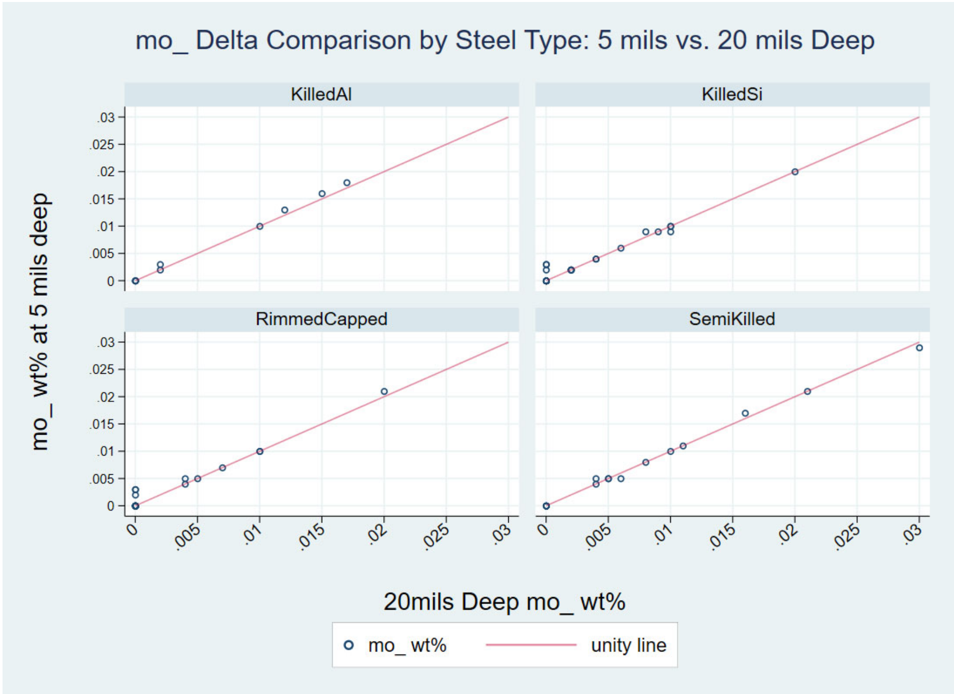

Nitrogen (N)

Figure 67. Nitrogen Weight Percent Comparisons at 5 mils vs. 20 mils by Steel Type.

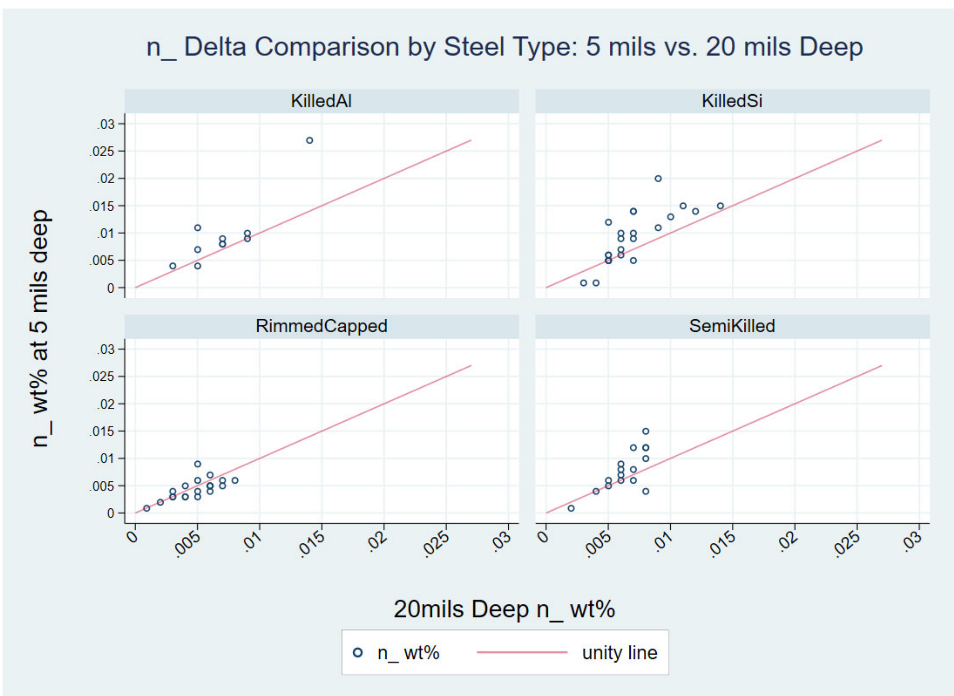

Niobium (Nb)

Figure 68. Niobium Weight Percent Comparisons at 5 mils vs. 20 mils by Steel Type.

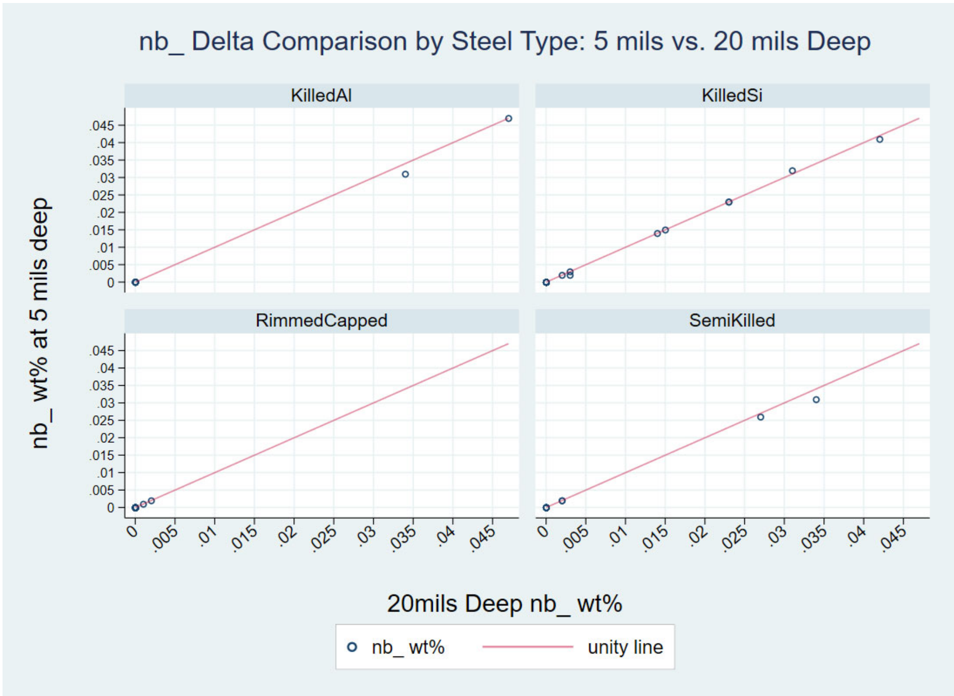

Nickel (Ni)

Figure 69. Nickel Weight Percent Comparisons at 5 mils vs. 20 mils by Steel Type.

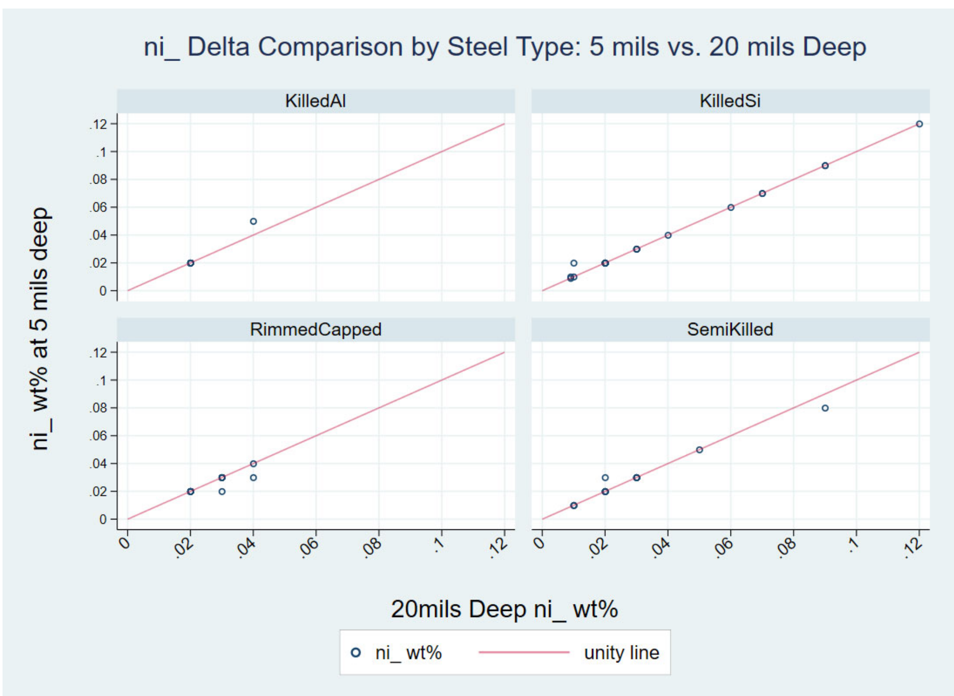

Phosphorus (P)

Figure 70. Phosphorus Weight Percent Comparisons at 5 mils vs. 20 mils by Steel Type.

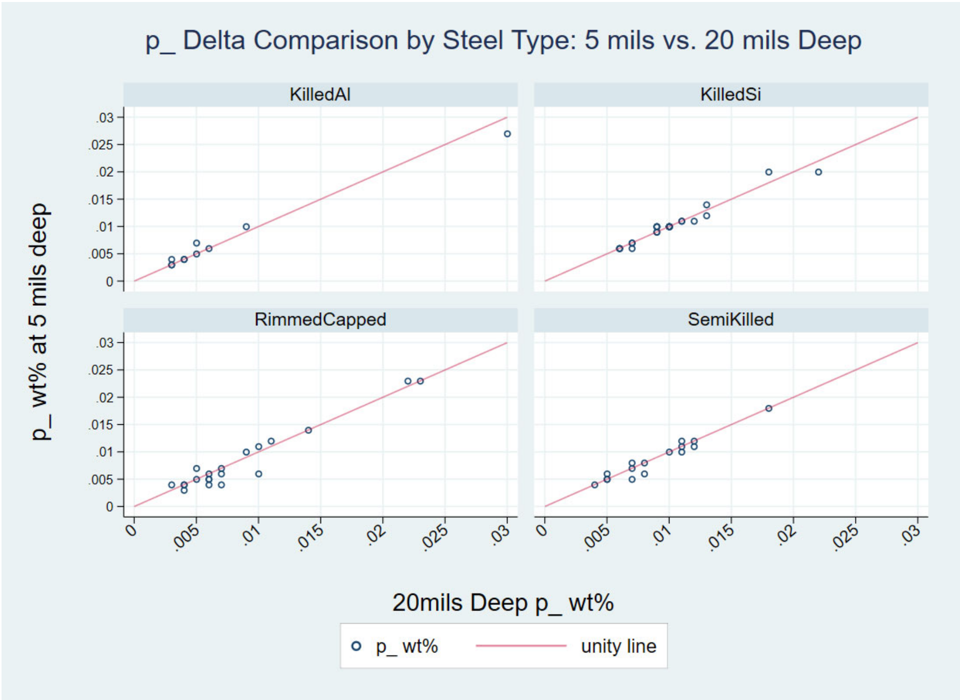

Sulfur (S)

Figure 71. Sulfur Weight Percent Comparisons at 5 mils vs. 20 mils by Steel Type.

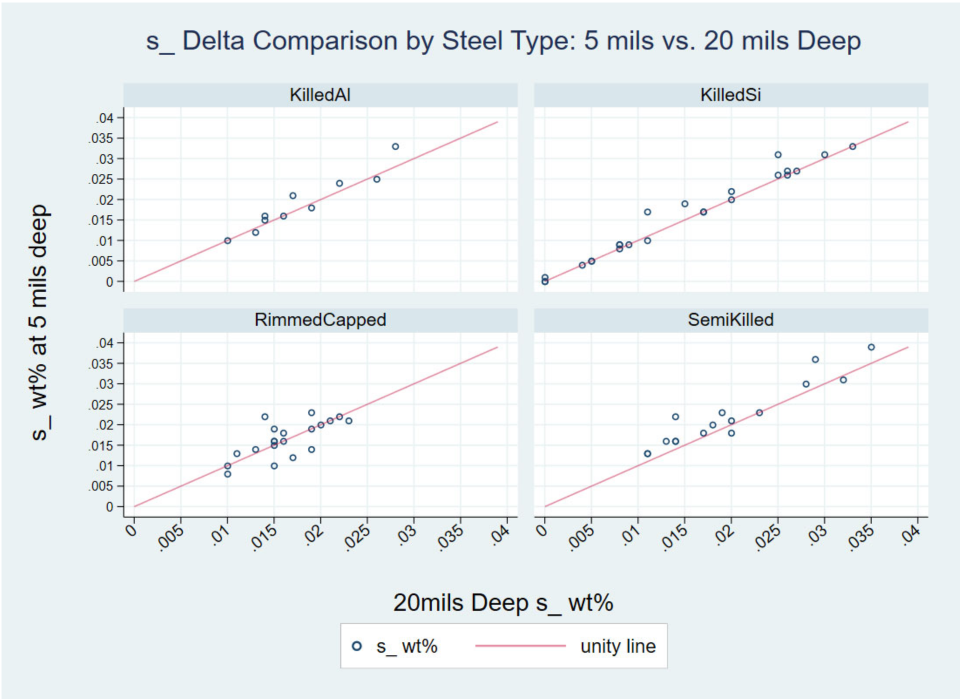

Silicon (Si)

Figure 72. Silicon Weight Percent Comparisons at 5 mils vs. 20 mils by Steel Type.

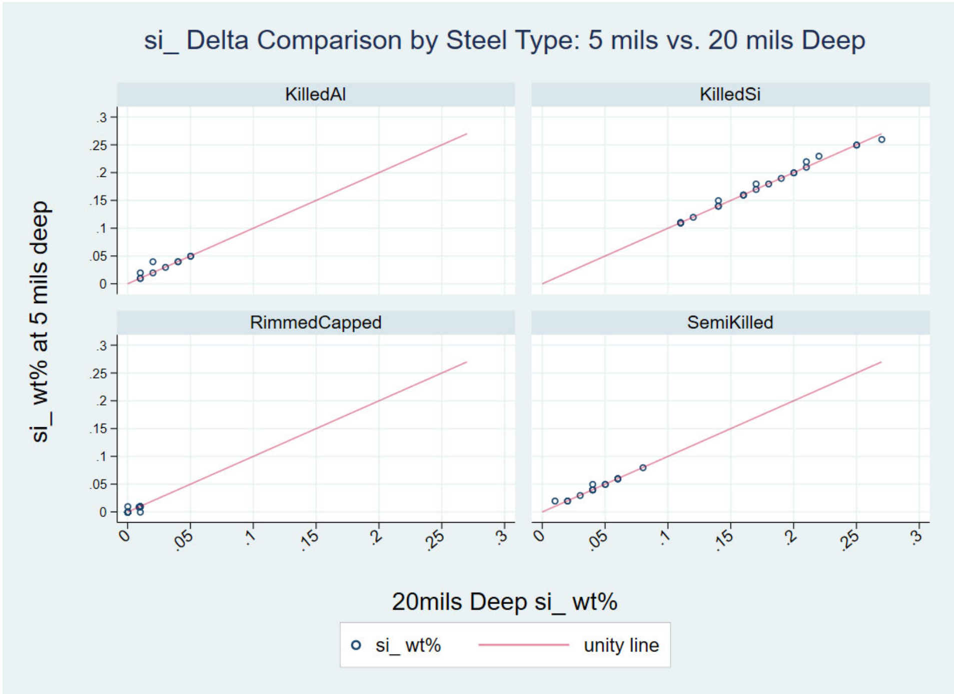

Titanium (Ti)

Figure 73. Titanium Weight Percent Comparisons at 5 mils vs. 20 mils by Steel Type.

Vanadium (V)

Figure 74. Vanadium Weight Percent Comparisons at 5 mils vs. 20 mils by Steel Type.

Chemistry Kernel Density Overlays by Element by Depth/Technique

The chemistry kernel density overlays by element in Figure 75 to Figure 77 provide similar information as the unity plots in the last section. The same trends can be seen, but distribution features such as unimodal or bimodal are evident as well.

The carbon distribution in the third panel of Figure 75 is noteworthy. As was discussed in the last section, the lower surface carbon levels of the 5 mil depth can be seen to be generally lower (curve is shifted to the right of the others).

Aluminum (Al), Boron (Br), Carbon (C), Chromium (Cr), Copper (Cu), and Manganese (Mn)

Figure 75. Chemistry Kernel Density Overlays by Element by Depth/Technique.

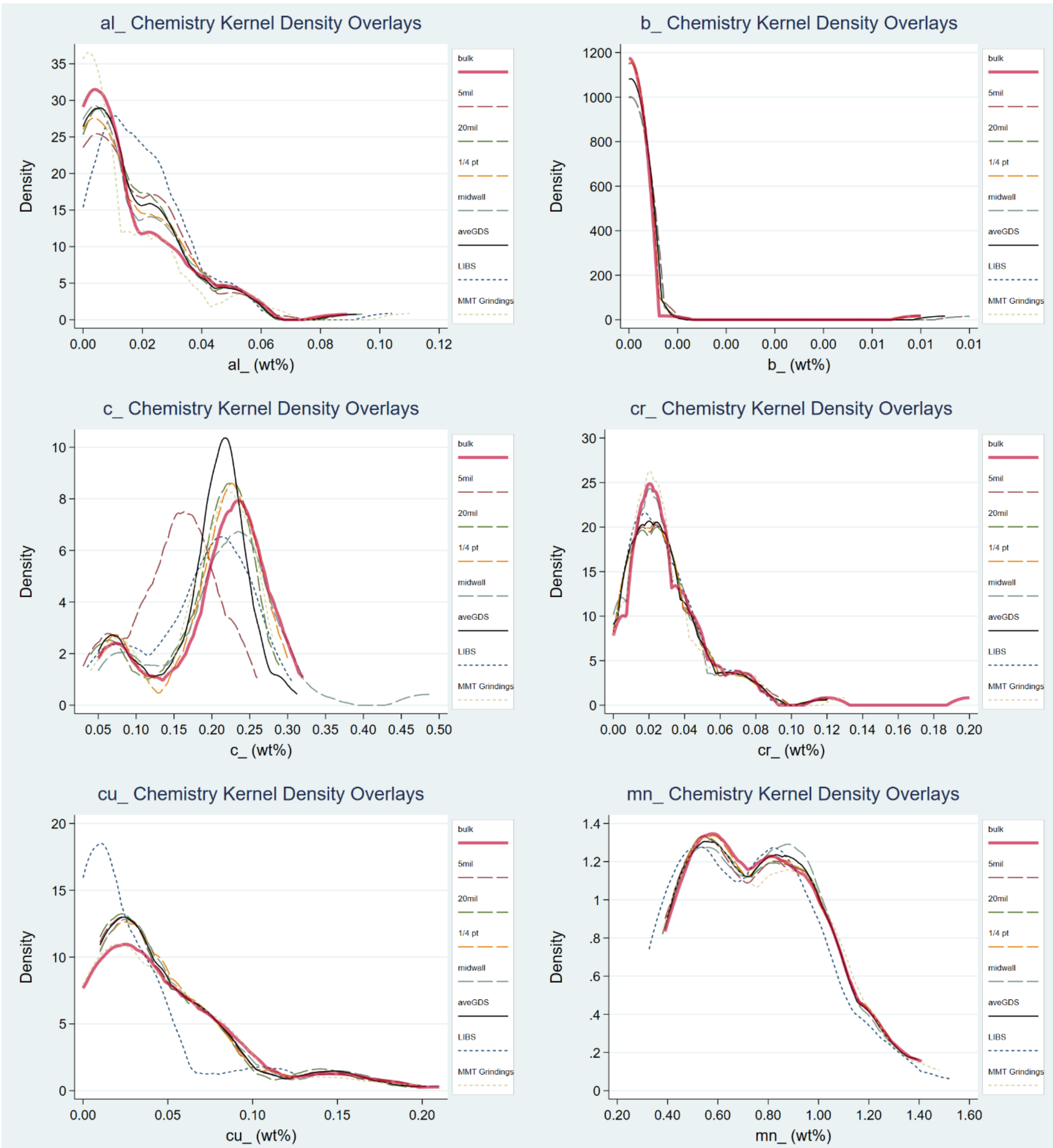

Molybdenum (Mo), Nitrogen (N), Niobium (Nb), Nickel (Ni), Phosphorus (P), and Sulfur (S)

Figure 76. Chemistry Kernel Density Overlays by Element by Depth/Technique.

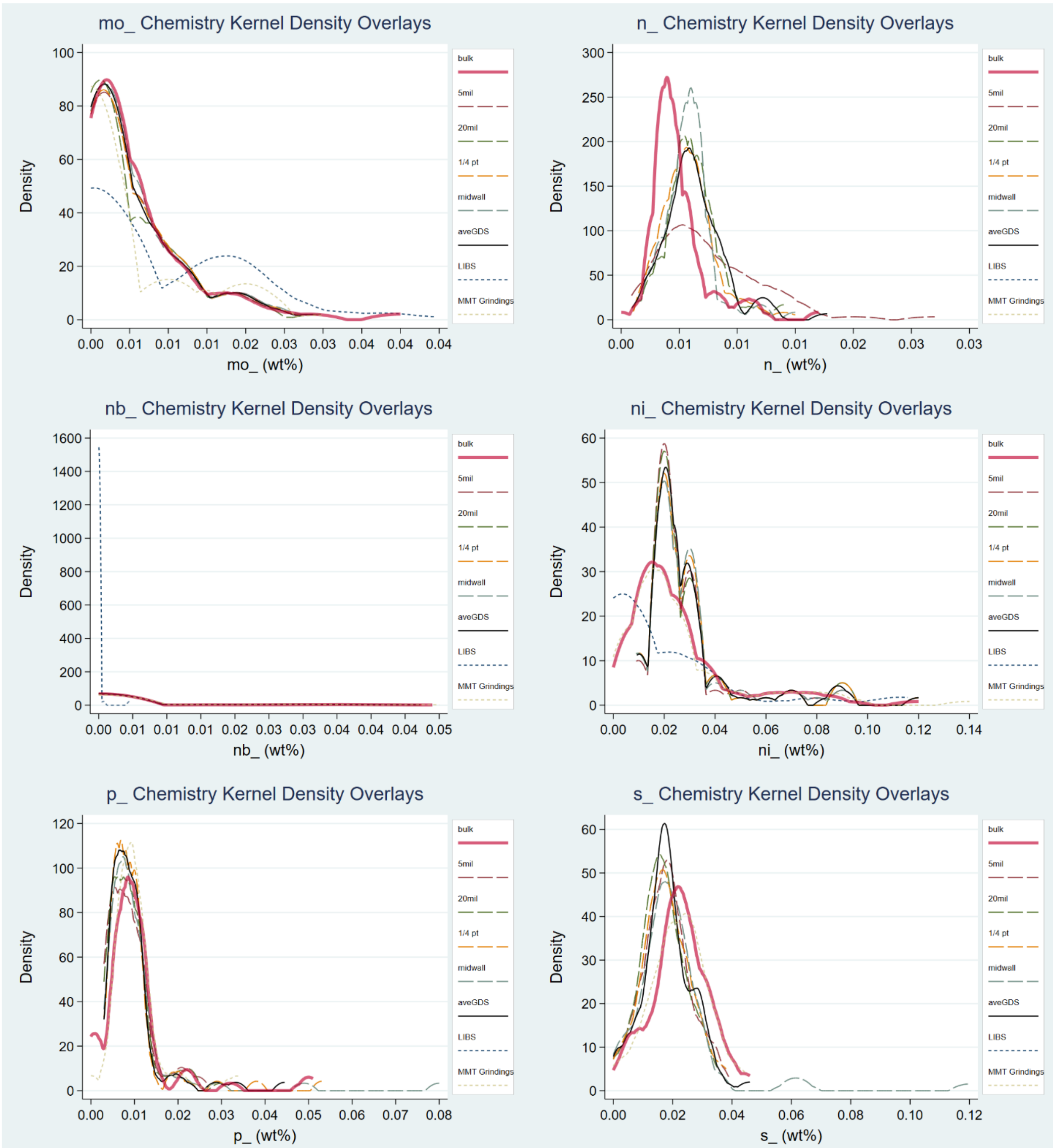

Silicon (Si), Titanium (Ti), and Vanadium (V)

Figure 77. Chemistry Kernel Density Overlays by Element by Depth/Technique.

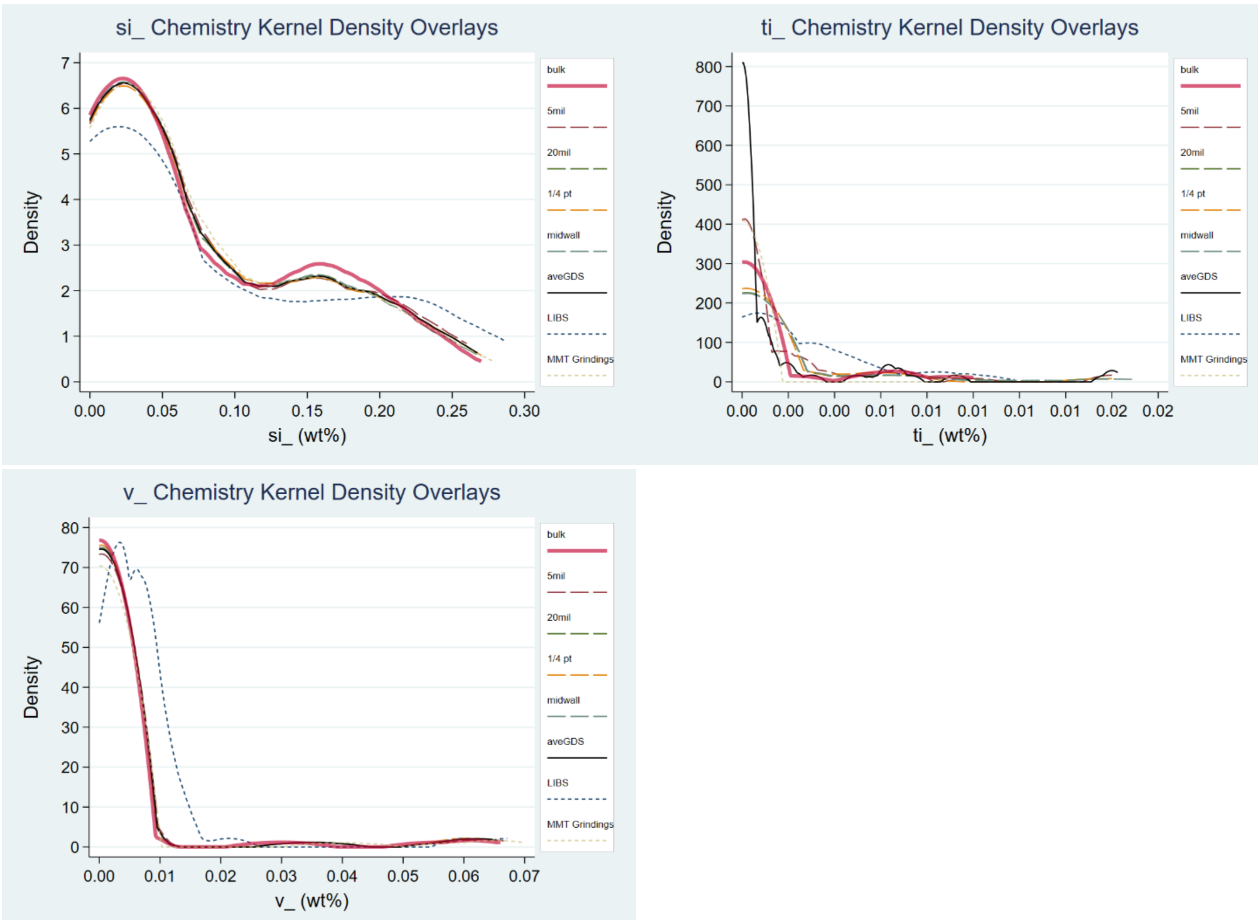

Chapter 4: Material Toughness (Supplemental Section)

4.1 Overview

This section of the report is provided as a supplemental section with the hope that the data provided and limited discussion will be helpful for researchers and technology developers moving forward as they attempt to develop and validate NDE technology to determine steel toughness in the field without cutout and testing.

A subset of 30 of the 70 pipeline samples had extensive Charpy V-notch (CVN) toughness testing completed on them. The data for these is provided in Appendix B in the form of a column database in Excel.

This section plots the results of the testing which included CVN absorbed energy, lateral expansion, and percent shear over various temperatures. Enough temperatures were performed to establish the CVN upper shelf energy level.

Frontics also tested these 30 pipeline samples in the form of coupons for KIC testing. Those results are presented in Attachment #4 but are not compared directly to these since the testing direction and mode are different between the Frontics tests and the CVN tests.

In general, the CVN energy went down when temperature was reduced and phosphorous and sulfur levels increased for non-HSLA steels.

The research team feels that this Chapter will provide an excellent foundation for future research and development as new field-ready and non-destructive toughness test methods are developed.

Figure 78 to Figure 89 are presented in the remainder of this supplemental chapter without further comment.

Absorbed Energy, Lateral Expansion, and Percent Shear Overlay

Figure 78. Charpy Absorbed Energy, Lateral Expansion, and % Shear Overlay.

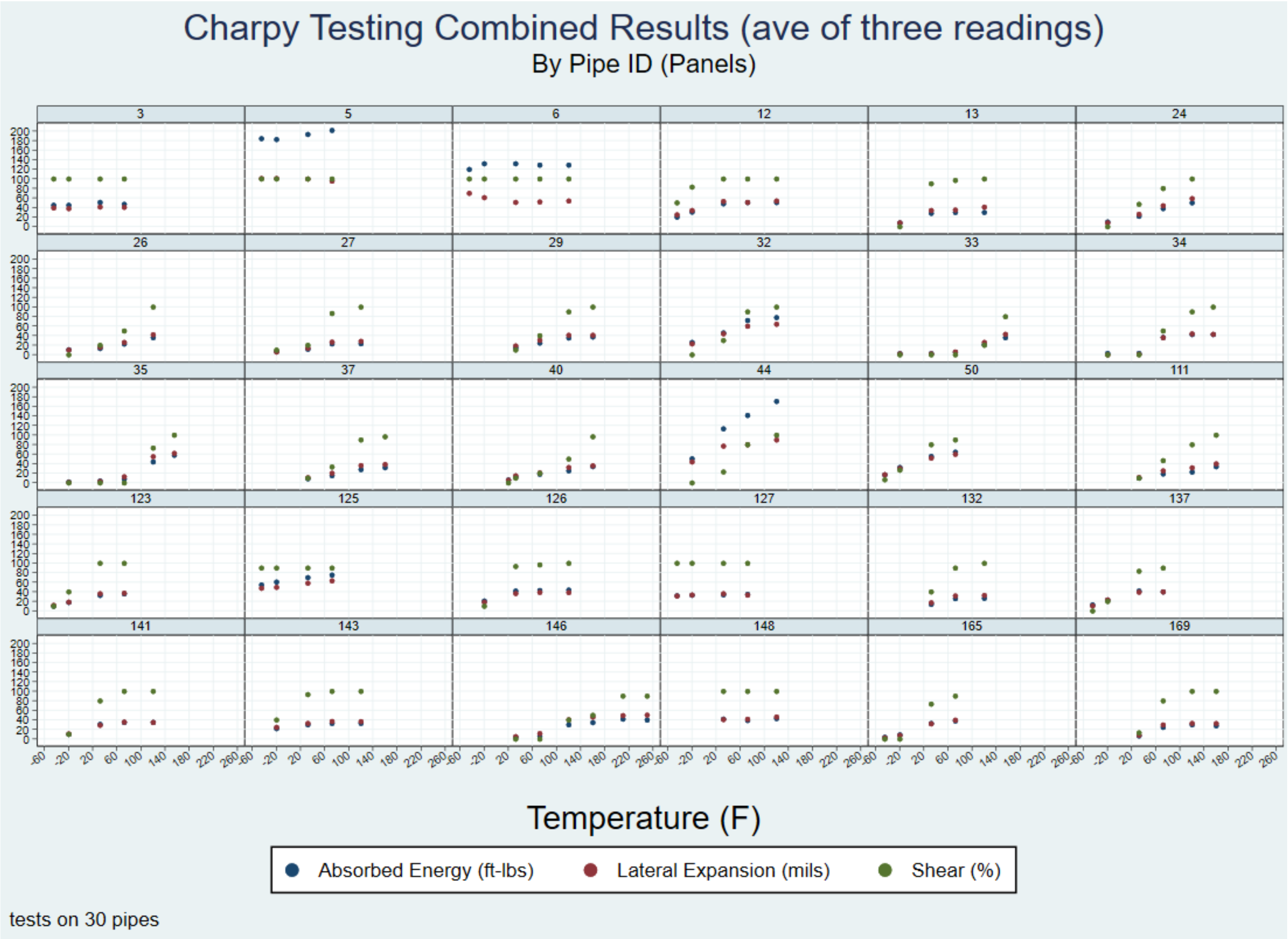

Matrix Plot of Upper Shelf Energy vs. Key Variables

Figure 79. Matrix Plot of Charpy Upper Shelf Energy vs. Key Variables.

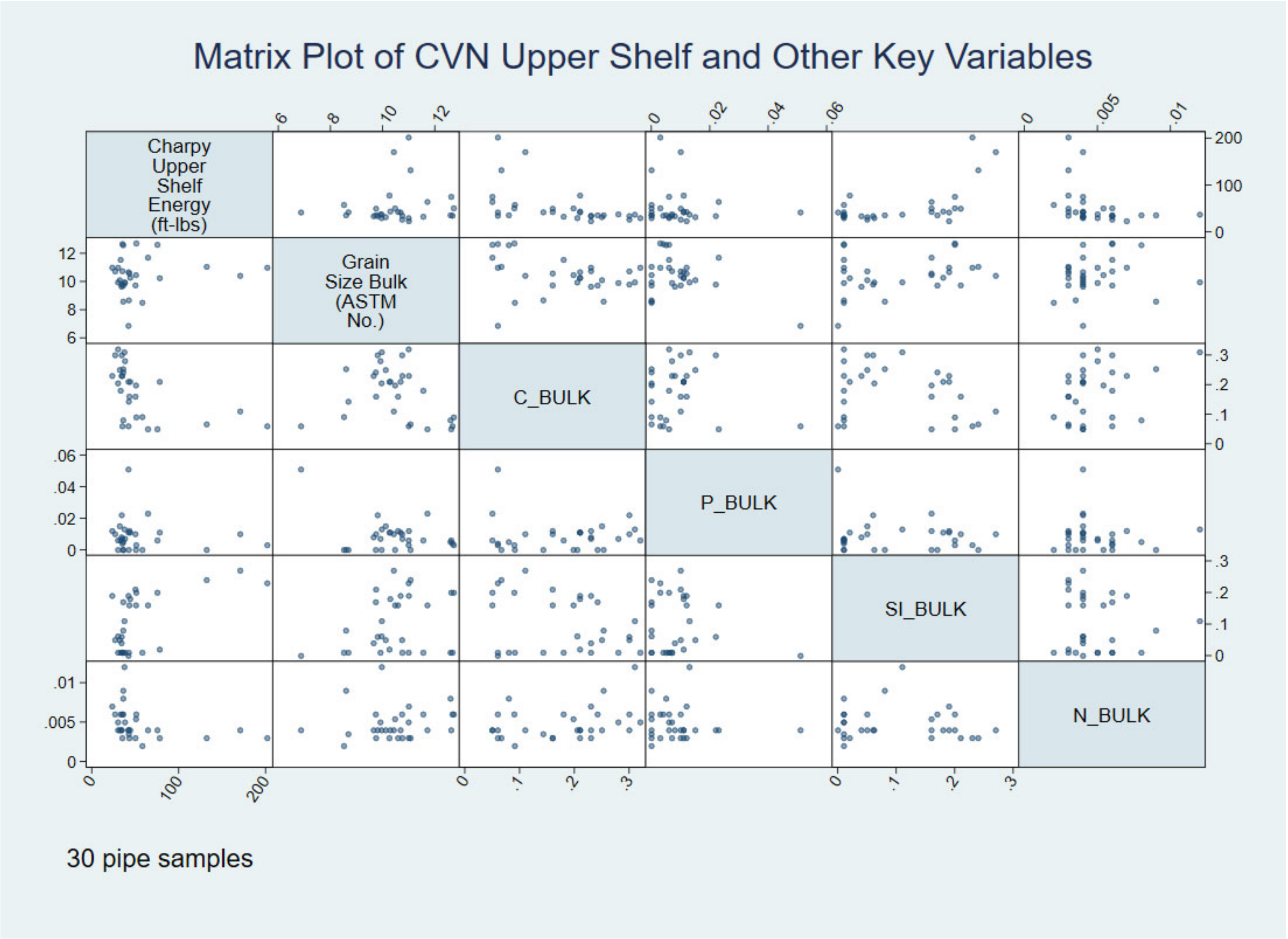

Mean Upper Shelf Energy by Pipe Chemistry Grade

Figure 80. Charpy Mean Upper Shelf Energy by Pipe Chemistry Grade.

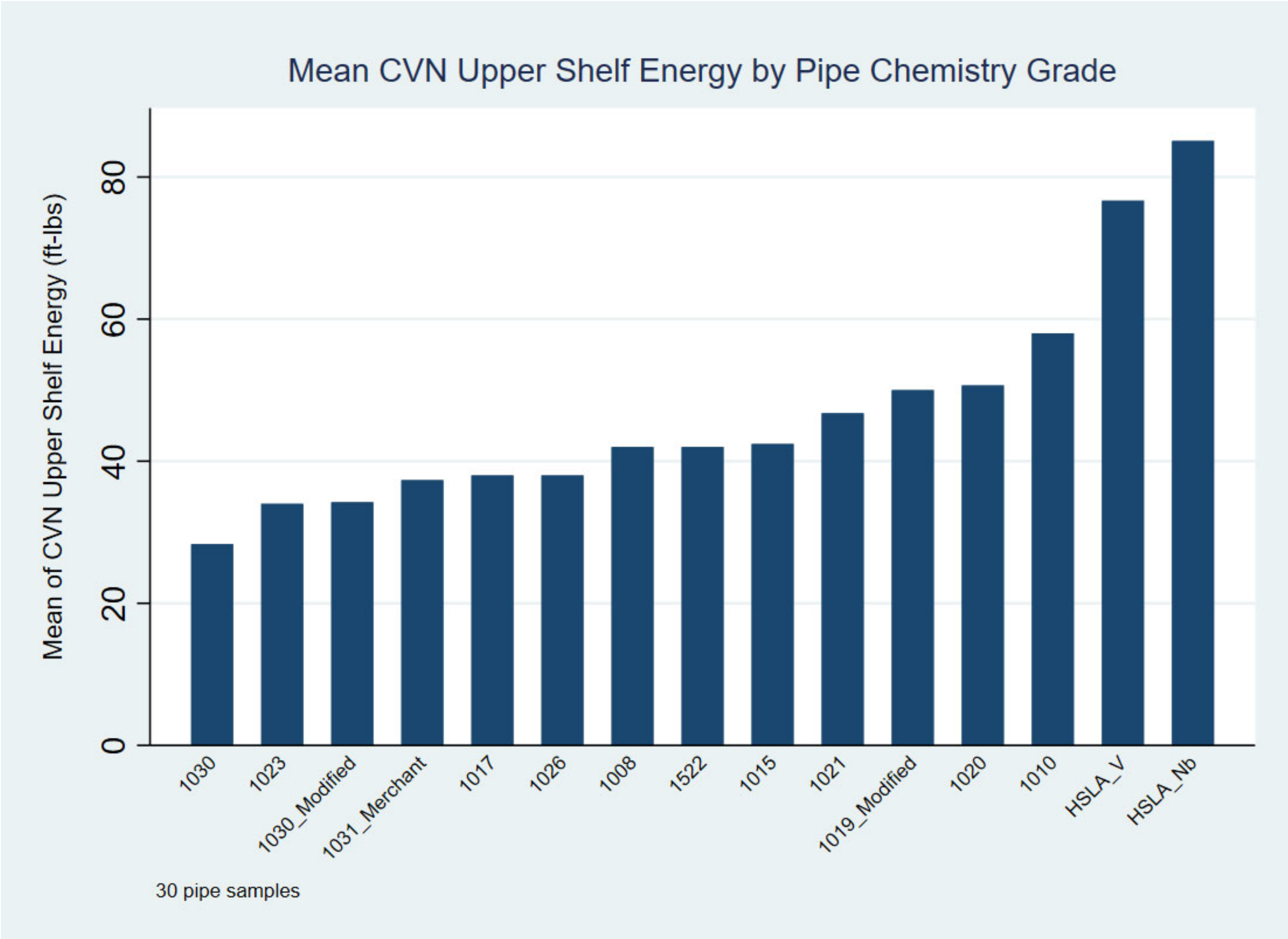

Mean Upper Shelf Energy by Pipe Steel Type

Figure 81. Charpy Mean Upper Shelf Energy by Pipe Steel Type.

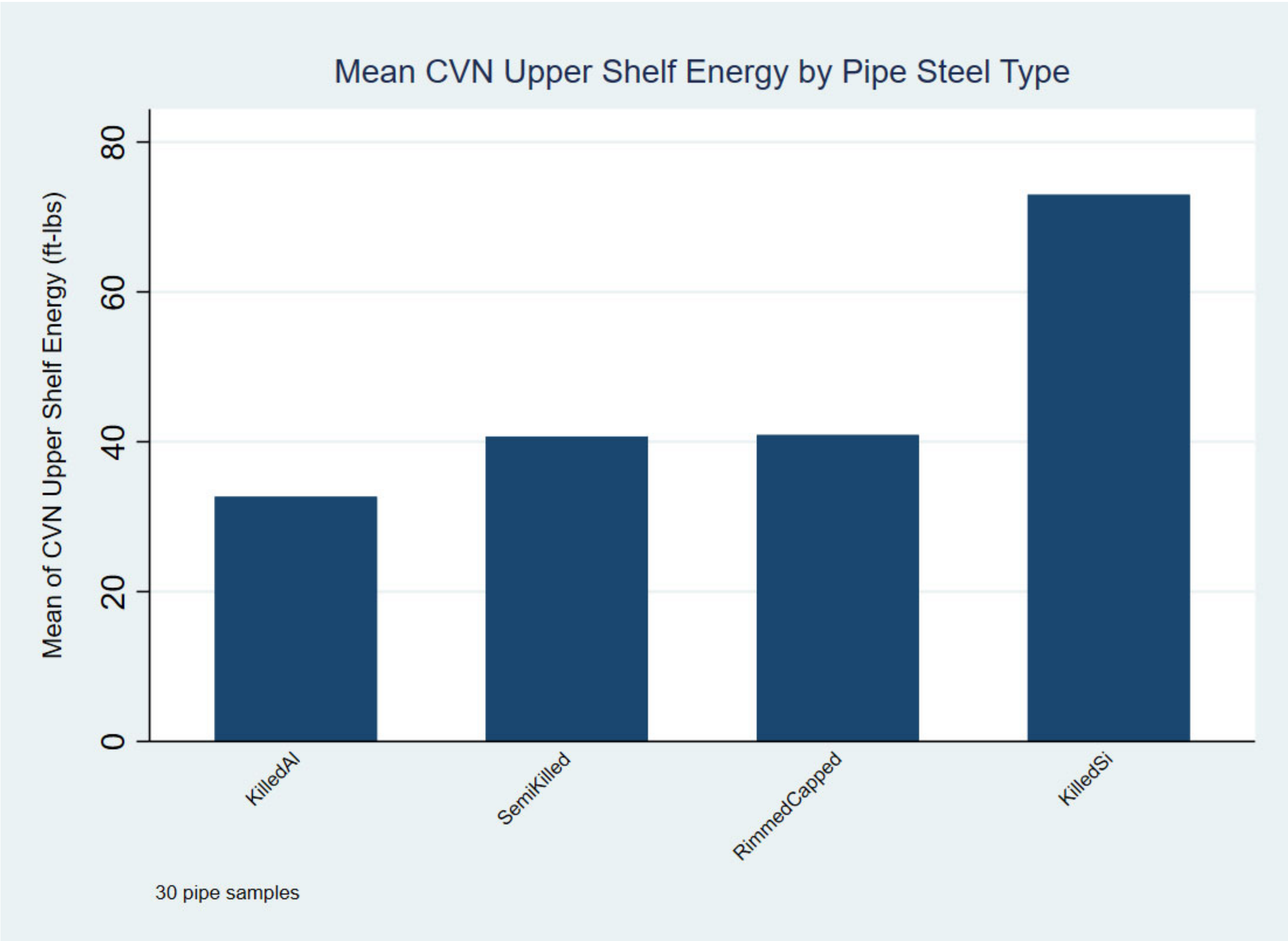

Mean Upper Shelf Energy by Pipe Grade and Steel Type

Figure 82. Mean CVN Upper Shelf Energy by Pipe Grade and Steel Type.

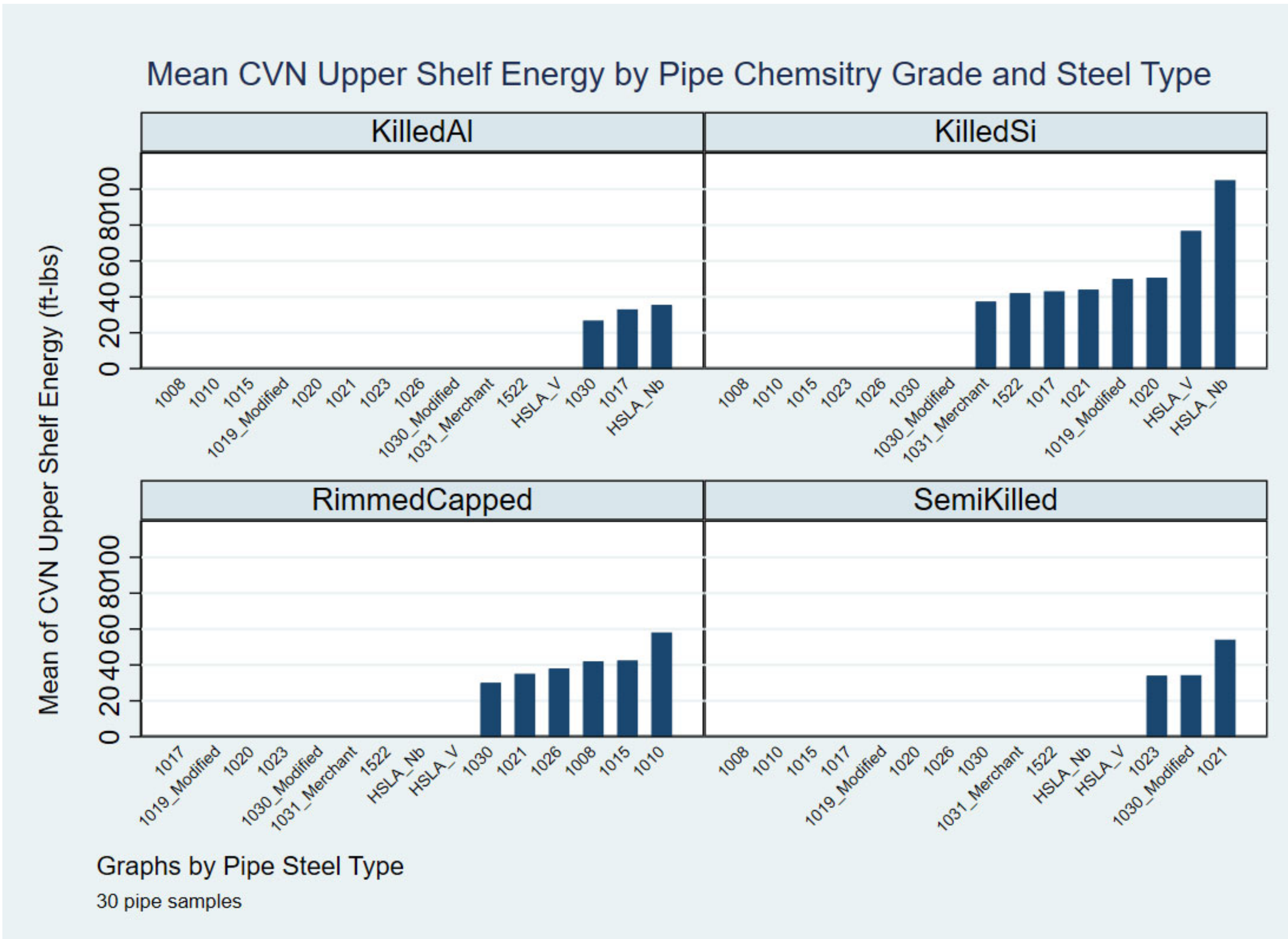

4.2 Effect of Carbon, Temperature, and Grade

Absorbed Energy by Carbon Level and HSLA vs. Non-HSLA Grade

Figure 83. Charpy Absorbed Energy by Carbon Level and HSLA vs. Non-HSLA Grade.

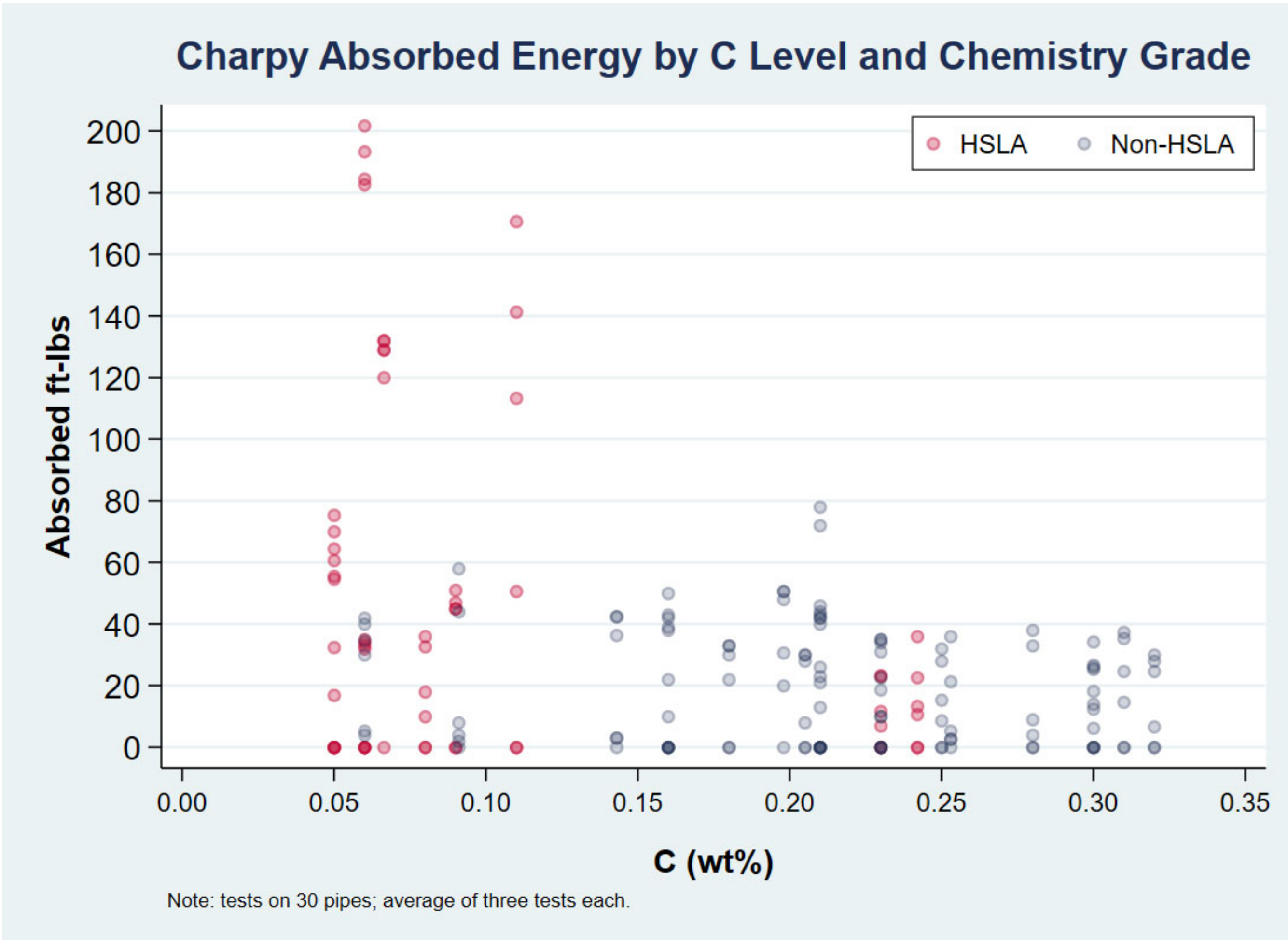

Absorbed Energy by Carbon Level and Temperature

Figure 84. Charpy Absorbed Energy by Carbon Level and Temperature.

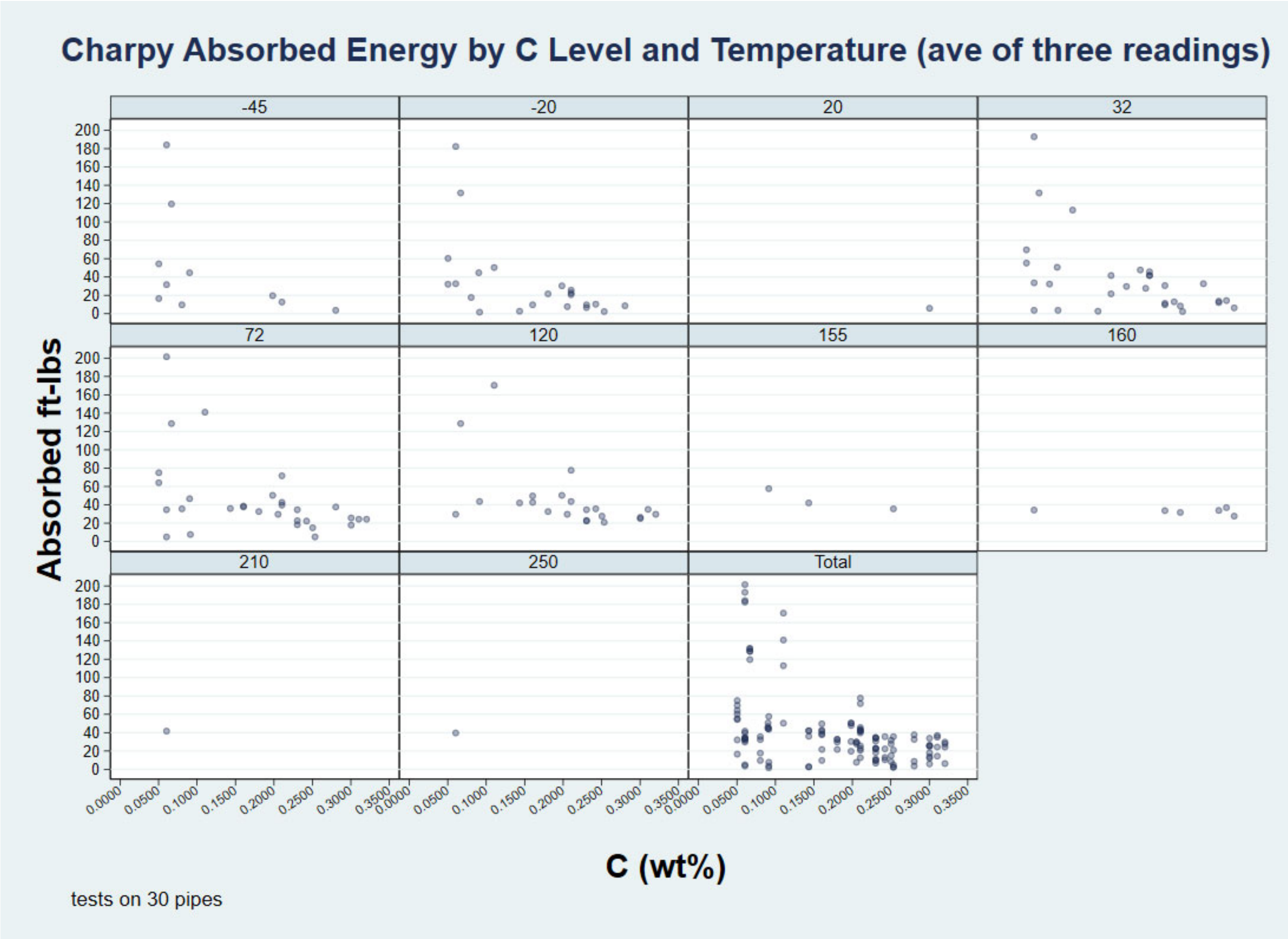

Absorbed Upper Shelf Energy by Carbon Level and HSLA vs. Non-HSLA Grade

Figure 85. Absorbed Upper Shelf Energy by C Level and HSLA vs. Non-HSLA Grade.

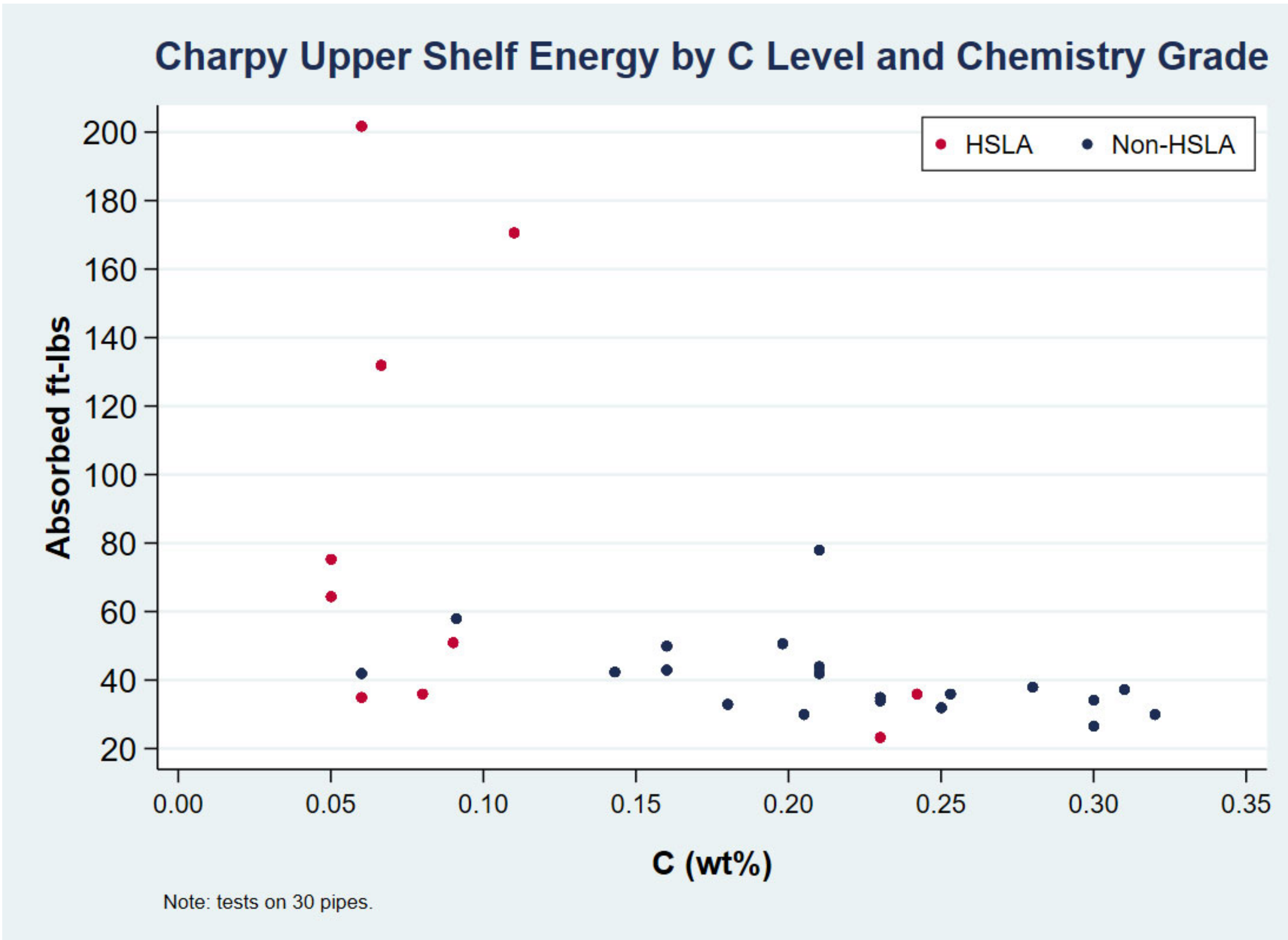

4.3 Effect of Manganese and Temperature on Toughness

Figure 86. Charpy Absorbed Energy by Manganese Level and Temperature.

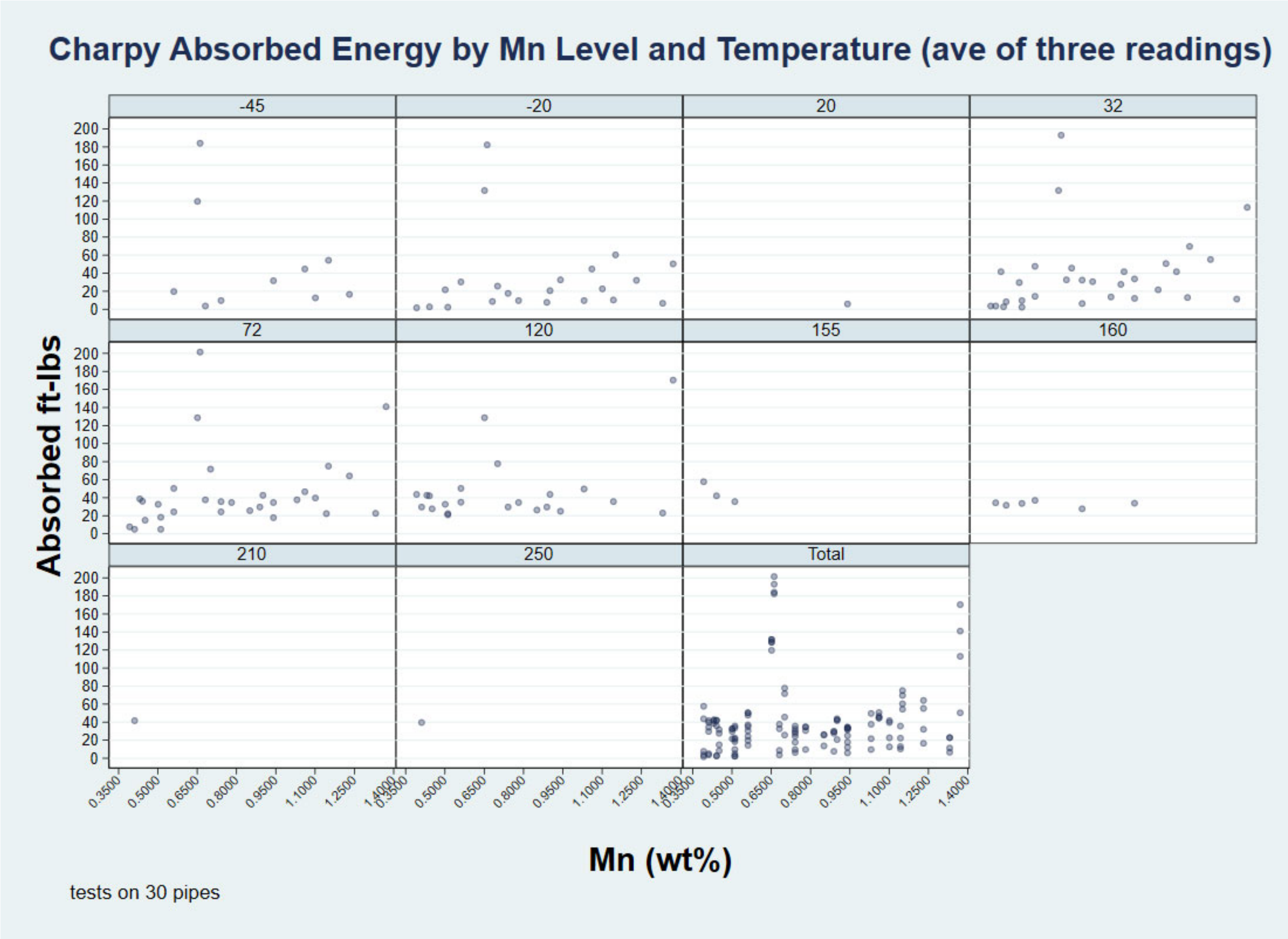

4.4 Effect of Sulfur, Phosphorous, and Temperature on Toughness

Figure 87. Mean Sulfur and Phosphorous Levels by Steel Type.

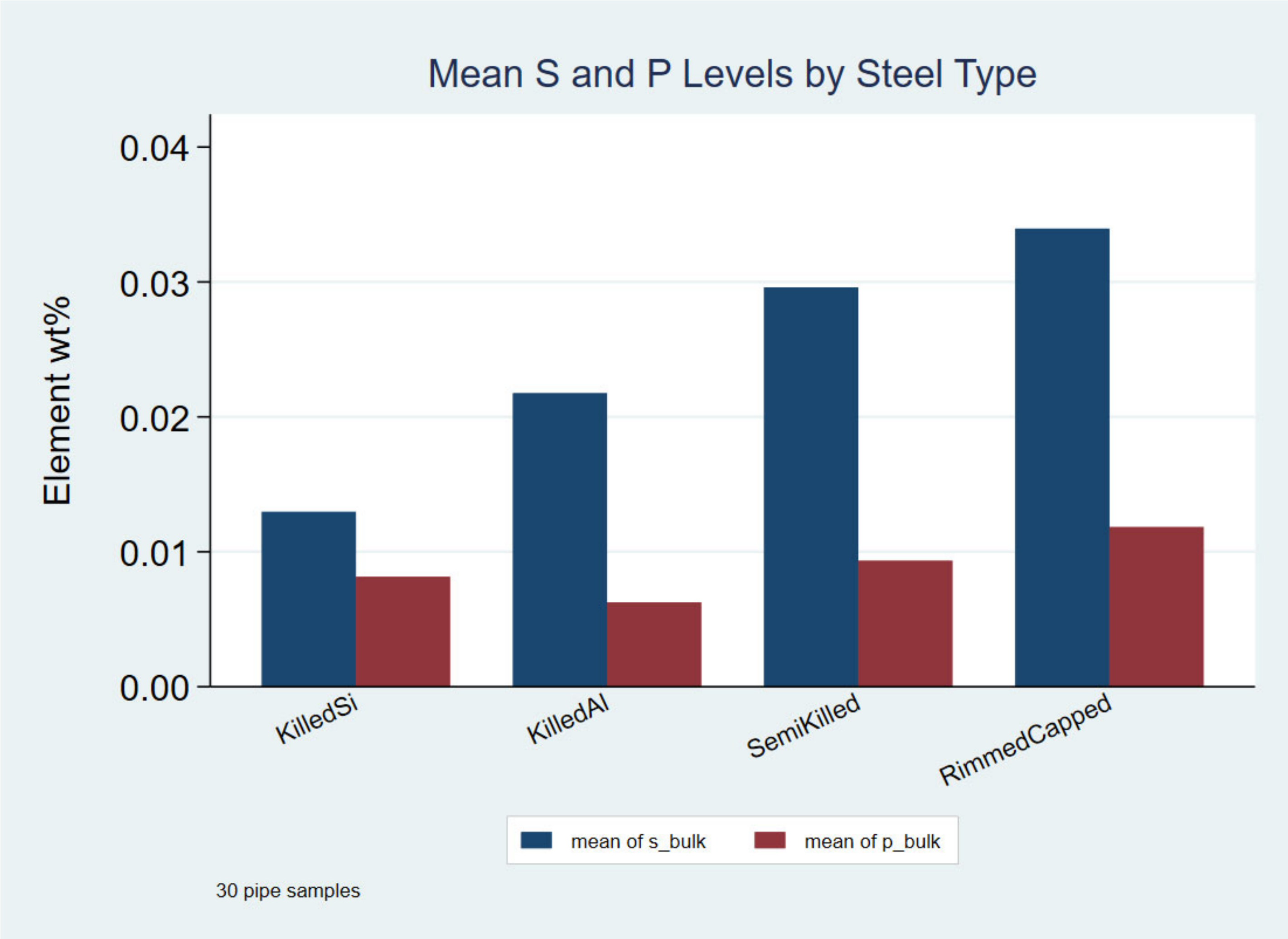

Figure 88. Charpy Absorbed Energy by Phosphorous Level and Temperature.

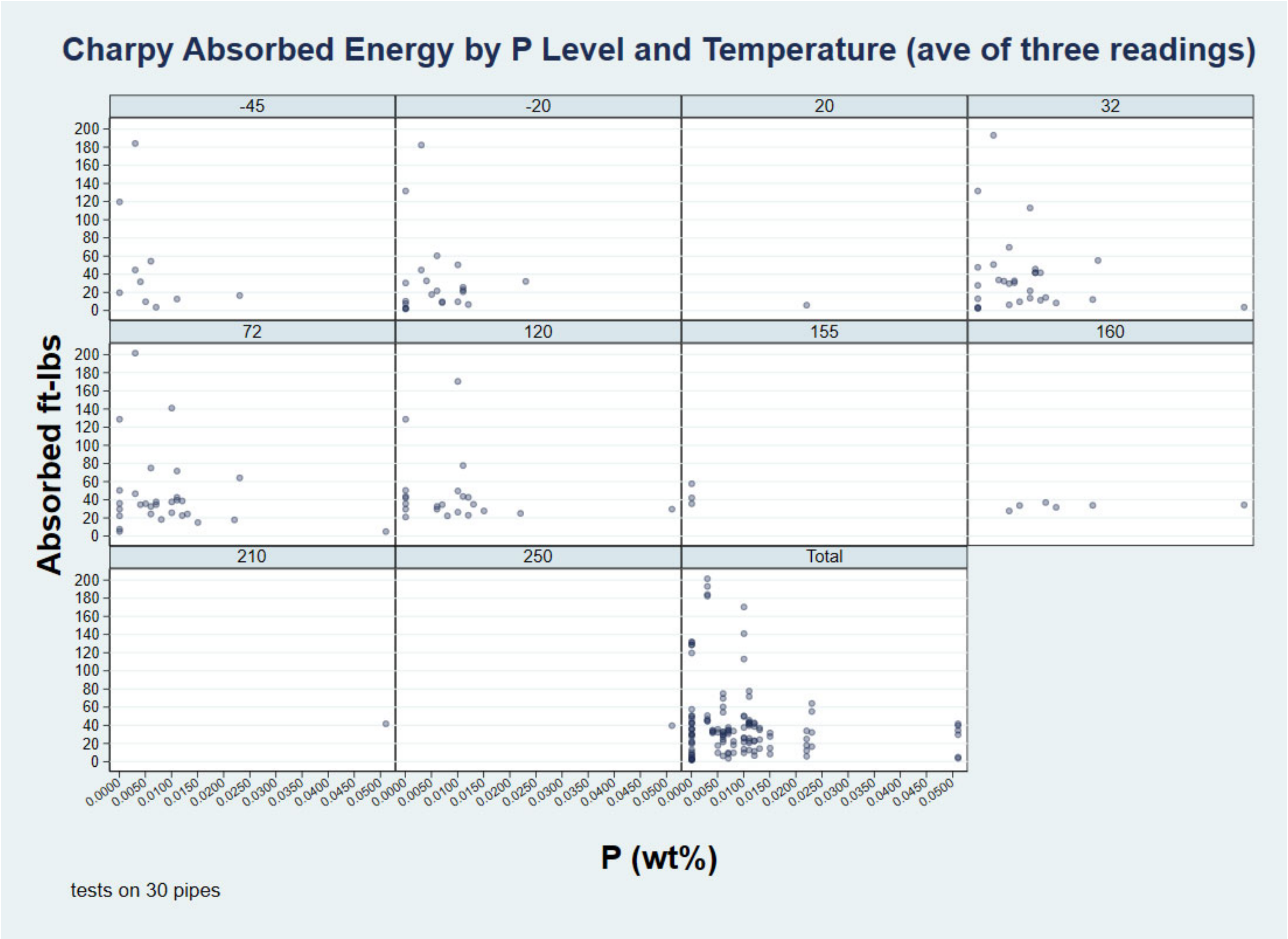

Figure 89. Charpy Absorbed Energy by Sulfur Level and Temperature.

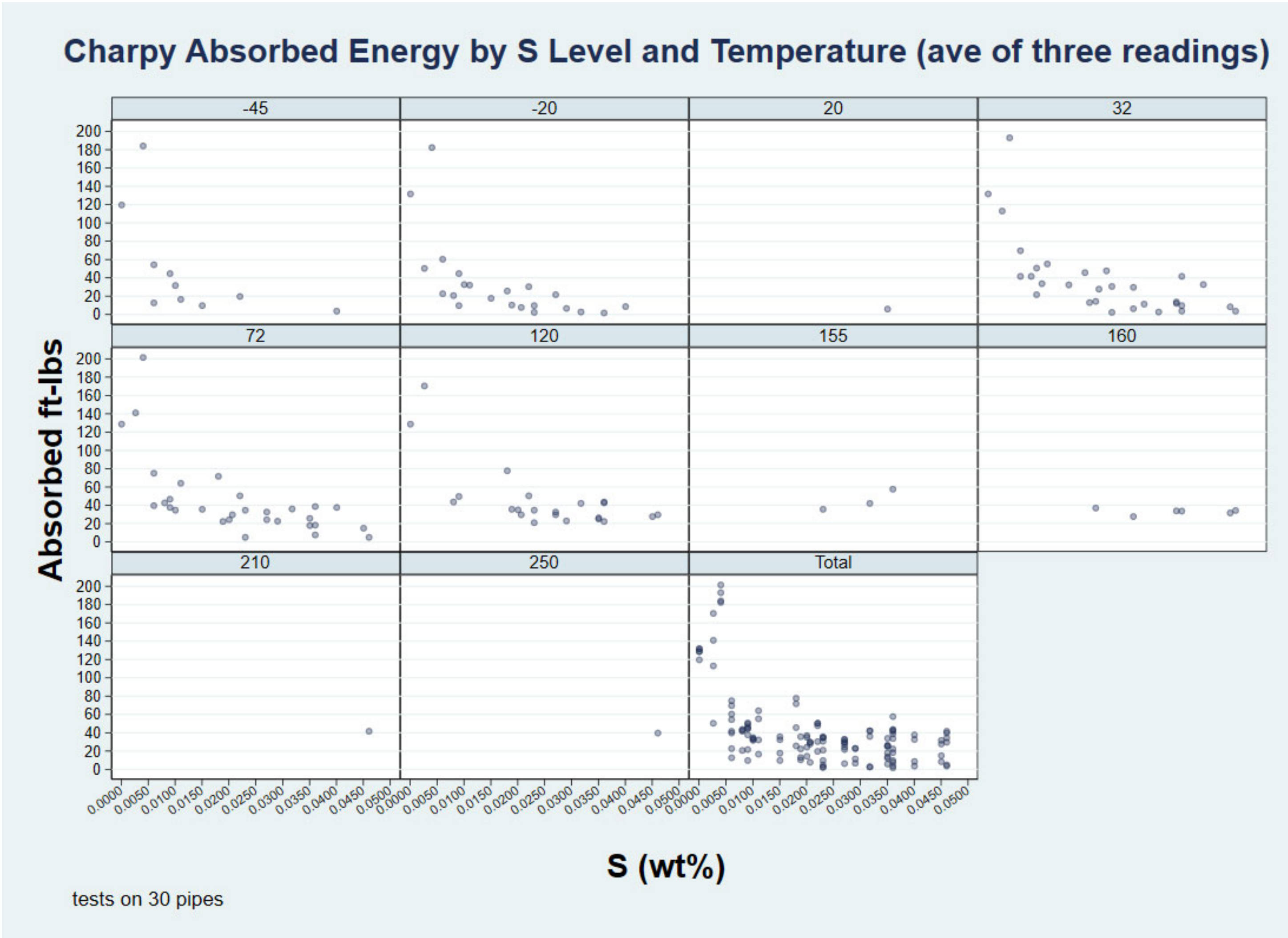

PART III: MODELING

Part III contains:

- Chapter 5: Causally Based and NDE Operator Provided Regression
- Chapter 6: Advanced Modeling Suite Analysis: OLS, BMA, BNM, GPM, and MBGPM

Chapter 5: Causally Based and NDE Operator Provided Regressions

5.1 Regression Modeling Overview and Nomenclature

This chapter contains the regression and model fits (when provided) from the nondestructive technology and the causal models from the analysis, as well as historical models from the literature. The abbreviations for the models in the plots are as follows and are used throughout the report:

- LRM: Linear Regression Model; surface-to-bulk
- OLS: Ordinary Least Squares; surface-to-bulk
- BRM: Bayesian Regression Model; surface-to-bulk
- ANN: Artificial Neural Network; surface-to-bulk
- DAE: an OLS model based on causal relationships
- MXX: various models from the historic literature based various model fits; surface-to-bulk
- Surface: raw surface yield strength values (no model applied) from NDE technology
- 0.2% Offset: lab testing of tensile bars using the 0.2% offset method
- 0.5% EUL: lab testing tensile bars using the 0.5% elongation under load method

Advanced data analytics modeling techniques are also presented in Chapter 6 and do not contain the causal relationships in this Chapter.

Regressed Delta Between Lab and NDE Strengths

Regressions were completed on the delta or difference between the bulk testing and the NDE predicted value. Therefore, the delta was defined for the YS and UTS as:

ys_delta = (lab full wall yield strength) - (NDE yield strength prediction)

uts_delta = (lab full wall ultimate tensile strength) - (NDE ultimate tensile strength prediction)

Dependent and Independent Regression Variables

These delta's are the dependent variables (DV). To get the prediction for bulk strength from either relationship one would subtract the NDE prediction from the delta strength calculated via the fitted regression equations from the surface measurable independent variables (IV) used for each equation.

Choice of Lab Yield Strength Method

The lab full-wall yield strength used for the Frontics technology was the 0.2% offset yield strength and for the MMT technology, the 0.5% elongation under load per their request and the basis of the technology. As shown in Chapter 3, the two types of yield strengths tracked nearly identically as one would expect for these types of steels, so the distinction was not critical but followed in any event.

Form of Regression Equations and Nomenclature

Instead of listing all forms of the equations used for regression with every term and each coefficient, the listings below will be in a more general nature to allow one to see the specific independent variables, their power, and their interactions.

By listing the models in this fashion, users of the models may set up the equations in the correct form with their software platform of choice and use their units of choice.

The model listing uses the variable nomenclature from the regression fitting to prevent transcription errors. The prefix and operators used are defined as follows and are common in the statistical analysis field:

- Prefix of "c." on an IV is used when it is a continuous variable and interacted with another variable. The prefix is not needed when the variable is standalone, i.e., interacted.
- Prefix of "i." on an IV is used when it is a categorical (aka factor) variable and interacted with another variable. The prefix is not needed when the variable is standalone, i.e., interacted.
- The "#" operator is a two factor interaction without the single factor terms included. Additional variables may be chained together to obtain two, three, etc. interaction variable. A single factor can be interacted with itself to create a squared term and so on.
- The "##" operation is a full factor interaction that includes the single factor terms in the regression as well.

Model Naming Convention for Historical and Newly Developed Causal Equations

The models used are based on metallurgical principles and those starting with "M" are from the literature and cited. The models starting with "DAE" are custom metallurgical models developed under this project and in every case the final "DAE" forms that were down selected outperformed the literature models and the NDE maker's regression models if provided.

The causality of each model is a function of the choices of IV and how they are interacted or not. The choices for the structure of the DAE prefixed models were based on the range of API steels tested and expected in the field. These include lower to moderate carbon steels with ferritic and/or pearlitic phase structures.

The inclusion of the key alloy elements used to strengthen the steels through solid solution and precipitation strengthening were accounted for.

Surface Obtained Variables for Independent Variables

- All the values for the IV's were selected and input from the surface obtained data.
- The chemistry element values were from the surface at 5 mils deep as was the ratio (fraction) of ferrite to pearlite microstructures, which was based on carbon content and the lever rule. This was checked with actual microscopy and found to be entirely consistent.
- The grain diameter was based on surface measurements.
- The diameter of the pipe was a known quantity.

Steel Type Classifying Methodology Based on Surface Chemistry

The steel types were inferred from the chemistry as follows and this well-established relationship proved highly accurate:

Figure 90. Steel Type as Defined by Silicon and Aluminum Weight Percent's.

Si		Al		Steel Type	De-oxidized?
>=	<	>=	<		
0.10		Regardless		Si Killed	Yes
	0.10	0.02		Al Killed	Yes
0.02	0.10		0.02	Semi-Killed	Partially
	0.02		0.02	Rimmed/Capped	No

Rimmed/Capped Steels

Rimmed or Capped steels are produced from non-deoxidized liquid steel cast into ingots. While carbon will segregate at a micro level in all steels, in a rimmed ingot it also occurs at a macro level. As the liquid steel cools very low C iron will freeze to the ingot wall first because it has a higher freezing point than iron with more carbon in solution. Because the ingot is not deoxidized the liquid steel will appear to roll or boil in the mold as the dissolved gases come out of solution. This is called the rimming action and brings fresh liquid metal to the solidification front. The carbon is ejected towards the inside by the rolling liquid metal, if only a small rim zone is desired, the ingot can be mechanically capped, shutting down the evolution of gases and ending the rimming action.

Rimmed/Capped are grouped as a one group and the following is provided as additional helpful information:

- Greater crop of ingot on rimmed
- Rimmed has very good surface quality
- Rimmed steel exhibits rim zone visible to the unaided eye on an etched specimen at 3ft
- Thin rim zone hard to tell apart rim vs. mechanically capped for ≥ 1015 steels

- Bulk Yield Tensile Elongation (YTE) properties likely similar between rimmed and rimmed/capped

HSLA Steels

High Strength Low Alloy (HSLA) steels were grouped into just one category using the category below based on the alloying element as prescribed in ASTM standards:

- Classified: HSLA_Nb if Nb >= 0.005 wt%
- Classified: HSLA_V >=0.02 wt%

5.2 Generic Form of All Causal Regression Models

Yield Strength Models

Overview

The yield strength models discussed in the section above are presented below in their generic form. Each single or interacted term from the model will have a coefficient as well a single constant for the regression solution. After testing an exhaustive number of models this set was narrowed down to the 12 candidate models listed below.

Many historic models recorded in the literature were tested but it became evident that although these models did have some merit, that the lack of ubiquitous computing power from the decades that they were developed potentially resulted in a limited number of terms for the least square regressions and exclusion of some key, higher order terms. With the availability of very powerful personal computers and equally importantly the associated statistical analysis packages, there was no restrictions on the causal model terms and forms selected for modeling.

The best model for the Frontics NDE technology was found to be DAE_1_3 and for the MMT technology to be DAE_1_4mmt. These two yield strength models outperformed all the other models used for the respective technologies. Note the coefficients for the top performing yield and ultimate tensile strength causal models are listed in **Appendix C**. The regression summaries are also provided in the same Appendix section.

Top Performing Models

The **DAE_1_3 model** is boxed (in green) since when used with the Frontics NDE technology unmodeled surface data, it produced the tightest predicted vs. actual predictions and a neutral (or no) bias towards the conservative or non-conservative side for accuracy. This model also had the tightest spread or precision as measured by the regression output and confidence interval. As will be shown in a later section, the 95% confidence interval of the regression output for the average yield strength prediction completely encompassed the unity line based on the lab results for yield strength.

The **DAE_1_4mmt model** is boxed (in blue) since when used with the MMT technology unmodeled surface data, it produced the best results from the MMT NDE technology. However, the output of the MMT NDE technology using this model or the others provided by the technology provider demonstrated a bias for certain steels, as shown in Chapter 3, and will be demonstrated on the regression outputs vs. full lab testing overlays in this section.

Constructed variables from standard variables are as follows:

- n_sqrt = sqrt(n_5mil) : square root of nitrogen percent at 5 mils
- v_sqrt = sqrt(v_5mil) : square root of vanadium percent at 5 mils
- dNegSqrt = gd_surface^(-0.5) : grain diameter raised to the -½ power
- xp = pearlite_perc_5m/100 : fraction of pearlite microstructure
- xf = 1-xp (note, this is the fraction of ferrite present) : fraction of ferrite microstructure
- xfcubrt = xf^(1/3) : cubic root of ferrite fraction
- oneminusxfcubrt = (1-xfcubrt) : 1-cubic root of ferrite fraction
- mnRecip = (1/mn_5mil) : reciprocal of manganese percent at 5 mils
- DdivT = diameter_nominal/wall_thickness_as_recieved : nominal pipe diameter / wall thickness

These terms are used in the listings below. The literature equations are shown for Frontics NDE as an example. MMT provided three sets of models as noted earlier.

Custom Yield Strength Metallurgically Based Models Developed in this Project

DAE_1_1
Custom model
regress ys_deltaFront :

- cu_5mil
- mn_5mil
- p_5mil
- si_5mil
- n_sqrt
- c.xp#(c.c_5mil#c.c_5mil)
- c.nb_5mil#c.c_5mil
- c.xf#c.mn_5mil
- c.mn_5mil#c.dNegSqrt
- c.xf#c.mn_5mil#c.dNegSqrt

DAE_1_2
Custom model reduced terms (statistically *significant* terms only retained)
regress ys_deltaFront :

- mn_5mil
- si_5mil
- n_sqrt
- c.xf#c.mn_5mil
- c.mn_5mil#c.dNegSqrt
- c.xf#c.mn_5mil#c.dNegSqrt

DAE_1_3 (used with Frontics NDE data)
Custom blended model (DAE_1_1 plus categorical i.steelType and c.diameter_nominal variables)
regress ys_deltaFront :

- i.steelType
- cu_5mil
- mn_5mil
- p_5mil
- si_5mil
- n_sqrt
- diameter_nominal
- c.xp#(c.c_5mil#c.c_5mil)
- c.nb_5mil#c.c_5mil
- c.xf#c.mn_5mil
- c.mn_5mil#c.dNegSqrt
- c.xf#c.mn_5mil#c.dNegSqrt

DAE_1_4mmt (used with MMT NDE data)
Used DAE1_3 and applied to MMT surface but also added i.seamless and i.hsla
regress ys_deltaMMT :

- i.steelType
- i.seamless
- i.hsla
- cu_5mil
- mn_5mil
- p_5mil
- si_5mil
- n_sqrt
- diameter_nominal
- c.xp#(c.c_5mil#c.c_5mil)
- c.nb_5mil#c.c_5mil
- c.xf#c.mn_5mil
- c.mn_5mil#c.dNegSqrt
- c.xf#c.mn_5mil#c.dNegSqrt

Yield Strength Models from the Literature

Note: the square brackets after the model numbers below, e.g. **[X]**, are the references for the source of the model terms and the full citations are located in the Reference section of this report.

Low Carbon

M_17_1 [2]
regress ys_deltaFront :

- mn_5mil
- si_5mil
- n_sqrt
- dNegSqrt

M_17_2 [3]
regress ys_deltaFront :

- mn_5mil
- si_5mil
- n_5mil dNegSqrt

M_17_3 [4, 5]
regress ys_deltaFront :

- mn_5mil
- si_5mil
- p_5mil
- cu_5mil
- n_5mil
- dNegSqrt

Medium Carbon

M_17_4 [2, 6]
regress ys_deltaFront :

- xfcubrt
- c.xfcubrt#c.mn_5mil
- c.xfcubrt#c.dNegSqrt
- oneminusxfcubrt
- si_5mil
- n_sqrt

M_17_5 [5, 7]
regress ys_deltaFront :

- mn_5mil
- si_5mil
- p_5mil
- n_5mil
- c.xf#c.dNegSqrt
- c.xf#c.c_5mil
- c.xf#c.dNegSqrt#c.mnRecip
- xp
- c.xp#(c.c_5mil#c.c_5mil)

M_17_6 [5, 8]
regress ys_deltaFront :

- p_5mil
- n_sqrt
- xf
- c.xf#c.mn_5mil
- c.xf#c.dNegSqrt
- xp

M_17_7 [5, 9]
regress ys_deltaFront :

- si_5mil
- p_5mil
- n_sqrt
- xf
- c.xf#c.mn_5mil
- c.xf#c.dNegSqrt
- xp

M_6_7 [10]
regress ys_deltaFront :

- xfcubrt
- c.xfcubrt#c.mn_5mil
- c.xfcubrt#c.dNegSqrt
- oneminusxfcubrt
- si_5mil
- v_sqrt
- n_sqrt

Custom Ultimate Tensile Strength Metallurgically Based Models Developed in this Project

The modeling of the ultimate tensile strength is a much simpler formula from a causal basis. It is highly dependent on manganese and carbon content. There are only minimal differences between all of the models for ultimate tensile, both the custom and the historic models in the literature.

DAE_2_1
Custom model
regress uts_deltaFront :

- mn_5mil
- si_5mil
- c_5mil
- p_5mil
- ni_5mil
- n_5mil
- dNegSqrt
- xfcubrt
- c.xfcubrt#c.n_sqrt
- c.xfcubrt#c.dNegSqrt
- c.xf#c.dNegSqrt
- c.xf#c.n_sqrt

DAE_2_2
Custom model reduced terms (statistically significant only)
regress uts_deltaFront :

- mn_5mil
- si_5mil
- c_5mil
- n_5mil

DAE_2_3 (used with Frontics NDE data)
Custom model (DAE_2_1 plus categorical and diameter terms)
regress uts_deltaFront :

- i.seamless
- c.diameter_nominal
- mn_5mil
- si_5mil
- c_5mil

DAE_2_4mmt (used with MMT NDE data) same model as DAE_2_3 above
Used DAE_2_3 and applied to MMT surface
regress uts_deltaMMT :

- i.seamless
- c.diameter_nominal
- mn_5mil
- si_5mil
- c_5mil

From the Literature Ultimate Tensile Strength Models

As noted in the custom model section, there are only minimal differences in the predictions from the custom and historical models from the literature.

Low Carbon

M_17_8 [2]
regress uts_deltaFront :

- mn_5mil
- si_5mil
- xp
- dNegSqrt

M_17_9 [4, 5]
regress uts_deltaFront :

- c_5mil
- mn_5mil
- si_5mil
- p_5mil
- ni_5mil
- n_5mil
- dNegSqrt

Medium Carbon

M_17_11 [5, 7]
regress uts_deltaFront :

- mn_5mil
- si_5mil
- p_5mil
- n_5mil
- c.xf#c.dNegSqrt
- xf

M_6-12 [11]
regress uts_deltaFront :

- c_5mil
- mn_5mil
- cr_5mil
- mo_5mil
- ni_5mil
- cu_5mil
- v_5mil
- ti_5mil

Strength Model: Akaike's and Bayesian information criterion

The goodness of fit information criterion (IC) are presented in Table 9 with two well-established measures: Akaike and Bayesian ICs. The lower the number, the better the fit.

Overall, the custom Frontics model fits (DAE1_3 and DAE2_3) exhibited the best fit to the as received surface yield and ultimate tensile strength data.

Table 9. Goodness of Fit Information Criterion (IC).

YIELD STRENGTH

Model	N	ll(null)	ll(model)	df	AIC	BIC
DAE1_1	70	-227.1678	-207.6279	11	437.2558	461.9892
DAE1_2	70	-227.1678	-210.4472	7	434.8944	450.6339
DAE1_3	**70**	**-227.1678**	**-181.7053**	**15**	**393.4106**	**427.138**
DAE1_4mmt	**70**	**-249.3438**	**-211.597**	**17**	**457.1941**	**495.4185**
M17_1	70	-227.1678	-215.0362	5	440.0723	451.3148
M17_2	70	-227.1678	-215.3869	5	440.7739	452.0163
M17_3	70	-227.1678	-214.8678	7	443.7357	459.4752
M17_4	70	-227.1678	-213.6304	6	439.2608	452.7518
M17_5	70	-227.1678	-212.7236	10	445.4473	467.9322
M17_6	70	-227.1678	-216.5796	6	445.1591	458.6501
M17_7	70	-227.1678	-212.7666	7	439.5331	455.2726
M6_7	70	-227.1678	-213.1484	7	440.2968	456.0362

ULTIMATE TENSILE STRENGTH

Model	N	ll(null)	ll(model)	df	AIC	BIC
DAE2_1	70	-192.7823	-180.6376	13	387.2752	416.5056
DAE2_2	70	-192.7823	-184.491	5	378.982	390.2244
DAE2_3	**70**	**-192.7823**	**-181.9819**	**6**	**375.9638**	**389.4548**
DAE2_4mmt	**70**	**-202.1882**	**-184.2985**	**6**	**380.597**	**394.088**
M17_8	70	-192.7823	-186.8327	5	383.6654	394.9079
M17_9	70	-192.7823	-183.4155	8	382.831	400.8189
M17_11	70	-192.7823	-183.761	7	381.5219	397.2614
M6_12	70	-192.7823	-187.3027	9	392.6054	412.8418

Overview of Strength Distribution Overlays by Technique and Model

The strength distributions of all seventy pipeline steels are plotted as kernel density overlays in Figure 91 to Figure 94.

The lab full-wall 0.2% offset and 0.5% EUL are plotted with the Frontics and MMT surface yield strength values (no model applied) in Figure 91. As discussed in an earlier chapter, the MMT data without a model application is skewed to the right. The Frontics data is also skewed to the right but to a lesser extent. The possible reasons for this were explained earlier. Also, note the excellent correspondence between the two lab yield strengths as one would expect for the tested grades.

Figure 91. Yield Strength Density Overlays Lab Full-Wall vs. NDE Surface.

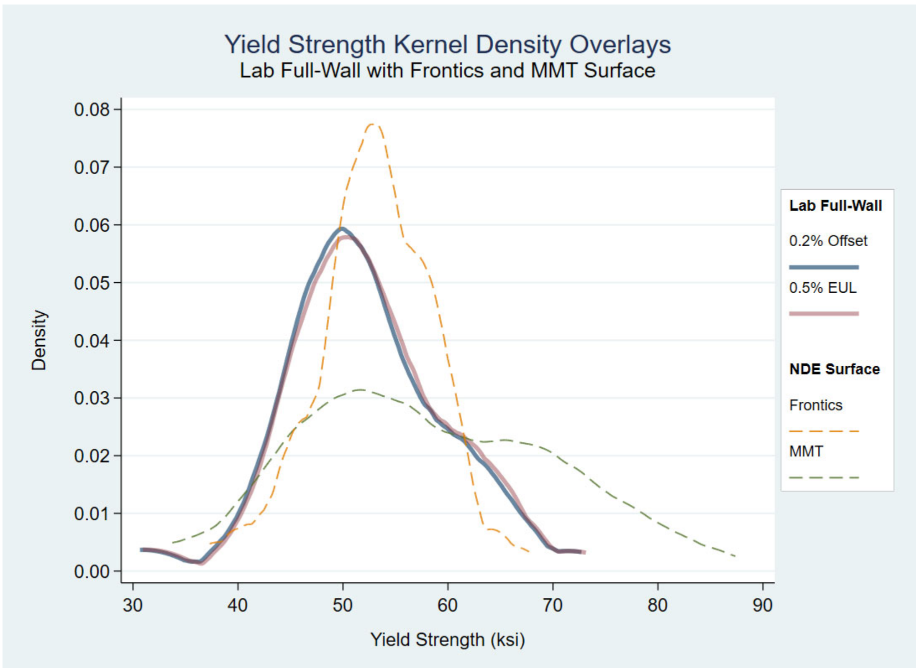

Figure 92 is a similar plot for ultimate tensile strength and shows very strong correlation between all values across the entire distribution. The UTS almost does not require a model correction and one would expect this from excellent correlations of surface hardness to bulk correlations of UTS for ferritic steels.

Figure 93 is a plot of key importance. It shows the yield strength distribution across all seventy pipeline samples for the lab full-wall vs. the posterior models. The Frontics causal model DAE1_3 tracks very closely to the lab tests and maintains a conservative tact from a distribution standpoint. The MMT casual model DAE1_4 is much tighter to the lab testing distribution vs. the surface data (alone) that was shown in Figure 91. This demonstrates the importance of incorporating causal modeling into the regression forms vs. straight numerical manipulations and methods.

Figure 92. Tensile Strength Density Overlays Lab Full-Wall vs. NDE Surface.

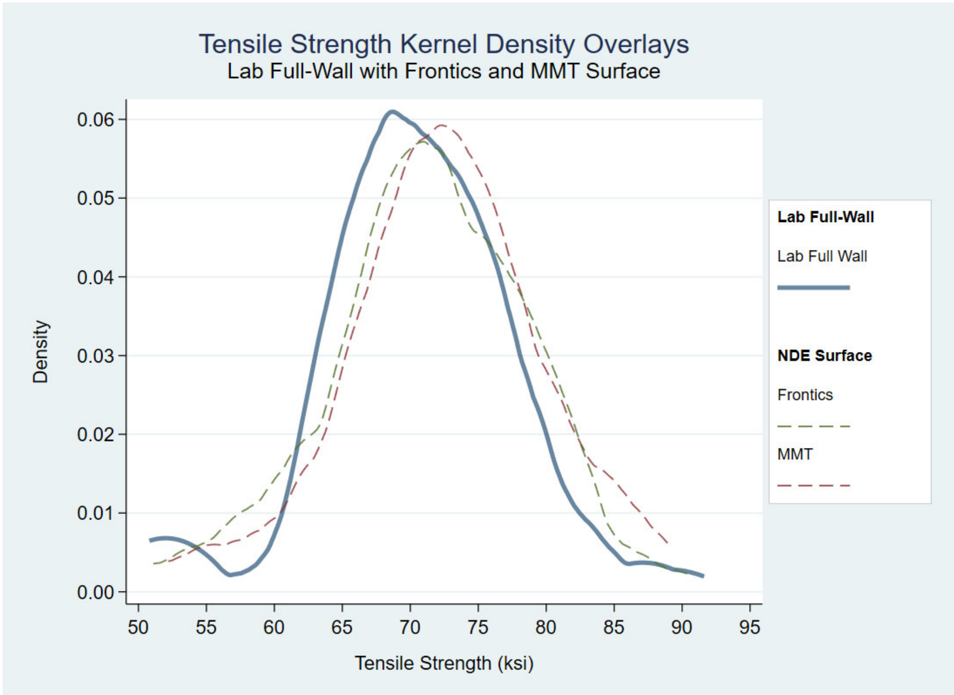

Figure 93. Yield Strength Density Overlays by Model and/or Technique.

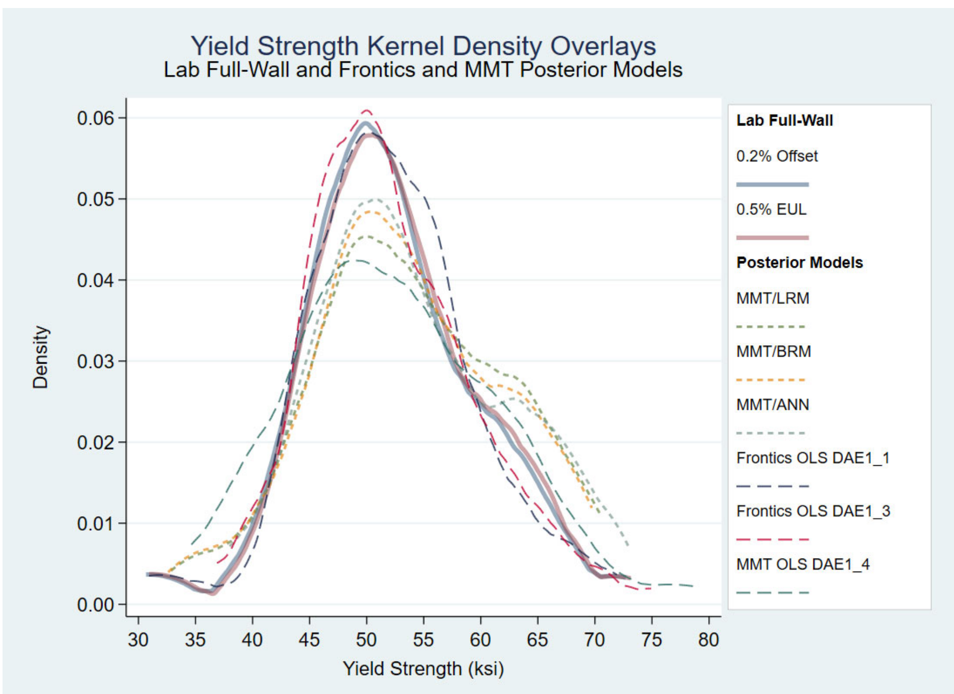

The ultimate tensile strength density overlays for the lab full-wall samples and the posterior models are shown in Figure 94. The causal models from both Frontics and MMT show excellent correspondence to the lab distributions. The MMT LRM, BRM, and ANN models have a slight shift to the right across the entire distribution.

Figure 94. Tensile Strength Density Overlays by Model and/or Technique.

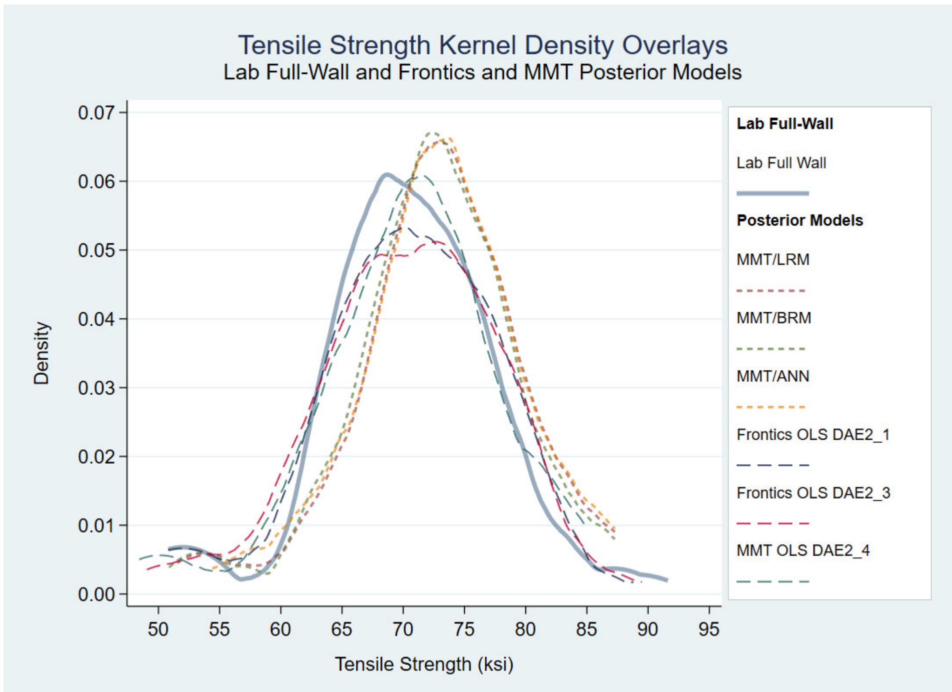

Predicted vs. Actuals for Strength Modeling

Predicted vs. Actuals Analysis Results and Parameters

In addition to measuring the goodness of fit and reviewing the strength distributions, the descriptive statistical summary of the predicted vs. actuals is presented in Table 10.

Table 10. Predicted vs. Actual Summaries of Custom and Historic Strength Models.

Variable	Obs	Mean	Std. dev.	Min	Max
YIELD STRENGTH (PREDICTED - ACTUAL)					
MMTsurf	70	5.865089	8.763753	-6.46122	31.59893
FrSurf	70	1.051026	6.255806	-14.84624	14.2341
MMTLRM	70	1.873716	5.997773	-10.76926	18.5156
FrDAE1_1	70	2.59e-08	4.732098	-11.20118	12.83836
FrDAE1_2	70	-2.81e-07	4.926578	-11.87904	13.27007
FrDAE1_3	**70**	**-4.58e-09**	**3.267567**	**-9.54355**	**6.214282**
FrM17_1	70	-2.64e-07	5.260369	-11.85199	12.47081
FrM17_2	70	-9.90e-08	5.286794	-12.00762	12.60092
FrM17_3	70	7.96e-08	5.247735	-12.1762	11.09503
FrM17_4	70	-8.34e-08	5.155783	-12.14778	13.08197
FrM17_5	70	-2.63e-08	5.089425	-11.62083	12.01248
FrM17_6	70	-1.85e-07	5.37764	-11.82852	11.49874
FrM17_7	70	-8.47e-08	5.092547	-11.42083	12.63856
FrM6_7	70	7.34e-08	5.1204	-11.81877	12.6513
DAE1_4mmt	**70**	**-2.06e-08**	**5.00817**	**-8.40642**	**11.95433**
ULTIMATE TENSILE STRENGTH (PREDICTED - ACTUAL)					
MMTsurfUTS	70	1.960932	4.378291	-7.803658	14.97856
FrSurfUTS	70	.9492044	3.827792	-8.73988	12.8939
MMTLRMUTS	70	2.395658	3.406963	-6.786992	9.602815
FrDAE2_1	70	-3.54e-07	3.218106	-7.52321	9.438433
FrDAE2_2	70	1.23e-08	3.400224	-9.551435	8.877146
FrDAE2_3	**70**	**5.85e-08**	**3.280505**	**-9.590734**	**7.389406**
FrM17_8	70	8.33e-08	3.515896	-8.778169	9.442286
FrM17_9	70	3.40e-07	3.348381	-8.718896	9.127207
FrM17_11	70	-2.60e-07	3.364948	-8.723165	9.135706
FrM6_12	70	-2.46e-07	3.539581	-10.00585	10.0049
DAE2_4mmt	**70**	**-4.82e-07**	**3.390887**	**-8.836629**	**6.232567**

The difference between the predicted strength minus the lab full-wall strength is the metric and the table summarizes the mean, standard deviation, minimum, and maximum of the seventy pipeline samples.

The surface data from the NDE techniques have positive mean values and up to 31.6 ksi positive bias in the case of MMT and 14.2 ksi positive bias for yield strength for Frontics.

The models provide a significant improvement from the plain surface data. The best custom models for yield strength have an effective mean of zero, meaning that the predicted minus the actual average delta (aka bias) is zero. Additionally, the min/max range in round numbers is shifted for MMT from -6 / + 32 ksi (Figure 95) to -8 / +12 ksi (Figure 97).

The same is true for Frontics which shifts from -15 / +14 ksi (Figure 95) to -10 / + 6 ksi (Figure 97). This is a vast improvement for both the HSD and AIS NDE predictions. The inclusion of the causal variables both continuous and categorical improve the models by including weighted (through coefficients) terms in the models to account for steel type, seamless, HSLA, etc.

The table and plots also shows similar but not as dramatic improvements for the ultimate tensile strength. Again, the custom models (based on causal relationships) provide the best fits that simultaneously minimize the non-conservative yield and ultimate tensile strength predictions, always important from a design basis for a pipeline system. Note the superior strength delta overlays for the causal models in Figure 98.

Predicted vs. Actuals Strength Delta Distribution Overlays by Technique and Model

The predicted vs. actual

Figure 95. Yield Strength Delta Density Overlays for NDE Surface Techniques.

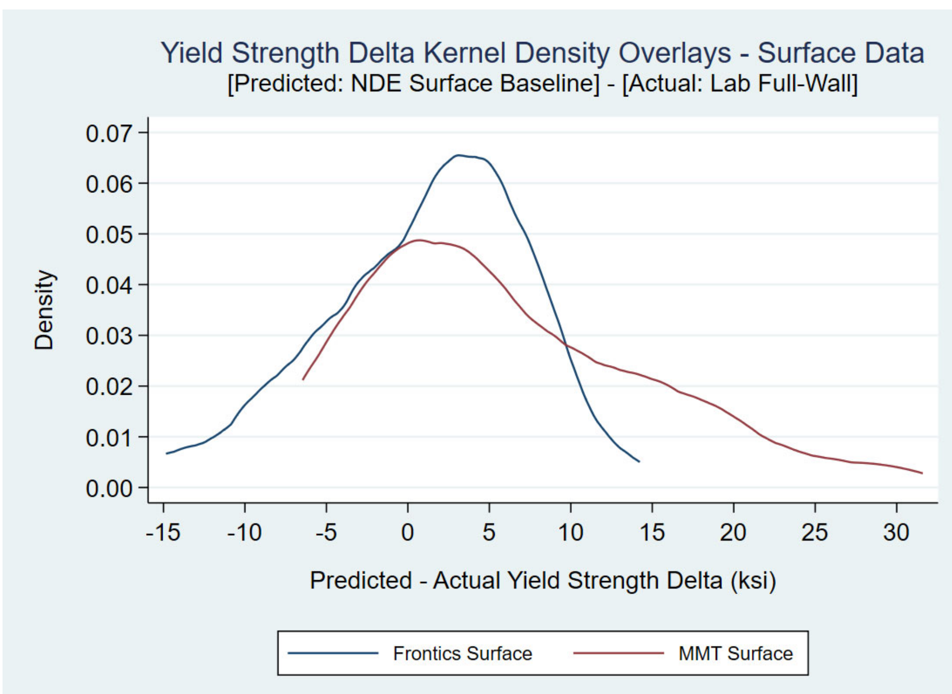

Figure 96. Tensile Strength Delta Density Overlays for NDE Surface Techniques.

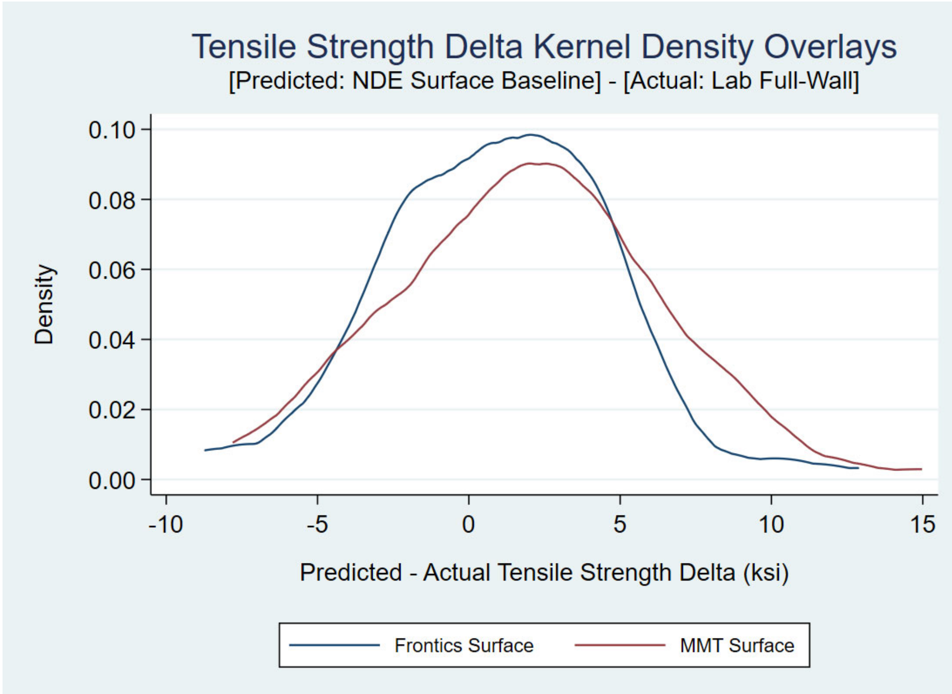

Figure 97. Yield Strength Delta Density Overlays for Model Fits.

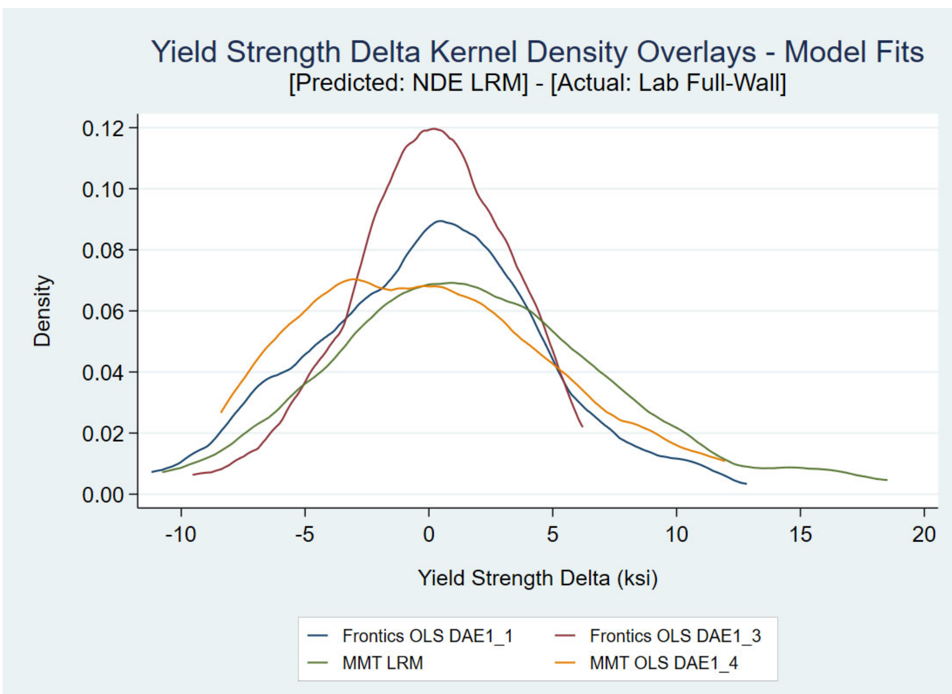

Figure 98. Tensile Strength Delta Density Overlays for Model Fits.

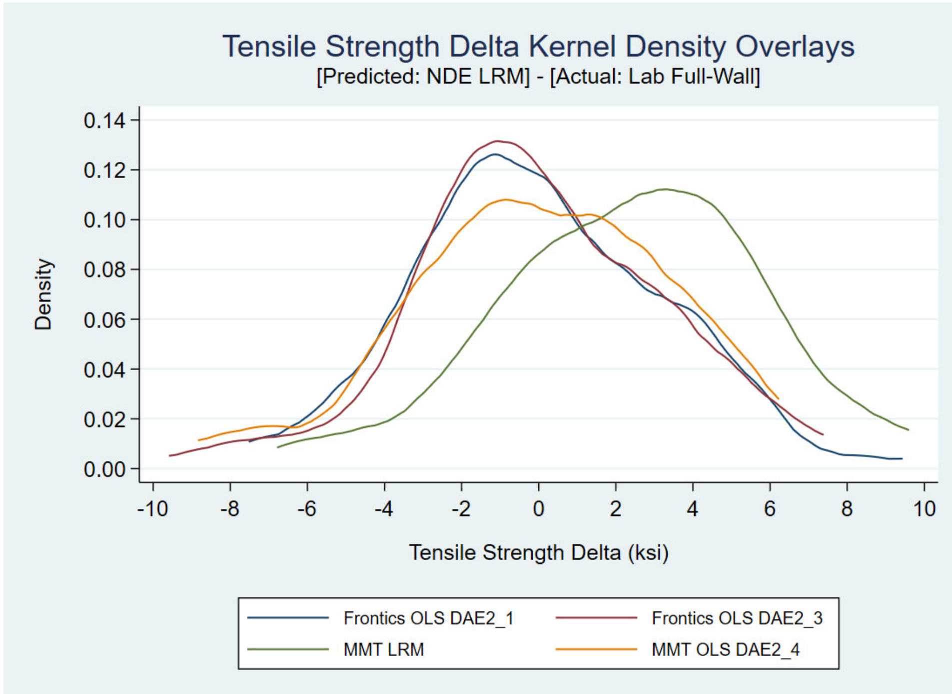

Strength Trend Comparison by Technique and Preferred Models by Steel Type

Figure 99 is a plot of yield strength for lab full-wall and the posterior models by steel type. The casual model (DAE1_3) for Frontics does well at matching the distribution of lab yield strengths for all steel types.

The casual model for MMT (DAE1_4) and the MMT LRM model also do well for silicon killed steels but are biased or skewed higher for aluminum killed steels slightly. For semi-killed steels both these models are biased/skewed higher and for rimmed/capped steels they are biased/skewed lower as compared to the lab full-wall results.

As discussed earlier, this is presumably due to the outer (near surface) layers of the pipeline steel having a higher yield strength in HSLA and non-seamless steels and a lower relative yield strength in the same outer layers for rimmed/capped steels for reasons already explained earlier in this report.

The tensile strengths are nearly consistent across all models and steel types since the factors that affect the yield strength distribution across the pipe wall do not do the same with the tensile strength values.

Figure 101 and Figure 102 are similar plots but only have two panels: one for welded long seams and one for seamless pipe. The causal model which expressly considers the seam type is closer to the lab full-wall yield and tensile distributions than the MMT LRM distribution. This is discussed in more detail in the next sections with distribution plots.

Figure 99. Lab Full-Wall and Best LRM Model Yield Strengths by Steel Type.

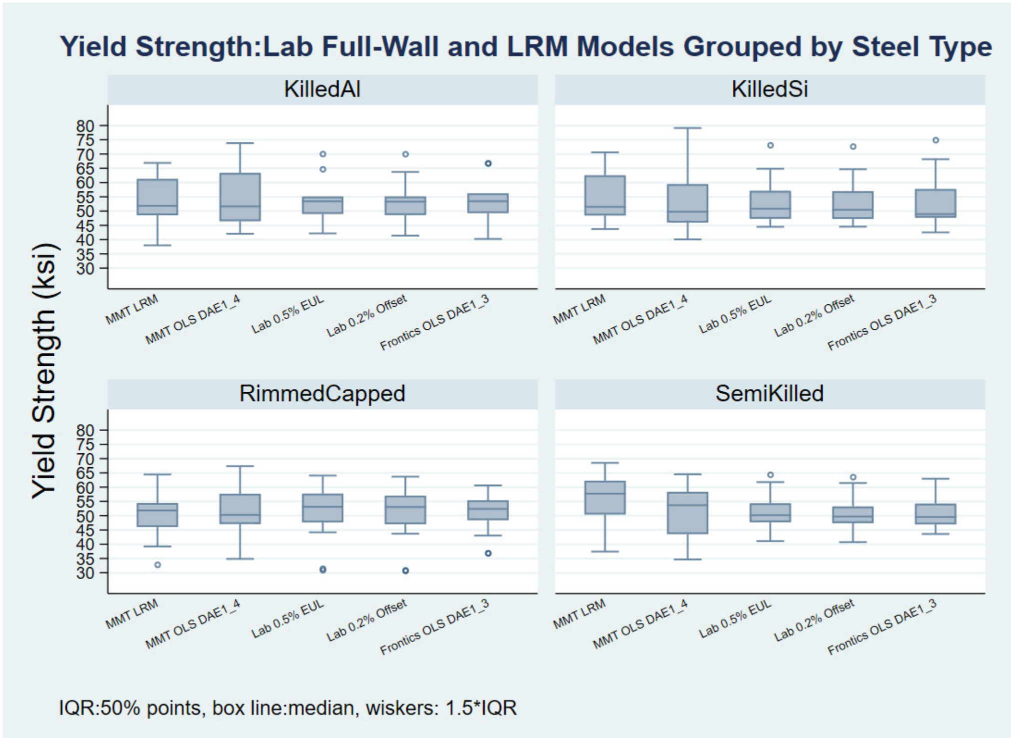

Figure 100. Lab Full-Wall and Best LRM Model Tensile Strengths by Steel Type.

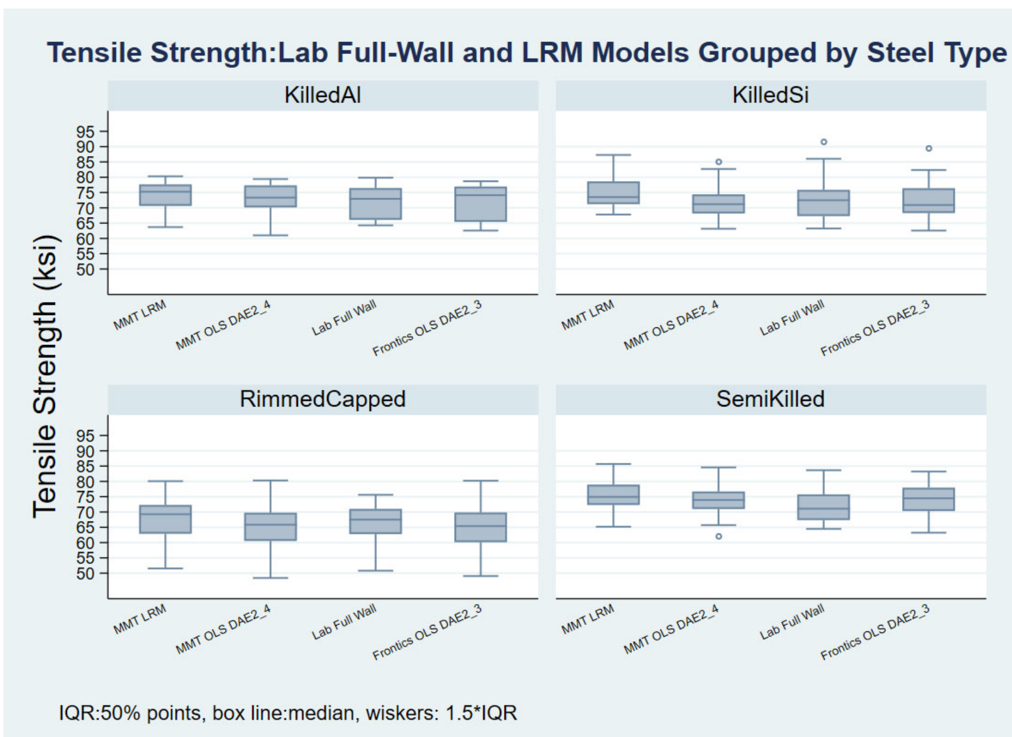

Strengths by Weld Seam Type

Figure 101. Lab Full-Wall and Best LRM Model Yield Strengths by Long Seam Category.

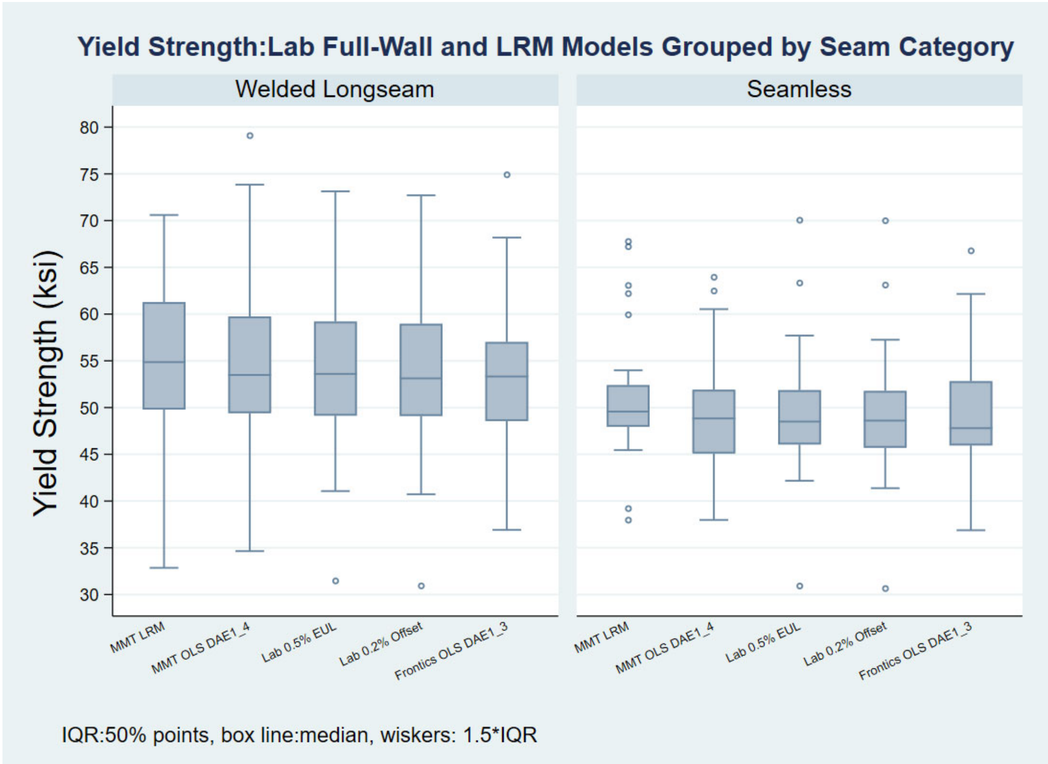

Figure 102. Lab Full-Wall and Best LRM Model Tensile Strengths by Long Seam Category.

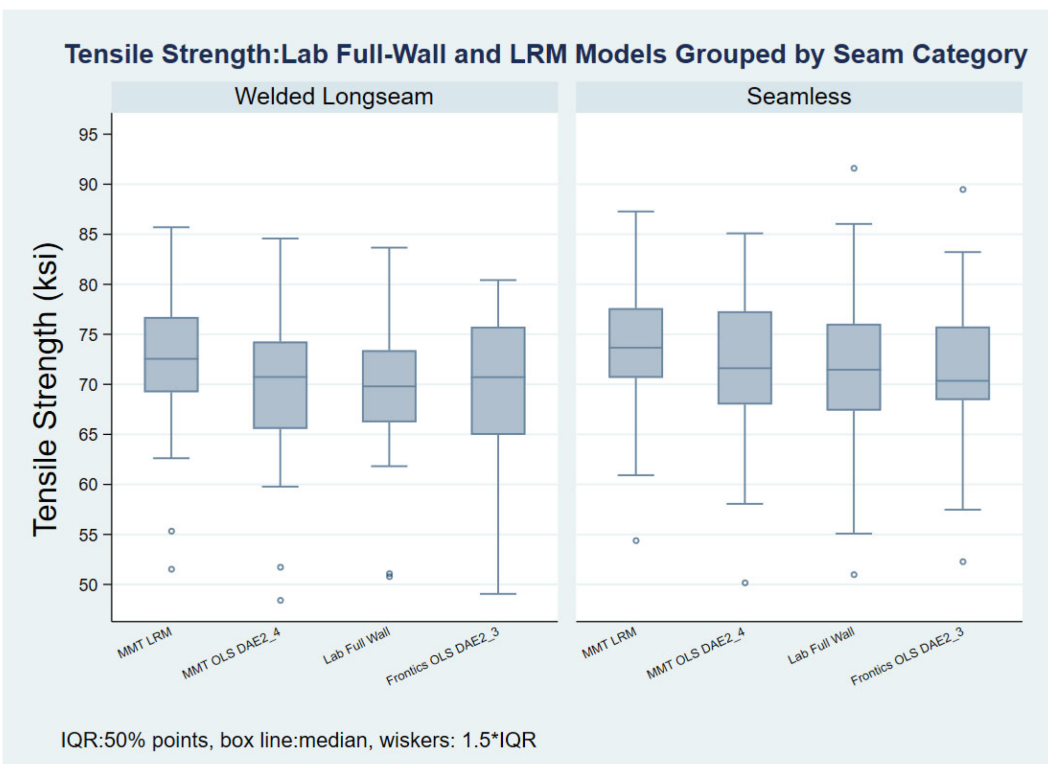

5.2 Overall Strength Comparisons of Lab, Surface, and Top Models

Yield Strength General Discussion

This section is the important comparison of the model performance vs. the lab full-wall strengths plotted as a unity plot with 95% confidence and prediction intervals. Figure 103 and Figure 104 are plots of the data without the confidence and prediction limits overlaid and are included for completeness.

The discussion below will be focused on the same data but with the intervals overlaid on the data in Figure 105 and Figure 106 for yield strength and ultimate tensile strength respectively.

The best predictions for yield strength were made by the Frontics AIS data with a causal model (DAE1_3) applied. This model is boxed in green in the center panel of Figure 105. One can see that the inner (blue) confidence interval overlaps the unity line for yield strength at a 95% confidence level.

Additionally, the wider prediction intervals (khaki shading) are relatively tight and encompass 95% of the seventy pipeline samples. This is an excellent model and works across all steel types, grades, diameters, thicknesses, etc.

The posterior yield strength models (LRM, BRM, and ANN) were improved upon with a causal model (DAE1_4) as far tightness of the predictions toward the unity line. However, as discussed in the report, the inherent baseline surface NDE data has a bias towards non-conservative predictions for steels at approximately 50 ksi or higher. This is evident by the slope of all the MMT posterior models, including the causal model. The models are rotated clockwise about ~50 ksi.

The MMT technology provides accurate strength data of the material it interrogates, however as pointed out in this report, it appears to be more localized towards the outer layers of the pipe wall. Conversely, the Frontics technology appears to penetrate deeper into the pipe wall to average a yield strength reading over a deeper (into the pipe wall thickness) profile. This explains the shift in the MMT values as described in detail in the earlier sections of this report, especially when comparing trends with seamless vs. non-seamless, HSLA vs. non-HSLA pipe, and rimmed/capped vs. killed/semi-killed steels and grades.

Confidence Interval Intersections with Full-Wall Lab Strength Unity Lines

There are additional ways to present the predicted vs. actual strengths, but the method outlined below provides an easy way to see how much the predictions are biased, what direction (high or low), and at what confidence – all relative to the full-wall destructive tensile testing.

A. The confidence interval is the zone where one might say based on the destructive tests vs. the model predictions and running a regression of the same, we plot the predicted (dashed line) line and the absolute unity (red line).
B. This allows us to elegantly compare on average (for the confidence interval) and pointwise (for the prediction interval) where we are 95% confident that the destructive yield strength would fall *based* on the model predictions applied to the data

C. The confidence band then allows us to select (with our selected 95% confidence level) where the predicted YS zone (confidence interval) would be equivalent to the lab/destructive value, and where on average it would be higher (non-conservative) or lower (overly conservative).

A detailed discussion of the confidence intervals around the model fits is presented below and references Figure 105b.

1. In Figure 105b, the green vertical line is where the 95% lower confidence level (LCL) is above the unity line and the red vertical level is where the 95% model regression upper confidence level (UCL) is below the unit line. When the unity line falls between this upper and lower bound we can say the average YS prediction zone is effectively equivalent to the lab/predicted interval.
2. The intercepts between the LCL and UCL are annotated on the x-axis. This is the most useful way to approach this relationship, since one will not know the actual (destructive full wall) YS ahead of time, i.e., a priori.
3. In Figure 105b, if we reference the subplots from 1 to 9 from left to right and top to bottom:
    a. The NDE technology (without other factors/variables) has a regression fit in subplots 2 and 3.
    b. The models that use causal relations and surface-obtained data including NDE YS values, chemistry, grain size, steel type, weld type, etc. are in subplots 4 to 6.
    c. MMT provided their own models in subplots 7 to 9 (factors in those models are unknown, only the generic form).
4. The subplot-by-subplot discussion is below:
    a. Subplot 1 represents two different lab (destructive) full wall tensile tests vs. each other. The two yield strength characterization methods matched well. One is the 0.2% offset method and the other the 0.5% elongation under load method.
    b. Subplot 2 is the surface (no posterior model applied to the Frontics predictions) of the 95% confidence bands run the entire length of the DOE. One could say the 95% prediction zone overlaps the unity line and the prediction is equivalent on average to the full/destructive YS value.
    c. Subplot 3 is the surface (no posterior model applied to the MMT predictions) of the 95% confidence bands that intersect the unity line from 43.5 to 50 ksi.
        i. To the right of the red line at 50 ksi, the prediction zone is higher than the actual destructive YS and therefore could be termed non-conservative.
        ii. To the left of the green line at 43.5 ksi, the prediction zone is lower than the actual YS and is conservative or might be termed overly conservative.
        iii. In between the red and green lines, one could say the 95% prediction zone overlaps the unity line and the prediction is equivalent on average to the full/destructive YS value between these values.
        iv. The explanation of (i) and (ii) hold for subplots 4 to 9 below, i.e., same meaning of the lines.

d. Subplot 4 was an optional model not used but was discussed in the narrative of the report.
e. Subplot 5 is the optimal causal OLS model applied to the suite of surface data for Frontics and the 95% bands overlap the unity line the entire length of the DOE.
f. Subplot 6 is the optimal causal OLS model applied to the same for MMT and the 95% bands overlap the unity line between 47 and 55 ksi.
g. Subplots 7, 8, and 9 are using the MMT model predictions (from MMT) for their LRM, BRM, and ANN and one can see the overlap of the 95% intervals at 41 to 52, 41 to 53, and 38 to 52 ksi respectively.

Ultimate Tensile Strength Discussion

The ultimate tensile strength comparisons in Figure 106 start out with a tighter and more accurate surface to bulk prediction from the raw, un-modeled data for both NDE technologies. Here we see both the Frontics and MMT causal fits provide excellent predictions of bulk ultimate tensile strength from the surface data passed through the causal models, DAE2_3 and DAE2_4, respectively. For both Frontics and MMT, the 95% confidence interval overlaps the unity line and the prediction interval is particularly tight across the entire strength range.

Summary

The NDE technologies from Frontics and MMT are viable for yield and ultimate tensile strength predictions and have proven their accuracy and calibrations well across standardized and homogeneous materials. However, the MMT HSD technology might benefit from additional yield strength modeling or refinement for pipeline steels that are not isotropic or constant strength across the pipewall thickness (depth).

The MMT technology does well with seamless pipe where the material has been normalized/annealed (making it isotropic/homogenous across the pipe wall) but can exhibit a non-conservative bias when compared to the full-wall results when the outer areas of the wall are stronger than the inner or midwall area of the pipe thickness. Similarly, for rimmed steels the opposite can be true since the outer layers can have a lower carbon content and yield strength compared to the inner wall of the pipeline cross section.

As a further check on the findings from Chapters 1 through 5, the next chapter results in similar and expanded modeling conclusions, based on numerous and robust advanced data analytics and modeling techniques.

Unity Plots of Strength Comparisons of Lab, Surface, and Top Models

Figure 103. Yield Strength Comparisons of Lab, Surface, and Top Models.

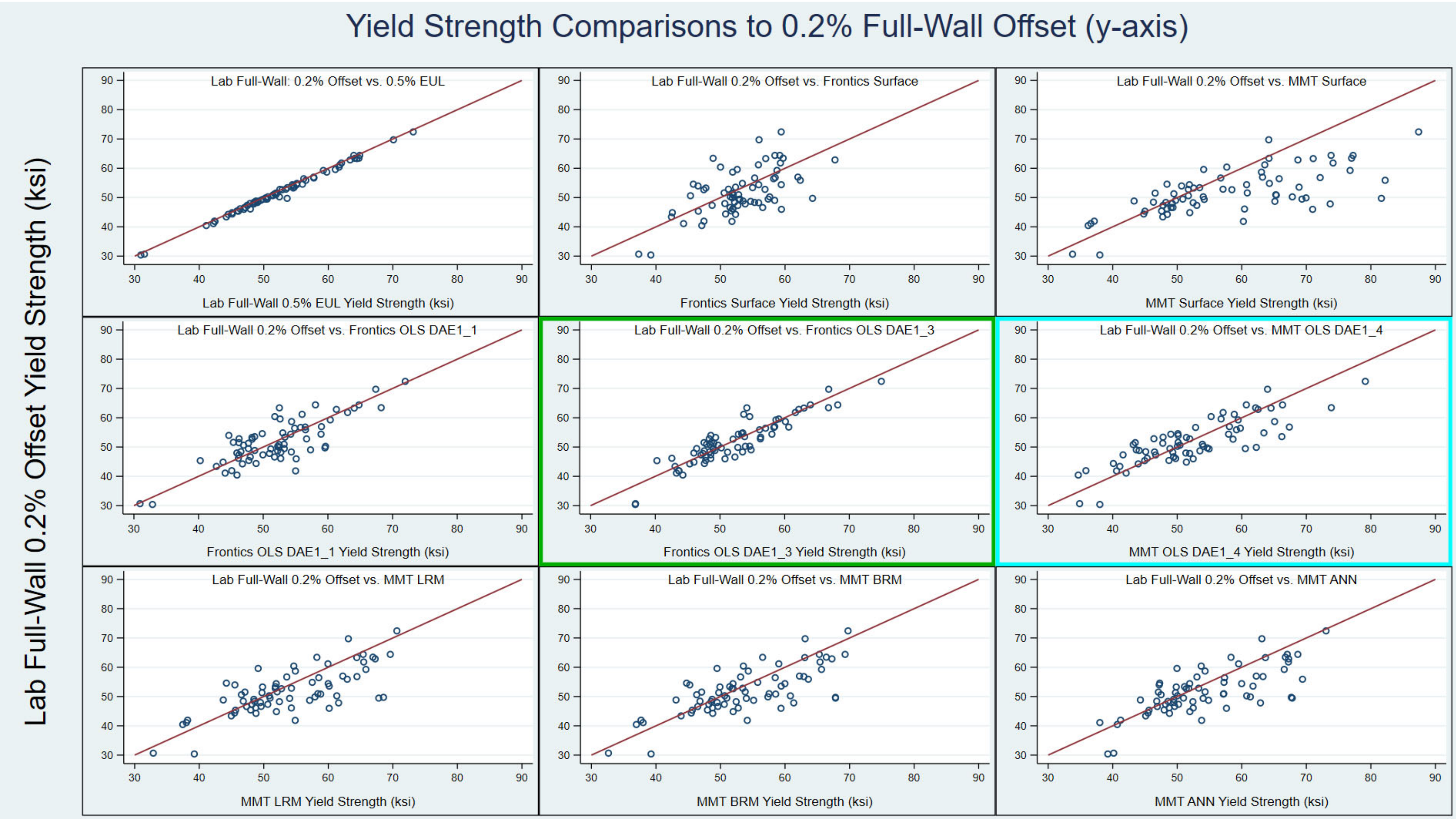

Figure 104. Tensile Strength for Lab, Surface, and Top Models.

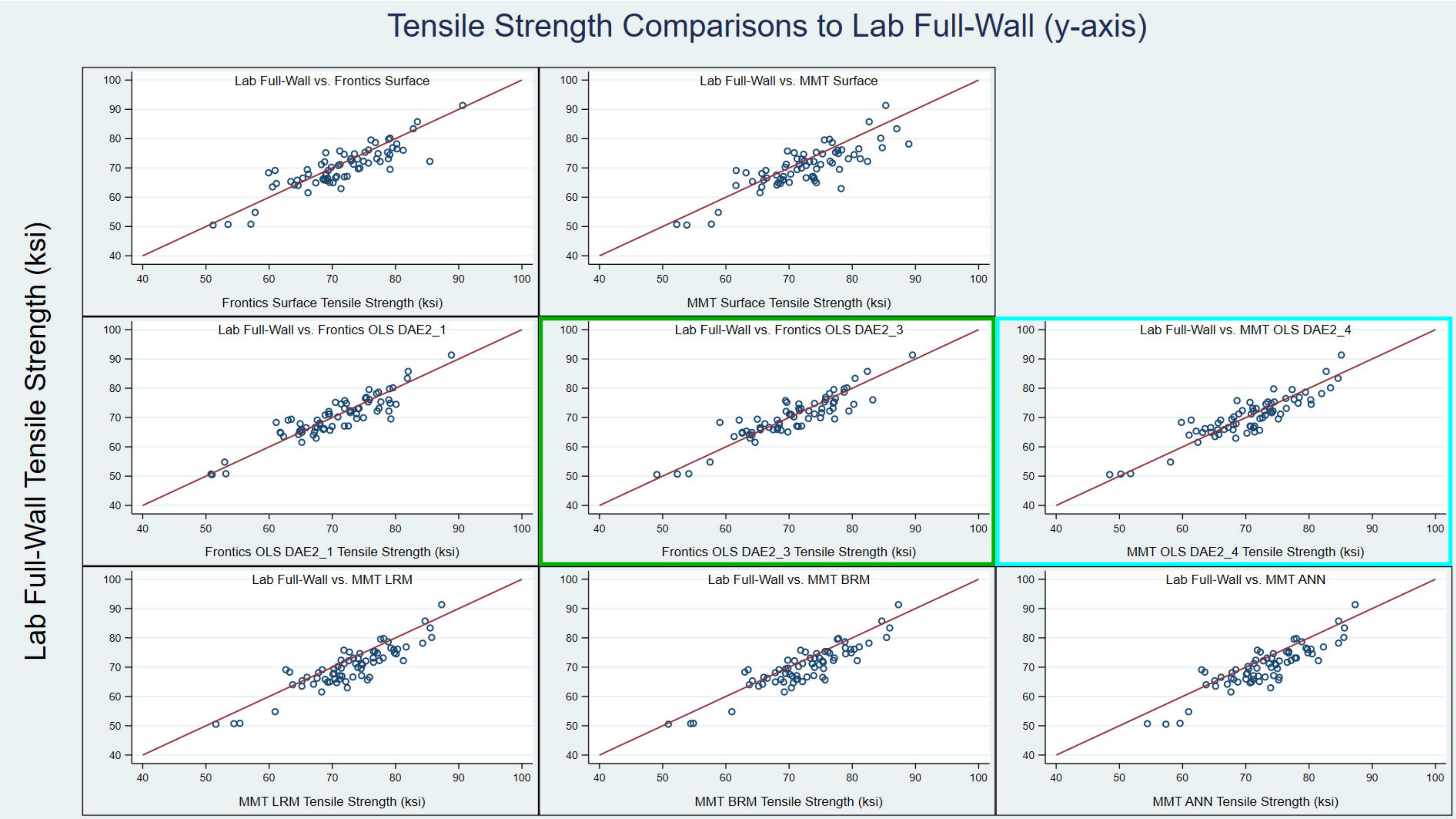

Unity Plots of Strength Comparisons of Lab, Surface, and Top Models with OLS Confidence Bands

Figure 105. Yield Strength Comparisons of Lab, Surface, and Top Models with CI & PI.

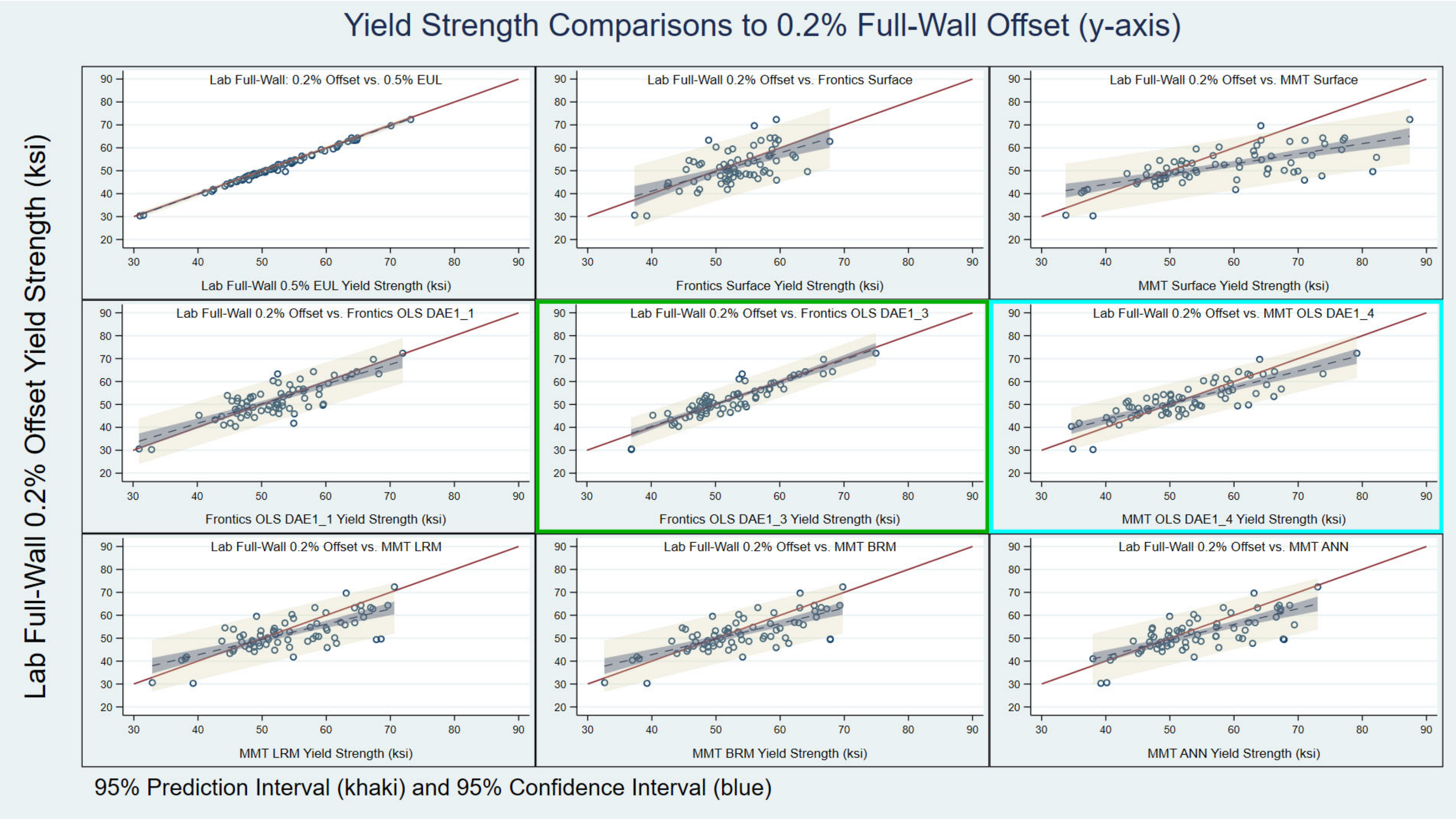

Figure 105. Yield Strength Comparisons of Lab, Surface, and Top Models with CI & PI.

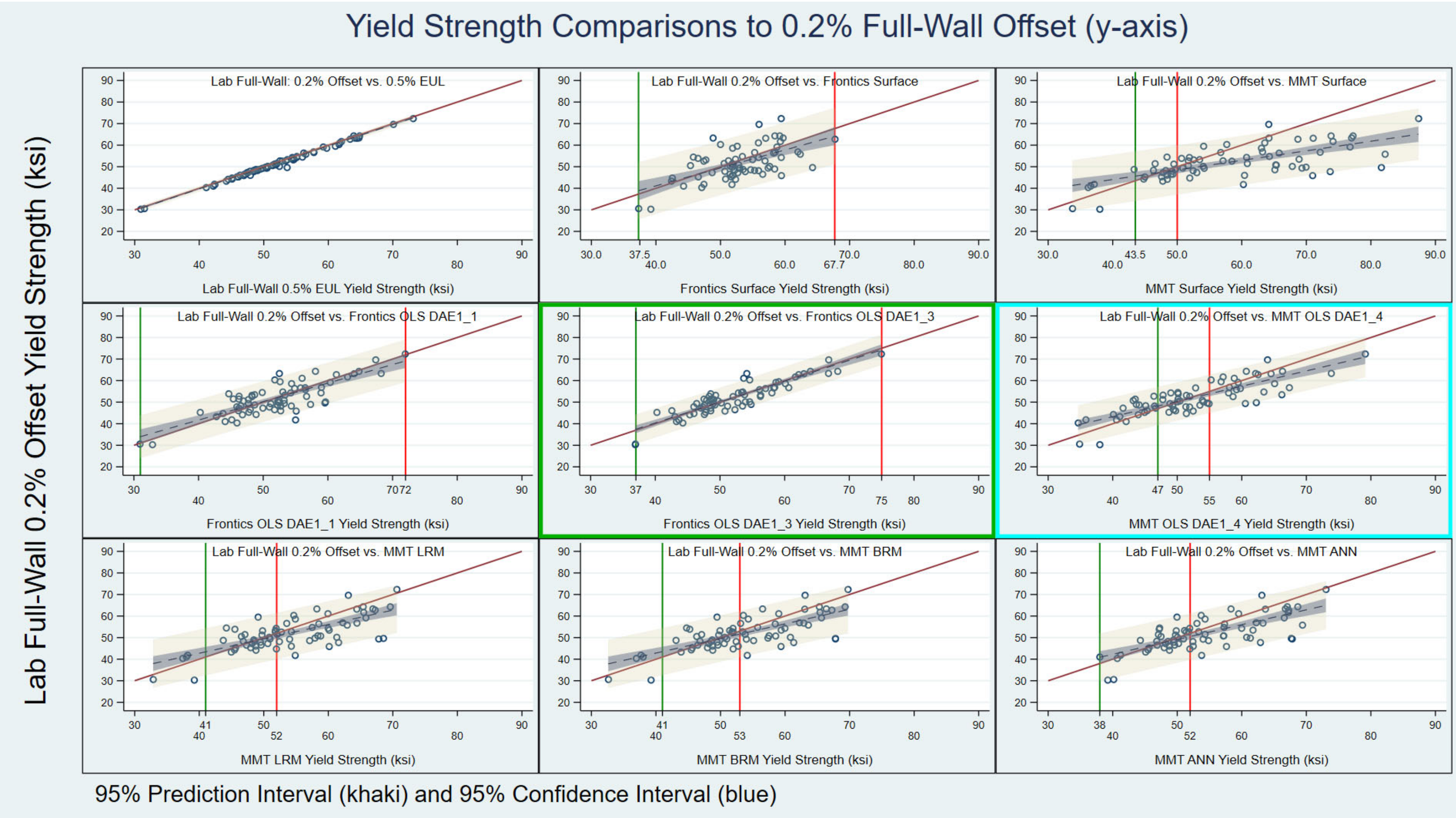

(b) Same as Figure 105a but with intersections of the confidence intervals and the unity line annotated with green and red vertical lines.

Figure 106. Tensile Strength for Lab, Surface, and Top Models with OLS CI & PI.

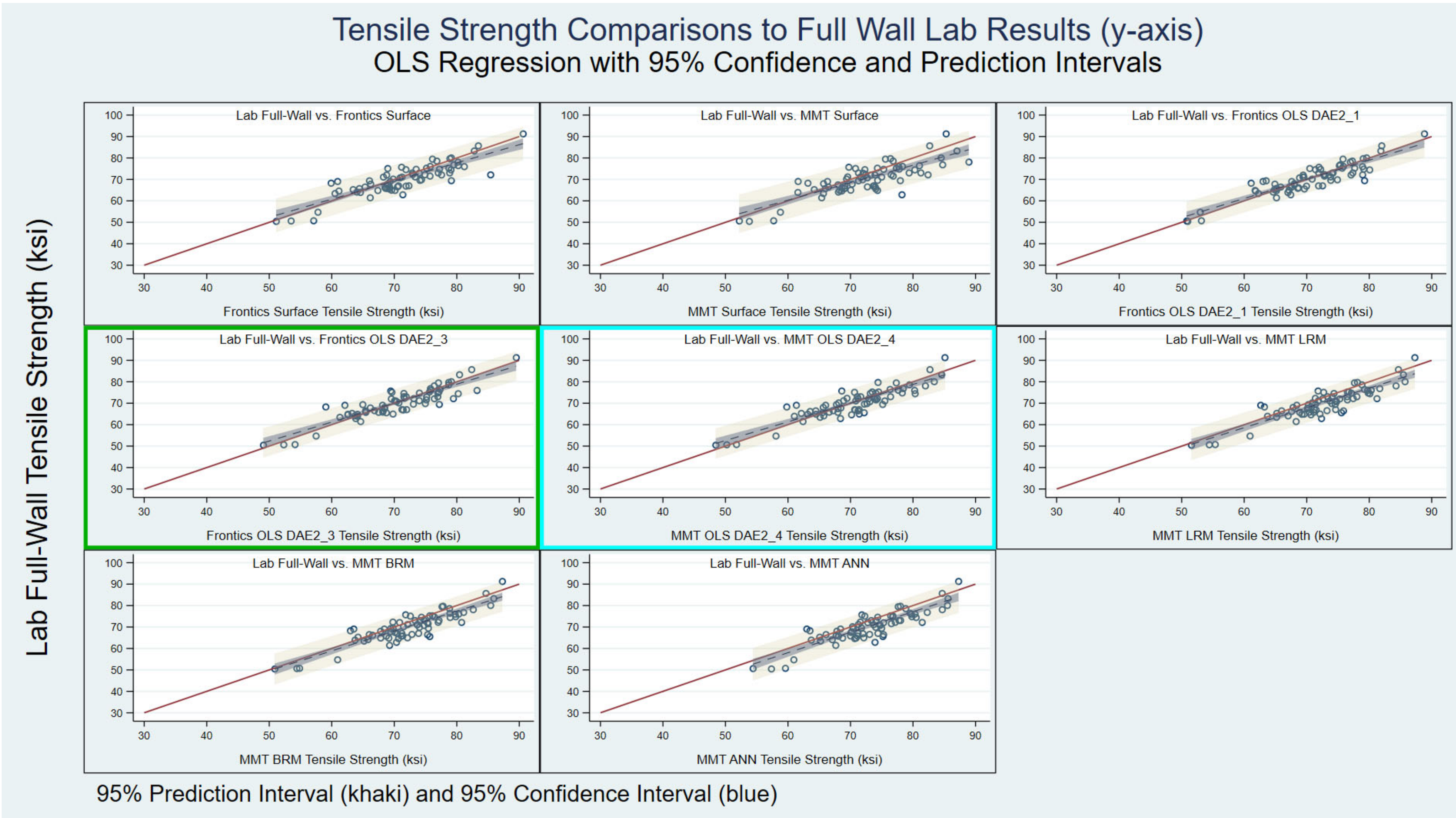

Chapter 6: Data Analytics Modeling: OLS, BMA, BNM, GPM, and MBGPM

6.1 Summary

Pipeline infrastructure and its safety are critical for the functioning of the U.S. economy and our standard of living. Accurate pipe material strength estimation is critical for the integrity and risk assessment of aging pipeline infrastructure systems. Existing techniques focus on the single modality deterministic estimation of pipe strength and ignores inhomogeneity and uncertainties. A systemic data-driven analytics modeling approach is proposed to accurately estimate the pipe yield strength and ultimate strength. This approach uses information fusion of multimodality surface measurement, e.g., surface chemical compositions, pipe overview data, hardness, and grain size. The study starts with variable selection and model selection by using Bayesian model averaging method. Ranking of variables are obtained and the strength estimation is performed by using identified most important variables. Model selection using ordinary least-squares linear model and quadratic model is done first for future model fusion. Following this, weighted parametric model with strong robustness is constructed by Bayesian updating model averaging method which shows outstanding regression performance and validation performance. Next, non-parametric Bayesian network model is applied to encode both continuous and categorical data. The flexibility of proposed Bayesian networks model provides easy ways for both prognostic (forward) and diagnostic (backward) reasoning. Gaussian process model is introduced to deal with possible nonlinear relationships. Uniform approximation and projection method is proposed to accomplish low dimensional representation. Manifold-base Gaussian process model is applied in two-dimensional Laplace space with dimension reduction. All the proposed models are evaluated using 70-sample pipe dataset and regression performance and validation performance of each model are justified. Conclusions from the proposed study are drawn. The "R" programming language/environment source code used to generate regressions and other output for this chapter is provided for both Windows and Apple Mac platforms in Appendix D.

6.2 Introduction

Pipeline infrastructure is one of the transportation systems for water, sewage, natural gas, petroleum, and refined products. Being recognized as one of the safest ways to transport flammable materials such as natural gas and petroleum, the United State (US) has become the leading nation that constructs the most millage length in the gas pipeline. There are three types of pipeline systems found along the transportation route bringing natural gas from the point of production to the point of use. The three main pipeline systems are Gathering Pipeline system, Transmission Pipeline system, and Distribution Pipeline System as shown in Figure 107. Gathering pipeline system gathers raw natural gas from production wells and transports it to large cross-country transmission pipelines. Transmission pipeline systems transport natural gas thousands of miles from processing facilities across many parts of the continental United States. Natural gas distribution pipeline systems can be found in thousands of communities from coast to coast and distribute natural gas to homes and businesses through large distribution lines mains and service lines. The latest data by 2017 shows that the US has recorded a total gas distribution main and estimated service length of 2,235,880 miles across the nation. For both onshore and offshore line, US has total 300,650 miles of Transmission pipeline and 18,357 miles of Gathering pipelines, respectively[12].

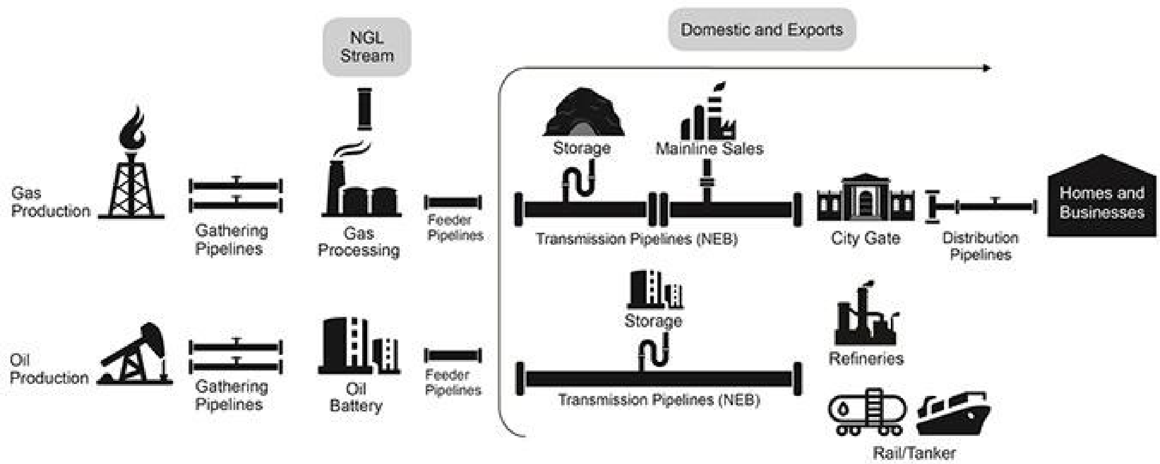

Figure 107. Schematic Diagram of the Gas Pipeline System

The Integrity Verification Process requires the testing for the aging pipe strength and toughness estimation and is one of the most critical components for the balance of safety and economy. This is one of the research topics in the PHMSA solicitation and is the focus of the proposed study. Many existing techniques are available for the pipe strength and toughness estimation, which are mainly based on single modality surface mechanical hardness and stress-strain measurements[13, 14]. Statistical analysis has been done for pipe steels on the mean and scatter of hardness-inferred strength[15]. One critical gap is that most estimation techniques focus on single measurement and did not fully utilize various sources of information from multiple types of measurement techniques. In principle, each measurement may contain complementary information for the true material strength and an information fusion approach can increase the efficiency and accuracy for estimation. Another critical gap is the systematic inclusion of uncertainties in the strength estimation. Some known sources of these uncertainties are: 1) material intrinsic randomness; 2) material spatial variability; 3) manufacturing and installation variability; and 4) operational and environmental conditions. Reduction of the impact of these uncertainties to the final strength estimation is critical to enhance the confidence in integrity assessment.

Accurate pipe material strength estimation is critical for the integrity and risk assessment of aging pipeline infrastructure systems. In order to measure the mechanical properties of the pipelines, nondestructive testing is needed without destroying the serviceability of the pipeline part or system. Some indirect methods are proposed through the relationship between the yield/ ultimate strength and surface material properties such as chemical composition, volume fraction and hardness. In this project, several models are proposed for both yield strength and ultimate strength estimation given pipe surface chemical compositions, overview data, hardness, and grain size. This chapter is organized as follows.

First, variable selection and model selection are conducted by Bayesian model averaging (BMA) which illustrates the importance of each variable and potential preferable parametric models for pipe strength estimation. Next, the chosen ordinary least-squares (OLS) models are further evaluated with full data regression and split data validation. Following this, in order to deal with model uncertainty, Bayesian updating model averaging (BUMA) is proposed to merge single linear model and quadratic model together. Besides parametric model construction, there are some non-parametric modelling methods can be used for pipe strength estimation. Bayesian network model (BNM) is applied which encodes continuous variables and categorical variables as well. As for potential non-linear relationship among different type of data, Gaussian process model (GPM) is introduced. Manifold based Gaussian process (MFGP) model combining Uniform Approximation and Projection with Gaussian process is demonstrated for dimension reduction computational efficiency improvement.

6.3 Variable Selection & Model Selection

Variable and feature selection have become the focus of many studies for which datasets with tens or hundreds of thousands of variables are available. The objective of variable selection is three-fold: improving the prediction performance of the predictors, providing faster and more cost-effective predictors, and providing a better understanding of the underlying process that generated the data[16]. Model uncertainty is a problem that arises frequently in applied statistics which tries to explain the variation of the response variable and determine whether the model is robust enough to deal with additional explanatory variables or perturbations of the data. Bayesian model averaging (BMA) has become a popular alternative to model selection.

Bayesian model averaging addresses model uncertainty in a canonical regression problem. Suppose a linear model structure, with y being the dependent variable, α_γ a constant, β_γ the coefficients, and ε a normal independent and identically distributed error term with variance σ^2:

$$y = \alpha_\gamma + X_\gamma \beta_\gamma + \varepsilon, \qquad \varepsilon \sim N(0, \sigma^2 I). \tag{1}$$

A problem arises when there are many potential explanatory variables in a matrix X: Which variables $X_\gamma \in \{X\}$ should be included in the model? And how important are they? The direct approach to do inference on a single linear model that includes all variables is inefficient or even infeasible with limited number of observations.

BMA tackles the problem by estimating models for all possible combinations of $\{X\}$ and constructing a weighted average over all of them. If X contains K potential variables, this means 2^K variable combinations and thus 2^K models. The model weights for this averaging stem from posterior model probabilities that arise from Bayes' theorem:

$$p(M_\gamma | y, X) = \frac{p(y|M_\gamma, X)\,p(M_\gamma)}{p(y|X)} = \frac{p(y|M_\gamma, X)\,p(M_\gamma)}{\sum_{s=1}^{2^K} p(y|M_s, X)\,p(M_s)}. \tag{2}$$

Hence, $p(y|X)$ denotes the integrated likelihood which is constant over all models. Therefore, the posterior model probability (PMP) is proportional to the integrated likelihood of model M_γ and its prior model probability $p(M_\gamma)$. By re-normalization of the product, one can infer the model weighted posterior distribution for any estimator θ of the coefficient β_γ:

$$p(\theta|y,X) = \sum_{\gamma=1}^{2^K} p(\theta|M_\gamma, y, X)\frac{p(M_\gamma|y,X)p(M_\gamma)}{\sum_{s=1}^{2^K} p(M_s|y,X)p(M_s)}. \quad (3)$$

The model prior $p(M_\gamma)$ has to be assumed by the researcher and should reflect prior beliefs. A popular choice is to set a uniform prior probability for each model $p(M_\gamma) \propto 1$ to represent the lack of prior knowledge.

With a small number of variables, it is straightforward to enumerate all potential variable combinations to obtain posterior results. For a larger number of covariates, this becomes more time consuming. In such a case, Markov-Chain Monte Carlo (MCMC) sampling is usually to approximate the posterior distribution. BMA mostly relies on the Metropolis-Hastings algorithm, which "walks" through the model space as follows: At step i, the sampler stands at a certain "current" model M_i with PMP $p(M_i|y,X)$. In step $i+1$ a candidate model M_j is proposed. The sampler switches from the current model to model M_j with probability $p_{i,j}$:

$$p_{i,j} = min\left(1, p(M_j|y,X)/p(M_i|y,X)\right). \quad (4)$$

In case model M_j is rejected, the sampler moves to the next step and proposes a new model M_k against M_i. In case model M_j is accepted, it becomes the current model and has to survive against further models in the next step. In this manner, the number of times each model is kept will converge to the distribution of posterior model probabilities $p(M_i|y,X)$.

There are several R packages available to solve variable selection and model selection following the major steps described above. For example, the BMS (Bayesian model sampling) package using R implements Bayesian model averaging for linear regression models. With the BMS package, users are allowed to specify their own model priors and offers a possibility of subjective inference by setting "prior inclusion probabilities" according to the researcher's beliefs. Furthermore, graphical analysis of results is provided by numerous built-in plot functions of posterior densities, predictive densities, and graphical illustrations to compare results under different prior settings. Another choice for model selection in linear regression is Bayesian adaptive sampling (BAS) package, that samples models without replacement from the space of models. For problems that permit enumeration of all models, BAS is guaranteed to enumerate the model space in 2^K iterations[18].

In this study, we used BAS package to do the variable selection and model selection. We used 70-sample full dataset with 22 variables included in the initial selection step which are LAB SPECTRO 5 mil surface chemical compositions, 5 mil pearlite (PL), pipe overview data nominal diameter (ND) and wall thickness (WT), rockwell hardness at the outer diameter (Hod) and 5 mil grain size (GS, $GS^{1/2}$, $GS^{-1/2}$). The variable indexes are shown in Table 11. For yield strength estimation, the response y would be the difference between Lab Full Wall 0.2% offset yield strength (YS_t) and the yield strength got from surface techniques (YS_s) which can be written as $y = YS_t - YS_s$. Similarly, for ultimate strength estimation, the delta term $y = UTS_t - UTS_s$. By doing variable selection and model selection, variable posterior inclusion probability (PIP) ranks are achieved as well as several linear models and quadratic models are selected for further investigations.

Table 11. Variables Used for Yield Strength and Ultimate Strength Estimation

Index	**1**	**2**	**3**	**4**	**5**	**6**	**7**	**8**	**9**	**10**	**11**
Variable	C	Mn	P	S	Al	Cr	Cu	Mo	Nb	Ni	Si
Index	**12**	**13**	**14**	**15**	**16**	**17**	**18**	**19**	**20**	**21**	**22**
Variable	Ti	V	B	N	PL	Hod	GS	GSsqrt	GSsqrtneg	ND	WT

Yield Strength

Linear model

22 variables are used in BMA approach with Frontics yield strength baseline, the response here is the delta term $y = YS_t - YS_s$. The PIP for all the input variables and the rank list of linear terms are shown in Table 12, which indicate the importance of each variable in terms of using linear model. It should be noted that the response here is the delta term instead of the benchmark yield strength Thus, it is not safe to say the variable with the highest PIP would still be the most useful in predicting yield strength directly. The delta term is to modify the yield strength got from surface techniques (YS_s). By doing this, the predictive Yield strength can be calculated. Furthermore, Top 20 best linear models are shown in Figure 108, where each column is a single linear model and 19 rows indicate 18 input variables and an intercept term, where colored cell means that the variable in such row is included in the model in corresponding column. And more specific properties of these 20 linear models are shown in Table 13. where "1" means included and "0" means not included intuitively, BF is Bayesian factor, "PostProbs" is posterior model probabilities, "R2" is R square, and Dim is the dimension of linear models.

As can be seen in Table 12. the top 5 variables are ND, N, Nb, Mo and Mn from the variable selection results which means they are more useful to predict the yield strength delta term. The top 5 variables are having relative high PIP. However, they are not necessarily to be included in the best linear model. To find the best yield strength linear model, we still need to look at the model selection part. Posterior model probability (PMP) and R square (R2) are two chosen criterions for regression model selection. BMA approach naturally selects the best model with the largest PMP like model M1 in yellow shaded column. Nevertheless, in regarding to inevitable model uncertainties, another model M8 in blue shaded column with the largest R square among top 20 yield strength linear model has been selected as well for further comparison. Considering higher PMP and larger R2 at the same time will guarantee better model performance. The results of using MMT yield strength baseline are shown in Table 14, Figure 109 and Table 15. The top 5 variables are ND, S, N, Cu and Mo. M1 with highest PMP, and M8 with largest R2.

Table 12. Rank of Variables for Yield Strength Linear Model (Frontics)

Rank	**1**	**2**	**3**	**4**	**5**	**6**	**7**	**8**
Variable	ND	N	Nb	Mo	Mn	GSsqrtneg	Si	GSsqrt
PIP	1.000	0.980	0.897	0.780	0.384	0.325	0.301	0.293
Rank	**9**	**10**	**11**	**12**	**13**	**14**	**15**	**16**
Variable	GS	PL	C	Hod	Ti	S	P	V
PIP	0.280	0.263	0.263	0.222	0.194	0.192	0.163	0.153
Rank	**17**	**18**	**19**	**20**	**21**	**22**		
Variable	Cr	Al	Ni	WT	Cu	B		
PIP	0.141	0.135	0.132	0.131	0.126	0.113		

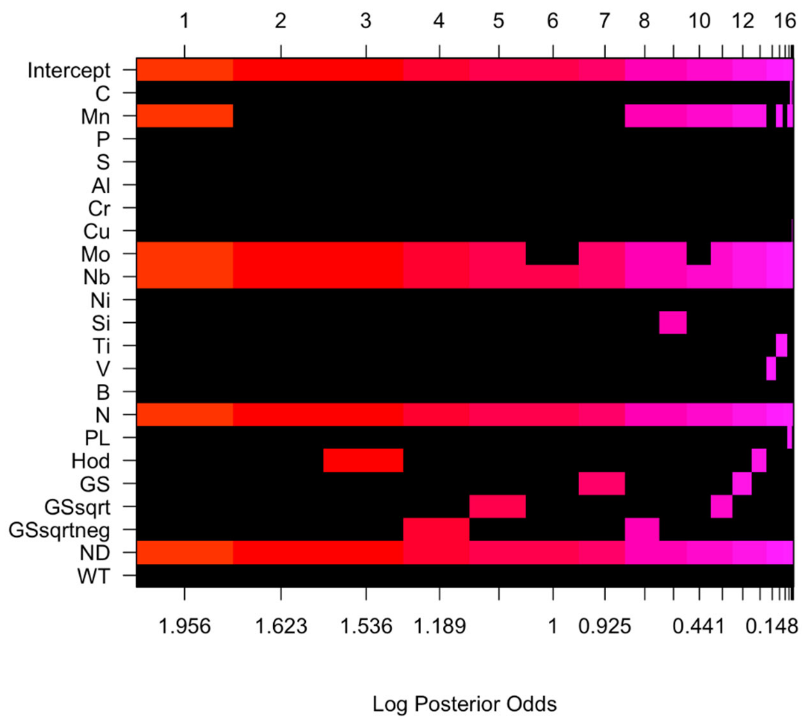

Figure 108. Top 20 Yield Strength Linear Models (Frontics)

Table 13. Properties of Top 20 Yield Strength Linear Models (Frontics)

	M1	M2	M3	M4	M5	M6	M7	M8	M9	M10
Intercept	1	1	1	1	1	1	1	1	1	1
C	0	0	0	0	0	0	0	0	0	0
Mn	1	0	0	0	0	0	0	1	1	1
P	0	0	0	0	0	0	0	0	0	0
S	0	0	0	0	0	0	0	0	0	0
Al	0	0	0	0	0	0	0	0	0	0
Cr	0	0	0	0	0	0	0	0	0	0
Cu	0	0	0	0	0	0	0	0	0	0
Mo	1	1	1	1	1	0	1	1	1	0
Nb	1	1	1	1	1	1	1	1	1	1
Ni	0	0	0	0	0	0	0	0	0	0
Si	0	0	0	0	0	0	0	0	1	0
Ti	0	0	0	0	0	0	0	0	0	0
V	0	0	0	0	0	0	0	0	0	0
B	0	0	0	0	0	0	0	0	0	0
N	1	1	1	1	1	1	1	1	1	1
PL	0	0	0	0	0	0	0	0	0	0
Hod	0	0	1	0	0	0	0	0	0	0
GS	0	0	0	0	0	0	1	0	0	0
GSsqrt	0	0	0	0	1	0	0	0	0	0
GSsqrtneg	0	0	0	1	0	0	0	1	0	0
ND	1	1	1	1	1	1	1	1	1	1
WT	0	0	0	0	0	0	0	0	0	0
BF	1	0.716	0.631	0.468	0.394	0.381	0.364	0.250	0.236	0.224
PostProbs	0.015	0.011	0.010	0.007	0.006	0.006	0.005	0.004	0.004	0.003
R2	0.580	0.550	0.575	0.571	0.569	0.513	0.568	0.589	0.588	0.535
dim	6	5	6	6	6	4	6	7	7	5
	M11	**M12**	**M13**	**M14**	**M15**	**M16**	**M17**	**M18**	**M19**	**M20**
Intercept	1	1	1	1	1	1	1	1	1	1
C	0	0	0	0	0	0	0	1	0	1
Mn	1	1	1	0	1	0	1	1	1	1
P	0	0	0	0	0	0	0	0	0	0
S	0	0	0	0	0	0	0	0	0	0
Al	0	0	0	0	0	0	0	0	0	0
Cr	0	0	0	0	0	0	0	0	0	0
Cu	0	0	0	0	0	0	0	0	1	0
Mo	1	1	1	1	1	1	1	1	1	1
Nb	1	1	1	1	1	1	1	1	1	1
Ni	0	0	0	0	0	0	0	0	0	0
Si	0	0	0	0	0	0	0	0	0	0
Ti	0	0	0	0	1	1	0	0	0	0
V	0	0	0	1	0	0	0	0	0	0
B	0	0	0	0	0	0	0	0	0	0
N	1	1	1	1	1	1	1	1	1	1
PL	0	0	0	0	0	0	1	1	0	0
Hod	0	0	1	0	0	0	0	0	0	0
GS	0	1	0	0	0	0	0	0	0	0
GSsqrt	1	0	0	0	0	0	0	0	0	0
GSsqrtneg	0	0	0	0	0	0	0	0	0	0
ND	1	1	1	1	1	1	1	1	1	1
WT	0	0	0	0	0	0	0	0	0	0
BF	0.215	0.202	0.187	0.159	0.160	0.154	0.146	0.146	0.158	0.146
PostProbs	0.003	0.003	0.003	0.003	0.002	0.002	0.002	0.002	0.002	0.002
R2	0.587	0.586	0.586	0.558	0.584	0.557	0.583	0.583	0.584	0.583
dim	6	8	9	8	8	8	7	8	9	9

Table 14. Rank of Variables for Yield Strength Linear Model (MMT)

Rank	**1**	**2**	**3**	**4**	**5**	**6**	**7**	**8**
Variable	ND	S	N	Cu	Mo	PL	C	B
PIP	1.000	0.416	0.309	0.305	0.275	0.250	0.249	0.228
Rank	**9**	**10**	**11**	**12**	**13**	**14**	**15**	**16**
Variable	V	GS	WT	Si	GSsqrt	GSsqrtneg	Cr	Ti
PIP	0.183	0.171	0.168	0.166	0.165	0.156	0.135	0.135
Rank	**17**	**18**	**19**	**20**	**21**	**22**		
Variable	Ni	P	Nb	Mn	Al	Hod		
PIP	0.130	0.130	0.127	0.122	0.120	0.118		

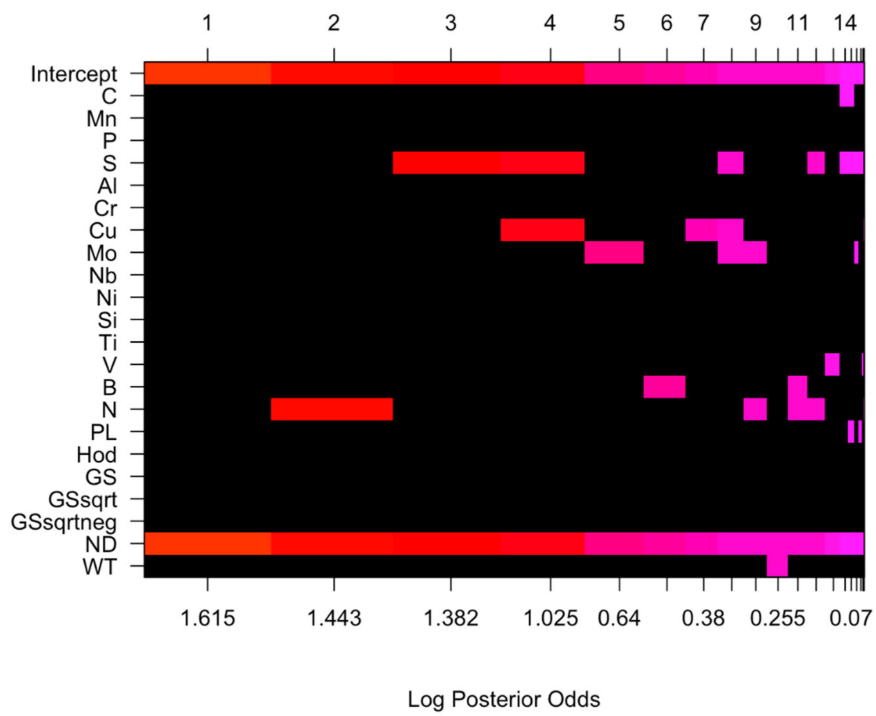

Figure 109. Top 20 Yield Strength Linear Models (MMT)

Table 15. Properties of Top 20 Yield Strength Linear Models (MMT)

	M1	M2	M3	M4	M5	M6	M7	M8	M9	M10
Intercept	1	1	1	1	1	1	1	1	1	1
C	0	0	0	0	0	0	0	0	0	0
Mn	0	0	0	0	0	0	0	0	0	0
P	0	0	0	0	0	0	0	0	0	0
S	0	0	1	1	0	0	0	1	0	0
Al	0	0	0	0	0	0	0	0	0	0
Cr	0	0	0	0	0	0	0	0	0	0
Cu	0	0	0	1	0	0	1	1	0	0
Mo	0	0	0	0	1	0	0	1	1	0
Nb	0	0	0	0	0	0	0	0	0	0
Ni	0	0	0	0	0	0	0	0	0	0
Si	0	0	0	0	0	0	0	0	0	0
Ti	0	0	0	0	0	0	0	0	0	0
V	0	0	0	0	0	0	0	0	0	0
B	0	0	0	0	0	1	0	0	0	0
N	0	1	0	0	0	0	0	0	1	0
PL	0	0	0	0	0	0	0	0	0	0
Hod	0	0	0	0	0	0	0	0	0	0
GS	0	0	0	0	0	0	0	0	0	0
GSsqrt	0	0	0	0	0	0	0	0	0	0
GSsqrtneg	0	0	0	0	0	0	0	0	0	0
ND	1	1	1	1	1	1	1	1	1	1
WT	0	0	0	0	0	0	0	0	0	1
BF	1	0.716	0.631	0.468	0.394	0.381	0.364	0.250	0.236	0.224
PostProbs	0.015	0.011	0.010	0.007	0.006	0.006	0.005	0.004	0.004	0.003
R2	0.580	0.550	0.575	0.571	0.569	0.513	0.568	0.589	0.588	0.535
dim	2	3	3	4	3	3	3	5	4	3

	M11	M12	M13	M14	M15	M16	M17	M18	M19	M20
Intercept	1	1	1	1	1	1	1	1	1	1
C	0	0	0	1	1	0	0	0	0	0
Mn	0	0	0	0	0	0	0	0	0	0
P	0	0	0	0	0	0	0	0	0	0
S	0	1	0	1	1	1	1	1	0	1
Al	0	0	0	0	0	0	0	0	0	0
Cr	0	0	0	0	0	0	0	0	0	0
Cu	0	0	0	0	0	0	0	0	1	0
Mo	0	0	0	0	0	1	0	0	0	0
Nb	0	0	0	0	0	0	0	0	0	0
Ni	0	0	0	0	0	0	0	0	0	0
Si	0	0	0	0	0	0	0	0	0	0
Ti	0	0	0	0	0	0	0	0	0	0
V	0	0	1	0	0	0	0	1	0	0
B	1	0	0	0	0	0	0	0	0	0
N	1	1	0	0	0	0	0	0	1	0
PL	0	0	0	0	1	0	1	0	0	0
Hod	0	0	0	0	0	0	0	0	0	0
GS	0	0	0	0	0	0	0	0	0	0
GSsqrt	0	0	0	0	0	0	0	0	0	0
GSsqrtneg	0	0	0	0	0	0	0	0	0	0
ND	1	1	1	1	1	1	1	1	1	1
WT	0	0	0	0	0	0	0	0	0	1
BF	0.215	0.202	0.187	0.159	0.160	0.154	0.146	0.146	0.158	0.146
PostProbs	0.003	0.003	0.003	0.003	0.002	0.002	0.002	0.002	0.002	0.002
R2	0.587	0.586	0.586	0.558	0.584	0.557	0.583	0.583	0.584	0.583
dim	4	4	3	4	5	4	4	4	4	4

Quadratic model

In order to do the variable selection and model selection for yield strength quadratic model, we use the top 5 variables (ND, N, Nb, Mo and Mn) to do the expansion. Then we got 20 expanded variables including the original 5 linear terms, 5 power terms and 10 interactive terms as shown in Table 16. Following the same procedures as we did in previous subsection, the rank list of variables for yield strength quadratic modelling is achieved in Table 17, as well as top 20 best quadratic models shown in Figure 110. In Table 18, model M1 with the highest PMP and model M13 with largest R2 and lower dimension are selected for further validation in the next section. The results of using MMT yield strength baseline are shown in Table 19, Table 20, Figure 111 and Table 21.

Table 16. Variables Used for Yield Strength Quadratic Model (Frontics)

Index	**1**	**2**	**3**	**4**	**5**	**6**	**7**	**8**	**9**	**10**
Variable	ND	N	Nb	Mo	Mn	ND2	N2	Nb2	Mo2	Mn2
Index	**11**	**12**	**13**	**14**	**15**	**16**	**17**	**18**	**19**	**20**
Variable	NDN	NDNb	NDMo	NDMn	NNb	NMo	NMn	NbMo	NbMn	MoMn

Table 17. Rank of Variables for Yield Strength Quadratic Model (Frontics)

Rank	**1**	**2**	**3**	**4**	**5**	**6**	**7**	**8**	**9**	**10**
Variable	N	N2	ND	NDN	Mo2	NNb	NbMo	Mo	NbMn	NMo
PIP	0.9991	0.9810	0.8984	0.8016	0.6109	0.5488	0.5001	0.4974	0.4846	0.4770
Rank	**11**	**12**	**13**	**14**	**15**	**16**	**17**	**18**	**19**	**20**
Variable	Mn	MoMn	Nb	NMn	NDMo	Mn2	ND2	NDMn	Nb2	NDNb
PIP	0.3715	0.3320	0.3277	0.3060	0.2753	0.2492	0.1945	0.1897	0.1881	0.1664

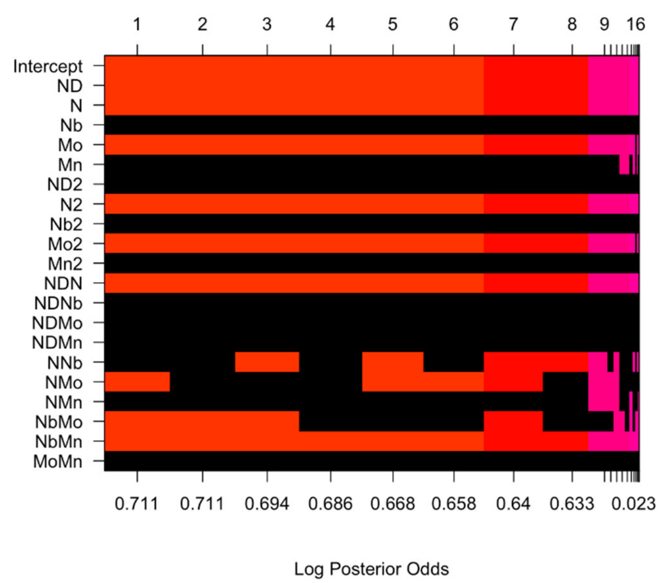

Figure 110. Top 20 Yield Strength Quadratic Models (Frontics)

Table 18. Properties of Top 20 Yield Strength Quadratic Models (Frontics)

	M1	M2	M3	M4	M5	M6	M7	M8	M9	M10
Intercept	1	1	1	1	1	1	1	1	1	1
ND	1	1	1	1	1	1	1	1	1	1
N	1	1	1	1	1	1	1	1	1	1
Nb	0	0	0	0	0	0	0	0	0	0
Mo	1	1	1	1	1	1	1	1	1	1
Mn	0	0	0	0	0	0	0	0	0	0
ND2	0	0	0	0	0	0	0	0	0	0
N2	1	1	1	1	1	1	1	1	1	1
Nb2	0	0	0	0	0	0	0	0	0	0
Mo2	1	1	1	1	1	1	1	1	1	1
Mn2	0	0	0	0	0	0	0	0	0	0
NDN	1	1	1	1	1	1	1	1	1	1
NDNb	0	0	0	0	0	0	0	0	0	0
NDMo	0	0	0	0	0	0	0	0	0	0
NDMn	0	0	0	0	0	0	0	0	0	0
NNb	0	0	1	0	1	0	1	1	1	0
NMo	1	0	0	0	1	1	1	0	1	1
NMn	0	0	0	0	0	0	0	0	1	1
NbMo	1	1	1	0	0	0	1	0	0	0
NbMn	1	1	1	1	1	1	1	1	1	1
MoMn	0	0	0	0	0	0	0	0	0	0
BF	1	1.000	1.000	1.000	1.000	1.000	1.000	1.000	0.509	0.509
PostProbs	0.003	0.003	0.003	0.003	0.003	0.003	0.003	0.003	0.002	0.002
R2	0.699	0.699	0.699	0.699	0.699	0.699	0.699	0.699	0.711	0.711
dim	10	9	10	8	10	9	11	9	11	10
	M11	**M12**	**M13**	**M14**	**M15**	**M16**	**M17**	**M18**	**M19**	**M20**
Intercept	1	1	1	1	1	1	1	1	1	1
ND	1	1	1	1	1	1	1	1	1	1
N	1	1	1	1	1	1	1	1	1	1
Nb	0	0	0	0	0	0	0	0	0	0
Mo	1	1	1	1	1	0	1	1	1	0
Mn	0	1	1	0	1	0	1	0	0	0
ND2	0	0	0	0	0	0	0	0	0	0
N2	1	1	1	1	1	1	1	1	1	1
Nb2	0	0	0	0	0	0	0	0	0	0
Mo2	1	1	1	1	1	0	1	1	1	0
Mn2	0	0	0	0	0	0	0	0	0	0
NDN	1	1	1	1	1	1	1	1	1	1
NDNb	0	0	0	0	0	0	0	0	0	0
NDMo	0	0	0	0	0	0	0	0	0	0
NDMn	0	0	0	0	0	0	0	0	0	0
NNb	1	0	0	0	1	0	1	1	0	1
NMo	1	0	0	0	0	0	0	0	1	0
NMn	1	0	0	1	0	0	0	1	1	0
NbMo	1	1	0	1	0	1	1	1	1	0
NbMn	1	1	1	1	1	1	1	1	1	1
MoMn	0	0	0	0	0	0	0	0	0	0
BF	0.509	0.510	0.510	0.509	0.510	0.506	0.510	0.509	0.509	0.506
PostProbs	0.002	0.002	0.002	0.002	0.002	0.002	0.002	0.002	0.002	0.002
R2	0.711	0.711	0.711	0.711	0.711	0.654	0.711	0.711	0.711	0.654
dim	12	10	9	10	10	7	11	11	11	7

Table 19. Variables Used for Yield Strength Quadratic Model (MMT)

Index	1	2	3	4	5	6	7	8	9	10
Variable	ND	S	N	Cu	Mo	ND2	S2	N2	Cu2	Mo2
Index	**11**	**12**	**13**	**14**	**15**	**16**	**17**	**18**	**19**	**20**
Variable	NDS	NDN	NDCu	NDMo	SN	SCu	SMo	NCu	NMo	CuMo

Table 20. Rank of Variables for Yield Strength Quadratic Model (MMT)

Rank	1	2	3	4	5	6	7	8	9	10
Variable	S	S2	ND	NMo	NDCu	SN	ND2	NCu	Cu2	N2
PIP	0.6706	0.5727	0.5071	0.4637	0.4517	0.4448	0.4407	0.3783	0.3702	0.3667
Rank	**11**	**12**	**13**	**14**	**15**	**16**	**17**	**18**	**19**	**20**
Variable	Mo2	N	NDS	Cu	NDMo	SMo	Mo	SCu	CuMo	NDN
PIP	0.3450	0.3433	0.3427	0.2995	0.2421	0.2373	0.2198	0.2103	0.1786	0.1675

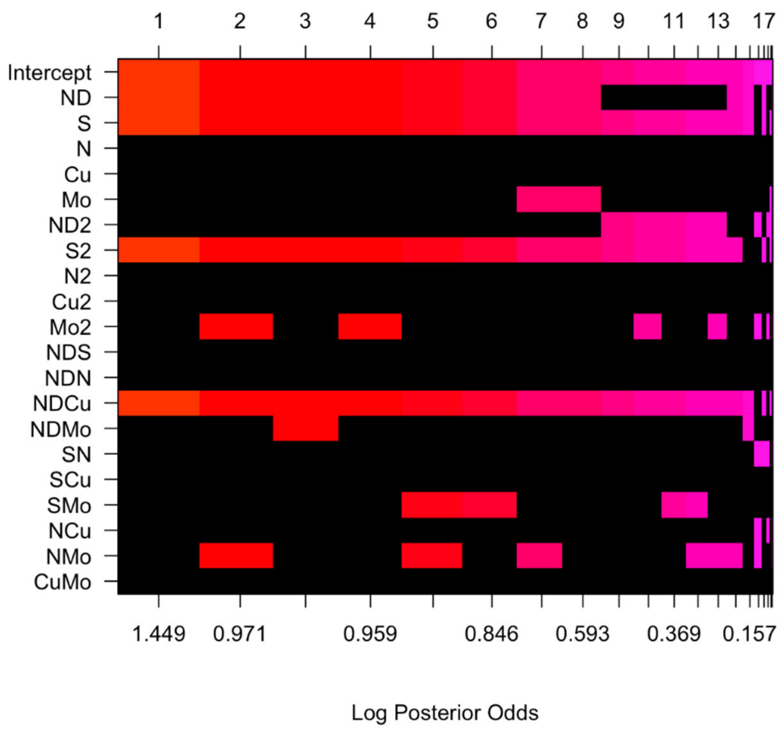

Figure 111. Top 20 Yield Strength Quadratic Models (MMT)

Table 21. Properties of Top 20 Yield Strength Quadratic Models (MMT)

	M1	M2	M3	M4	M5	M6	M7	M8	M9	M10
Intercept	1	1	1	1	1	1	1	1	1	1
ND	1	1	1	1	1	1	1	1	0	0
S	1	1	1	1	1	1	1	1	1	1
N	0	0	0	0	0	0	0	0	0	0
Cu	0	0	0	0	0	0	0	0	0	0
Mo	0	0	0	0	0	0	1	1	0	0
ND2	0	0	0	0	0	0	0	0	1	1
S2	1	1	1	1	1	1	1	1	1	1
N2	0	0	0	0	0	0	0	0	0	0
Cu2	0	0	0	0	0	0	0	0	0	0
Mo2	0	1	0	1	0	0	0	0	0	1
NDS	0	0	0	0	0	0	0	0	0	0
NDN	0	0	0	0	0	0	0	0	0	0
NDCu	1	1	1	1	1	1	1	1	1	1
NDMo	0	0	1	0	0	0	0	0	0	0
SN	0	0	0	0	0	0	0	0	0	0
SCu	0	0	0	0	0	0	0	0	0	0
SMo	0	0	0	0	1	1	0	0	0	0
NCu	0	0	0	0	0	0	0	0	0	0
NMo	0	1	0	0	1	0	1	0	0	0
CuMo	0	0	0	0	0	0	0	0	0	0
BF	1	0.632	0.655	0.632	0.580	0.580	0.454	0.454	0.419	0.339
PostProbs	0.003	0.002	0.002	0.002	0.002	0.001	0.001	0.001	0.001	0.001
R2	0.627	0.644	0.645	0.644	0.643	0.643	0.641	0.641	0.618	0.638
dim	8	8	8	9	9	9	8	9	8	9

	M11	M12	M13	M14	M15	M16	M17	M18	M19	M20
Intercept	1	1	1	1	1	1	1	1	1	1
ND	0	0	0	1	1	0	1	0	0	1
S	1	1	1	1	1	0	1	0	1	0
N	0	0	0	0	0	0	0	0	0	0
Cu	0	0	0	0	0	0	0	0	0	0
Mo	0	0	0	0	0	0	0	0	1	0
ND2	1	1	1	0	0	1	0	1	1	0
S2	1	1	1	1	0	0	1	0	1	0
N2	0	0	0	0	0	0	0	0	0	0
Cu2	0	0	0	0	0	0	0	0	0	0
Mo2	0	0	1	0	0	1	0	1	0	1
NDS	0	0	0	0	0	0	0	0	0	0
NDN	0	0	0	0	0	0	0	0	0	0
NDCu	1	1	1	1	1	0	1	0	1	0
NDMo	0	0	0	0	1	0	0	0	0	0
SN	0	0	0	0	0	1	1	1	0	1
SCu	0	0	0	0	0	0	0	0	0	0
SMo	1	1	0	0	0	0	0	0	0	0
NCu	0	0	0	0	0	1	0	1	0	1
NMo	0	1	1	1	0	1	0	0	0	1
CuMo	0	0	0	0	0	0	0	0	0	0
BF	0.384	0.384	0.339	0.331	0.283	0.232	0.256	0.232	0.247	0.219
PostProbs	0.001	0.001	0.001	0.001	0.001	0.001	0.001	0.001	0.001	0.001
R2	0.639	0.639	0.638	0.638	0.613	0.611	0.635	0.611	0.635	0.610
dim	6	7	7	6	5	6	6	5	6	6

Ultimate Strength

Linear model

Similarly, we used 22 variables in Table 11 as inputs for variable selection and model selection of ultimate strength. The rank list of variables in terms of ultimate strength linear model is achieved in Table 22. Top 20 best models are shown in Figure 112. Again, we selected model M1 with the highest PMP and model M5 with largest R2 among top 20 models. And all the detail information is shown in Table 23. The results of using MMT yield strength baseline are shown in Table 24, Figure 113 and Table 25.

Table 22. Rank of Variables for Ultimate Strength Linear Model (Frontics)

Rank	**1**	**2**	**3**	**4**	**5**	**6**	**7**	**8**
Variable	ND	PL	C	S	Si	N	Ni	Cr
PIP	0.676	0.446	0.446	0.422	0.365	0.289	0.208	0.205
Rank	**9**	**10**	**11**	**12**	**13**	**14**	**15**	**16**
Variable	WT	Mn	GSsqrtneg	GSsqrt	GS	B	Cu	Ti
PIP	0.196	0.188	0.173	0.169	0.168	0.166	0.153	0.151
Rank	**17**	**18**	**19**	**20**	**21**	**22**		
Variable	Al	Hod	Nb	P	V	Mo		
PIP	0.134	0.131	0.129	0.127	0.124	0.115		

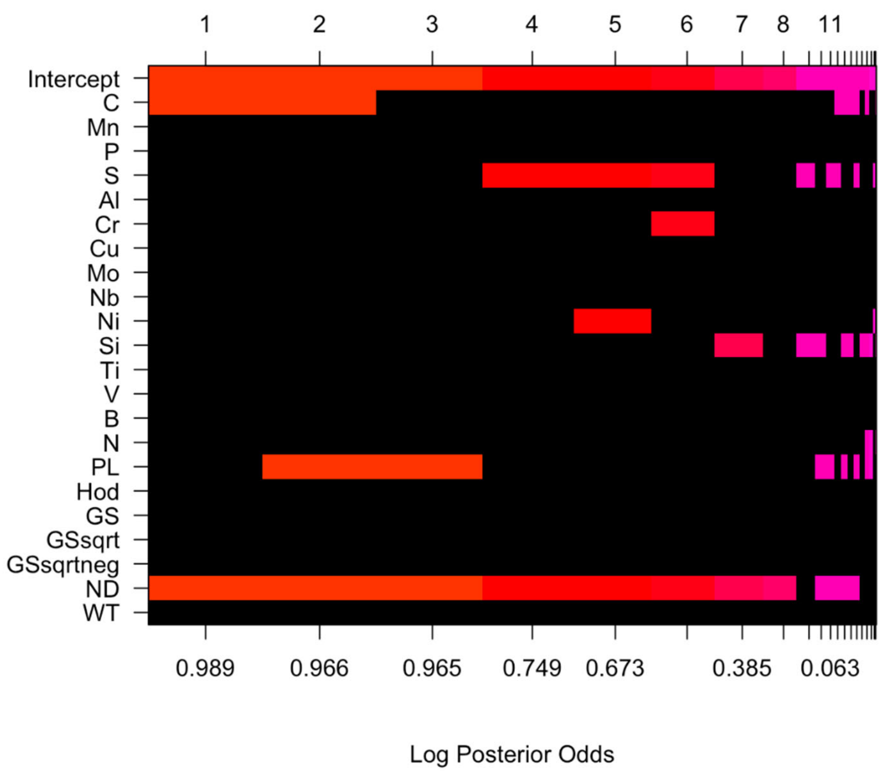

Figure 112. Top 20 Ultimate Strength Linear Models (Frontics)

Table 23. Properties of Top 20 Ultimate Strength Linear Models (Frontics)

	M1	M2	M3	M4	M5	M6	M7	M8	M9	M10
Intercept	1	1	1	1	1	1	1	1	1	1
C	1	1	0	0	0	0	0	0	0	0
Mn	0	0	0	0	0	0	0	0	0	0
P	0	0	0	0	0	0	0	0	0	0
S	0	0	0	1	1	1	0	0	1	0
Al	0	0	0	0	0	0	0	0	0	0
Cr	0	0	0	0	0	1	0	0	0	0
Cu	0	0	0	0	0	0	0	0	0	0
Mo	0	0	0	0	0	0	0	0	0	0
Nb	0	0	0	0	0	0	0	0	0	0
Ni	0	0	0	0	1	0	0	0	0	0
Si	0	0	0	0	0	0	1	0	1	1
Ti	0	0	0	0	0	0	0	0	0	0
V	0	0	0	0	0	0	0	0	0	0
B	0	0	0	0	0	0	0	0	0	0
N	0	0	0	0	0	0	0	0	0	0
PL	0	1	1	0	0	0	0	0	0	1
Hod	0	0	0	0	0	0	0	0	0	0
GS	0	0	0	0	0	0	0	0	0	0
GSsqrt	0	0	0	0	0	0	0	0	0	0
GSsqrtneg	0	0	0	0	0	0	0	0	0	0
ND	1	1	1	1	1	1	1	1	0	1
WT	0	0	0	0	0	0	0	0	0	0
BF	1	1.000	1.000	0.764	0.714	0.663	0.547	0.524	0.403	0.402
PostProbs	0.004	0.004	0.004	0.003	0.003	0.003	0.002	0.002	0.002	0.002
R2	0.181	0.181	0.181	0.175	0.222	0.220	0.167	0.114	0.160	0.209
dim	3	4	3	3	4	4	3	2	3	4
	M11	**M12**	**M13**	**M14**	**M15**	**M16**	**M17**	**M18**	**M19**	**M20**
Intercept	1	1	1	1	1	1	1	1	1	1
C	0	1	1	1	1	0	1	0	0	1
Mn	0	0	0	0	0	0	0	0	0	0
P	0	0	0	0	0	0	0	0	0	0
S	1	1	0	0	1	0	0	0	1	0
Al	0	0	0	0	0	0	0	0	0	0
Cr	0	0	0	0	0	0	0	0	0	0
Cu	0	0	0	0	0	0	0	0	0	0
Mo	0	0	0	0	0	0	0	0	0	0
Nb	0	0	0	0	0	0	0	0	0	0
Ni	0	0	0	0	0	0	0	0	1	0
Si	0	0	1	1	0	1	1	1	0	1
Ti	0	0	0	0	0	0	0	0	0	0
V	0	0	0	0	0	0	0	0	0	0
B	0	0	0	0	0	0	0	0	0	0
N	0	0	0	0	0	0	1	1	0	1
PL	1	0	1	0	1	0	1	1	0	0
Hod	0	0	0	0	0	0	0	0	0	0
GS	0	0	0	0	0	0	0	0	0	0
GSsqrt	0	0	0	0	0	0	0	0	0	0
GSsqrtneg	0	0	0	0	0	0	0	0	0	0
ND	1	1	1	1	1	0	0	0	0	0
WT	0	0	0	0	0	0	0	0	0	0
BF	0.391	0.391	0.402	0.402	0.391	0.399	0.392	0.392	0.373	0.392
PostProbs	0.002	0.002	0.002	0.002	0.002	0.002	0.002	0.002	0.001	0.001
R2	0.209	0.209	0.209	0.209	0.209	0.107	0.209	0.209	0.158	0.209
dim	4	4	5	4	5	2	5	4	3	4

Table 24. Rank of Variables for Ultimate Strength Linear Model (MMT)

Rank	1	2	3	4	5	6	7	8
Variable	N	Ti	PL	C	V	B	Nb	P
PIP	0.985	0.661	0.550	0.546	0.481	0.361	0.325	0.320
Rank	**9**	**10**	**11**	**12**	**13**	**14**	**15**	**16**
Variable	GS	GSsqrt	GSsqrtneg	Si	Cu	ND	S	Mn
PIP	0.302	0.298	0.282	0.281	0.279	0.272	0.239	0.204
Rank	**17**	**18**	**19**	**20**	**21**	**22**		
Variable	Ni	WT	Hod	Al	Cr	Mo		
PIP	0.187	0.178	0.145	0.132	0.123	0.119		

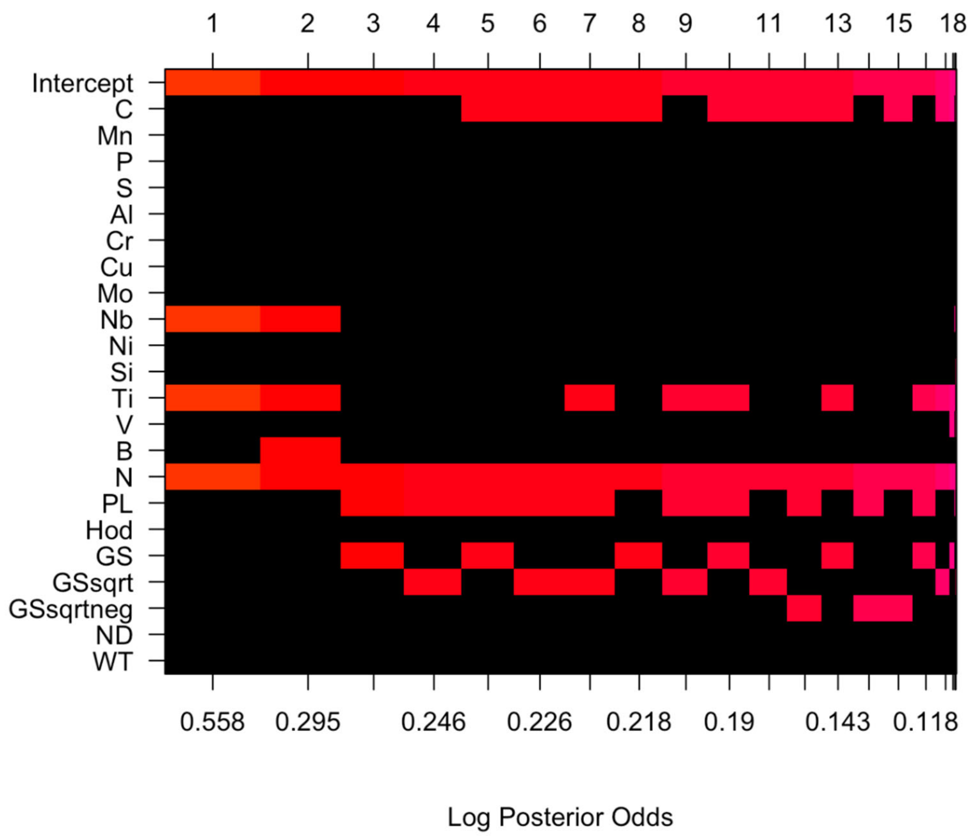

Figure 113. Top 20 Ultimate Strength Linear Models (MMT)

Table 25. Properties of Top 20 Ultimate Strength Linear Models (MMT)

	M1	M2	M3	M4	M5	M6	M7	M8	M9	M10
Intercept	1	1	1	1	1	1	1	1	1	1
C	0	0	0	0	1	1	1	1	0	1
Mn	0	0	0	0	0	0	0	0	0	0
P	0	0	0	0	0	0	0	0	0	0
S	0	0	0	0	0	0	0	0	0	0
Al	0	0	0	0	0	0	0	0	0	0
Cr	0	0	0	0	0	0	0	0	0	0
Cu	0	0	0	0	0	0	0	0	0	0
Mo	0	0	0	0	0	0	0	0	0	0
Nb	1	1	0	0	0	0	0	0	0	0
Ni	0	0	0	0	0	0	0	0	0	0
Si	0	0	0	0	0	0	0	0	0	0
Ti	1	1	0	0	0	0	1	0	1	1
V	0	0	0	0	0	0	0	0	0	0
B	0	1	0	0	0	0	0	0	0	0
N	1	1	1	1	1	1	1	1	1	1
PL	0	0	1	1	1	1	1	0	1	1
Hod	0	0	0	0	0	0	0	0	0	0
GS	0	0	1	0	1	0	0	1	0	1
GSsqrt	0	0	0	1	0	1	1	0	1	0
GSsqrtneg	0	0	0	0	0	0	0	0	0	0
ND	0	0	0	0	0	0	0	0	0	0
WT	0	0	0	0	0	0	0	0	0	0
BF	1	0.769	0.705	0.714	0.705	0.714	0.659	0.705	0.659	0.693
PostProbs	0.001	0.001	0.001	0.001	0.001	0.001	0.001	0.001	0.001	0.001
R2	0.372	0.404	0.365	0.366	0.365	0.366	0.402	0.365	0.402	0.402
dim	4	5	4	4	5	5	6	4	5	6

	M11	M12	M13	M14	M15	M16	M17	M18	M19	M20
Intercept	1	1	1	1	1	1	1	1	1	1
C	1	1	1	0	1	0	1	1	0	1
Mn	0	0	0	0	0	0	0	0	0	0
P	0	0	0	0	0	0	0	0	0	0
S	0	0	0	0	0	0	0	0	0	0
Al	0	0	0	0	0	0	0	0	0	0
Cr	0	0	0	0	0	0	0	0	0	0
Cu	0	0	0	0	0	0	0	0	0	0
Mo	0	0	0	0	0	0	0	0	0	0
Nb	0	0	0	0	0	0	0	0	1	0
Ni	0	0	0	0	0	0	0	0	0	0
Si	0	0	0	0	0	0	0	0	0	1
Ti	0	0	1	0	0	1	1	1	1	0
V	0	0	0	0	0	0	0	1	0	1
B	0	0	0	0	0	0	0	0	0	0
N	1	1	1	1	1	1	1	1	1	1
PL	0	1	0	1	0	1	0	0	1	0
Hod	0	0	0	0	0	0	0	0	0	0
GS	0	0	1	0	0	1	0	1	0	0
GSsqrt	1	0	0	0	0	0	1	0	0	1
GSsqrtneg	0	1	0	1	1	0	0	0	0	0
ND	0	0	0	0	0	0	0	0	0	0
WT	0	0	0	0	0	0	0	0	0	0
BF	0.714	0.699	0.693	0.699	0.699	0.693	0.659	0.553	0.575	0.565
PostProbs	0.001	0.001	0.001	0.001	0.001	0.001	0.001	0.001	0.001	0.001
R2	0.366	0.365	0.402	0.365	0.365	0.402	0.402	0.434	0.399	0.434
dim	1	1	1	1	1	1	1	1	1	1

Quadratic model

Top 5 variables (ND, PL, C, S and Si) in Table 22 are expanded to 20 variables for ultimate strength quadratic variable selection and model selection as shown in Table 26. The rank list of variables in terms of ultimate strength quadratic model is achieved in Table 27. Top 20 best models are shown in Figure 114. Model M1 with the highest PMP and model M9 with largest R2 among top 20 quadratic models are selected in Table 28. Note that all the R2s of ultimate strength linear models and quadratic models are relatively small, i.e., less than 0.3 which infers an obvious randomness of ultimate strength delta term. This randomness can be partially explained by linear model and quadratic model. The results of using MMT yield strength baseline are shown in Table 29, Table 30, Figure 115 and Table 31.

Table 26. Variables Used for Ultimate Strength Quadratic Model (Frontics)

Index	**1**	**2**	**3**	**4**	**5**	**6**	**7**	**8**	**9**	**10**
Variable	ND	PL	C	S	Si	ND2	PL2	C2	S2	Si2
Index	**11**	**12**	**13**	**14**	**15**	**16**	**17**	**18**	**19**	**20**
Variable	NDPL	NDC	NDS	NDSi	PLC	PLS	PLSi	CS	CSi	SSi

Table 27. Rank of Variables for Ultimate Strength Quadratic Model (Frontics)

Rank	**1**	**2**	**3**	**4**	**5**	**6**	**7**	**8**	**9**	**10**
Variable	ND	NDS	ND2	S	PL	C	NDC	NDPL	PL2	C2
PIP	0.400	0.320	0.316	0.296	0.293	0.292	0.258	0.247	0.242	0.242
Rank	**11**	**12**	**13**	**14**	**15**	**16**	**17**	**18**	**19**	**20**
Variable	PLC	S2	CS	PLS	CSi	NDSi	PLSi	SSi	Si	Si2
PIP	0.241	0.235	0.223	0.222	0.207	0.206	0.206	0.192	0.191	0.163

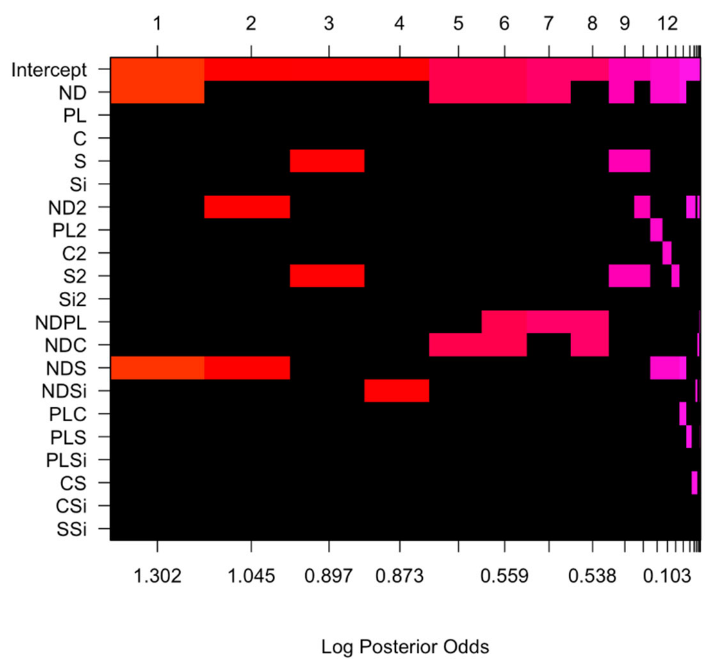

Figure 114. Top 20 Ultimate Strength Quadratic Models (Frontics)

Table 28. Properties of Top 20 Ultimate Strength Quadratic Models (Frontics)

	M1	M2	M3	M4	M5	M6	M7	M8	M9	M10
Intercept	1	1	1	1	1	1	1	1	1	1
ND	1	0	0	0	1	1	1	0	1	0
PL	0	0	0	0	0	0	0	0	0	0
C	0	0	0	0	0	0	0	0	0	0
S	0	0	1	0	0	0	0	0	1	1
Si	0	0	0	0	0	0	0	0	0	0
ND2	0	1	0	0	0	0	0	0	0	1
PL2	0	0	0	0	0	0	0	0	0	0
C2	0	0	0	0	0	0	0	0	0	0
S2	0	0	1	0	0	0	0	0	1	1
Si2	0	0	0	0	0	0	0	0	0	0
NDPL	0	0	0	0	0	1	1	1	0	0
NDC	0	0	0	0	1	1	0	1	0	0
NDS	1	1	0	0	0	0	0	0	0	0
NDSi	0	0	0	1	0	0	0	0	0	0
PLC	0	0	0	0	0	0	0	0	0	0
PLS	0	0	0	0	0	0	0	0	0	0
PLSi	0	0	0	0	0	0	0	0	0	0
CS	0	0	0	0	0	0	0	0	0	0
CSi	0	0	0	0	0	0	0	0	0	0
SSi	0	0	0	0	0	0	0	0	0	0
BF	1	0.787	0.651	0.636	0.465	0.465	0.465	0.465	0.373	0.334
PostProbs	0.004	0.003	0.003	0.003	0.002	0.002	0.002	0.002	0.002	0.001
R2	0.220	0.214	0.210	0.160	0.202	0.202	0.202	0.202	0.245	0.242
dim	3	3	3	2	3	4	3	3	4	4
	M11	**M12**	**M13**	**M14**	**M15**	**M16**	**M17**	**M18**	**M19**	**M20**
Intercept	1	1	1	1	1	1	1	1	1	1
ND	1	1	1	1	0	0	0	0	0	0
PL	0	0	0	0	0	0	0	0	0	0
C	0	0	0	0	0	0	0	0	0	0
S	0	0	0	0	0	0	0	0	0	0
Si	0	0	0	0	0	0	0	0	0	0
ND2	0	0	0	0	1	1	0	1	1	0
PL2	1	0	0	0	0	0	0	0	0	0
C2	0	1	0	0	0	0	0	0	0	0
S2	0	0	1	0	0	0	0	0	0	0
Si2	0	0	0	0	0	0	0	0	0	0
NDPL	0	0	0	0	0	0	0	0	1	0
NDC	0	0	0	0	0	0	0	1	0	0
NDS	1	1	1	1	0	0	0	0	0	0
NDSi	0	0	0	0	0	0	1	0	0	1
PLC	0	0	0	1	0	0	0	0	0	0
PLS	0	0	0	0	1	0	0	0	0	1
PLSi	0	0	0	0	0	0	0	0	0	0
CS	0	0	0	0	0	1	1	0	0	0
CSi	0	0	0	0	0	0	0	0	0	0
SSi	0	0	0	0	0	0	0	0	0	0
BF	0.300	0.294	0.291	0.297	0.283	0.295	0.275	0.266	0.289	0.264
PostProbs	0.001	0.001	0.001	0.001	0.001	0.001	0.001	0.001	0.001	0.001
R2	0.240	0.239	0.239	0.240	0.191	0.192	0.190	0.190	0.191	0.189
dim	4	4	4	4	3	3	3	3	3	3

Table 29. Variables Used for Ultimate Strength Quadratic Model (MMT)

Index	1	2	3	4	5	6	7	8	9	10
Variable	N	Ti	PL	C	V	N2	Ti2	PL2	C2	V2
Index	**11**	**12**	**13**	**14**	**15**	**16**	**17**	**18**	**19**	**20**
Variable	NTi	NPL	NC	NV	TiPL	TiC	TiV	PLC	PLV	CV

Table 30. Rank of Variables for Ultimate Strength Quadratic Model (MMT)

Rank	1	2	3	4	5	6	7	8	9	10
Variable	Ti	Ti2	V	TiV	NTi	V2	N	N2	PL	C
PIP	0.635	0.547	0.511	0.502	0.500	0.471	0.442	0.435	0.390	0.390
Rank	**11**	**12**	**13**	**14**	**15**	**16**	**17**	**18**	**19**	**20**
Variable	NC	NPL	CV	PLV	NV	PLC	C2	PL2	TiC	TiPL
PIP	0.373	0.356	0.322	0.320	0.317	0.306	0.305	0.304	0.302	0.285

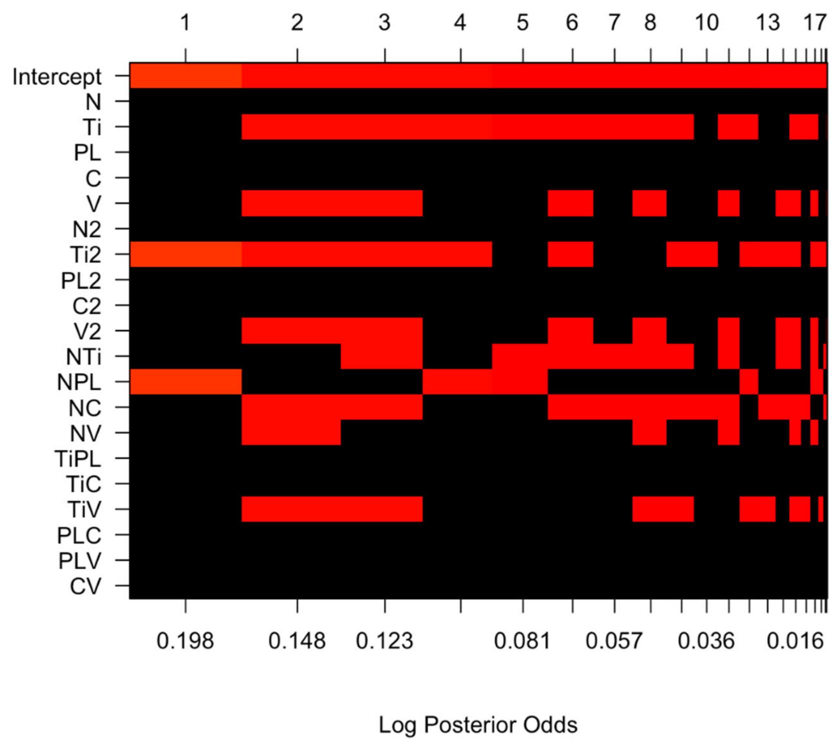

Figure 115. Top 20 Ultimate Strength Quadratic Models (MMT)

Table 31. Properties of Top 20 Ultimate Strength Quadratic Models (MMT)

	M1	M2	M3	M4	M5	M6	M7	M8	M9	M10
Intercept	1	1	1	1	1	1	1	1	1	1
N	0	0	0	0	0	0	0	0	0	0
Ti	0	1	1	1	1	1	1	1	1	0
PL	0	0	0	0	0	0	0	0	0	0
C	0	0	0	0	0	0	0	0	0	0
V	0	1	1	0	0	1	0	1	0	0
N2	0	0	0	0	0	0	0	0	0	0
Ti2	1	1	1	1	0	1	0	0	1	1
PL2	0	0	0	0	0	0	0	0	0	0
C2	0	0	0	0	0	0	0	0	0	0
V2	0	1	1	0	0	1	0	1	0	0
NTi	0	0	1	0	1	1	1	1	1	0
NPL	1	0	0	1	1	0	0	0	0	0
NC	0	1	1	0	0	1	1	1	1	1
NV	0	1	0	0	0	0	0	1	0	0
TiPL	0	0	0	0	0	0	0	0	0	0
TiC	0	0	0	0	0	0	0	0	0	0
TiV	0	1	1	0	0	0	0	1	1	0
PLC	0	0	0	0	0	0	0	0	0	0
PLV	0	0	0	0	0	0	0	0	0	0
CV	0	0	0	0	0	0	0	0	0	0
BF	0.989	1.000	1.000	0.929	0.929	1.000	0.930	1.000	0.930	0.997
PostProbs	0.0003	0.0003	0.0003	0.0003	0.0003	0.0003	0.0003	0.0003	0.0003	0.0003
R2	0.329	0.406	0.406	0.328	0.328	0.406	0.328	0.406	0.328	0.329
dim	3	8	8	4	4	7	4	8	6	3

	M11	M12	M13	M14	M15	M16	M17	M18	M19	M20
Intercept	1	1	1	1	1	1	1	1	1	1
N	0	0	0	0	0	0	0	0	0	0
Ti	1	1	0	0	1	1	1	0	0	1
PL	0	0	0	0	0	0	0	0	0	0
C	0	0	0	0	0	0	0	0	0	0
V	1	0	0	1	1	0	1	0	0	1
N2	0	0	0	0	0	0	0	0	0	0
Ti2	0	1	1	1	1	0	1	1	1	0
PL2	0	0	0	0	0	0	0	0	0	0
C2	0	0	0	0	0	0	0	0	0	0
V2	1	0	0	1	1	0	1	0	0	1
NTi	1	0	0	1	1	0	1	0	1	0
NPL	0	1	0	0	0	0	1	1	0	0
NC	1	0	1	1	1	1	0	0	1	1
NV	1	0	0	0	1	0	1	0	0	0
TiPL	0	0	0	0	0	0	0	0	0	0
TiC	0	0	0	0	0	0	0	0	0	0
TiV	0	1	1	0	1	1	0	1	0	0
PLC	0	0	0	0	0	0	0	0	0	0
PLV	0	0	0	0	0	0	0	0	0	0
CV	0	0	0	0	0	0	0	0	0	0
BF	1.000	0.929	0.997	0.936	1.000	0.930	0.905	0.989	0.997	1.000
PostProbs	0.0003	0.0003	0.0003	0.0003	0.0003	0.0003	0.0003	0.0003	0.0003	0.0003
R2	0.406	0.328	0.329	0.405	0.406	0.328	0.404	0.329	0.329	0.406
dim	7	5	4	6	9	4	8	4	4	5

Discussion and Conclusion

In this section, Bayesian variable section and model selection are conducted with the BAS package. For both yield strength and ultimate strength, variable ranking is obtained to explain the importance of such variables in linear models and quadratic models as well. In consideration of model uncertainties, two reasonable models are selected for further investigation in each case. One is the model with the highest posterior model probability, and the other is the model with the largest R square. The regression performance and predictive performance will be evaluated comprehensively in the next section.

6.4 Ordinary Least Square Model

Ordinary least-squares (OLS) model is one of the most popular statistical techniques used in the social sciences. It is used to predict values of a continuous response variable using one or more explanatory variables and can also identify the strength of the relationships between inputs and responses[19]. OLS chooses the parameters of a linear function of a set of explanatory variables by the principle of least squares: minimizing the sum of the squares of the differences between the observed dependent variable in the given dataset and those predicted by the linear function. Geometrically, this is seen as the sum of the squared distances, parallel to the axis of the dependent variable, between each data point in the set and the corresponding point on the regression surface—the smaller the differences, the better the model fits the data. The resulting estimator can be expressed by a simple formula, especially in the case of a simple linear regression, in which there is a single regressor on the right side of the regression equation. The OLS estimator is identical to the maximum likelihood estimator (MLE) under the normality assumption for the error terms. From the properties of MLE, we can infer that the OLS estimator is asymptotically efficient if the normality assumption is satisfied [20].

Suppose the data consists of n observations $\{y_i, x_i\}_{i=1}^n$. Each observation i includes a scalar response y_i and a column vector x_i of values of p parameters (regressors) x_{ij} for $j = 1, \cdots, p$. In a linear regression model, the response variable, y_i, is a linear function of the regressors:

$$y_i = \beta_1 x_{i1} + \beta_2 x_{i2} + \cdots + \beta_p x_{ip} + \varepsilon_i, \quad (5)$$

or in vector form,

$$y_i = \boldsymbol{x}_i^T \boldsymbol{\beta} + \varepsilon_i, \quad (6)$$

where $\boldsymbol{x_i}$ is a column vector of the ith observations of all the explanatory variables. β is a $p \times 1$ vector of unknown parameters. The scalars ε_i represent unobserved random errors, which accounts for influences upon the responses y_i from sources other than the explanators $\boldsymbol{x_i}$. This model can also be written in matrix notation as

$$\boldsymbol{y} = X\boldsymbol{\beta} + \boldsymbol{\varepsilon}, \quad (7)$$

where $\boldsymbol{y}$ and $\boldsymbol{\varepsilon}$ are $n \times 1$ vectors of the values of the response variable and the errors for the various observations, and X is an $n \times p$ matrix of regressors, also sometimes called the design matrix, whose row i is $\boldsymbol{x}_i^T$ and contains the ith observations on all the explanatory variables. As a rule, the constant term is always included in the set of regressors X, by taking $x_{i1} = 1$ for all $i = 1, \cdots, n$. The coefficient β_1 corresponding to this regressor is called the intercept.

Regressors do not have to be independent: there can be any desired relationship between the regressors. For instance, we might suspect the response depends linearly both on a value and its square. In this case we would include one regressor whose value is just the square of another regressor. Thus, the model would be quadratic in the second regressor, which can be called as quadratic model although the model is still linear in the parameters β.

In this section, OLS linear model and quadratic model are applied to predict pipeline yield strength and ultimate strength given 70 pipe samples with 18 features including surface identities and pipe overview data. All the continuous variables used in linear models for both yield strength and ultimate strength are shown in Table. Twenty continuous variables used in quadratic models for yield strength estimation are used in Table which including linear terms, power terms and interactive terms. Similarly, 20 continuous variables applied to quadratic models for ultimate strength as shown in Table. Lab full wall 0.2% offset yield strength and ultimate strength are treated as benchmarks to evaluate both regression performance and predictive performance for each model.

Yield Strength Estimation

Linear model

Full Data Regression

From previous model selection section, based on Frontics yield strength baselines, there are two linear models have been selected for yield strength estimation. One is the linear model with the largest posterior (ASU_F_LM1_YS), the other one is with the largest R square (ASU_F_LM2_YS) among the top 20 best linear models. These two linear models have greater potential to achieve better performance than other models. To start with model performance evaluation, full 70-sample dataset is used to address the regression performance. All the predictive values are compared to the Lab Full Wall 0.2% Offset yield strength which can be seen as the benchmark. Comparison results are shown in Figure 116 – Figure 119. The results of using MMT yield strength baseline are shown in Figure 120 - Figure 123. Numerical comparison of regression performance is shown in Table 32. From the result, the linear model ASU_F_LM2_YS has smaller RMSE than ASU_F_LM1_YS. This indicate that ASU_F_LM2_YS would achieve better regression performance. Statistical analysis of the difference between the predicted and the observed is shown in Table 33.

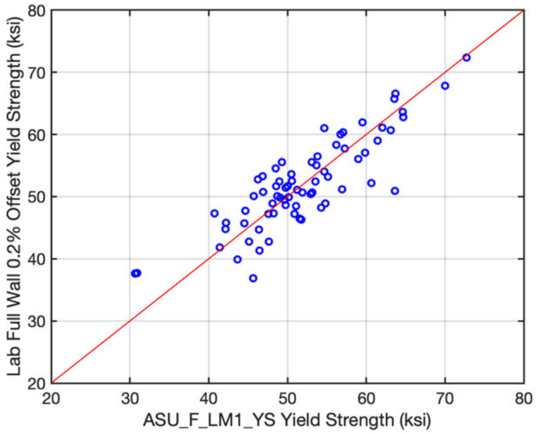

Figure 116. Unit Plot of Lab 0.2% Offset vs. ASU_F_LM1_YS

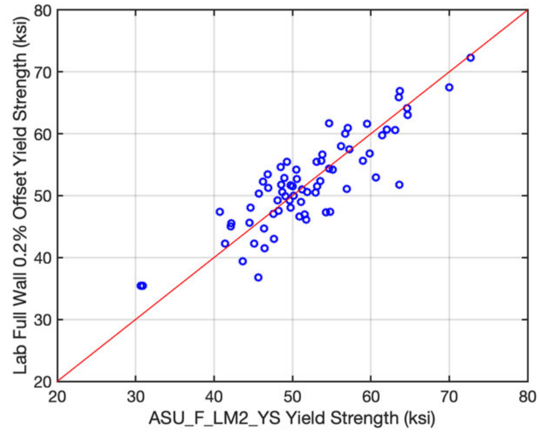

Figure 117. Unit Plot of Lab 0.2% Offset vs. ASU_F_LM2_YS

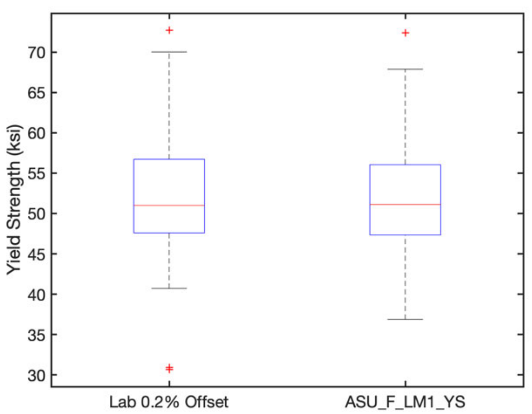

Figure 118. Boxplot of Lab 0.2% Offset vs. ASU_F_LM1_YS

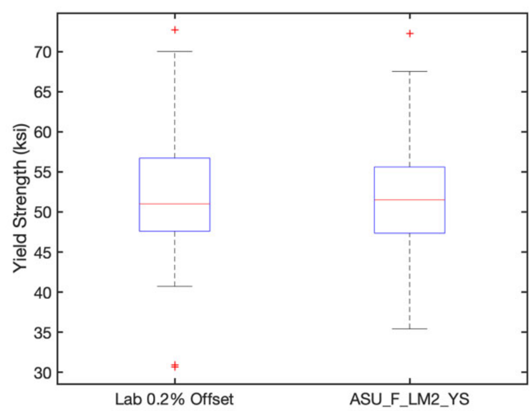

Figure 119. Boxplot of Lab 0.2% offset vs. ASU_F_LM2_YS

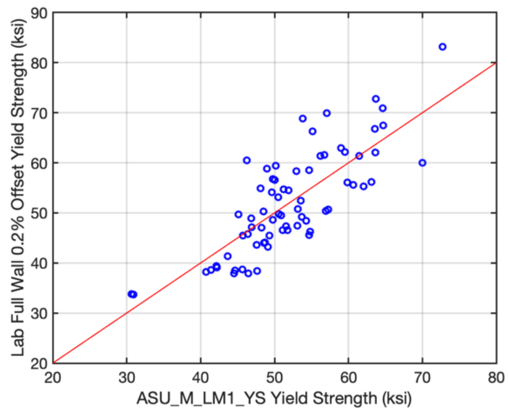

Figure 120. Unit Plot of Lab 0.2% Offset vs. ASU_M_LM1_YS

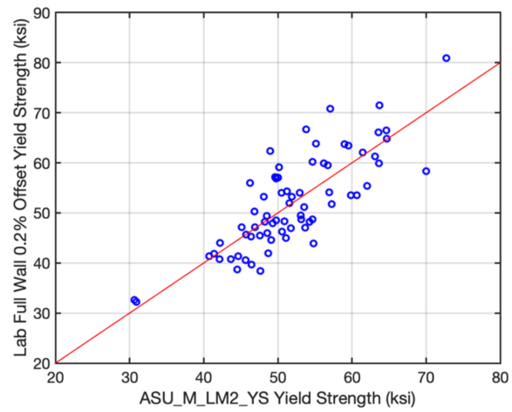

Figure 121. Unit Plot of Lab 0.2% Offset vs. ASU_M_LM2_YS

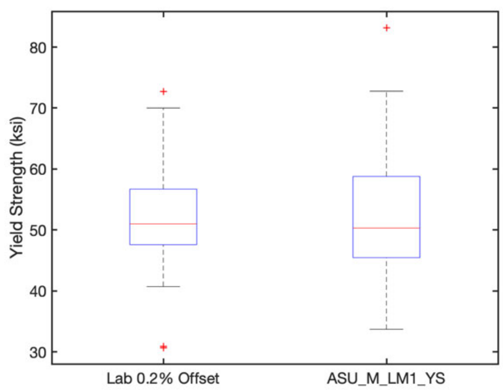

Figure 122. Boxplot of Lab 0.2% Offset vs. ASU_M_LM1_YS

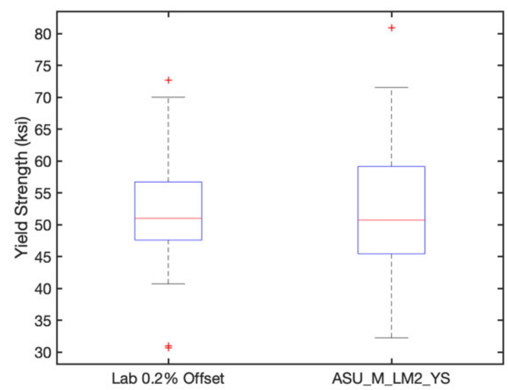

Figure 123. Boxplot of Lab 0.2% offset vs. ASU_M_LM2_YS

Table 32. Properties of Yield Strength Linear Model (Frontics & MMT)

	ASU_F_LM1_YS	ASU_F_LM2_YS	ASU_M_LM1_YS	ASU_M_LM2_YS
R2_Delta	0.5802	0.5889	0.5144	0.5799
adj_R2_Delta	0.5474	0.5498	0.5072	0.5541
R2_YS/UTS	0.7270	0.7326	0.3799	0.4635
adj_R2_YS/UTS	0.7056	0.7072	0.3708	0.4305
RMSE_Delta	4.0244	3.9823	6.0630	5.6390
RMSE_YS/UTS	4.0235	3.9814	6.0634	5.6397
BIC	423.32	426.10	463.71	466.30
AIC	407.58	408.11	456.96	452.81
$\chi^2 = \sum_{i=1}^{70} \frac{(o_i - e_i)^2}{e_i}$	23.03	22.00	48.58	41.58
Log Likelihood	-180.7334	-196.0552	-225.4803	-220.4054

Table 33. Predicted vs. Actual STATs for All Obs. (Yield Strength Linear Model)

	Obs	Mean	Std. Dev	Min	Max
ASU_F_LM1_YS	70	-1.70E-04	4.0529	-6.9499	12.7852
ASU_ F_LM2_YS	70	-1.69E-04	4.0105	-7.0247	11.8946
ASU_M_LM1_YS	70	-5.29E-03	6.1079	-14.9869	10.0456
ASU_ M_LM2_YS	70	-5.29E-03	5.6811	-13.7486	11.6824

Split Data Validation

Hold-out cross validation is applied to model validation. We randomly draw 5 test samples from the full dataset, and 65 samples would be left automatically to be the training set. Next, use the 65-sample training set do the parametric learning. The following step is delta term prediction for the 5 test samples. Recall that we treat the yield strength got from surface techniques YS_s as the baseline of predictive values. Thus, sum up the predictive delta and corresponding YS_s will lead to final predictive yield strength. After 500 iterations, we got averaged RMSE for delta term and yield strength as well. The results are shown in the Table 34 below. It is easy to find that ASU_ F_LM1_YS has relatively small RMSEs which pretty match to the regression performance comparison.

Table 34. Performance Comparison of Yield Strength Linear Model (Frontics & MMT)

	AvgRMSE.Delta	AvgRMSE.YS
ASU_F_LM1_YS	4.2444	4.1732
ASU_ F_LM2_YS	4.3273	4.2911
ASU_M_LM1_YS	5.9965	6.0794
ASU_ M_LM2_YS	5.9372	5.9485

Quadratic model

Full Data Regression

In previous section, the largest posterior quadratic model (ASU_F_QM1_YS) and the largest R square model (ASU_F_QM2_YS) are selected out. The procedures of doing quadratic model regression are exactly the same as linear model regression except the variables used here not only included linear terms but also power terms and interactive terms. Compare predictive values with benchmark delta and benchmark yield strength, the unit plots and boxplots are shown in Figure 124 - Figure 127. The results of using MMT yield strength baseline are shown in Figure 128 - Figure 131. As can be seen in Table 35, the RMSEs of using ASU_F_QM1_YS quadratic model and ASU_F_QM2_YS quadratic model are 3.4051and 3.3372 respectively. So, it is fair to say ASU_F_QM2_YS with smaller RMSE has better performance regarding to full data ultimate strength regression. Statistical analysis of the difference between the predicted and the observed is shown in Table 36.

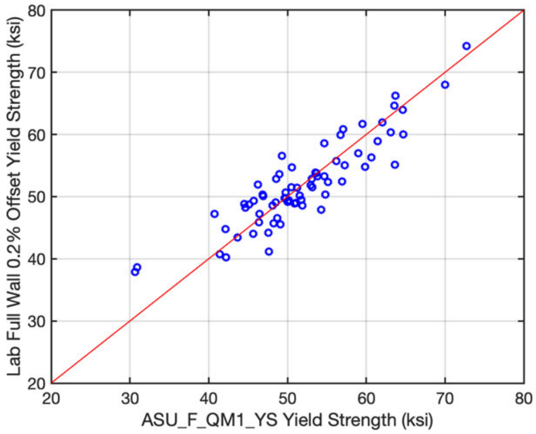

Figure 124. Unit Plot of Lab 0.2% Offset vs. ASU_F_QM1_YS

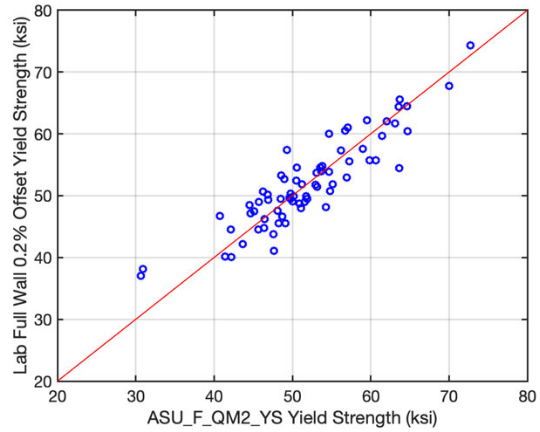

Figure 125. Unit Plot of Lab 0.2% Offset vs. ASU_F_QM2_YS

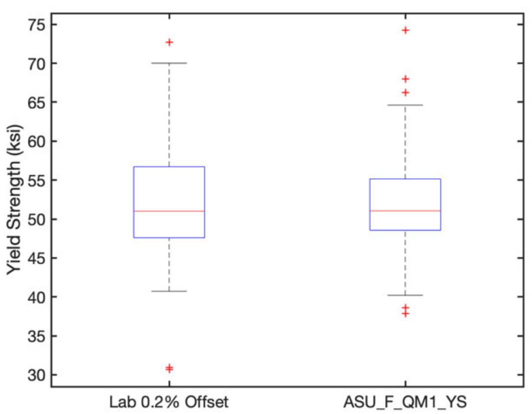

Figure 126. Boxplot of Lab 0.2% Offset vs. ASU_F_QM1_YS

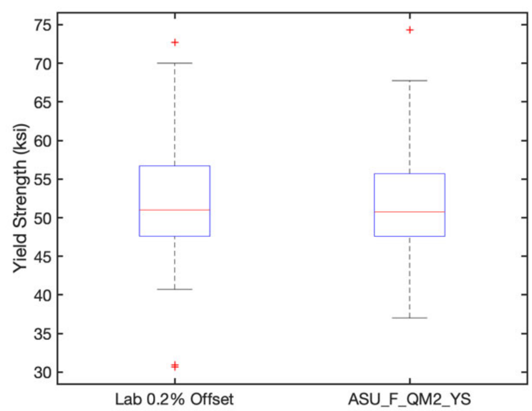

Figure 127. Boxplot of Lab 0.2% offset vs. ASU_F_QM2_YS

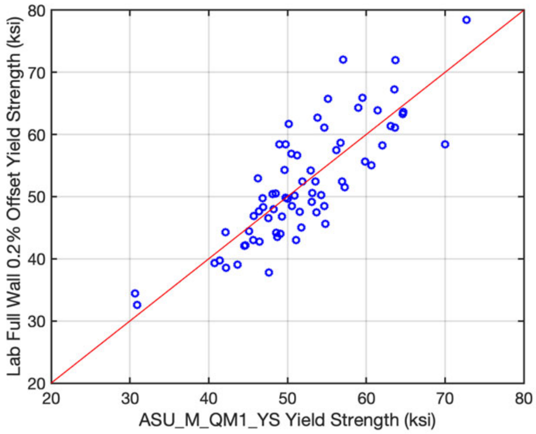

Figure 128. Unit Plot of Lab 0.2% Offset vs. ASU_M_QM1_YS

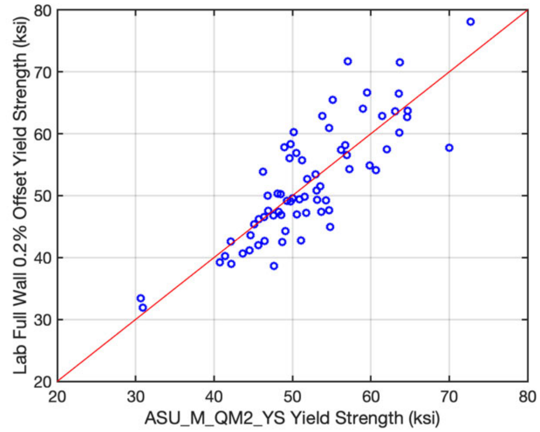

Figure 129. Unit Plot of Lab 0.2% Offset vs. ASU_M_QM2_YS

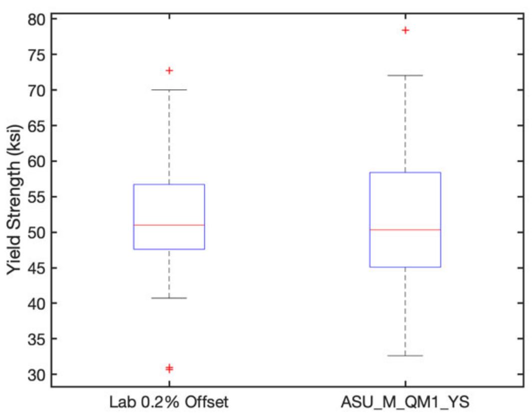

Figure 130. Boxplot of Lab 0.2% Offset vs. ASU_M_QM1_YS

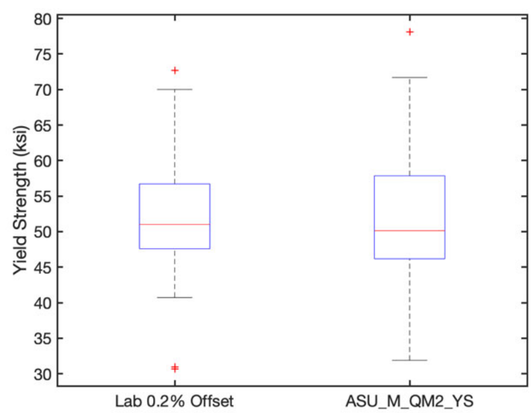

Figure 131. Boxplot of Lab 0.2% offset vs. ASU_M_QM2_YS

Table 35. Properties of Yield Strength Quadratic Model (Frontics & MMT)

	ASU_F_QM1_YS	ASU_F_QM2_YS	ASU_M_QM1_YS	ASU_M_QM2_YS
R2_Delta	0.6994	0.7112	0.6269	0.6446
adj_R2_Delta	0.6543	0.6734	0.6039	0.6168
R2_YS/UTS	0.8044	0.8122	0.5239	0.5463
adj_R2_YS/UTS	0.7751	0.7875	0.4946	0.5108
RMSE_Delta	3.4056	3.3378	5.3142	5.1867
RMSE_YS/UTS	3.4051	3.3372	5.3132	5.1866
BIC	416.94	409.88	458.00	458.84
AIC	392.21	387.39	444.51	443.10
$\chi^2 = \sum_{i=1}^{70} \frac{(o_i - e_i)^2}{e_i}$	17.16	16.20	36.87	34.83
Log Likelihood	-185.1048	-183.6972	-216.253	-214.5519

Table 36. Predicted vs. Actual STATs for All Obs. (Yield Strength Quadratic Model)

	Obs	Mean	Std. Dev	Min	Max
ASU_F_QM1_YS	70	-1.69E-04	3.4298	-7.6571	8.5254
ASU_ F_QM2_YS	70	-1.69E-04	3.3614	-8.0537	9.2141
ASU_M_QM1_YS	70	-5.29E-03	5.3521	-14.9512	11.6132
ASU_ M_QM2_YS	70	-5.29E-03	5.2246	-14.6021	12.2812

Split Data Validation

Similarly, the 70-sample dataset used for yield strength linear model validation has been split into training set and test set for 500 times. After 500 iterations, we got averaged RMSEs of both predictive delta term and predictive yield strength for quadratic models above. The comparison results are shown in Table 37. The RMSEs of ASU_QM2_YS are smaller than it of ASU_QM1_YS. And the models of Frontics baseline are all better than ones with MMT baseline.

Table 37. Performance Comparison of Yield Strength Quadratic Model (Frontics & MMT)

	AvgRMSE.Delta	AvgRMSE.YS
ASU_F_QM1_YS	3.8648	3.8192
ASU_ F_QM2_YS	3.6333	3.5914
ASU_M_QM1_YS	5.5362	5.5683
ASU_ M_QM2_YS	5.4421	5.4494

Ultimate Strength Estimation

Linear model

Full Data Regression

For ultimate strength estimation, we just follow the same ways as did for yield strength. ASU_F_LM1_UTS with the largest posterior and ASU_F_LM2_UTS with the largest R square were chosen among the top 20 best linear model for ultimate strength to evaluate model performance further. Comparison results between predictive value and Lab Full Wall 0.2% offset ultimate strength (benchmark) are shown in from Figure 132 to Figure 135. The results of using MMT yield strength baseline are shown in Figure 136 - Figure 139. Numerical results can be read in Table 38. ASU_F_LM2_UTS linear model with the smallest RMSE shows the best regression performance. Statistical analysis of the difference between the predicted and the observed is shown in Table 39.

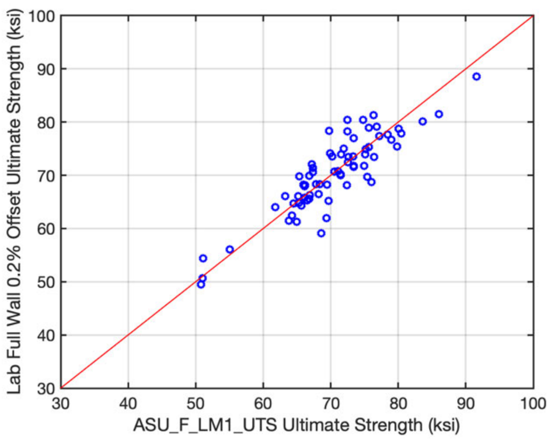

Figure 132. Unit Plot of Lab 0.2% Offset vs. ASU_F_LM1_UTS

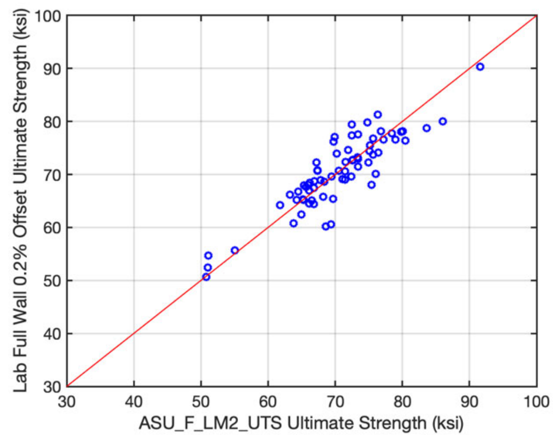

Figure 133. Unit Plot of Lab 0.2% Offset vs. ASU_F_LM2_UTS

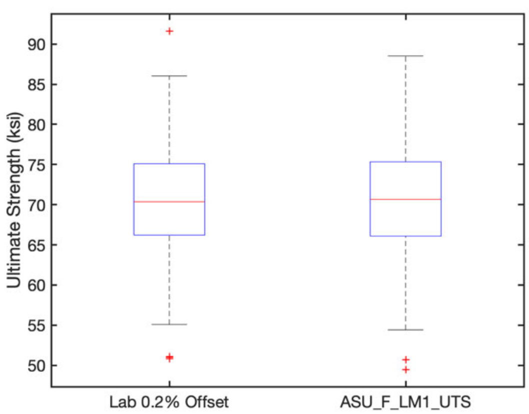

Figure 134. Boxplot of Lab 0.2% Offset vs. ASU_F_LM1_UTS

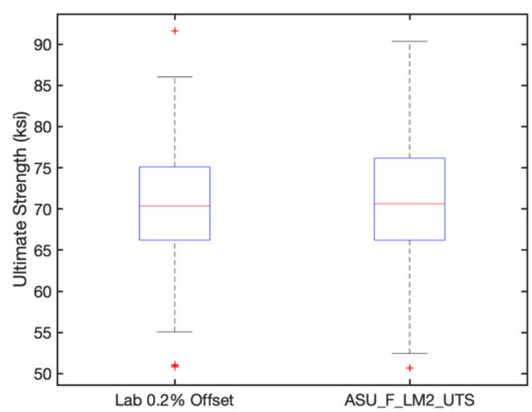

Figure 135. Boxplot of Lab 0.2% offset vs. ASU_F_LM2_UTS

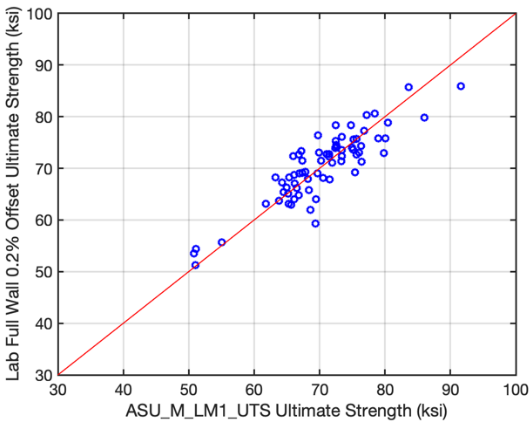

Figure 136. Unit Plot of Lab 0.2% Offset vs. ASU_M_LM1_UTS

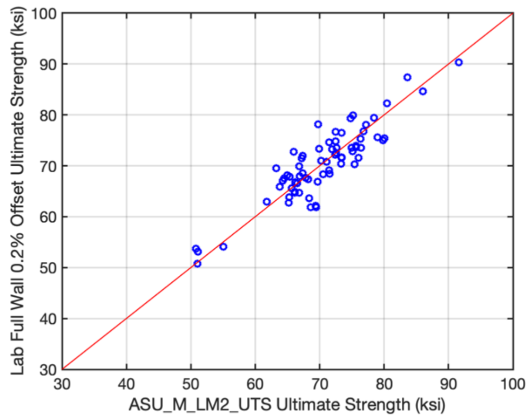

Figure 137. Unit Plot of Lab 0.2% Offset vs. ASU_M_LM2_UTS

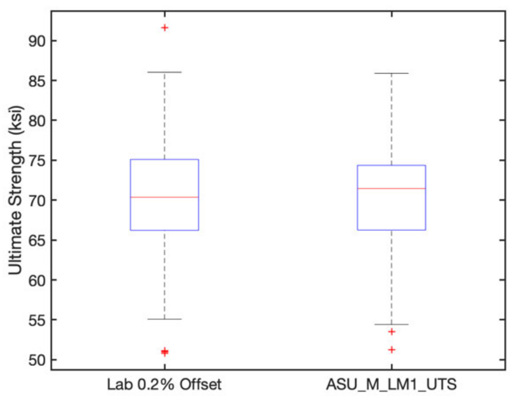

Figure 138. Boxplot of Lab 0.2% Offset vs. ASU_M_LM1_UTS

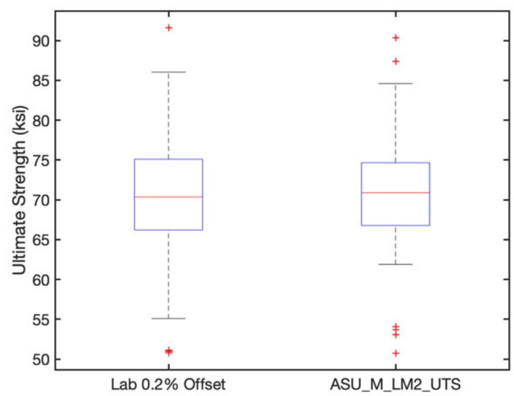

Figure 139. Boxplot of Lab 0.2% offset vs. ASU_M_LM2_UTS

Table 38. Properties of Ultimate Strength Linear Model (Frontics & MMT)

	ASU_F_LM1_UTS	ASU_F_LM2_ UTS	ASU_M_LM1_ UTS	ASU_M_LM2_ UTS
R2_Delta	0.1812	0.2220	0.3716	0.4343
adj_R2_Delta	0.1692	0.1866	0.3623	0.3901
R2_YS/UTS	0.7719	0.7832	0.7716	0.7941
adj_R2_YS/UTS	0.7685	0.7734	0.7682	0.7780
RMSE_Delta	3.4386	3.3519	3.4462	3.2698
RMSE_YS/UTS	3.4385	3.3519	3.4407	3.2665
BIC	388.55	389.23	393.11	394.25
AIC	379.56	377.99	381.87	378.51
$\chi^2 = \sum_{i=1}^{70} \frac{(o_i - e_i)^2}{e_i}$	11.61	11.02	11.62	10.67
Log Likelihood	-185.7799	-183.9931	-185.9	-182.2558

Table 39. Predicted vs. Actual STATs for All Obs. (Ultimate Strength Linear Model)

	Obs	Mean	Std. Dev	Min	Max
ASU_F_LM1_UTS	70	-2.64E-05	3.4633	-8.5363	9.5370
ASU_ F_LM2_UTS	70	-2.63E-05	3.3761	-7.1641	8.8400
ASU_M_LM1_UTS	70	-7.96E-03	3.4656	-6.5668	10.0843
ASU_ M_LM2_UTS	70	-7.96E-03	3.2901	-8.3577	7.5372

Split Data Validation

To analyze the linear models for ultimate strength more comprehensively, again we did data splitting for 500 iterations with 65-sample training set and 5-sample test set for each time. And the predictive performance of these selected linear models is evaluated by comparing averaged RMSE as shown in the Table 40. ASU_LM1_UTS performed the best with the smallest RMSE 3.3593.

Table 40. Performance Comparison of Ultimate Strength Linear Model (Frontics & MMT)

	AvgRMSE.Delta	AvgRMSE.YS
ASU_F_LM1_UTS	3.3592	3.3593
ASU_ F_LM2_UTS	3.4261	3.4262
ASU_M_LM1_UTS	3.4523	3.4471
ASU_ M_LM2_UTS	3.4129	3.4088

Quadratic model

Full Data Regression

Besides linear model analysis, it is necessary to evaluate the quadratic models as well which got in Section. The quadratic model ASU_F_QM1_UTS has the largest posterior is compared to the quadratic model ASU_F_QM2_UTS. Comparison results between predictive value and Lab Full Wall 0.2% offset ultimate strength (benchmark) are shown in from Figure 140 to Figure 143. The results of using MMT yield strength baseline are shown in Figure 144 - Figure 147. And numerical results are shown in Table 41. ASU_F_QM2_UTS and ASU_M_QM2_UTS are both doing well. Statistical analysis of the difference between the predicted and the observed is shown in Table 42.

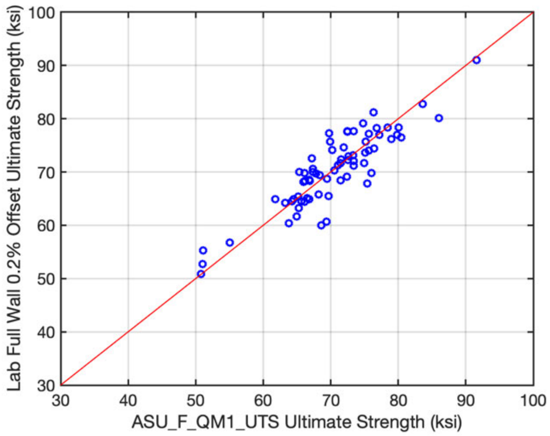

Figure 140. Unit Plot of Lab 0.2% Offset vs. ASU_F_QM1_UTS

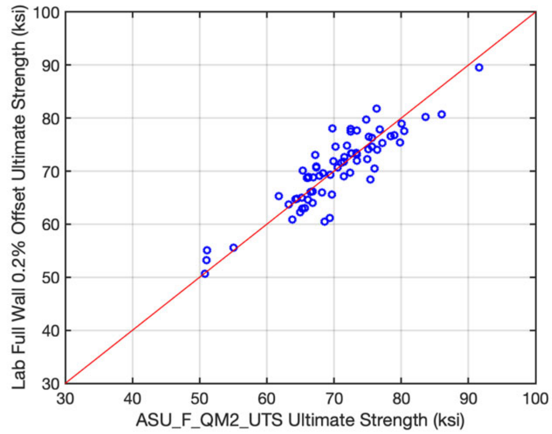

Figure 141. Unit Plot of Lab 0.2% Offset vs. ASU_F_QM2_UTS

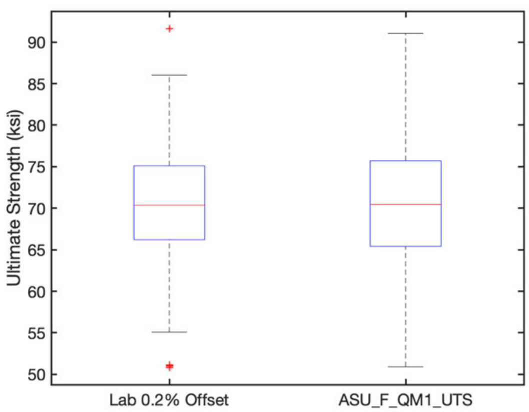

Figure 142. Boxplot of Lab 0.2% Offset vs. ASU_F_QM1_UTS

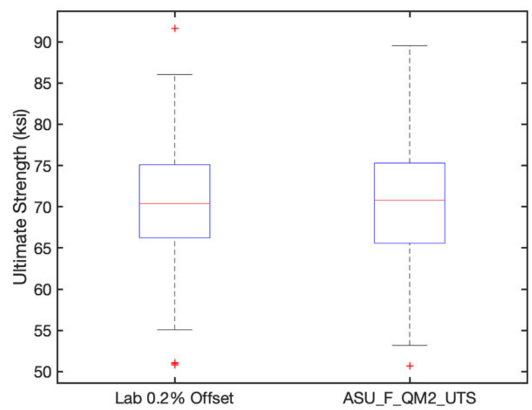

Figure 143. Boxplot of Lab 0.2% offset vs. ASU_F_M2_UTS

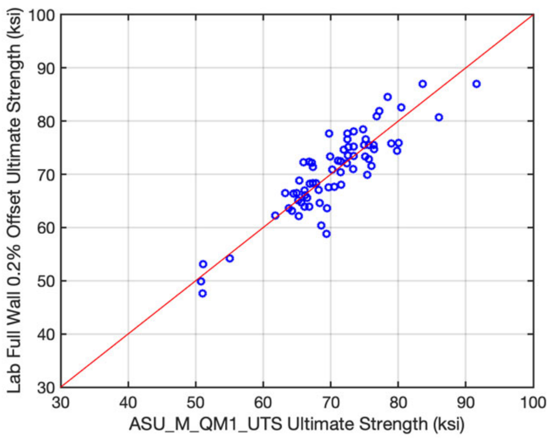

Figure 144. Unit Plot of Lab 0.2% Offset vs. ASU_M_QM1_UTS

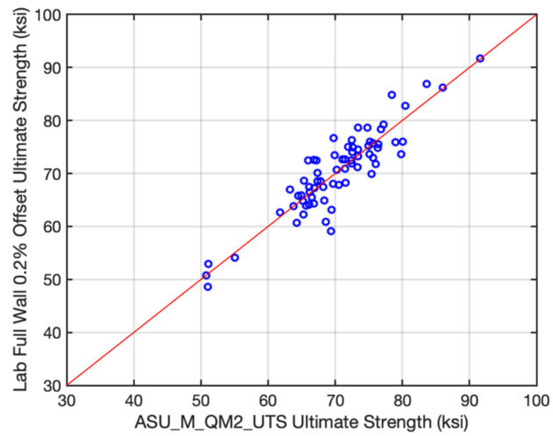

Figure 145. Unit Plot of Lab 0.2% Offset vs. ASU_M_QM2_UTS

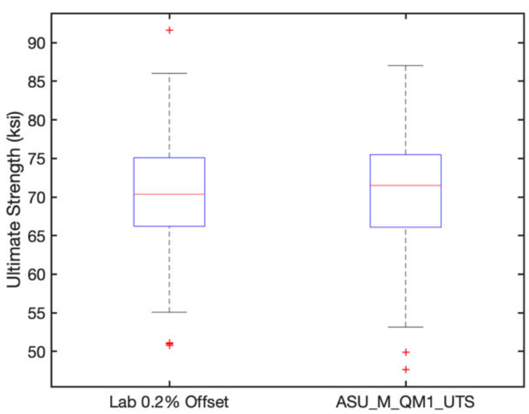

Figure 146. Boxplot of Lab 0.2% Offset vs. ASU_M_QM1_UTS

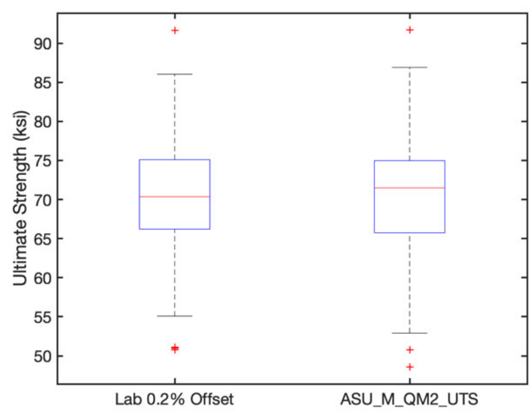

Figure 147. Boxplot of Lab 0.2% offset vs. ASU_M_QM2_UTS

Table 41. Properties of Ultimate Strength Quadratic Model (Frontics & MMT)

	ASU_F_QM1_UTS	ASU_F_QM2_ UTS	ASU_M_QM1_ UTS	ASU_M_QM2_ UTS
R2_Delta	0.2196	0.2445	0.3289	0.4241
adj_R2_Delta	0.1963	0.2102	0.3089	0.3591
R2_YS/UTS	0.7825	0.7895	0.7561	0.7908
adj_R2_YS/UTS	0.7760	0.7799	0.7489	0.7672
RMSE_Delta	3.3570	3.3029	3.5612	3.2991
RMSE_YS/UTS	3.3572	3.3032	3.5551	3.2929
BIC	385.19	387.17	393.46	404.00
AIC	376.20	375.92	384.46	383.76
$\chi^2 = \sum_{i=1}^{70} \frac{(o_i - e_i)^2}{e_i}$	11.18	10.79	12.38	10.75
Log Likelihood	-184.0996	-182.9622	-188.2316	-182.8801

Table 42. Predicted vs. Actual STATs for All Obs. (Ultimate Strength Quadratic Model)

	Obs	Mean	Std. Dev	Min	Max
ASU_F_QM1_UTS	70	-1.69E-04	3.4298	-7.6571	8.5254
ASU_ F_QM2_UTS	70	-1.69E-04	3.3614	-8.0537	9.2141
ASU_M_QM1_UTS	70	-5.29E-03	5.3521	-14.9512	11.6132
ASU_ M_QM2_UTS	70	-5.29E-03	5.2246	-14.6021	12.2812

Split Data Validation

500 times data splitting are carried out evaluate the quadratic model predictive performance with the same training and test size. The averaged RMSEs are shown in the Table 43. The quadratic model ASU_F_QM1_UTS shows the best predictive performance among these four models which is different from the conclusion got from regression cases. In other words, although the model ASU_M_QM2_UTS did well in regression, it is not reliable in predicting ultimate strength.

Table 43. Performance Comparison of UTS Quadratic Model (Frontics & MMT)

	AvgRMSE.Delta	AvgRMSE.YS
ASU_F_QM1_UTS	3.2585	3.2587
ASU_ F_QM2_UTS	3.2760	3.2763
ASU_M_QM1_UTS	3.4949	3.4888
ASU_ M_QM2_UTS	4.2897	4.2841

Discussion and Conclusion

All the OLS models including linear models and quadratic models are chosen from model selection in the previous section. If the model uncertainties in Bayesian model averaging process is considered, it's not safe to say that the model with the largest posterior would perform the best. That's why we additionally selected the model with the largest R square among the top 20 models in each scenario. By comparing RMSEs, we can conclude that the models with the largest R square are slightly better than those with the largest posterior. However, the model selection approach based on Bayesian model averaging is very important. Larger model posterior could guarantee good regression performance and predictive performance. That would contribute to narrow down the scale of selection for OLS models.

6.5 Bayesian Updating Model Averaging

Bayesian Updating Model Averaging (BUMA) is an extension of the usual Bayesian inference methods in which one does not only include parameter uncertainty through the prior distribution, but also include model uncertainty using Bayes' theorem and therefore allowing for allow for direct model selection, combined estimation, and prediction[21]. The predictions of pipeline yield strength under realistic service conditions include various uncertainties. Those uncertainties come from material property, manufacturing process, model choice, model parameters, mechanism modeling, measurement data, as well as numerical evaluations[22]. For a specific model, the associated model parameters also have statistical uncertainties introduced by regression analysis with experimental data. The justification of using a particular model depends on the actual problem. One approach to justify using one model is to update the initial belief on that model using measurement data from experiments. Bayesian updating is one of the most commonly used methods[23]. The model determination can be made based on the results of Bayes factors in a hypothesis testing context[24]. Comparing with typical Bayesian model averaging (BMA), BUMA not only can deal with both parametric linear model and non-parametric model. Each model is treated as a black box and the initial belief of model prior is updated by training set which would lead to averaged posterior model probability.

The probabilistic inference is usually associated with a specific model M_k and it is conditional on the assumption that the model is the correct one which can fully describe the physical phenomenon. However, when the mechanism is not exactly clear, multiple models may be available to simplify the actual complicated mechanism. The joint distribution of an event X and model M_k with a n_k dimensional parameter or hyperparameter can be expressed as

$$p(X, M_k) = P(M_k)p(X|M_k), \tag{8}$$

where $k \in \mathrm{K}$ is the model index, $P(M_k)$ is the prior probability assigned to model M_k, and $p(X|M_k)$ is the conditional probability distribution of event X given model M_k. Notice that we treat each model as a black box which simplified the uncertainties of model parameters. According to Bayes theorem, the total probability of event X as

$$P(X) = \sum_{k \in K} P(M_k)\, P(X|M_k), \tag{9}$$

where $P(X|M_k)$ is the global likelihood for model M_k. And the posterior probability of model M_k reads

$$P(M_k|X) = \frac{P(M_k)P(X|M_k)}{P(X)}. \quad (10)$$

Suppose every response Y_i is distributed to a normal distribution with mean y_i and standard deviation σ. y_i is true value or the benchmark. Then, the likelihood of each Y_i given input X_i, model M_k and σ is written as

$$P(Y_i|X_i, M_k, \sigma) = \frac{1}{\sqrt{2\pi\sigma}} exp\left(-\frac{(y_i - Y_i)^2}{2\sigma^2}\right). \quad (11)$$

According to the above equation, the posterior is proportional to prior times likelihood,

$$P(M_k|X_i, Y_i, \sigma) \propto P(M_k) \cdot P(Y_i|X_i, M_k, \sigma). \quad (12)$$

Without any clear information about the mechanism, we applied uniform priors to the three models which means at the beginning the priors of each model are exactly the same,

$$P(M_1) = P(M_2) = \cdots = P(M_k) = \frac{1}{k}. \quad (13)$$

Then a weight is added to each model and got a global weighted model as follow,

$$M_{weighted} = \sum_{k\in K} w_k \cdot M_k. \quad (14)$$

where w_k equals to posterior model probability, and $\sum_{k\in K} w_k = 1$.

From previous section, there are total four models have been selected for both yield strength and ultimate strength which including two linear models and two quadratic models. In this section, Model priors would be initiated as $P(M_{L1}) = P(M_{L2}) = P(M_{q1}) = P(M_{q2}) = 1/4$. By utilizing Bayesian updating model averaging, four models are merged together to be an averaged model. The performance of the averaged model would be evaluated with full data and split data as well.

Yield Strength Estimation

Full Data Regression

A weighted model for yield strength estimation is merged by two linear models and two quadratic models. First, we used full 70-sample dataset to train there four models and got the records of all the predictive yield strength. Then, likelihoods are calculated with predictive yield strength and benchmark yield strength. Since posterior model probability is proportional to model prior times likelihood, we can retrain the weighted model. To be more specific, given initial uniform prior, posterior would be calculated after plugging in likelihoods of first sample of each model. Next, the new posteriors can be seen as new priors for next iteration. Following the same procedure, the posteriors would be updated for 70 times and the final posteriors show the preference of each model. We called the final posteriors as weights for each model which used to construct the weighted model. Variables and trained weighs for each model are shown in Table 44.

According to equation (14), predictive delta term and yield strength of the weighted model can be calculated. All the predictive values are compared to the Lab Full Wall 0.2% Offset yield strength as shown in Figure 148 - Figure 151. As can be seen in Table 44, ASU_F_QM2_YS has the largest weight among the four single models. As for using MMT yield strength baseline, ASU_M_QM2_YS has the largest weight as shown in Table 45. More detailed numerical comparisons are read in Table 46 and Table 47. From the results, the best OLS models ASU_ F_QM2_YS has smaller RMSE than the weighted model, but the weighted model ASU_F_BUMA_YS has narrower range of residue. And ASU_F_BUMA_YS is much better than ASU_M_BUMA_YS.

Table 44. Variables and Weighs for Each Yield Strength OLS model (Frontics)

Model	Variables	Weight
ASU_F_LM1_YS (M_{L1})	Mn, Mo, Nb, N, ND	0.00055
ASU_ F_LM2_YS (M_{L2})	Mn, Mo, Nb, N, GSsqrtneg, ND	0.00089
ASU_ F_QM1_YS (M_{q1})	ND, N, Mo, N2, Mo2, NDN, NMo, NbMo, NbMn	0.34444
ASU_ F_QM2_YS (M_{q2})	ND, N, Mo, Mn, N2, Mo2, NDN, NbMn	0.65412

Table 45. Variables and Weighs for Each Yield Strength OLS model (MMT)

Model	Variables	Weight
ASU_M_LM1_YS (M_{L1})	ND	8.697e-07
ASU_ M_LM2_YS (M_{L2})	S, Cu, Mo, ND	8.998e-04
ASU_ M_QM1_YS (M_{q1})	ND, S, S2, NDCu	0.13446
ASU_ M_QM2_YS (M_{q2})	ND, S, S2, NDCu, NDMo	0.86464

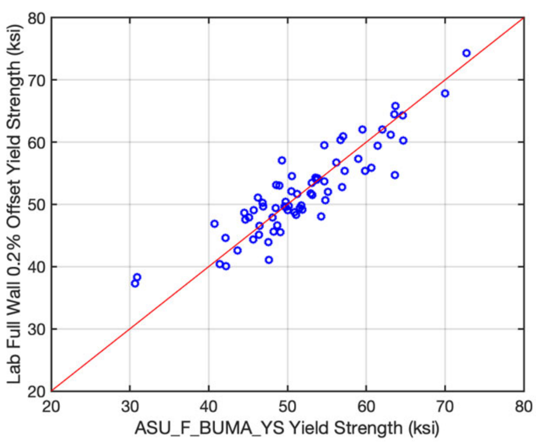

Figure 148. Unit Plot of Lab 0.2% Offset vs. ASU_F_BUMA_YS

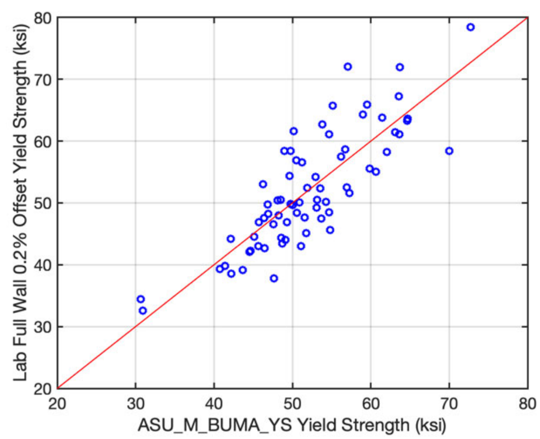

Figure 149. Unit Plot of Lab 0.2% Offset vs. ASU_M_BUMA_YS

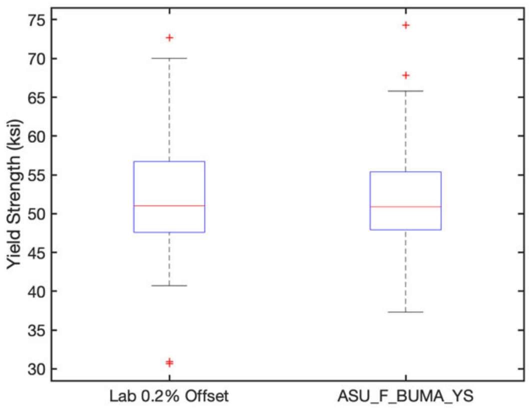

Figure 150. Boxplot of Lab 0.2% Offset vs. ASU_F_BUMA_YS

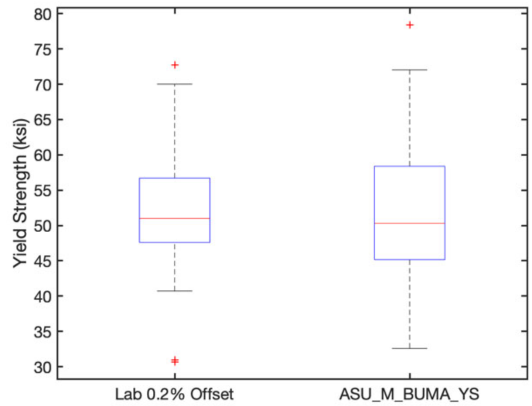

Figure 151. Boxplot of Lab 0.2% offset vs. ASU_M_BUMA_YS

Table 46. Yield Strength Bayesian Weighted Model vs. OLS Model (Frontics & MMT)

	ASU_F_QM2_YS	ASU_F_BUMA_YS	ASU_M_QM2_YS	ASU_M_ BUMA _ YS
R2_Delta	0.7112	0.7101	0.6446	0.6282
adj_R2_Delta	0.6734	0.6490	0.6168	0.5862
R2_YS/UTS	0.8122	0.8114	0.5463	0.5255
adj_R2_YS/UTS	0.7875	0.7717	0.5108	0.4720
RMSE_Delta	3.3378	3.3444	5.1867	5.3048
RMSE_YS/UTS	3.3372	3.3439	5.1866	5.3038
$\chi^2 = \sum_{i=1}^{70} \frac{(o_i - e_i)^2}{e_i}$	16.20	16.37	34.83	36.73

Table 47. Predicted vs. Actual STATs for All Obs. (YS Bayesian Weighted vs. OLS Model)

	Obs	Mean	Std. Dev	Min	Max
ASU_ F_QM2_YS	70	-1.69E-04	3.3614	-8.0537	9.2141
ASU_F_BUMA_YS	70	-1.70E-04	3.3681	-7.7592	8.9813
ASU_ M_QM2_UTS	70	-5.29E-03	5.2246	-14.6021	12.2812
ASU_ M_BUMA_YS	70	-5.29E-03	5.3427	-14.9366	11.6382

Split Data Validation

Hold-out cross validation is applied to model validation. We randomly draw 5 test samples from the full dataset, and 65 samples would be left automatically to be the training set. Similar to what we did in the regression part, the performance of single model is evaluated first. 500 iterations are carried out for validation and the number of the largest posterior for each model is counted. The results are shown in Table 48. ASU_F_QM2_YS did the best in four groups of validation. And ASU_F_LM2_YS always did the worst. It is safe to say that ASU_F_QM2_YS got better performance among these four single models while it is not the dominant one. Now, it is more valuable to check the performance of the weighted model. The comparison results are shown in Table 49. In this case, ASU_F_QM2_YS has the smallest RMSE 3.5914. While it is worth noting that the weighed model ASU_F_BUMA_YS has the second smallest RMSE 3.6766 which performed better than ASU_F_QM1_YS. The predictive performance of the weighted model is very close to ASU_F_QM2_YS. Similarly, the results of using MMT yield strength baseline are shown in Table 50 and Table 51. When comparing the predictive performance of two yield strength weighted models, ASU_F_BUMA_UTS is much better than ASU_M_BUMA_UTS.

Table 48. Performance of Yield Strength OLS Models (Frontics)

	Group 1	Group 2	Group 3	Group 4
ASU_F_LM1_YS	88	92	93	94
ASU_F_LM2_YS	69	63	60	68
ASU_F_QM1_YS	106	98	110	122
ASU_F_QM2_YS	237	247	237	216

Table 49. Performance of Yield Strength Weighted Model and OLS Models (Frontics)

	AvgRMSE.Delta	AvgRMSE.YS
ASU_F_LM1_YS	4.2444	4.1732
ASU_F_LM2_YS	4.3273	4.2911
ASU_F_QM1_YS	3.8648	3.8192
ASU_F_QM2_YS	3.6333	3.5914
ASU_F_BUMA_YS	3.6463	3.6766

Table 50. Performance of Yield Strength OLS Models (MMT)

	Group 1	Group 2	Group 3	Group 4
ASU_F_LM1_YS	145	125	126	115
ASU_F_LM2_YS	80	88	74	96
ASU_F_QM1_YS	116	129	121	122
ASU_F_QM2_YS	159	158	179	167

Table 51. Performance of Yield Strength Weighted Model and OLS Models (MMT)

	AvgRMSE.Delta	AvgRMSE.YS
ASU_F_LM1_YS	5.9965	6.0794
ASU_F_LM2_YS	5.9372	5.9485
ASU_F_QM1_YS	5.5362	5.5683
ASU_F_QM2_YS	5.4421	5.4494
ASU_F_BUMA_YS	5.4093	5.4740

Ultimate Strength Estimation

Full Data Regression

Variables and final trained weighs for each chosen ultimate strength models are shown in Table 52 and Table 53. The quadratic model ASU_F_QM2_UTS has the largest weight 0.46911. When using MMT ultimate strength baseline, ASU_F_QM2_UTS has the largest weight 0.48948. Predictive delta term and ultimate strength of the weighted model are calculated, and 70 predictive values are compared to the Lab Full Wall 0.2% Offset ultimate strength as shown in the unit plot Figure 152 - Figure 155. More detailed numerical comparisons are read in Table 54 and Table 55. From the results, the weighted model ASU_M_BUMA_UTS has the smallest RMSE 3.1405 which indicates the best regression performance. However, the performance of the weighted model ASU_F_BUMA_UTS is almost the same as ASU_M_BUMA_UTS when compare them with respected to the range of residue.

Table 52. Variables and Weighs for Each Ultimate Strength OLS model (Frontics)

Model	Variables	Weight
ASU_F_LM1_UTS (M_{L1})	C, ND	0.13085
ASU_ F_LM2_ UTS (M_{L2})	S, N, ND	0.11657
ASU_ F_QM1_ UTS (M_{q1})	ND, NDS	0.28347
ASU_ F_QM2_ UTS (M_{q2})	ND, S, S2	0.46911

Table 53. Variables and Weighs for Each Ultimate Strength OLS model (MMT)

Model	Variables	Weight
ASU_M_LM1_ UTS (M_{L1})	ND	0.09534
ASU_ M_LM2_ UTS (M_{L2})	S, Cu, Mo, ND	0.48948
ASU_ M_QM1_ UTS (M_{q1})	ND, S, S2, NDCu	0.03109
ASU_ M_QM2_ UTS (M_{q2})	ND, S, S2, NDCu, NDMo	0.38409

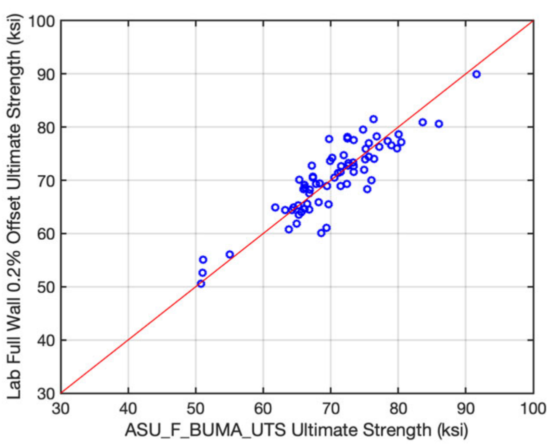

Figure 152. Unit Plot of Lab 0.2% Offset vs. ASU_F_BUMA_UTS

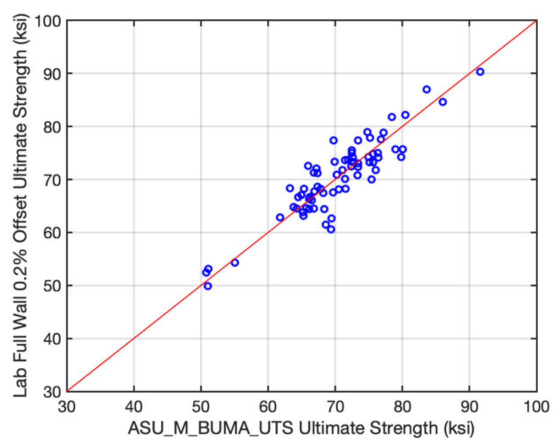

Figure 153. Unit Plot of Lab 0.2% Offset vs. ASU_M_BUMA_UTS

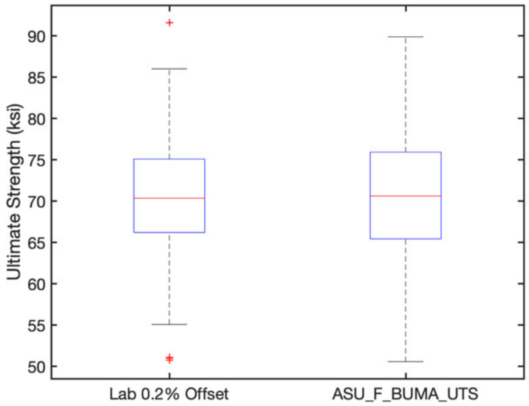

Figure 154. Boxplot of Lab 0.2% Offset vs. ASU_F_BUMA_UTS

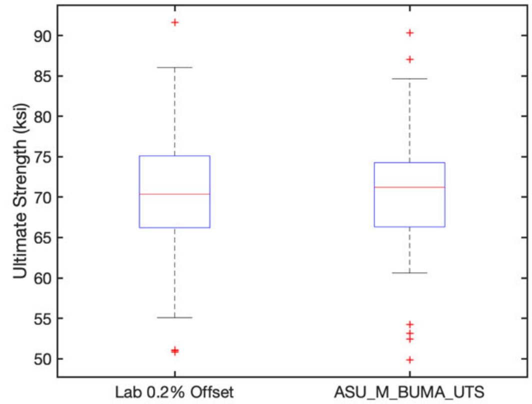

Figure 155. Boxplot of Lab 0.2% offset vs. ASU_M_BUMA_UTS

Table 54. Bayesian Ultimate Strength Weighted Model vs. OLS Model (Frontics & MMT)

	ASU_F_QM2_UTS	ASU_F_BUMA_UTS	ASU_M_LM2_UTS	ASU_M_ BUMA _UTS
R2_Delta	0.2445	0.2457	0.4343	0.4765
adj_R2_Delta	0.2102	0.1738	0.3901	0.3549
R2_YS/UTS	0.7895	0.7898	0.7941	0.8097
adj_R2_YS/UTS	0.7799	0.7698	0.7780	0.7655
RMSE_Delta	3.3029	3.3004	3.2698	3.1454
RMSE_YS/UTS	3.3032	3.3006	3.2665	3.1405
$\chi^2 = \sum_{i=1}^{70} \frac{(o_i - e_i)^2}{e_i}$	10.79	10.77	10.67	9.80

Table 55. Predicted vs. Actual STATs for All Obs. (UTS Bayesian Weighted vs. OLS Model)

	Obs	Mean	Std. Dev	Min	Max
ASU_ F_QM2_UTS	70	-1.69E-04	3.3614	-8.0537	9.2141
ASU_F_BUMA_UTS	70	-2.67E-05	3.3245	-7.9688	8.5147
ASU_M_LM1_UTS	70	-7.96E-03	3.4656	-6.5668	10.0843
ASU_ M_BUMA_UTS	70	-7.96E-03	3.1632	-7.5973	8.7915

Split Data Validation

500 times split data iterations with 65 training sample and 5 test sample are carried out for four groups of validation. And the number of the largest posterior for each model are counted. The results are shown in Table 56. ASU_F_LM2_UTS always did the worst while the linear model ASU_F_LM1_UTS did the best in four groups of validation. However, there is no single OLS model shows the dominant performance. Hence it is necessary to compare the performance of the weighted model with those four single models. The comparison results are shown in Table 57. In this case, by comparing averaged RMSEs, the quadratic model ASU_F_QM1_UTS has the best

predictive performance with the smallest RMSE 3.2587 followed by another quadratic model ASU_F_QM1_UTS and the weighted model ASU_F_BUMA_UTS. The results of using MMT ultimate strength baseline are shown in Table 58 and Table 59. ASU_M_LM2_UTS has the smallest averaged RMSE and the weighted model ASU_M_BUMA_UTS is the second best. When comparing the predictive performance of two weighted models, ASU_F_BUMA_UTS is better with smaller RMSE.

Table 56. Validation of Ultimate Strength OLS Models (Frontics)

	Group 1	Group 2	Group 3	Group 4
ASU_F_LM1_UTS	167	159	160	165
ASU_F_LM2_UTS	47	67	59	73
ASU_F_QM1_UTS	127	119	128	106
ASU_F_QM2_UTS	159	155	153	156

Table 57. Validation of Ultimate Strength Weighted Model and OLS Models (Frontics)

	AvgRMSE.Delta	AvgRMSE.YS
ASU_F_LM1_UTS	3.3592	3.3593
ASU_F_LM2_UTS	3.4261	3.4262
ASU_F_QM1_UTS	3.2585	3.2587
ASU_F_QM2_UTS	3.2760	3.2763
ASU_F_BUMA_UTS	3.2864	3.3393

Table 58. Performance of Ultimate Strength OLS Models (MMT)

	Group 1	Group 2	Group 3	Group 4
ASU_M_LM1_UTS	156	142	154	136
ASU_M_LM2_UTS	197	185	177	198
ASU_M_QM1_UTS	68	94	94	75
ASU_M_QM2_UTS	79	79	75	91

Table 59. Performance of Ultimate Strength Weighted Model and OLS Models (MMT)

	AvgRMSE.Delta	AvgRMSE.YS
ASU_M_LM1_UTS	3.4523	3.4471
ASU_M_LM2_UTS	3.4129	3.4088
ASU_M_QM1_UTS	3.4949	3.4888
ASU_M_QM2_UTS	4.2897	4.2841
ASU_M_BUMA_UTS	3.4376	3.4344

Discussion and Conclusion

For single parametric linear model and quadratic model, different datasets or training set may lead to different performance even dealing with the same problem. The weighted model constructed by Bayesian updating model averaging can tackle model uncertainties and data perturbation well. In regarding to RMSE comparison, the performance of the weighted model may not be the best all the time. But it is always very close to the best performance among the chosen models. In addition, weighted models are proven to effectively narrow down the range of residue which is more valuable in terms of predicting both yield strength and ultimate strength. What's more, Bayesian updating model averaging can not only deal with parametric model, but also has great potential to encode non-parametric model which may lead to a more robust weighted model.

6.6 Bayesian Network Model

Bayesian networks are part of a branch of statistical tools called advanced graphical models that can describe probabilistic relationships between variables[25]. A Bayesian network consists of two parts: a qualitative part in the form of a directed graph, and a quantitative part, in the form of conditional probability tables[26]. In a Bayesian network an important restriction is that the directed graph must be acyclic, in which the edges must not create loops or cycles within the network[27].

It is often assumed that the directed edges in Bayesian network represent causal relationships. The probability theory is not intrinsically able to express causality, so edge directions are not necessarily indicative of causal effects[28]. However, it can also be argued that there is a case for the usage of the term 'causal' for edges in manually constructed Bayesian networks, as they are usually designed to represent the prior understanding of the causal structure. These manually constructed Bayesian networks are usually sparse and their interpretation is clear and meaningful[29].

Bayesian networks are attractive for probabilistic reasoning because their structure allows them to be decomposed for efficient calculation of the joint distribution in typically sparse networks in practice. The flexible nature of Bayesian networks makes it ideal for the complex engineering problems. Bayesian networks can also carry out probabilistic inference easily and efficiently for each specific failure outcome by considering the variables involved, rather than updating the whole model[30]. Another significant benefit of Bayesian Networks is that they allow for the conditional dependencies or causal interactions between variables to be visualized. This provides an intuitive way of observing the relationships allowing stakeholders to make informed decisions in response to different hazard scenarios.

The first step of a Bayesian network construction is structure identification which is extremely important. The initial structure learning process can be performed by using structure-learning algorithms that use optimization methods to attempt to identify the relationships from the data to maximize likelihood or minimize measures such as the Bayesian Information Criterion (BIC), or can be guided manually using domain knowledge. In other words, there are typical two ways to derive the Bayesian network structure with given data: an automated learning method and a guided method utilizing literature and expert knowledge.

In the guided method, the data and knowledge are collected and used to build the structure of the Bayesian network worked in parallel. An approach similar to the one introduced by Babovic[31] was utilized to incorporate domain knowledge, where the Bayesian Network was constrained before combining with raw data. The domain knowledge consisted of information from experts and prior information available from historical data. However, in real world applications, previous expert knowledges may not be applicable to different scenarios and the causal relationships between variables are hard to obtain. Thus, the automated learning method comes up to solve these issues.

The automated learning method is based on several optimization algorithm. The hill-climbing algorithm is the most used one which is a score-based technique that starts with an empty network structure of all variables, then proceeds by adding, removing, and reversing edges between nodes to maximize the goodness of fit of the model. The score for the goodness of fit in *bnlearn* package utilized the log-likelihood loss, which is the negated expected log likelihood; hence, the lower the score the better the fit[32, 33]. The structure of the Bayesian network was final when the score could no longer be improved.

In this section, automated learning Bayesian networks are constructed to predict pipeline yield strength and ultimate strength given 70 pipe samples with 23 features including surface identities and pipe overview data. All the variables used as inputs for the Bayesian network learning are shown in Table 60. For both yield strength and ultimate strength estimation, two different networks are obtained accordingly to analyze the model performance. One is a single Bayesian network and another is an averaged Bayesian network updated by iterations. Generally, there are 4 major streps to construct Bayesian network models. 1) Preprocessing and exploratory data analysis; 2) Learning the structure of a Bayesian network; 3) Learning the parameters of a Bayesian network; 4) Using the network as a regression or predictive model; Results and comparisons are shown in following subsections.

Table 60. Variables Used in Bayesian Network Models

Index	**1**	**2**	**3**	**4**	**5**	**6**	**7**	**8**	**9**	**10**	**11**	**12**
Variable	C	Mn	P	S	Al	Cr	Cu	Mo	Nb	Ni	Si	Ti
Index	**13**	**14**	**15**	**16**	**17**	**18**	**19**	**20**	**21**	**22**	**23**	
Variable	V	B	N	PL	Hod	GS	GSsqrt	GSsqrtneg	ND	WT	ST	

Yield Strength Estimation

Full Data Regression

Note that the y nodes in all the following Bayesian networks are the Delta terms which equal to the difference between full wall tensile data and surface indentation results. Here, $y = YS_t - YS_s$ where YS_s can be seen as the baseline of responses. The single Bayesian network is shown in Figure 174.

However, the quality of the single network crucially depends on whether variables are normally distributed and on whether the relationships that link them are linear. It is not clear that is the case for all of them in the current investigation. We also do not know about which arcs represent strong relationships, in which they are resistant to perturbations of the data. Fortunately, the averaged Bayesian network can address both issues at the same time as show in Figure 156. The main approach of averaged Bayesian network is to resample the data using bootstrap and to learn a separate network from each bootstrap sample. The method will check how often each possible arc appears in the networks and eventually construct a consensus network with the arcs that appear more frequently. Also, the threshold can be customized that will be used to decide whether an arc is strong enough to be included in the consensus network. The regression and comparison results are showing as below.

In the single Bayesian network of yield strength regression, the delta item y has five parent nodes which are ND, Mo, N, Nb and Mn. Besides these directed edges from surface identities and pipe overview variables to the delta node. There are also edges between surface identities and pipe overview variables. These relationships are helpful to get better understanding of the entire causal structure which leads to more eligible reliability pipe strength analysis. The bootstrap step of training the averaged Bayesian network is essentially based on the single network. While in the averaged Bayesian network, four nodes including ND, Mo, N and Nb are the parent nodes of y. The difference between the single network and the averaged network is caused by model uncertainties. The power of the averaged Bayesian network is to show strong and weak relationship explicitly and visually among the variables, and also to improve the robustness of the Bayesian network model. As can be seen in Figure 157, ND, N and Nb have stronger relationship directed to the delta node y than Mo.

Both the single Bayesian network and the averaged Bayesian network are used as regression models for yield strength estimation. Predictive values for each sample are compared to Lab full wall 0.2% offset yield strength, and comparison results are shown in Figure 158 – Figure 161. As for using MMT yield strength baseline, single Bayesian network and weighted Bayesian network model are shown in Figure 162 and Figure 163. Comparing to benchmark yield strength as shown in Figure 164 - Figure 167. Numerical results of regression performance are shown in Table 61 and Table 62, including R square, adjust R square root mean square error (RMSE), chi-squared value and range of residue. From the results, the performance of these Bayesian networks is quite similar to OLS linear models in terms of comparing RMSEs while with larger residue ranges.

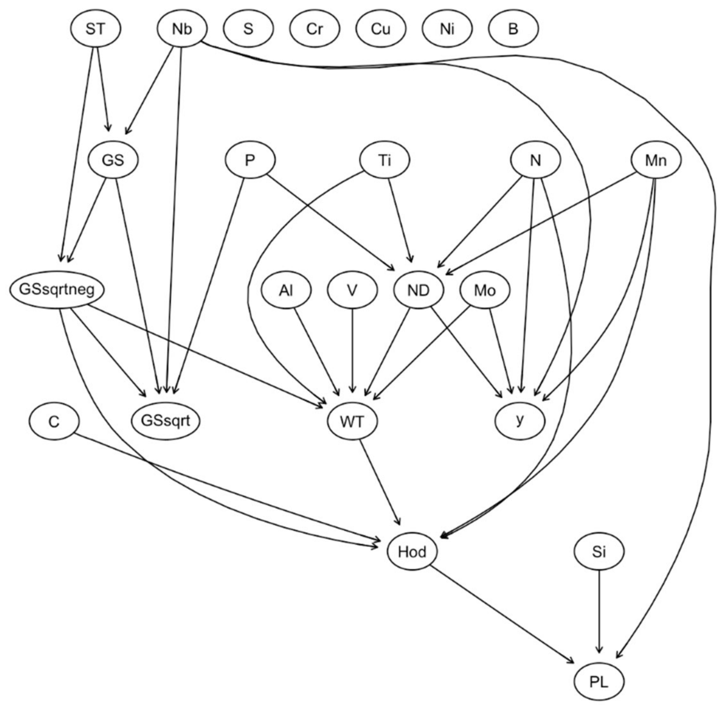

Figure 156. Single Bayesian network (ASU_F_BN1_YS)

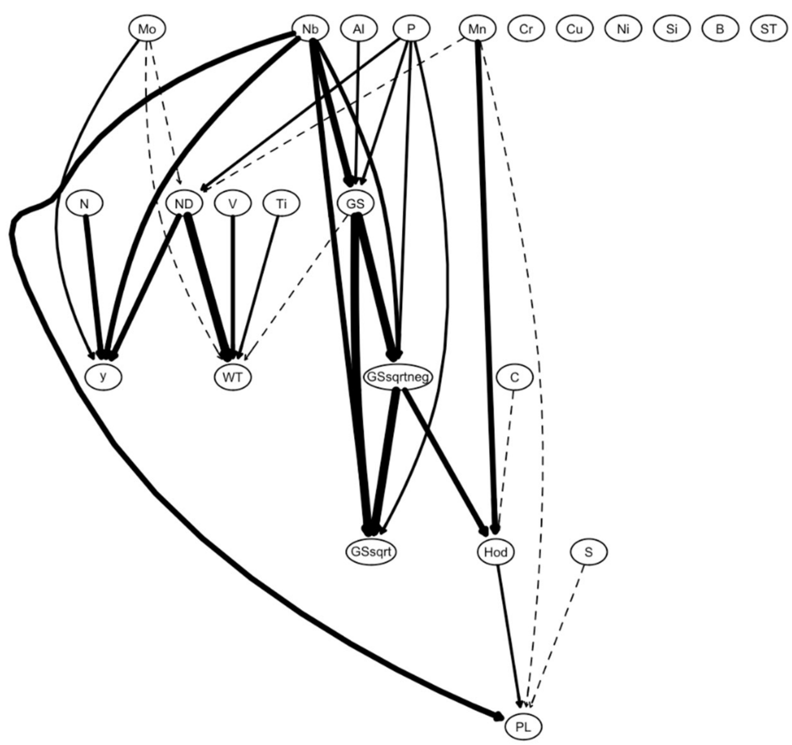

Figure 157. Averaged Bayesian network (ASU_F_BN2_YS)

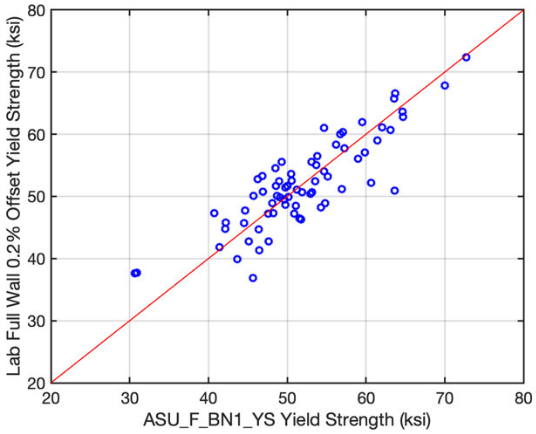

Figure 158. Unit Plot of Lab 0.2% Offset vs. ASU_F_BN1_YS

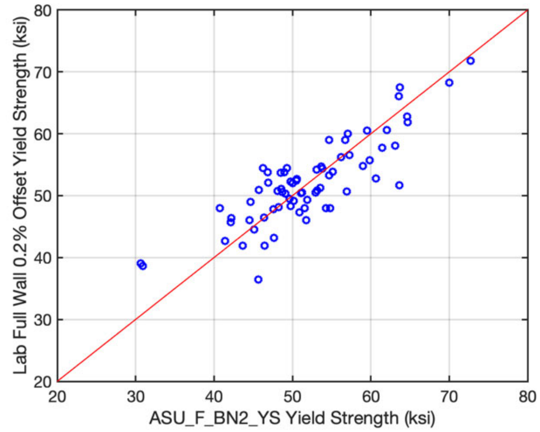

Figure 159. Unit Plot of Lab 0.2% Offset vs. ASU_F_BN2_YS

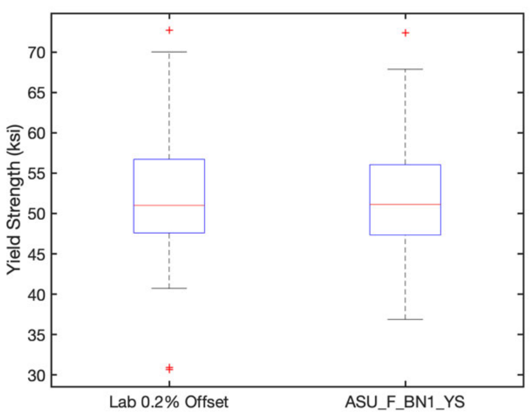

Figure 160. Boxplot of Lab 0.2% Offset vs. ASU_F_BN1_YS

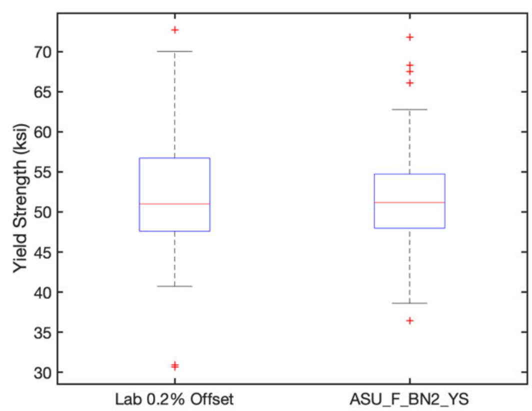

Figure 161. Boxplot of Lab 0.2% offset vs. ASU_F_BN2_YS

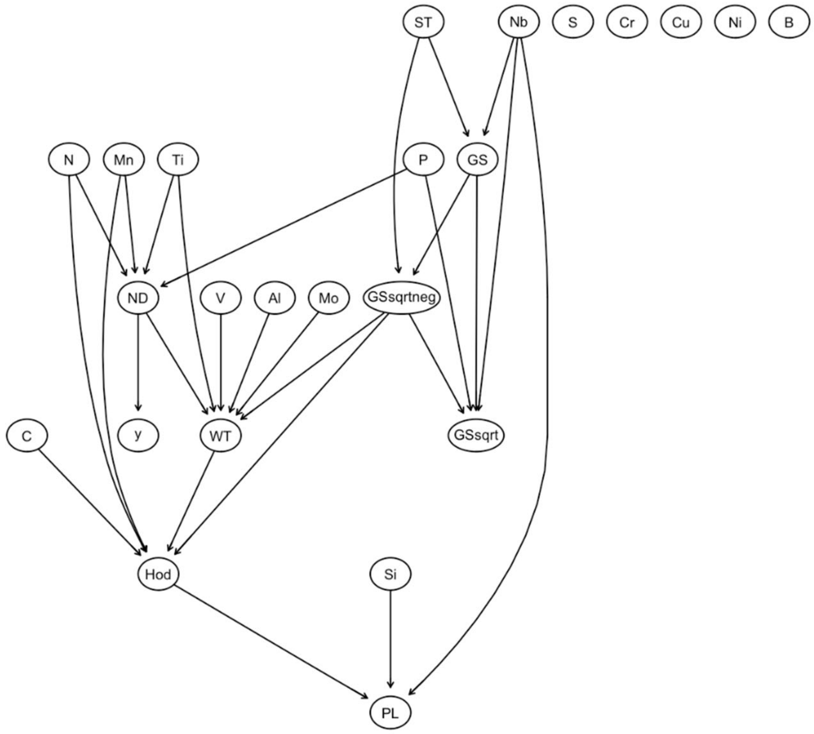

Figure 162. Single Bayesian network (ASU_M_BN1_YS)

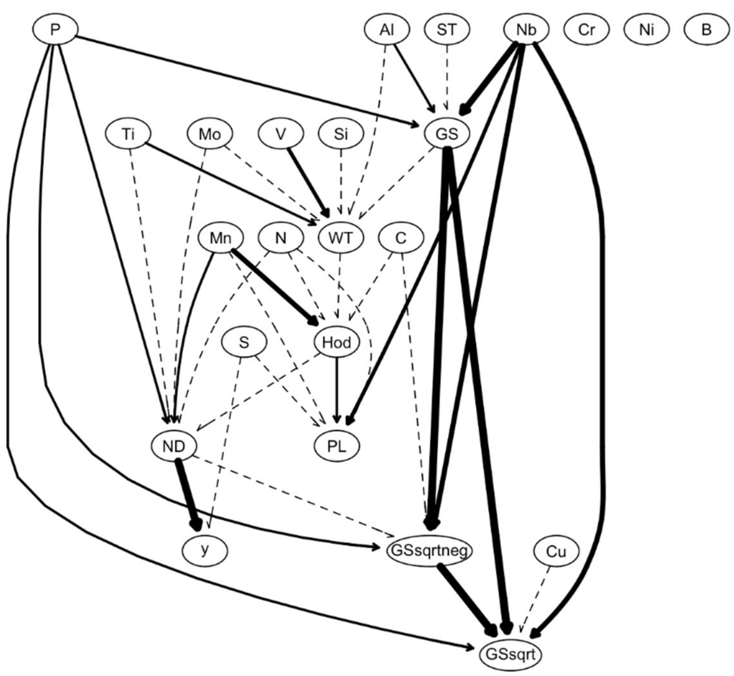

Figure 163. Averaged Bayesian network (ASU_M_BN2_YS)

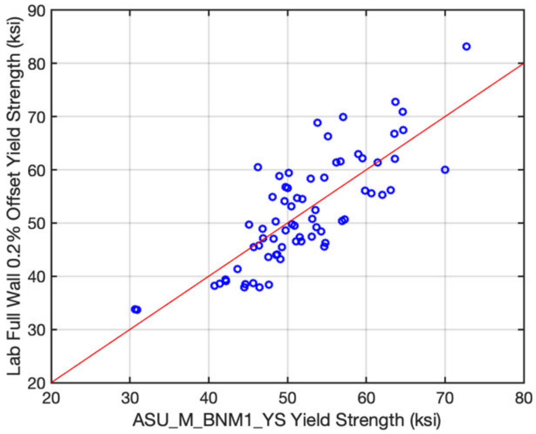

Figure 164. Unit Plot of Lab 0.2% Offset vs. ASU_M_BN1_YS

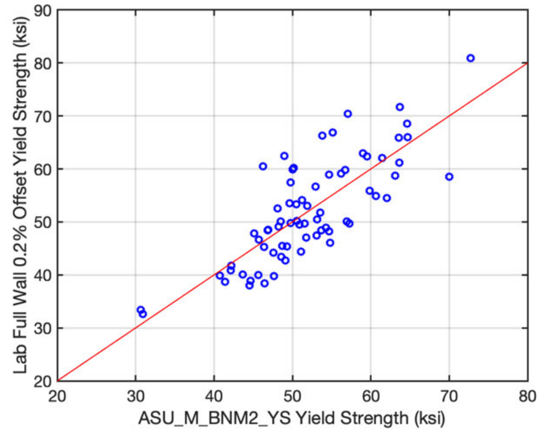

Figure 165. Unit Plot of Lab 0.2% Offset vs. ASU_M_BN2_YS

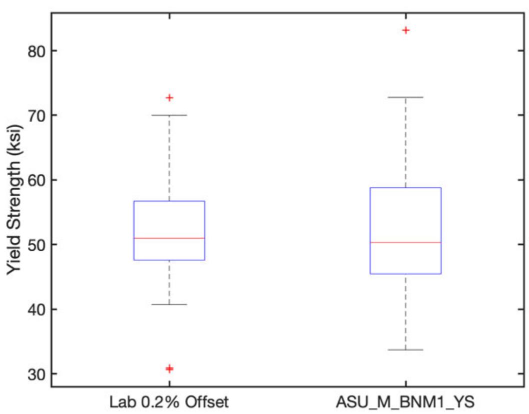

Figure 166. Boxplot of Lab 0.2% Offset vs. ASU_M_BN1_YS

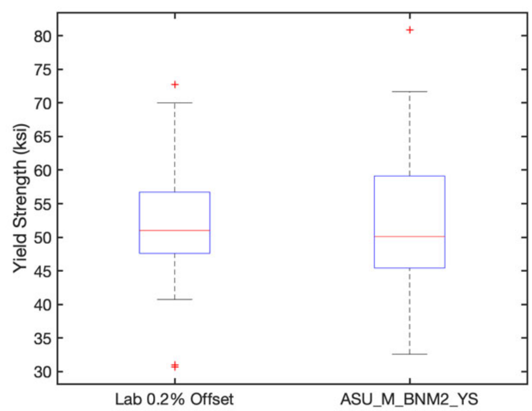

Figure 167. Boxplot of Lab 0.2% offset vs. ASU_M_BN2_YS

Table 61. Properties of Yield Strength Bayesian Network (Frontics & MMT)

	ASU_F_BN1_YS	ASU_F_BN2_YS	ASU_M_BN1_YS	ASU_M_BN2_YS
R2_Delta	0.5802	0.5496	0.5144	0.5395
adj_R2_Delta	0.5474	0.5219	0.5072	0.5257
R2_YS/UTS	0.7270	0.7070	0.3799	0.4119
adj_R2_YS/UTS	0.7056	0.6890	0.3708	0.3944
RMSE_Delta	4.0244	4.1683	6.0630	5.9042
RMSE_YS/UTS	4.0235	4.1676	6.0634	5.9048
$\chi^2 = \sum_{i=1}^{70} \frac{(o_i - e_i)^2}{e_i}$	23.03	25.21	48.58	46.16

Table 62. Predicted vs. Actual STATs for All Obs. (Yield Strength Bayesian Network)

	Obs	Mean	Std. Dev	Min	Max
ASU_F_BN1_YS	70	-1.70E-04	4.0529	-6.9499	12.7852
ASU_ F_ BN2_YS	70	-1.69E-04	4.1981	-8.4076	12.0304
ASU_M_BN1_YS	70	-5.29E-03	6.1079	-14.9869	10.0456
ASU_M_BN2_YS	70	-5.29E-03	5.9481	-14.2204	11.4708

Split Data Validation

To evaluate the performance of two networks further, we split the 70-sample dataset into training and test parts. 5 samples were randomly selected from the dataset to be a testing set, and the rest 65 samples would work as the training set correspondingly. Parametric learning is done with the training set, and then using the 5 test samples to do validation. After 500 iterations, the general predictive performance of the single Bayesian network and the averaged Bayesian network are shown in Table 63. For predictive performance with the 70-sample dataset, the single Bayesian network is slightly better than the averaged Bayesian network. It's reasonable that when we carry out model averaging, the performance of averaged model usually approximates the best model instead of being the best. However, the averaged model is much better to deal with perturbations of the data, which means when having different dataset, the single network would have poorer performance while the averaged network would still be usable.

Table 63. Performance Comparison of Yield Strength BN Models (Frontics & MMT)

	AvgRMSE.Delta	AvgRMSE.YS
ASU_F_BN1_YS	4.2809	4.2802
ASU_ F_BN2_YS	4.3181	4.3176
ASU_M_BN1_YS	5.9155	5.9155
ASU_ M_BN2_YS	5.9708	5.9689

Ultimate Strength Estimation

Full Data Regression

Following the same procedure in yield strength estimation, we used the full data to do the regression first. A single Bayesian network and an averaged Bayesian network for ultimate strength are achieved as shown in Figure 168 and Figure 169 respectively. In the single network, ND, and C are the parent nodes of delta term y. In the averaged network, y has three parent nodes ND, S and C . However, the relationships between S, C and y are not strong. Predictive values for each sample are compared to Lab full wall 0.2% offset ultimate strength, and comparison results are shown in Figure 170 – Figure 173. On the other hand, with MMT ultimate strength baseline, A single Bayesian network and an averaged Bayesian network are constructed in Figure 174 and Figure 175. In the single Bayesian network, the delta term has three parent nodes Ti, Nb and N which are the same in the averaged Bayesian network model.

Numerical results of regression performance are shown in Table 64 and Table 65. As for ultimate strength full data regression, the performance of averaged networks is similar to the single networks. By comparing the range of residue, it can be concluded that ultimate strength Bayesian network models with Frontics baseline are better than with MMT baseline.

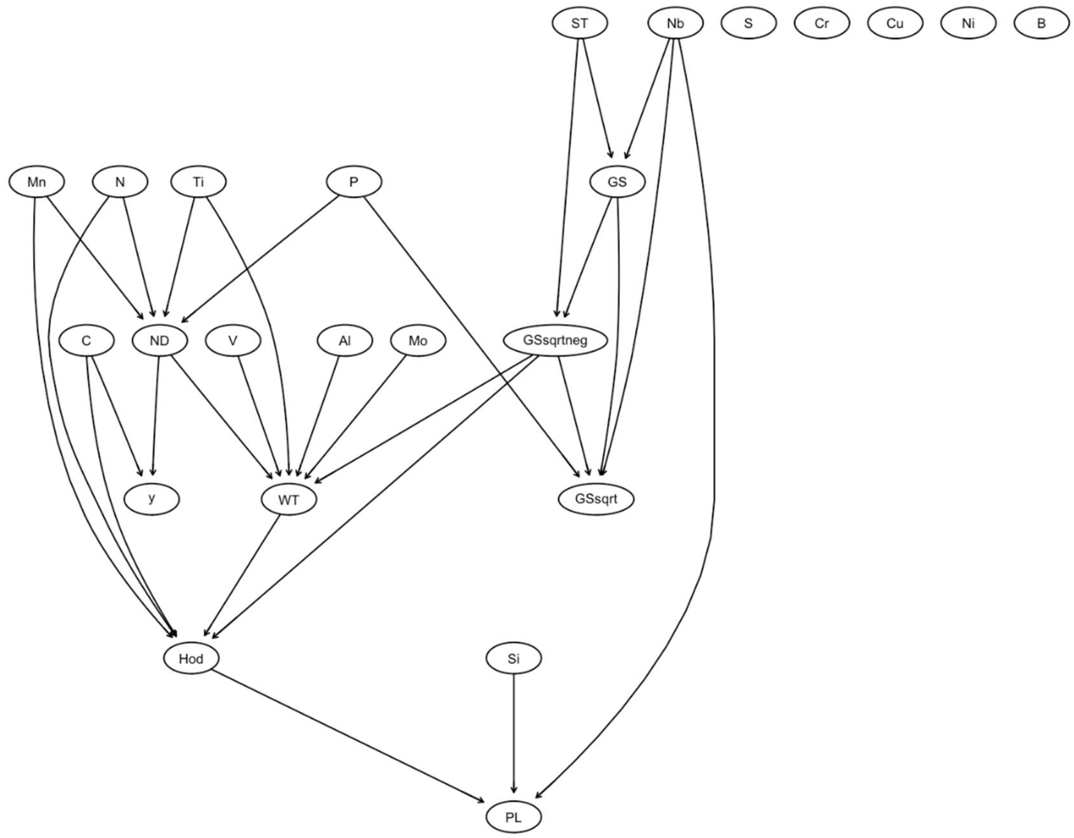

Figure 168. Single Bayesian network (ASU_F_BN1_UTS)

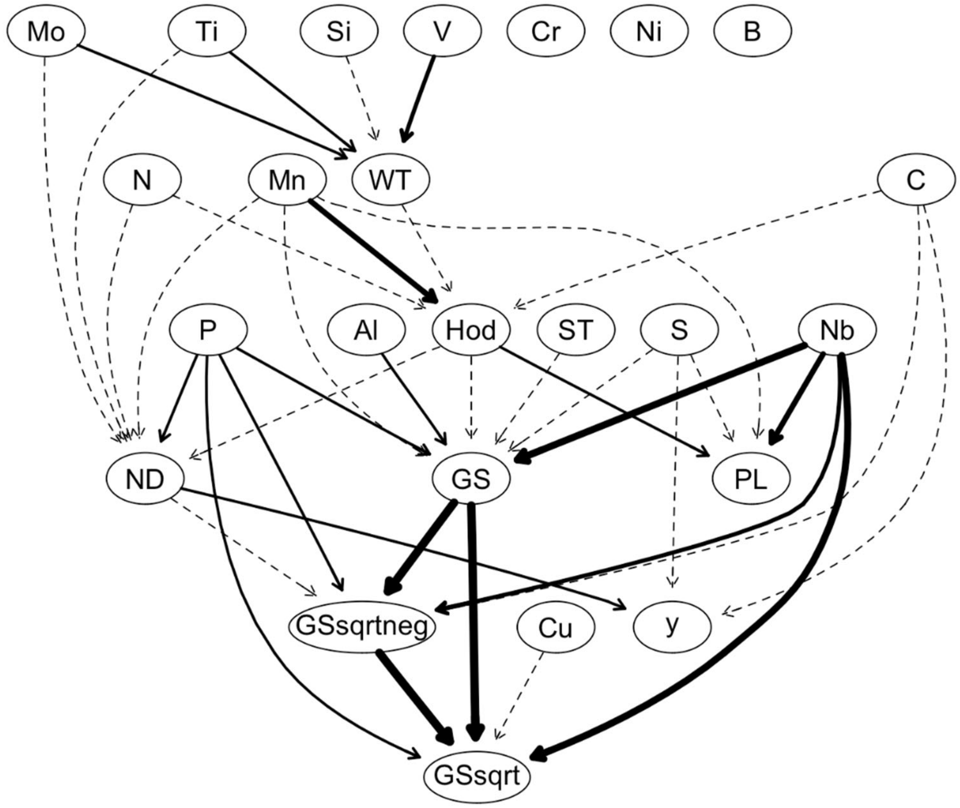

Figure 169. Averaged Bayesian network (ASU_F_BN2_UTS)

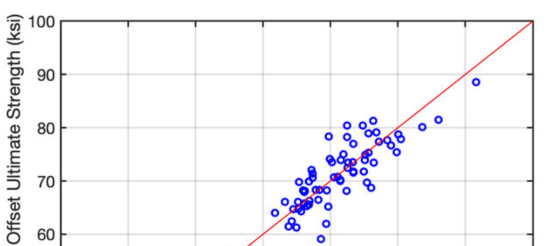

Figure 170. Unit Plot of Lab 0.2% Offset vs. ASU_F_BN1_UTS

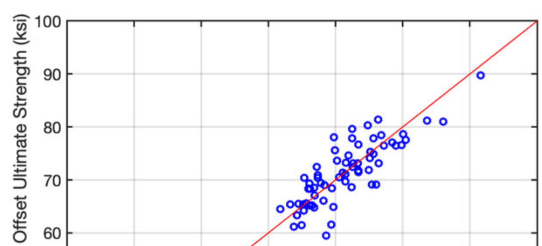

Figure 171. Unit Plot of Lab 0.2% Offset vs. ASU_F_BN2_UTS

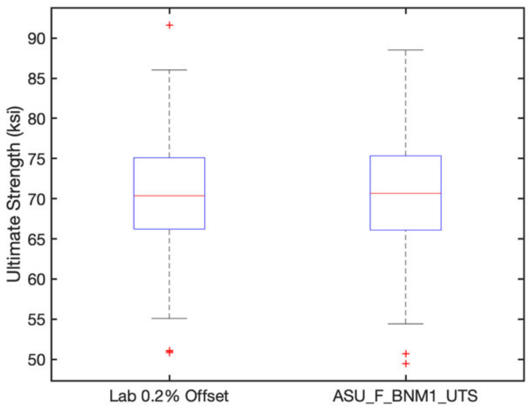

Figure 172. Boxplot of Lab 0.2% Offset vs. ASU_F_BN1_UTS

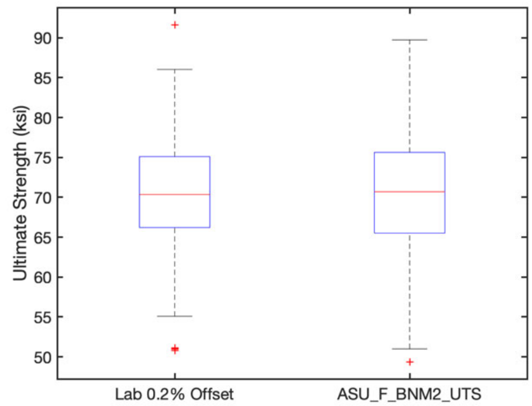

Figure 173. Boxplot of Lab 0.2% offset vs. ASU_F_BN2_UTS

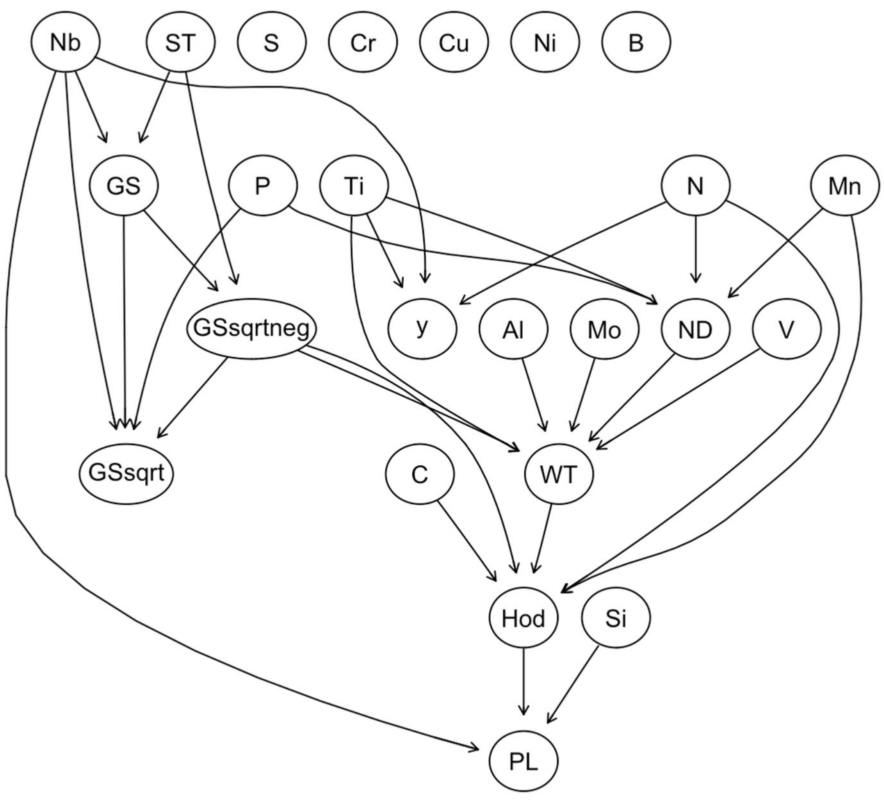

Figure 174. Single Bayesian network (ASU_M_BN1_UTS)

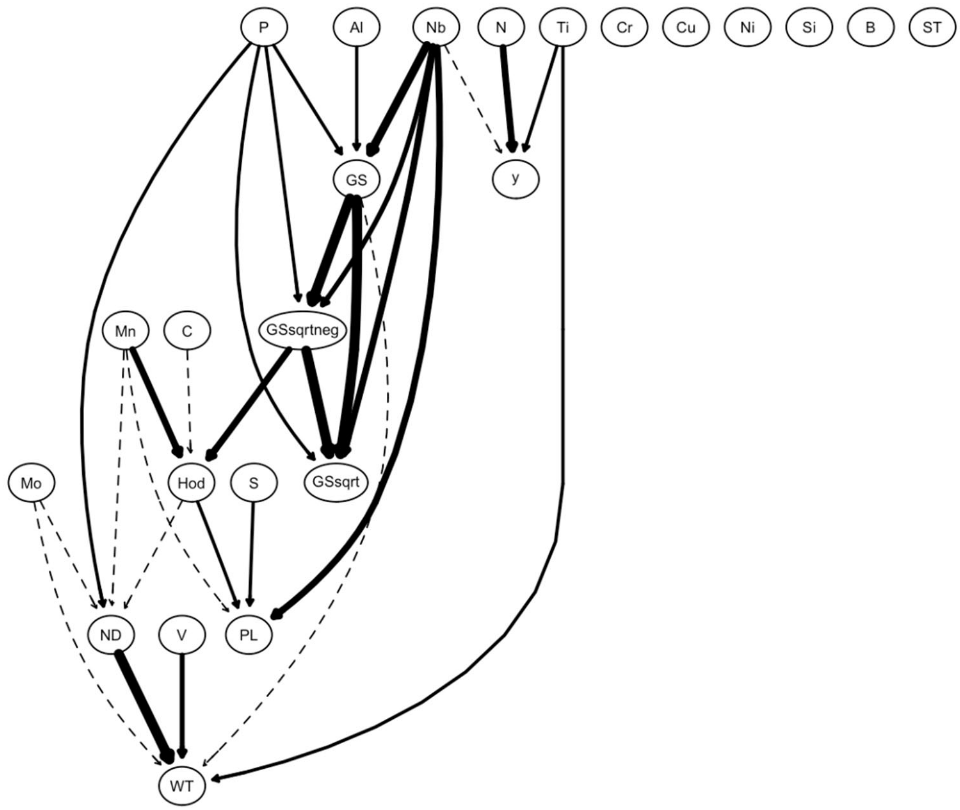

Figure 175. Averaged Bayesian network (ASU_M_BN2_UTS)

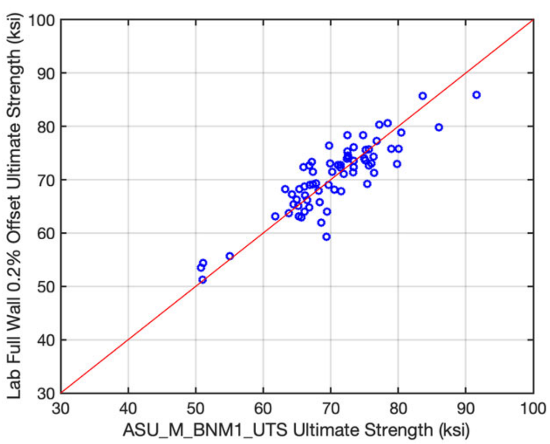

Figure 176. Unit Plot of Lab 0.2% Offset vs. ASU_M_BN1_UTS

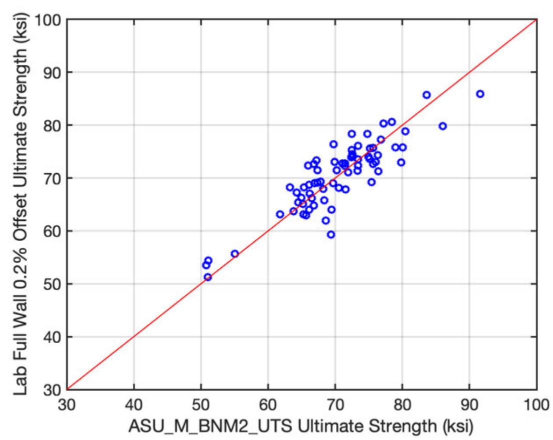

Figure 177. Unit Plot of Lab 0.2% Offset vs. ASU_M_BN2_UTS

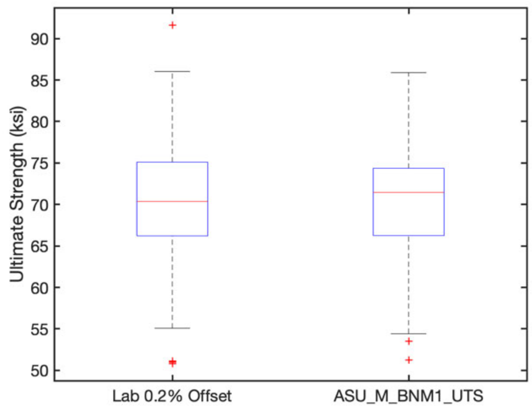

Figure 178. Boxplot of Lab 0.2% Offset vs. ASU_M_BN1_UTS

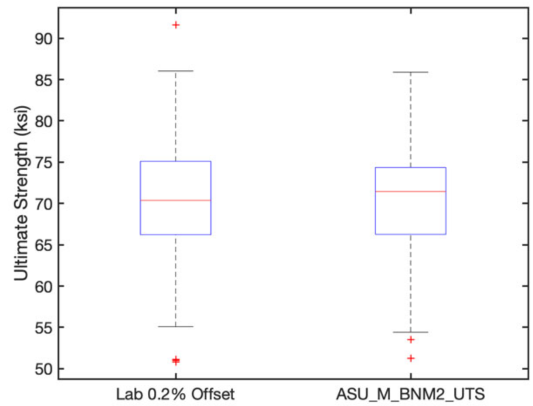

Figure 179. Boxplot of Lab 0.2% offset vs. ASU_M_BN2_UTS

Table 64. Properties of Ultimate Strength Bayesian Network (Frontics & MMT)

	ASU_F_BN1_UTS	ASU_F_BN2_UTS	ASU_M_BN1_UTS	ASU_M_BN2_UTS
R2_Delta	0.1812	0.2085	0.3716	0.3716
adj_R2_Delta	0.1568	0.1725	0.3430	0.3430
R2_YS/UTS	0.7719	0.7795	0.7716	0.7716
adj_R2_YS/UTS	0.7651	0.7694	0.7612	0.7612
RMSE_Delta	3.4386	3.3809	3.4462	3.4462
RMSE_YS/UTS	3.4385	3.3809	3.4407	3.4407
$\chi^2 = \sum_{i=1}^{70} \frac{(o_i - e_i)^2}{e_i}$	11.61	11.26	11.62	11.62

Table 65. Predicted vs. Actual STATs for All Obs. (Ultimate Strength Bayesian Network)

	Obs	Mean	Std. Dev	Min	Max
ASU_F_BN1_UTS	70	-2.64E-05	3.4633	-8.5363	9.5370
ASU_ F_ BN2_UTS	70	-2.57E-05	3.4053	-8.2337	9.1392
ASU_M_BN1_UTS	70	-7.96E-03	3.4656	-6.5668	10.0843
ASU_M_BN2_UTS	70	-7.96E-03	3.4656	-6.5668	10.0843

Split Data Validation

To validate the predictive performance of above two Bayesian networks, again we draw the 5 test samples from the entire dataset and the rest 65 samples as training set for each iteration. The general results for 500 iterations are shown in the Table 66. For Frontics ultimate strength baseline, the predictive performance of the averaged Bayesian network model ASU_ F_BN2_UTS is slightly better than the single one ASU_F_BN1_UTS. For MMT baseline, the single Bayesian network

ASU_M_BN1_UTS shows better performance than ASU_ M_BN2_UTS although they have the same regression performance.

Table 66. Validation Performance Comparison of UTS BN Models (Frontics & MMT)

	AvgRMSE.Delta	AvgRMSE.YS
ASU_F_BN1_UTS	3.3731	3.3729
ASU_ F_BN2_UTS	3.3576	3.3577
ASU_M_BN1_UTS	3.4467	3.4420
ASU_ M_BN2_UTS	3.5321	3.5274

Discussion and Conclusion

In this section, the automated learning Bayesian network with both continuous and categorical variables are applied to yield strength and ultimate strength estimation. Single Bayesian networks and averaged Bayesian networks are constructed with full 70-sample dataset which including surface identities data and pipe overview data. By doing this, the regression performance of all the networks are achieved as well. 5 test data Hold-out cross validations with 500 iterations are used to evaluate the predictive performance of each network. For both yield strength estimation and ultimate strength estimation, the performance of single Bayesian network and averaged Bayesian network are quite similar. In general speaking, the Bayesian network models with Frontics baseline are performed better than those with MMT baseline. Note that all the results got by using Bayesian network are comparable to the results from linear models in previous section. However, the relationships between all the variables can be expressed explicitly by using the automated learning Bayesian network without doing the variable selection and the model selection. In addition, the averaged Bayesian network has nature abilities to deal with perturbations of the data which is very impressive.

6.7 Gaussian Process Model

Gaussian process regression has its basis in Bayesian probability theory[34]. The most used Gaussian process is a non-parametric model, we do not have to worry about whether it is possible for the model to fit the data. Even when a lot of observations have been added, there may still be some flexibility left in the functions[35]. If more datapoints were added one would see the mean function adjust itself to pass through these points, and that the posterior uncertainty would reduce close to the observations. However, non-parametric models rely on local neighborhood training data to make predictions, thus they perform poorly when applied to regions of the state space that are not densely covered by the training dataset. This problem becomes particularly critical as the state space grows[36]. Since some input variables in our research are obtained surface indentation techniques which are very expensive, so it is not possible to get plenty of datapoints to cover the entire sate space. While the parametric approach can capture a great deal of prior knowledge that does not need to be learned from data. It quite necessary to combine the benefits of parametric and non-parametric approaches. Then the semi-parametric Gaussian Process seems like a better option which can combines the interpretability of parametric models with the accuracy of non-parametric models. That means considering the parametric models for the mean function, and the Gaussian Process just has to model the residual errors[37].

A Gaussian Process (GP) defines a prior over functions, which can be converted into a posterior over functions once we have some observed data. In other words, it defines a distribution over the function's values at a finite, but arbitrary, set of points, say $\boldsymbol{x_1}, \ldots, \boldsymbol{x_N}$. A GP assumes that $p\big(f(\boldsymbol{x_1}), \ldots, f(\boldsymbol{x_N})\big)$ is jointly Gaussian, with mean $\boldsymbol{\mu}(\boldsymbol{x})$ and covariance $\Sigma(\boldsymbol{x})$ given by $\Sigma_{ij} = k(\boldsymbol{x_i}, \boldsymbol{x_j})$, where k us a positive definite kernel function. In our research, we use GPs for regression. Let the prior on the regression function to be a GP, denoted by

$$f(\boldsymbol{x}) \sim GP\big(m(\boldsymbol{x}), k(\boldsymbol{x}, \boldsymbol{x}')\big), \tag{15}$$

where m(x) is the mean function and $k(x, x')$ is the kernel or covariance function, i.e.,

$$m(\boldsymbol{x}) = E[f(x)], \tag{16}$$

$$k(\boldsymbol{x}, \boldsymbol{x}') = E\big[\big(f(\boldsymbol{x}) - m(\boldsymbol{x})\big)\big(f(\boldsymbol{x}') - m(\boldsymbol{x}')\big)\big]. \tag{17}$$

For any finite set of points, this process defines a joint Gaussian:

$$p(\mathbf{f}|\mathbf{X}) = N(\mathbf{f}|\boldsymbol{\mu}, \mathbf{K}), \tag{18}$$

where $K_{ij} = k(x_i, x_j)$ and $\boldsymbol{\mu} = \big(m(x_1), \ldots, m(x_N)\big)$.

Note that it is common to use a mean function of $m(\boldsymbol{x}) = 0$, since the GP is flexible enough to model the mean arbitrarily well. Suppose we have a training set $D = \{(x_i,\ f_i),\ i = 1 : N\}$, where $f_i = f(x_i)$ is the noise-free observation of the function evaluated at x_i. Given a test set $\mathbf{X}_*$ of size $N_* \times D$, we want to predict the function outputs $\mathbf{f}_*$. By definition of the GP, the joint distribution has the following form

$$\begin{pmatrix} \mathbf{f} \\ \mathbf{f}_* \end{pmatrix} \sim N\left(\begin{pmatrix} \boldsymbol{\mu} \\ \boldsymbol{\mu}_* \end{pmatrix}, \begin{pmatrix} \mathbf{K} & \mathbf{K}_* \\ \mathbf{K}_*^T & \mathbf{K}_{**} \end{pmatrix}\right), \tag{19}$$

where $\mathbf{K} = \mathrm{k}(\mathbf{X},\ \mathbf{X})$ is $N \times N$, $\mathbf{K}_* = \mathrm{k}(\mathbf{X},\ \mathbf{X}_*)$ is $N \times N_*$, and $\mathbf{K}_{**} = \mathrm{k}(\mathbf{X}_*,\ \mathbf{X}_*)$ is $N_* \times N_*$. By the standard rules for conditioning Gaussians, the posterior has the following form

$$p(\mathbf{f}_*|\mathbf{X}_*, \mathbf{X}, \mathbf{f}) = N(\mathbf{f}_*|\boldsymbol{\mu}_*, \boldsymbol{\Sigma}_*), \quad (20)$$

$$\boldsymbol{\mu}_* = \boldsymbol{\mu}(\boldsymbol{X}_*) + \boldsymbol{K}_*^{\boldsymbol{T}} \boldsymbol{K}^{-\mathbf{1}}(\mathbf{f} - \boldsymbol{\mu}(\mathbf{X})), \quad (21)$$

$$\boldsymbol{\Sigma}_* = \mathbf{K}_{**} - \mathbf{K}_*^{\boldsymbol{T}}\mathbf{K}^{-\mathbf{1}}\mathbf{K}_*, \quad (22)$$

Sometimes it is useful to use a parametric model such as a linear model for the mean of the process, as follows:

$$f(\mathbf{x}) = \beta^T \phi(\mathbf{x}) + r(\mathbf{x}), \quad (23)$$

where $r(\mathbf{x}) \sim \mathrm{GP}(0,\ k(\mathbf{x}, \mathbf{x}'))$ models the residuals. This combines a parametric and a non-parametric model which is known as a semi-parametric Gaussian Process model. If we assume $\beta \sim N(b, B)$, we can integrate these parameters out to get a new GP:

$$p(\mathbf{f}_*|\mathbf{X}_*, \mathbf{X}, \mathbf{y}) = N(\overline{\mathbf{f}}_*, \mathrm{cov}[f_*]), \quad (24)$$

$$\overline{\mathbf{f}}_* = \Phi_*^T \bar{\beta} + \mathbf{K}_*^T \mathbf{K}_y^{-1}(y - \boldsymbol{\Phi}\bar{\beta}), \quad (25)$$

$$\bar{\beta} = \left(\boldsymbol{\Phi}^T \mathbf{K}_y^{-1}\boldsymbol{\Phi} + \mathbf{B}^{-1}\right)^{-1}\left(\boldsymbol{\Phi}\mathbf{K}_y^{-1}\boldsymbol{y} + \mathbf{B}^{-1}\mathbf{b}\right), \quad (26)$$

$$\mathrm{cov}[f_*] = \mathbf{K}_{**} - \mathbf{K}_*^{\boldsymbol{T}}\mathbf{K}_y^{-1}\mathbf{K}_* + \mathbf{R}^{\mathrm{T}}\left(\mathbf{B}^{-1} + \boldsymbol{\Phi}\mathbf{K}_y^{-1}\boldsymbol{\Phi}^T\right)^{-1}\mathbf{R}, \quad (27)$$

$$\mathbf{R} = \boldsymbol{\Phi}_* - \boldsymbol{\Phi}\mathbf{K}_y^{-1}(y - \boldsymbol{\Phi}\bar{\beta}). \quad (28)$$

The predictive mean is the output of the linear model plus a correction term due to the GP, and the predive covariance is the usual GP covariance plus an extra term due to the uncertainty in β.

Yield Strength Estimation

Full Data Regression

From previous variable selection section, with Frontics baseline, the top 3 variables for using yield strength linear model are ND, N and Nb. As for MMT baseline, the top 3 variables are ND, S and N. In this subsection, we applied gaussian process with these three variables to do yield strength full data regression. In consideration of the limited data size we have, a linear trend is added to the GP model which can be seen as a semi gaussian process model. Compare with the Lab Full Wall 0.2% benchmark yield strength YS_t, 70 predictive yield strength of using three-dimensional GP model are shown in Figure 180 - Figure 183. Numerical regression performance is shown in Table 67 and Table 68. From the result, the RMSEs of the GP models are much larger than the models we used in previous sections.

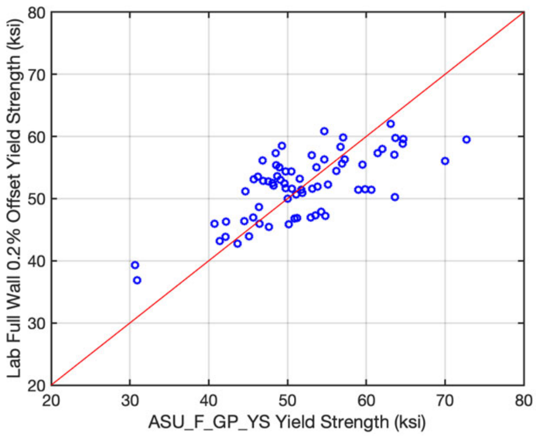

Figure 180. Unit Plot of Lab 0.2% Offset vs. ASU_F_GP_YS

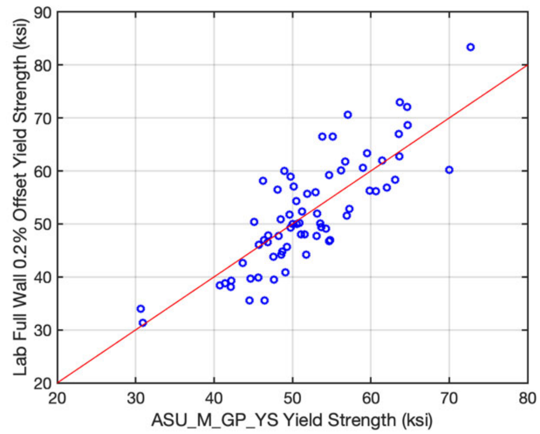

Figure 181. Unit Plot of Lab 0.2% Offset vs. ASU_M_GP_YS

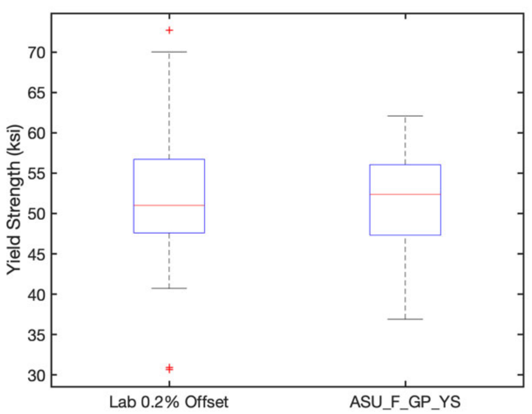

Figure 182. Boxplot of Lab 0.2% Offset vs. ASU_F_GP_YS

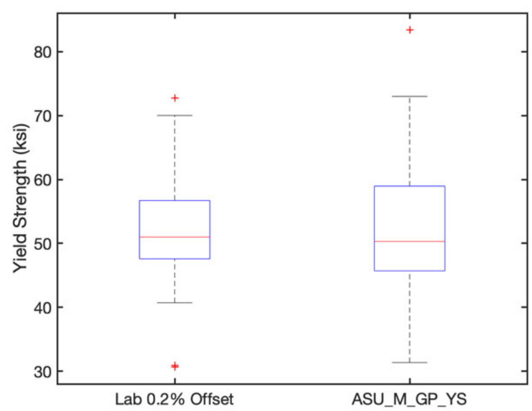

Figure 183. Boxplot of Lab 0.2% offset vs. ASU_M_GP_YS

Table 67. Properties of Yield Strength GP Model (Frontics & MMT)

	ASU_F_GP_YS	ASU_M_GP_YS
R2_Delta	0.2249	0.5472
adj_R2_Delta	0.1897	0.5266
R2_YS/UTS	0.4957	0.4218
adj_R2_YS/UTS	0.4728	0.3955
RMSE_Delta	5.4682	5.8543
RMSE_YS/UTS	5.4681	5.8550
$\chi^2 = \sum_{i=1}^{70} \frac{(o_i - e_i)^2}{e_i}$	39.30	45.37

Table 68. Predicted vs. Actual STATs for All Obs. (Yield Strength GP Model)

	Obs	Mean	Std. Dev	Min	Max
ASU_F_GP_YS	70	-2.23E-04	5.5075	-9.2502	13.9659
ASU_ M_GP_YS	70	-5.45E-03	5.8981	-13.5168	10.8967

Split Data Validation

To evaluate the performance of the GP model further, 500 times hold-out cross validation has been done. Following the same procedures as we did for all the parametric model, the dataset is split into 65-sample training set and 5-sample test set. All the predictive values are compared to benchmark yield strength YS_t. The averaged RMSEs for 500 iterations are shown in Table 69. With less training sample, the performance of GP model is getting even worse.

Table 69. Validation Performance of Yield Strength GP Model (Frontics & MMT)

	AvgRMSE.Delta	AvgRMSE.YS
ASU_F_GP_YS	6.3216	6.3220
ASU_M_GP_YS	6.0545	6.0548

Ultimate Strength Estimation

Full Data Regression

In previous variable selection section, with Frontics baseline, the top 3 variables for using ultimate strength linear model are ND, PL, C. As for MMT baseline, the top 3 variables are N, Ti and PL. Just following the same procedures, we applied gaussian process with these three variables to do ultimate strength full data regression. Compare with the Lab Full Wall 0.2% benchmark ultimate strength UTS_t, 70 predictive ultimate strength of using three-dimensional GP model are shown in Figure 184 - Figure 187. Numerical regression performance is shown in Table 70 and Table 71. From the result, the GP model ASU_M_GP_UTS is better with smaller RMSE and narrower range of residue. However, it is still not plausible compared to the models we constructed before.

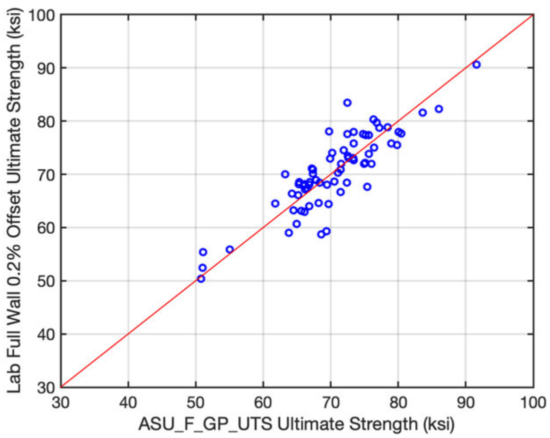

Figure 184. Unit Plot of Lab 0.2% Offset vs. ASU_F_GP_UTS

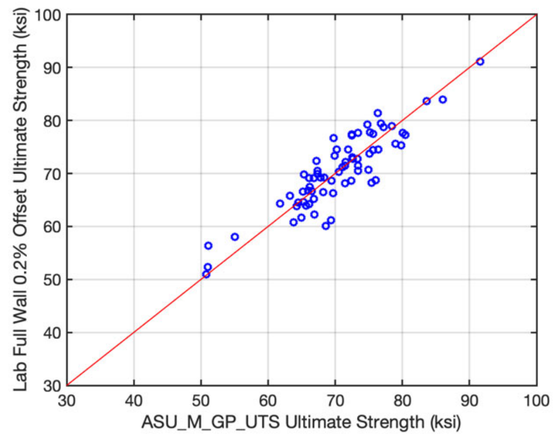

Figure 185. Unit Plot of Lab 0.2% Offset vs. ASU_M_GP_UTS

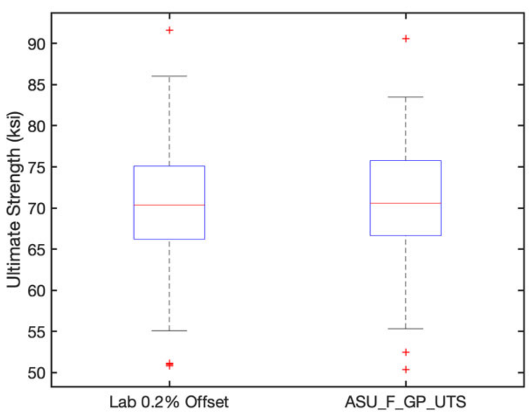

Figure 186. Boxplot of Lab 0.2% Offset vs. ASU_F_GP_UTS

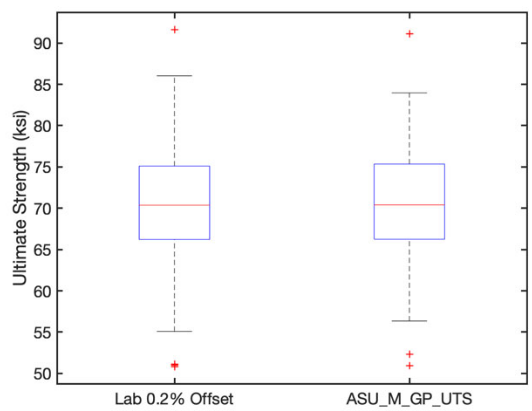

Figure 187. Boxplot of Lab 0.2% offset vs. ASU_M_GP UTS

Table 70. Properties of Ultimate Strength GP Model (Frontics & MMT)

	ASU_F_GP_UTS	ASU_M_GP_UTS
R2_Delta	0.2301	0.0329
adj_R2_Delta	0.1951	-0.0111
R2_YS/UTS	0.7855	0.7305
adj_R2_YS/UTS	0.7757	0.7182
RMSE_Delta	3.3343	3.7371
RMSE_YS/UTS	3.3345	3.7376
$\chi^2 = \sum_{i=1}^{70} \frac{(o_i - e_i)^2}{e_i}$	13.96	11.11

Table 71. Predicted vs. Actual STATs for All Obs. (Ultimate Strength GP Model)

	Obs	Mean	Std. Dev	Min	Max
ASU_F_GP_UTS	70	-3.69E-05	3.7646	-10.9794	10.0936
ASU_ M_GP_UTS	70	-5.17E-05	3.3585	-6.9063	8.5094

Split Data Validation

Similar to yield strength estimation, ultimate strength GP model also evaluated by 500 times hold-out cross validation. The averaged RMSEs are shown in Table 72. The RMSEs of these two GP models are relatively large.

Table 72. Validation Performance of Ultimate Strength GP Model (Frontics & MMT)

	AvgRMSE.Delta	AvgRMSE.UTS
ASU_F_GP_UTS	6.3216	6.3220
ASU_M_GP_UTS	6.0545	6.0548

Discussion and Conclusion

Although GP model is flexible enough, the performance of strength estimation for pipes is not plausible. There are two major reasons for the poor performance. One is that the randomness of the delta terms for both yield strength and ultimate strength is obvious. GP model is not good at dealing with the problems lack of pattern. The other reason would be the limited sample size. A larger dataset is extremely essential for training a non-parametric model like GP. As we can see from the results above, all the validation results are worse than the regression ones because of less training data. In other words, the performance of GP modeling would be getting worse when the dimension of GP model goes up with unchanged training set or the training set becomes smaller with unchanged dimensions. However, the GP modeling has a great potential to achieve better predictive performance and as long as having more training data which need to be evaluated in the future.

6.8 Manifold-Based Gaussian Process Model

Aging pipe data involve 18 features. A critical challenge is the curse-of-dimensionality to analyze this type of high dimensional data by using most existing methods. In other words, the amount of data needed for capturing tendency will increase with dimensions increasing, while the performance will exponentially decrease as well. The most efficiency way to avoid curse of dimensionality is dimension reduction for this stage. There are several dimension reduction techniques available to obtain the low dimensional embedding. Principal Components Analysis (PCA) is one of the most popular linear dimension reduction method, which requires all objects are statistically independent. t-distributed stochastic neighbor embedding (t-SNE) is the commonly used nonlinear dimension reduction method which majorly focus on local structure. Recently, a new nonlinear dimensionality reduction technique, called uniform manifold approximation and projection (UMAP) was introduced, which claimed to preserve as much of local and more of global structure than t-SNE[38, 39]. Therefore, the proposed model for this research is constructed by UMAP and Gaussian Process (GP) regression, where UMAP is used to find the low dimensional representation of high dimensional pipes' data and Gaussian Process (GP) regression model is used to study the low dimensional data points. The major benefit of using manifold learning-based GP regression is to analyze high dimensional/super-high dimensional data from the recognized low-dimensional pattern.

Theoretical foundations of Uniform Approximation and Projection (UMAP) include topological data analysis and manifold theory. For brief mathematical preliminaries, topology is a branch of mathematics focusing on whether certain properties of geometric objects are preserved by homeomorphisms or not, where a homeomorphism is a map between two topological spaces that is bijective (i.e., one-to-one and onto) and bi-continuous (i.e., with the map itself and its inverse both being continuous). A manifold is a topological space that "locally" resembles Euclidean space near each point; that is, any point in the space has a neighborhood in the space which is homeomorphic to an open ball of a Euclidean space.

UMAP has three major assumptions about the data: (a) the data is uniformly distributed on Riemannian manifold; (b) the Riemannian metric is locally constant; (c) the manifold is locally connected[38]. Based on those assumptions, a low dimensional projection can be obtained from constructed fuzzy simplicial complex, the obtained low dimensional projection should be topological equivalent to the constructed fuzzy simplicial complex based on Nerve Theorem [40]A detailed description can be found in in[38]. Here, UMAP is firstly used to find the low dimensional representation of high dimensional data in a L2-space. L2 spaces is known as the Lebasque space, in which a basic regression can be presented. We assume that the low dimensional patterns of high-dimensional data are distributed in this L2-space. For this stage, UMAP can work as both supervised learning and unsupervised learning. In the proposed method, supervised features are used for dimension reduction. As introduced above, it was claimed that UMAP can preserve as much of local and more of global data structure than t-Distributed Stochastic Neighbor (t-SNE) method. In other words, the low dimensional embedding calculated by UMAP have more topological information than other dimensionality reduction techniques.

From previous Gaussian Process Model section, we've already knew that the performance of GP model is very sensitive to data size and model dimension. Given limited sample size, using dimension reduction is the only possible way to improve the performance. Hence in this section, UMAP is proposed to accomplish low dimensional representation, and GP modeling would be applied in the embedded L2-space that the manifold based Gaussian process model (MFGP) can be seen as a two-dimensional GP model.

Yield Strength Estimation

Full Data Regression

There are total 22 variables including surface chemical compositions, pipe overall data, hardness and grain size as recalled in Table 11. UMAP is applied first for dimensionality reduction. With using both Frontics and MMT baseline, those 22 variables are represented in two-dimensional L2-space as shown in Figure 188 and Figure 189, where different colors in the plot indicate values of the response delta term which equals to the difference between YS_t and YS_s. As can be seen from the low dimensional results, the overall trend of responses can be captured by manifold learning. Then GP modeling is performed with respect to the L2-space. Both the predictive delta term and yield strength of 70 samples are calculated by MFGP modeling and compared to benchmarks. The comparison results are show in Figure 190 - Figure 193. Detailed numerical results can be read in Table 73 and Table 74. The regression performance of MFGP almost seems to be. In consideration of the possibility of overfitting issues, spit data validation should be evaluated further to justify the MFGP model comprehensively.

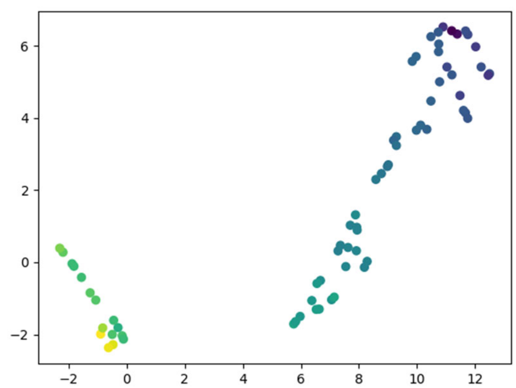

Figure 188. Low Dim. Representation in 2D L2-space for Yield Strength Est. (Frontics)

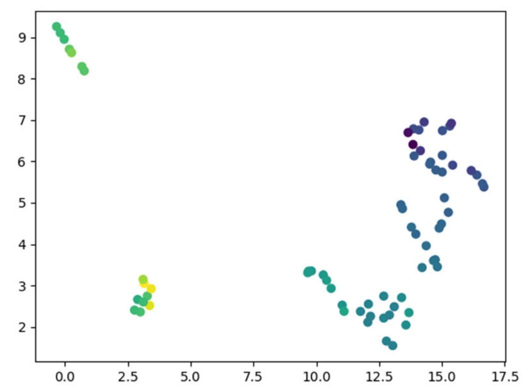

Figure 189. Low Dim. Representation in 2D L2-space for Yield Strength Est. (MMT)

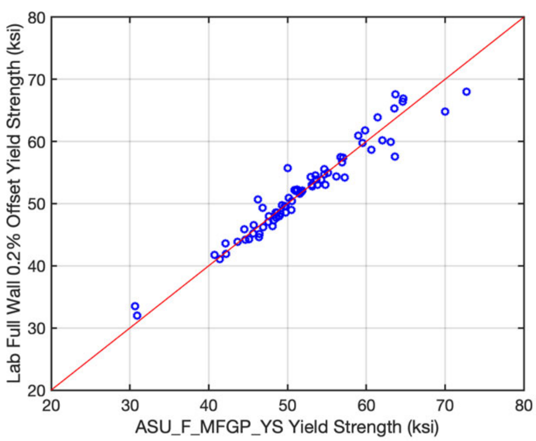

Figure 190. Unit Plot of Lab 0.2% Offset vs. ASU_F_MFGP_YS

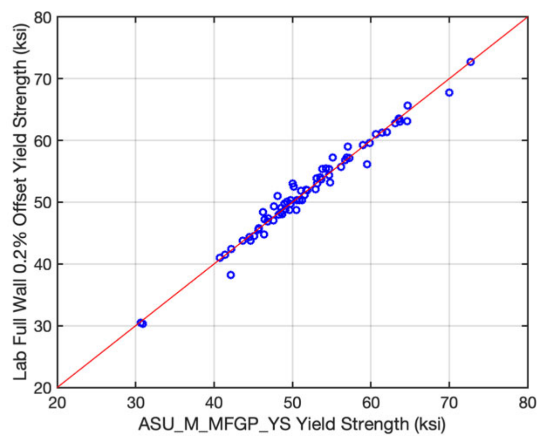

Figure 191. Unit Plot of Lab 0.2% Offset vs. ASU_M_MFGP_YS

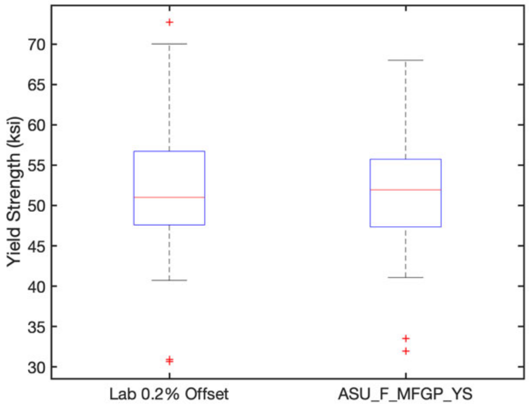

Figure 192. Boxplot of Lab 0.2% Offset vs. ASU_F_MFGP_YS

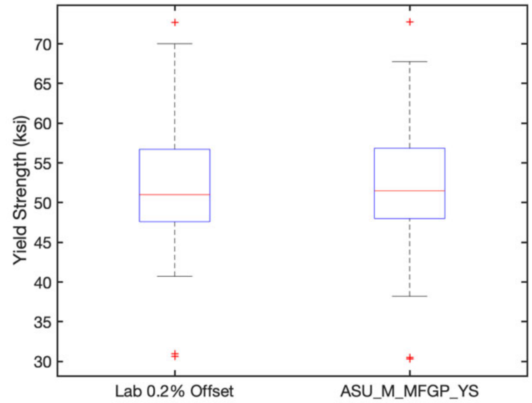

Figure 193. Boxplot of Lab 0.2% offset vs. ASU_M_MFGP YS

Table 73. Properties of Yield Strength MFGP Model (Frontics & MMT)

	ASU_F_MFGP_YS	ASU_M_MFGP_YS
R2_Delta	0.9035	0.9814
adj_R2_Delta	0.8583	0.9727
R2_YS/UTS	0.9372	0.9763
adj_R2_YS/UTS	0.9078	0.9652
RMSE_Delta	1.9293	1.1857
RMSE_YS/UTS	1.9293	1.1858
$\chi^2 = \sum_{i=1}^{70} \frac{(o_i - e_i)^2}{e_i}$	4.67	1.94

Table 74. Predicted vs. Actual STATs for All Obs. (Yield Strength MFGP Model)

	Obs	Mean	Std. Dev	Min	Max
ASU_F_MFGP_YS	70	-6.00E-03	1.9432	-5.7289	6.0717
ASU_ M_MFGP_YS	70	-1.55E-02	1.1942	-2.9868	3.9277

Split Data Validation

As we did many times in previous sections, 500 times hold-out cross validation is used in split data validation. The averaged RMSEs of using MFGP are shown in Table 78. From the result, the averaged RMSEs of both delta term and yield strength are 6.12 and 6.83 which are much larger than regression cases. Compared with the regression results, the performance of MFGP model is not desirable in doing split data validation for predicting yield strength.

Table 75. Validation Performance of Yield Strength MFGP Model

	AvgRMSE.Delta	AvgRMSE.YS
ASU_F_MFGP_YS	6.12	6.12
ASU_M_MFGP_YS	6.83	6.83

Ultimate Strength Estimation

Full Data Regression

Similar to yield strength estimation, the regression performance of MFGP model for ultimate strength is checked with full 70-sample dataset first. With both Frontics and MMT baseline, the original 22 variable are represented in two-dimensional L2-space as shown in Figure 194 and Figure 195. Predictive values are compared to benchmark as shown in Figure 196 and Figure 199. The numerical comparison results are shown in Table 76 and Table 77. As for ultimate strength regression, MFGP did extremely well.

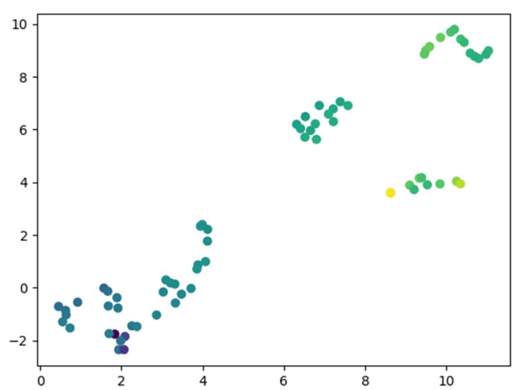

Figure 194. Low Dim. Representation in 2D L2-space for Ultimate Strength Est. (Frontics)

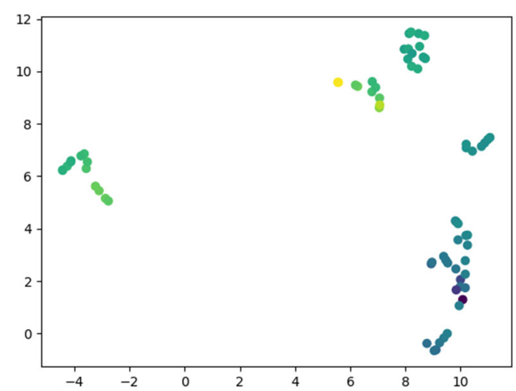

Figure 195. Low Dim. Representation in 2D L2-space for Ultimate Strength Est. (MMT)

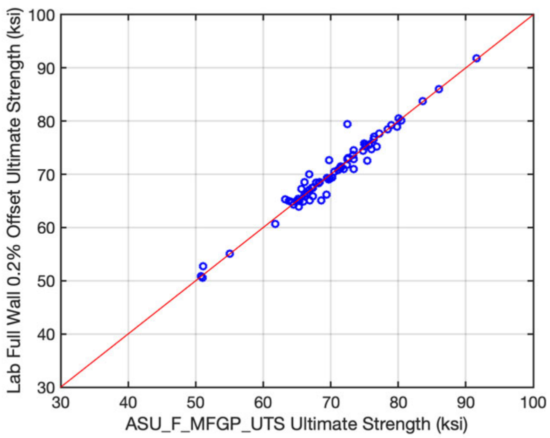

Figure 196. Unit Plot of Lab 0.2% Offset vs. ASU_F_MFGP_UTS

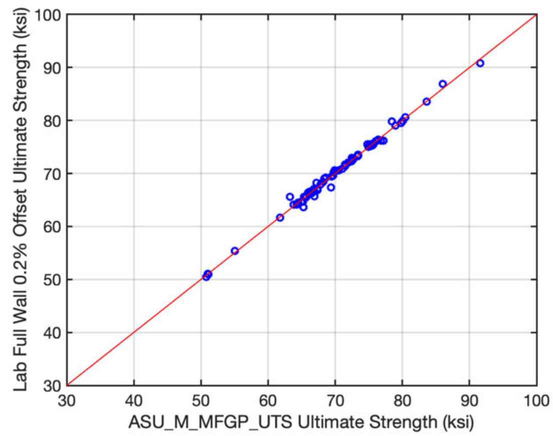

Figure 197. Unit Plot of Lab 0.2% Offset vs. ASU_M_MFGP_UTS

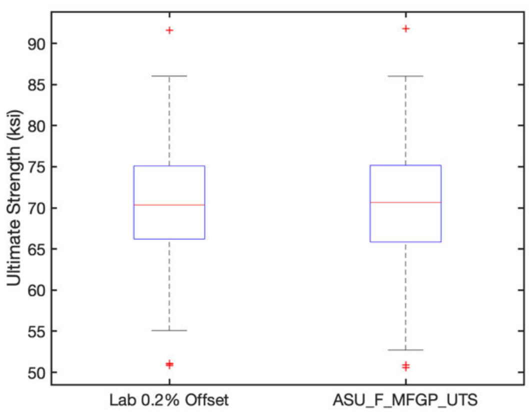

Figure 198. Boxplot of Lab 0.2% Offset vs. ASU_F_MFGP_UTS

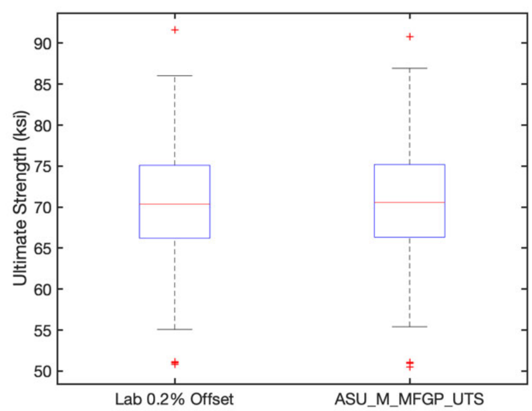

Figure 199. Boxplot of Lab 0.2% offset vs. ASU_M_MFGP UTS

Table 76. Properties of Ultimate Strength MFGP Model (Frontics & MMT)

	ASU_F_MFGP_UTS	ASU_M_MFGP_UTS
R2_Delta	0.8581	0.9818
adj_R2_Delta	0.7918	0.9733
R2_YS/UTS	0.9605	0.9934
adj_R2_YS/UTS	0.9420	0.9903
RMSE_Delta	1.4312	0.5864
RMSE_YS/UTS	1.4312	0.5866
$\chi^2 = \sum_{i=1}^{70} \frac{(o_i - e_i)^2}{e_i}$	2.05	0.35

Table 77. Predicted vs. Actual STATs for All Obs. (Ultimate Strength MFGP Model)

	Obs	Mean	Std. Dev	Min	Max
ASU_F_MFGP_UTS	70	-6.00E-03	1.9432	-5.7289	6.0717
ASU_ M_MFGP_UTS	70	-1.55E-02	1.1942	-2.9868	3.9277

Split Data Validation

The averaged RMSEs of 500 iterations for ultimate strength split data validation are shown in the Table 78. For both delta term and ultimate strength prediction, the RMSEs are the same 6.67 and 7.05 which is still much larger than it of regression case. Even larger than the pure GP model as we investigated in the previous section.

Table 78. Validation Performance of Ultimate Strength MFGP Model

	AvgRMSE.Delta	AvgRMSE.YS
ASU_F_MFGP_UTS	6.67	6.67
ASU_M_MFGP_UTS	7.05	7.05

Discussion and Conclusion

In this section, given 70 sample dataset, manifold-base Gaussian process (MFGP) is proposed to predict both yield strength and ultimate strength of pipes. Based on the results from both full data regression and split data validation, the performance of regression is significantly better than validation cases in terms of using MFGP. Statistically speaking, the proposed MFGP is not robust enough to deal with overfitting issues with relatively small training set. The major reason of this problem could be the constructed manifold is far away from the true manifold. In other words, off-manifold calibration can be not processed for high-dimensional data with only limited training sample. However, MFGP shows high computational efficiency for high-dimensional system that would be powerful for engineering application. Furthermore, by integrating UMAP, a non-deterministic method, with GP modeling, MFGP can partially explain the uncertainty during prediction process.

6.9 Conclusion

This report focused on data driven modeling of pipe yield strength and ultimate strength with Frontics and MMT baselines. Both parametric models and non-parametric models are proposed. Parametric models include ordinary least-squares (OLS) linear models (LM), quadratic models (QM) and Bayesian updating averaged model (BUMA). Taking uncertainties into consideration. All the single linear model and quadratic model with the highest posterior model probability or the largest R square are chosen from model selection with Bayesian model averaging approach. BUMA models are constructed by updating the posteriors of OLS models given uniform model priors. Non-parametric models are Bayesian network model (BNM), Gaussian process model (GP) and manifold-based Gaussian process model (MFGP). The automated learning Bayesian network model with continuous and categorical variables is applied with hill-climbing learning algorithm. GP model is introduced to tackle non-linear problems. And MFGP model combines dimension reduction with Gaussian process. The performance of all the proposed models are evaluated by full data regression and split data validation.

For yield strength estimation, considering regression performance, validation performance and the range of residue at the same time, the model ASU_F_QM1_YS would win the best followed by the Bayesian updating averaged model ASU_F_BUMA_YS. ASU_F_BUMA_YS has constantly excellent performance which has proven to effectively narrow down the range of residue. Although ASU_F_MFGP_YS shows the best performance in yield strength regression, it is not reliable for prediction. In regard to ultimate strength estimation, the best model would be ASU_F_QM1_UTS followed by ASU_F_QM2_UTS and ASU_F_BUMA_UTS. Note that the Bayesian updating averaged models are always closed to have the best performance. It's not hard to imagine given different dataset, the weighted model could achieve better performance since the natural abilities to deal with perturbance data.

In general speaking, Quadratic model with linear terms, power terms and interactive terms overperform pure linear model. However, the performance of single OLS model is case by case due to the lack of capacities of dealing with uncertainties. Bayesian updating averaged model would be the best preference among these models which integrates uncertainties during modeling process which is more robust and reliable. The performance of automated leaning Bayesian network is like linear model, and its predictive accuracy depends on whether the input variables are normally distributed. While the significant benefit of Bayesian Networks is that they allow for the conditional dependencies or causal interactions between variables to be visualized. The flexibility of Bayesian networks for both prognostic (forward) and diagnostic (backward) reasoning would be valuable for engineering application. The relatively poor performance of GP model and MFGP model could be caused by the randomness of delta terms and the limited data size. Having large database is the guarantee of better performance of non-parametric models.

6.10 Regression Table Summaries

Table 79. Summary of 70 samples Full Dataset Regression Performance (Frontics)

	R2_Delta	adj_R2_Delta	R2_YS/UTS	adj_R2_YS/UTS	RMSE_Delta	RMSE_YS/UTS	BIC	AIC	χ2	Log-likelihood
ASU_F_LM1_YS	0.5802	0.5474	0.7270	0.7056	4.0244	4.0235	423.32	407.58	23.03	-180.7334
ASU_F_LM2_YS	0.5889	0.5498	0.7326	0.7072	3.9823	3.9814	426.10	408.11	22.00	-196.0552
ASU_F_QM1_YS	0.6994	0.6543	0.8044	0.7751	3.4056	3.4051	416.94	392.21	17.16	-185.1048
ASU_F_QM2_YS	0.7112	0.6734	0.8122	0.7875	3.3378	3.3372	409.88	387.39	16.20	-183.6972
ASU_F_BUMA_YS	0.7101	0.6490	0.8114	0.7717	3.3444	3.3439			16.37	
ASU_F_BN1_YS	0.5802	0.5474	0.7270	0.7056	4.0244	4.0235			23.03	
ASU_F_BN2_YS	0.5496	0.5219	0.7070	0.6890	4.1683	4.1676			25.21	
ASU_F_GP_YS	0.2249	0.1897	0.4957	0.4728	5.4682	5.4681			39.30	
ASU_F_MFGP_YS	0.9035	0.8583	0.9372	0.9078	1.9293	1.9293			4.67	
ASU_F_LM1_UTS	0.1812	0.1692	0.7719	0.7685	3.4386	3.4385	388.55	379.56	11.61	-185.7799
ASU_F_LM2_UTS	0.2220	0.1866	0.7832	0.7734	3.3519	3.3519	389.23	377.99	11.02	-183.9931
ASU_F_QM1_UTS	0.2196	0.1963	0.7825	0.7760	3.3570	3.3572	385.19	376.20	11.18	-184.0996
ASU_F_QM2_UTS	0.2445	0.2102	0.7895	0.7799	3.3029	3.3032	387.17	375.92	10.79	-182.9622
ASU_F_BMA_UTS	0.2457	0.1738	0.7898	0.7698	3.3004	3.3006			10.77	
ASU_F_BN1_UTS	0.1812	0.1568	0.7719	0.7651	3.4386	3.4385			11.61	
ASU_F_BN2_UTS	0.2085	0.1725	0.7795	0.7694	3.3809	3.3809			11.26	
ASU_F_GP_UTS	0.2301	0.1951	0.7855	0.7757	3.3343	3.3345			13.96	
ASU_F_MFGP_UTS	0.8581	0.7918	0.9605	0.9420	1.4312	1.4312			2.05	

Table 80. Summary of 70 samples Full Dataset Regression Performance (MMT)

	R2_Delta	adj_R2_Delta	R2_YS/UTS	adj_R2_YS/UTS	RMSE_Delta	RMSE_YS/UTS	BIC	AIC	χ2	Log-likelihood
ASU_M_LM1_YS	0.5144	0.5072	0.3799	0.3708	6.0630	6.0634	463.71	456.96	48.58	-225.4803
ASU_M_LM2_YS	0.5799	0.5541	0.4635	0.4305	5.6390	5.6397	466.30	452.81	41.58	-220.4054
ASU_M_QM1_YS	0.6269	0.6039	0.5239	0.4946	5.3142	5.3132	458.00	444.51	36.87	-216.253
ASU_M_QM2_YS	0.6446	0.6168	0.5463	0.5108	5.1867	5.1866	458.84	443.10	34.83	-214.5519
ASU_M_BUMA_YS	0.6282	0.5862	0.5255	0.4720	5.3048	5.3038			36.73	
ASU_M_BN1_YS	0.5144	0.5072	0.3799	0.3708	6.0630	6.0634			48.58	
ASU_M_BN2_YS	0.5395	0.5257	0.4119	0.3944	5.9042	5.9048			46.16	
ASU_M_GP_YS	0.5472	0.5266	0.4218	0.3955	5.8543	5.8550			45.37	
ASU_M_MFGP_YS	0.9814	0.9727	0.9763	0.9652	1.1857	1.1858			1.94	
ASU_M_LM1_UTS	0.3716	0.3623	0.7716	0.7682	3.4462	3.4407	393.11	381.87	11.62	-185.9341
ASU_M_LM2_UTS	0.4343	0.3901	0.7941	0.7780	3.2698	3.2665	394.25	378.51	10.67	-182.2558
ASU_M_QM1_UTS	0.3289	0.3089	0.7561	0.7489	3.5612	3.5551	393.46	384.46	12.38	-188.2316
ASU_M_QM2_UTS	0.4241	0.3591	0.7908	0.7672	3.2991	3.2929	404.00	383.76	10.75	-182.8801
ASU_M_BMA_UTS	0.4765	0.3549	0.8097	0.7655	3.1454	3.1405			9.80	
ASU_M_BN1_UTS	0.3716	0.3430	0.7716	0.7612	3.4462	3.4407			11.62	
ASU_M_BN2_UTS	0.3716	0.3430	0.7716	0.7612	3.4462	3.4407			11.62	
ASU_M_GP_UTS	0.0329	-0.0111	0.7305	0.7182	3.7371	3.7376			11.11	
ASU_M_MFGP_UTS	0.9818	0.9733	0.9934	0.9903	0.5864	0.5866			0.35	

Table 81. Summary of Validation Performance (Frontics)

	AvgRMSE.Delta	AvgRMSE.YS/UTS
ASU_F_LM1_YS	4.2444	4.1732
ASU_F_LM2_YS	4.3273	4.2911
ASU_F_QM1_YS	3.8648	3.8192
ASU_F_QM2_YS	3.6333	3.5914
ASU_F_BUMA_YS	3.6463	3.6766
ASU_F_BN1_YS	4.2809	4.2802
ASU_F_BN2_YS	4.3181	4.3176
ASU_F_GP_YS	6.3216	6.3220
ASU_F_MFGP_YS	6.12	6.12
ASU_F_LM1_UTS	3.3592	3.3593
ASU_F_LM2_UTS	3.4261	3.4262
ASU_F_QM1_UTS	3.2585	3.2587
ASU_F_QM2_UTS	3.2760	3.2763
ASU_F_BMA_UTS	3.2864	3.3393
ASU_F_BN1_UTS	3.3731	3.3729
ASU_F_BN2_UTS	3.3576	3.3577
ASU_F_GP_UTS	3.8250	3.8254
ASU_F_MFGP_UTS	6.6700	6.6700

Table 82. Summary of Validation Performance (MMT)

	AvgRMSE.Delta	AvgRMSE.YS/UTS
ASU_M_LM1_YS	5.9965	6.0794
ASU_M_LM2_YS	5.9372	5.9485
ASU_M_QM1_YS	5.5362	5.5683
ASU_M_QM2_YS	5.4421	5.4494
ASU_M_BUMA_YS	5.4093	5.4740
ASU_M_BN1_YS	5.9155	5.9155
ASU_M_BN2_YS	5.9708	5.9689
ASU_M_GP_YS	6.0545	6.0548
ASU_M_MFGP_YS	6.8300	6.8300
ASU_M_LM1_UTS	3.4523	3.4471
ASU_M_LM2_UTS	3.4129	3.4088
ASU_M_QM1_UTS	3.4949	3.4888
ASU_M_QM2_UTS	4.2897	4.2841
ASU_M_BUMA_UTS	3.4376	3.4344
ASU_M_BN1_UTS	3.4467	3.4420
ASU_M_BN2_UTS	3.5321	3.5274
ASU_M_GP_UTS	3.9485	3.9487
ASU_M_MFGP_UTS	7.0500	7.0500

Table 83. Summary of Predicted vs. Actual STATs for All Obs. (Frontics)

Model	Obs	Mean	Std	Min	Max
ASU_F_LM1_YS	70	-1.70E-04	4.0529	-6.9499	12.7852
ASU_F_LM2_YS	70	-1.69E-04	4.0105	-7.0247	11.8946
ASU_F_QM1_YS	70	-1.69E-04	3.4298	-7.6571	8.5254
ASU_F_QM2_YS	70	-1.69E-04	3.3614	-8.0537	9.2141
ASU_F_BUMA_YS	70	-1.70E-04	3.3681	-7.7592	8.9813
ASU_F_BN1_YS	70	-1.70E-04	4.0529	-6.9499	12.7852
ASU_F_BN2_YS	70	-1.69E-04	4.1981	-8.4076	12.0304
ASU_F_GP_YS	70	-2.23E-04	5.5075	-9.2502	13.9659
ASU_F_MFGP_YS	70	-6.00E-03	1.9432	-5.7289	6.0717
ASU_F_LM1_UTS	70	-2.64E-05	3.4633	-8.5363	9.5370
ASU_F_LM2_UTS	70	-2.63E-05	3.3761	-7.1641	8.8400
ASU_F_QM1_UTS	70	-2.63E-05	3.3815	-7.4620	8.7143
ASU_F_QM2_UTS	70	-2.64E-05	3.3270	-8.2630	8.2132
ASU_F_BUMA_UTS	70	-2.67E-05	3.3245	-7.9688	8.5147
ASU_F_BN1_UTS	70	-2.64E-05	3.4633	-8.5363	9.5370
ASU_F_BN2_UTS	70	-2.57E-05	3.4053	-8.2337	9.1392
ASU_F_GP_UTS	70	-3.69E-05	3.7646	-10.9794	10.0936
ASU_F_MFGP_UTS	70	-2.73E-03	1.4415	-6.8812	3.5338

Table 84. Summary of Predicted vs. Actual STATs for All Obs. (MMT)

Model	Obs	Mean	Std	Min	Max
ASU_M_LM1_YS	70	-5.29E-03	6.1079	-14.9869	10.0456
ASU_M_LM2_YS	70	-5.29E-03	5.6811	-13.7486	11.6824
ASU_M_QM1_YS	70	-5.29E-03	5.3521	-14.9512	11.6132
ASU_M_QM2_YS	70	-5.29E-03	5.2246	-14.6021	12.2812
ASU_M_BUMA_YS	70	-5.29E-03	5.3427	-14.9366	11.6382
ASU_M_BN1_YS	70	-5.29E-03	6.1079	-14.9869	10.0456
ASU_M_BN2_YS	70	-5.29E-03	5.9481	-14.2204	11.4708
ASU_M_GP_YS	70	-5.45E-03	5.8981	-13.5168	10.8967
ASU_M_MFGP_YS	70	-1.55E-02	1.1942	-2.9868	3.9277
ASU_M_LM1_UTS	70	-7.96E-03	3.4656	-6.5668	10.0843
ASU_M_LM2_UTS	70	-7.96E-03	3.2901	-8.3577	7.5372
ASU_M_QM1_UTS	70	-7.96E-03	3.5808	-7.8360	10.5789
ASU_M_QM2_UTS	70	-7.96E-03	3.3167	-6.8648	10.2522
ASU_M_BUMA_UTS	70	-7.96E-03	3.1632	-7.5973	8.7915
ASU_M_BN1_UTS	70	-7.96E-03	3.4656	-6.5668	10.0843
ASU_M_BN2_UTS	70	-7.96E-03	3.4656	-6.5668	10.0843
ASU_M_GP_UTS	70	-5.17E-05	3.3585	-6.9063	8.5094
ASU_M_MFGP_UTS	70	-2.40E-02	0.5903	-2.3811	2.0700

PART IV: PROJECT CONCLUSIONS AND RECOMMENDATIONS

Part IV contains:

- Chapter 7: Conclusions
- Chapter 8: Recommendations

Chapter 7: Conclusions

1. The project successfully measured and categorized the mechanical, chemical, and physical differences across a broad range of pipe sample walls through methodical full-wall and bulk testing as compared to surface-collected physical, mechanical, and chemical NDE testing.
2. Differences in yield strength between the surface derived values and bulk, full-wall were analyzed via a sensitivity study and explained through the changes in surface yield strength due to primary steel production processes, seam type and pipe forming process, and steel chemistry. All these factors/variables can be determined from surface testing.
3. Based on the extensive testing and analysis an ambitious set of modeling tasks were completed include causal-based OLS and data analytics-based modeling. Successful models for yield strength and ultimate tensile strength were developed to predict bulk properties from purely surface obtained information for yield strength and tensile strength.
4. The optimum causal models combined with the Frontics AIS technology surface data achieved a 95% confidence in yield strength predictions by overlapping the full-wall yield strength from lab tests across the entire pipe sample DOE. The optimal models for the MMT HSD exhibited bias in the yield strength for certain pipe configurations related to non-isotropic properties across the pipe wall. The models reduced the bias of the MMT results, but could not completely adjust for it particularly at higher yield strengths.
5. Both NDE technologies optimal models, coupled with the surface data, achieved 95% confidence in ultimate tensile strength predictions by overlapping the full-wall ultimate tensile strength from lab testing across the entire pipe sample DOE.
6. Chemistry values were correlated successfully for 15 key elements, and the only significant variation of chemical properties across the pipe wall was noted from surface to bulk values for carbon and sulfur. A set of chemical element kernel distributions were developed to estimate the magnitude of these differences across the pipe wall based on steel type and other factors.
7. A supplemental body of detailed toughness testing was completed on over 40% of the pipe samples in the DOE and collected and analyzed as a supplemental task of the project. This work will provide invaluable to future NDE technology development aimed at estimating pipe toughness through surface nondestructive testing.

Chapter 8: Recommendations

1. The relations, models, and distributions developed under this project can be used to predict full-wall yield and ultimate strengths from surface-based NDE technology such as Frontics AIS and MMT HSD for *seamless* pipes.
2. The Frontics AIS technology also was successful at a 95% confidence for predicting *yield* strength across the entire pipe sample DOE on *non-seamless* pipes, i.e., pipes with long seam welds like ERW, SAW, etc.
3. Further research is warranted/advised into the promising MMT HSD technology to help reduce bias in the full-wall yield strength predictions based on surface readings for non-seamless pipe that have variation of yield strength across the pipe thickness cross section. The current models provided by the manufacturer and developed under this project could not remove the bias in these measurements, particularly for higher yield strengths.
4. The relations, models, and distributions developed under this project can be used to predict full-wall *ultimate tensile* strengths from surface-based NDE technology such as Frontics AIS and MMT HSD. Using the causal-based models developed, both technologies achieved a 95% confidence for predicting tensile strength across the entire pipe sample DOE, seamless or non-seamless.

PART V: APPENDICES, REFERENCES, AND ATTACHMENTS

Part V contains:

- Appendices
- References
- Attachments

Appendices

Appendix A: External File - Project Master Data Table for 70 Pipeline Samples in Excel (778KB). APPENDIX_A_MASTER_DATA_TABLE_V01.xlsx

Appendix B: External File - Charpy Toughness and Related Data 30 Pipeline Samples in Excel (195 KB). APPENDIX_B_CHARPY_DATA_TABLE_V01.xlsx

Appendix C: Contained in this report - Causal-Based Regression Output Tables.

Appendix D: External File - R-Code for Regressions in Chapter 6 in a ZIP file (53 KB). APPENDIX_D_CH6_R-CODE.zip

Appendix A: Project Master Data Table

External File - Project Master Data Table for 70 Pipeline Samples in Excel (778KB).

Filename: APPENDIX_A_MASTER_DATA_TABLE_V01.xlsx

Appendix B: Charpy Toughness and Related Data

External File - Charpy Toughness and Related Data 30 Pipeline Samples in Excel (195 KB).

Filename: APPENDIX_B_CHARPY_DATA_TABLE_V01.xlsx

Appendix C: Causal Model Regression Output Tables

DAE_1_3: Regress Results for Yield Strength Delta Frontics AIS

Source	SS	df	MS			
				Number of obs	=	70
				F(14, 55)	=	10.47
Model	1963.60968	14	140.257834	Prob > F	=	0.0000
Residual	736.712842	55	13.394779	R-squared	=	0.7272
				Adj R-squared	=	0.6577
Total	2700.32252	69	39.135109	Root MSE	=	3.6599

ys_deltaFront	Coefficient	Std. err.	t	P> t	[95% conf.	interval]
steelType						
KilledSi	-.9542302	3.113312	-0.31	0.760	-7.193446	5.284986
RimmedCapped	4.683697	1.881262	2.49	0.016	.9135635	8.45383
SemiKilled	-2.328979	1.613331	-1.44	0.155	-5.562166	.9042089
cu_5mil	-3.614347	11.58788	-0.31	0.756	-26.83699	19.60829
mn_5mil	148.406	51.12612	2.90	0.005	45.94696	250.865
p_5mil	90.78431	110.045	0.82	0.413	-129.7508	311.3194
si_5mil	.4295721	20.38887	0.02	0.983	-40.43063	41.28978
n_sqrt	-59.98384	24.70705	-2.43	0.018	-109.4979	-10.4698
diameter_nominal	-.5015118	.0960278	-5.22	0.000	-.6939558	-.3090678
c.xp#c.c_5mil#c.c_5mil	-393.9323	286.7953	-1.37	0.175	-968.6829	180.8182
c.nb_5mil#c.c_5mil	1707.823	604.7443	2.82	0.007	495.888	2919.757
c.xf#c.mn_5mil	-178.619	61.93398	-2.88	0.006	-302.7375	-54.50052
c.mn_5mil#c.dNegSqrt	-11.89951	3.400048	-3.50	0.001	-18.71336	-5.085658
c.xf#c.mn_5mil#c.dNegSqrt	14.79267	3.994075	3.70	0.000	6.788363	22.79698
_cons	6.326566	3.54775	1.78	0.080	-.7832827	13.43642

DAE_1_4mmt regress: Regress Results for Yield Strength Delta MMT HSD

Source	SS	df	MS			
				Number of obs	=	70
				F(16, 53)	=	6.43
Model	3357.80237	16	209.862648	Prob > F	=	0.0000
Residual	1730.64202	53	32.6536229	R-squared	=	0.6599
				Adj R-squared	=	0.5572
Total	5088.44438	69	73.7455707	Root MSE	=	5.7143

ys_deltaMMT	Coefficient	Std. err.	t	P> t	[95% conf.	interval]
KilledSi	6.737072	5.028333	1.34	0.186	-3.348488	16.82263
RimmedCapped	-.0747886	3.112577	-0.02	0.981	-6.317828	6.168251
SemiKilled	-1.874652	2.571982	-0.73	0.469	-7.033394	3.284091
Seamless	3.299899	1.907592	1.73	0.089	-.5262464	7.126044
HSLA	3.335258	4.687858	0.71	0.480	-6.067394	12.73791
cu_5mil	-17.05694	18.52519	-0.92	0.361	-54.21377	20.09989
mn_5mil	105.7867	80.17679	1.32	0.193	-55.02754	266.601
p_5mil	78.83774	174.3307	0.45	0.653	-270.8253	428.5008
si_5mil	-65.75388	34.93962	-1.88	0.065	-135.8339	4.326129
n_sqrt	13.45917	40.30981	0.33	0.740	-67.39207	94.31041
diameter_nominal	-.8242026	.1564516	-5.27	0.000	-1.138005	-.5104006
c.xp#c.c_5mil#c.c_5mil	-553.3381	455.354	-1.22	0.230	-1466.663	359.9864
c.nb_5mil#c.c_5mil	-639.764	1364.913	-0.47	0.641	-3377.433	2097.905
c.xf#c.mn_5mil	-114.2744	97.28292	-1.17	0.245	-309.3992	80.85046
c.mn_5mil#c.dNegSqrt	-6.362876	5.368521	-1.19	0.241	-17.13077	4.405013
c.xf#c.mn_5mil#c.dNegSqrt	6.793832	6.320528	1.07	0.287	-5.883542	19.47121
_cons	4.780465	5.79581	0.82	0.413	-6.844458	16.40539

DAE_2_3: Regress Results for Ultimate Tensile Strength Delta Frontics AIS

Source	SS	df	MS
Model	268.428819	5	53.6857638
Residual	742.558499	64	11.6024766
Total	1010.98732	69	14.6519901

Number of obs	=	70
F(5, 64)	=	4.63
Prob > F	=	0.0011
R-squared	=	0.2655
Adj R-squared	=	0.2081
Root MSE	=	3.4062

uts_deltaFront	Coefficient	Std. err.	t	P>|t|	[95% conf.	interval]
Seamless	1.897563	.9019652	2.10	0.039	.09568	3.699445
diameter_nominal	-.1607846	.0770479	-2.09	0.041	-.3147055	-.0068637
mn_5mil	1.809902	1.822556	0.99	0.324	-1.831072	5.450877
si_5mil	-11.90077	5.986043	-1.99	0.051	-23.85927	.0577227
c_5mil	15.86179	8.162154	1.94	0.056	-.4439844	32.16757
_cons	-2.652115	1.844633	-1.44	0.155	-6.337193	1.032964

DAE_2_4: Regress Results for Ultimate Tensile Strength Delta MMT HSD

Source	SS	df	MS
Model	529.320553	5	105.864111
Residual	793.370157	64	12.3964087
Total	1322.69071	69	19.1694306

Number of obs	=	70
F(5, 64)	=	8.54
Prob > F	=	0.0000
R-squared	=	0.4002
Adj R-squared	=	0.3533
Root MSE	=	3.5209

uts_deltaMMT	Coefficient	Std. err.	t	P>|t|	[95% conf.	interval]
Seamless	4.460485	.9323144	4.78	0.000	2.597973	6.322997
diameter_nominal	-.1253978	.0796404	-1.57	0.120	-.2844978	.0337022
mn_5mil	1.258266	1.883881	0.67	0.507	-2.505219	5.021752
si_5mil	-9.903803	6.187461	-1.60	0.114	-22.26468	2.457071
c_5mil	28.02344	8.436792	3.32	0.001	11.16901	44.87787
_cons	-6.553776	1.906701	-3.44	0.001	-10.36285	-2.744703

Appendix D: Charpy Toughness and Related Data

External File - R-Code for Regressions in Chapter 6 in a ZIP file (53 KB).

Filename: APPENDIX_D_CH6_R-CODE.zip

References

1. Chen, J., Ersoy, D., Yongming, L., *Probabilistic bulk property estimation using multimodality surface non-destructive measurements for vintage pipes.* Structural Safety, 2020. **87**.

2. Pickering, F.B., *Physical Metallurgy and the Deisn of Steels.* 1983, New York, NY: Applied Science Publishers.

3. Gladman, T., et. al., *Structure-Property Relationships in High-Strength Microalloyed Steels*, in *Microalloying '75*, M. Korchynsky, Editor. 1977, Union Carbide: New York, NY. p. 32-58.

4. Hodgson, P.D. and R.K. Gibbs, *A Mathematical Model to Predict the Mechanical Properties of Hot Rolled C-Mn and Microalloyed Steels.* ISIJ International, 1992. **32**(12): p. 1329-1338.

5. Lenard, J.G., et. al, *Mathematical and Physical Simulation of the Properties of Hot Rolled Products.* 1999, New York, NY: Elsevier.

6. Gladman, T., et al, *Some Aspects of the Structure-Property Realtionships in High Carbon Ferrite-Pearlite Steels.* J. Iron Steel Inst., 1972. **210**: p. 916-930.

7. Choquet, et. al. *Modeling of Forces, Struture and Final Properties During the Hot Rolling PRocess on the Hot Strip Mill.* in *Proc. Mathematical Mdoeling of Hot Rolling of Steel.* 1990. Hamilton, Canada.

8. Kuziak, et. al., *Modeling of the Microstructure and Mechanical Properites of Steels During Thermomechanical Processing.* 1997, NIST: Boulder, CO.

9. Majita, J., et. al. *Use of the Computer Simulation to Predict Mechanical Properties of C-Mn Steel after Thermomechanical Processing.* in *Metal Forming '96.* 1996. Mat. Proc. Techn.

10. Licka, S., et al, *Mathematical Model to Calculate Structure Development and Mechanical Properties of Hot-Rolled Plates and Strips*, in *Thermomechanical Processing of Microalloyed Austnite.* 1981, Metallurgical Society of AIME: New York, NY. p. 521-528.

11. Pickering, F.B., *High-Strength, Low-Alloy Steels - A Decade of Progress*, in *Microalloying '75.* 1975, Union Carbide Corp.: New York, NY. p. 9-31.

12. Guidebook, *US Department of Transportation, Pipeline and Hazardous Materials Safety Administration.* 2016, USA.

13. Lebedev, A., N. Muzyka, and N. Volchek, *Determination of damage accumulated in structural materials by the parameters of scatter of their hardness characteristics.* Stength of materials, 2002. **34(4)**: p. 317-321.

14. Lai, M. and K. Lim, *On the prediction of tensile properties from hardness tests.* Journal of materials science, 1991. **26(8)**: p. 2031-2036.

15. Hashemi, S., *Strength–hardness statistical correlation in API X65 steel.* Materials Science and Engineering: A, 2011. **528(3)**: p. 1648-1655.

16. Guyan, I. and A. Elisseeff, *An Introduction to Variable and Feature Selection.* Journal of Machine Learning Research, 2003. **3**: p. 1157-1182.

17. Zeugner, S. and M. Feldkircher, *Bayesian Model Averaging Employing Fixed and Flexible Priors: The BMS Package for R.* Journal of Statistical Software, 2015. **68**(4).

18. Clyde, M.A., J. Ghosh, and M.L. Littman, *Bayesian Adaptive Sampling for Variable Selection and Model Averaging.* Journal of Vomputational and Graophical Statistics, 2011. **20**: p. 80-101.

19. Faraway, J.J., *Practical Regression and Anova using R.* 2002.

20. Hayashi, F., *Econometrics.* 2001.

21. Guan, X., R. Jha, and Y. Liu, *Model selection, updating, and averaging for probabilistic fatigue damage prognosis.* Structural Satety, 2011. **33**: p. 242-249.

22. Gregory, P., *Bayesian logical data analysis for the physical sciences.* 2005.

23. Jeffreys, S., *Theory of probability.* Oxford University Press.

24. Clyde, M., M. Cetinkaya-Rundel, and C. Rundel, *An Introduction to Bayesian Thinking.* 2020.

25. Pearl , J., *Probabilistic reasoning in intelligent systems: networks of plausible inference.* 1988, San Francisco, CA, USA: Morgan Kaufmann.

26. Jensen, F.V. and T.D. Nielsen, *Bayesian networks and decision graphs.* 2007, New York, NY: Springer.

27. Wiegerinck, W., B. Kappen, and W. Burgers, *Bayesian networks for expert systems: theory and practical applications. In: Robert B, Groen FCA, editors.* Interactive collaborative information systems, 2010. **281**.

28. Nagarajan, R., M. Scutari, and S. Lèbre, *Bayesian networks in R: with applications in systems biology.* 2013, New York: Springer.

29. Pearl, J., *Causality: models, reasoning, and inference. 2nd ed.* 2009, New York: Cambridge University Press.

30. Lauritzen, S.L. and D.J. Spiegelhalter, *Local computations with probabilities on graphcial structures and their application to expert systems.* J R Stat Soc Ser B, 1988. **50**: p. 157-224.

31. Babovic, V., *Introducing knowledge into learning based on genetic programming.* Hydroinformatics, 2009. **11**(181).

32. Scutari, M., *Learning Bayesian Networks with the bnlearn R Package.* J Stat Softw, 2010. **35**(3): p. 1-22.

33. Koller, D. and N. Friedman, *Probabilistic Graphcial Models: principles and techniques*. 2009, Cambridge, MA, US; London, UK: The MIT Press.

34. Bijl, H., *Gaussian Process Regression Techniques*. 2016.

35. Rasmssen, C.E. and C.K. Williams, *Gaussian Process for Machine Learning*. 2006, London: The MIT Press.

36. Wu, T. and J. Movellan. *Semi-parametric Gaussian Process for Robot System Identification*. in *IEEE/RSJ Internetional Conference on Intelligent Robots and Systems*. 2012. Vilamoura.

37. Murphy, K.P., *Machine Learning*. 2012, London: The MIT Press.

38. Mclnnes, L., J. Healy, and J. Melville, *UMAP: Uniform Manifold Approximation and Projection for Dimension Reduction.* arXiv stat.ML, 2020.

39. Becht, E. and L. Mclnnes, *Dimensionality reduction for visualizing single-cell data using UMAP.* Nature biotechnology, 2019. **37**(1): p. 38-44.

40. Ghrist, R.W., *Elementary applied topology*. 2014, Seattle: Createspace.

END OF REPORT BODY

Attachments

This report contains the following six attachments appended in the following order:

Attachment #1: Frontics - Measurement of Yield strength, Tensile strength and Fracture toughness of API 5L pipe using Instrumented Indentation Testing

Attachment #2: Frontics - Measurement of Yield strength, Tensile strength and Fracture toughness of API 5L pipe using Instrumented Indentation Testing - Part II

Attachment #3: Frontics - Measurement of Yield strength, Tensile strength and Fracture toughness of API 5L pipe using Instrumented Indentation Testing - Additional Sample

Attachment #4: Frontics - Measurement of Yield strength, Tensile strength and Fracture toughness of API 5L pipe samples using Instrumented Indentation Testing - Coupon testing

Attachment #5: MMT - Procedure Bundle

Attachment #6: MMT - Final report for nondestructive HSD Testing for 70 cutout samples

Filenames:

- Attachment #1 - FARE-190603-1 Part I.pdf (328 pages)
- Attachment #2 - FARE-190603-1 Part II.pdf (298 pages)
- Attachment #3 - FARE-190723-1 Part I Appendix 2.pdf (8 pages)
- Attachment #4 - FARE-201122A.pdf (108 pages)
- Attachment #5 - 2020MMTProcedureBundle_2021.03.01.pdf (47 pages)
- Attachment #6 - 2021.02.10-MMTFinalNDEReportForGTI19006.pdf (267 pages)